DESIGN AND SYNTHESIS OF BORON-DIPYRROMETHENE (BODIPY) BASED FLUORESCENT AND COLORIMETRIC SENSORS FOR THE DETECTION OF GOLD AND MERCURY IONS

A Thesis Submitted to
the Graduate School of Engineering and Sciences of
İzmir Institute of Technology
in Partial Fulfillment of the Requirements for the Degree of

DOCTOR OF PHILOSOPHY

in Chemistry

by
Muhammed ÜÇÜNCÜ

May 2016
İZMİR

We approve the thesis of **Muhammed ÜÇÜNCÜ**

Examining Committee Members:

Assoc. Prof. Dr. Mustafa EMRULLAHOĞLU
Deparment of Chemistry, İzmir Institute of Technology

Prof. Dr. Mehtap EMİRDAĞ EANES
Deparment of Chemistry, İzmir Institute of Technology

Assist. Prof. Dr. Hadi M. ZAREIE
Deparment of Materials Science and Engineering, İzmir Institute of Technology

Assist. Prof. Dr. Tuna Subaşı
Deparment of Food Engineering, Ahi Evran University

Assist. Prof. Dr. Murat IŞIK
Deparment of Materials Science and Engineering, Bingöl University

26 May 2016

Assoc. Prof. Dr. Mustafa EMRULLAHOĞLU
Supervisor, Deparment of Chemistry,
İzmir Institute of Technology

Prof. Dr. Ahmet Emin EROĞLU
Head of the Deparment of Chemistry

Prof. Dr. Bilge KARAÇALI
Dean of the Graduate School of
Engineering and Science

ACKNOWLEDGEMENTS

During my PhD studies, there are many people to thank. I would like to express my deepest appreciation to the people who provide help, support and guidance through my graduate study at İzmir Institute of Technology. I am heartily thankful to my supervisor Assoc. Prof. Dr. Mustafa Emrullahoğlu for his patient guidance, encouragement and excellent advice throughout this study. This thesis could not have been written without his astute guidance. It was honor to study with him.

Also I would like to thank all old and new members of İYTE Emrullahoğlu research group, Ceren Cantürk, Hüseyin Zeybek and Ceyla Çetintaş. I would like to extend special thanks to Erman Karakuş for his support, help and friendship for twelve years.

I would like to thank to Melek Özkan, Özge Tüncel Çerik, Ayşenur Çataler Karakuş, Burcu Şengez, Selçuk Özdemir and Dane Rusçuklu for cell imaging studies, Assist. Prof. Dr. Tuna Subaşı, Dr. Ahmet E. Atik and Dr Filiz Yeşilırmak for HRMS analyses.

Special thanks to Prof. Dr. Mehtap Emirdağ Eanes, Assist. Prof. Dr. Hadi M. Zareie, Assist. Prof. Dr. Tuna Subaşı and Assist. Prof. Dr. Murat Işık for participating as committee member and for reviewing my work.

I would like to thank to the TUBITAK for fellowship support (2211-A) during my doctoral study.

I am deeply and forever indebted to my family for their love, support and encouragement throughout my entire life.

ABSTRACT

DESIGN AND SYNTHESIS OF BORON-DIPYRROMETHENE (BODIPY) BASED FLUORESCENT AND COLORIMETRIC SENSORS FOR THE DETECTION OF GOLD AND MERCURY IONS

The identification and quantification of heavy metal ions such as gold and mercury species in synthetic samples and living cells have crucial importance for scientific research. Even at very low concentrations, heavy metal ions can cause mortal consequences. Hence, there is a huge need for the development of new, sensitive, and selective methods to detect biologically active molecules, heavy metal ions, and anions that have significant effects on humans or animals. Up to now, trace metal analyses have been performed by classical spectroscopic methods such as atomic absorption and emission spectroscopy and inductively coupled plasma mass spectrometry. However, these methodologies require sophisticated devices and must be preceded by complicated sample preparation steps. In contrast to these time-consuming and expensive methods, fluorogenic and chromogenic methods that have high analyte sensitivity and selectivity and easy sample preparation steps and that use cheaper instrumentation have become important alternatives in recent years.

There are many organic dye molecules that act as signaling units for fluorogenic-sensing strategies such as rhodamine derivatives, fluorescein, coumarin, and BODIPY. For this thesis, we chose the BODIPY core as a signal reporter unit because of such unique properties as long excitation/emission wavelengths, high molar absorption coefficients and fluorescence quantum yields, and wide pH range for the sensing event. Also, BODIPY dyes can be easily derivatized from their various positions so that they produce an important advantage over other florophore molecules.

The main purpose of this thesis is to design and synthesize new BODIPY derivatives that bear highly selective and sensitive receptor units towards gold and mercury ions. In addition, to investigate the photophysical properties of designed molecules in the absence and presence of targeted metal ions in both synthetic samples and living cells.

ÖZET

ALTIN VE CIVA İYONLARININ TAYİNİ İÇİN BOR-DİPİROMETEN (BODIPY) BAZLI FLORESAN VE KOLORİMETRİK SENSÖRLERİN TASARIMI VE SENTEZİ

Altın ve civa iyonları gibi ağır metal iyonlarının sentetik örneklerde ve canlı hücrelerde tayin edilmesi ve miktarının belirlenmesi oldukça önemli bir çalışma alanıdır. Bu tür yapıların insan vücudunda birikmesinin telafisi mümkün olmayan hastalıklara yol açtığı bilinen bir gerçektir. Bu sebepten dolayı yeni, yüksek duyarlılıkta ve gelişmiş tayin yöntemlerine her daim ihtiyaç duyulmaktadır. Atomik absorpsiyon ve atomik emisyon spektroskopisi, indüktif eşleşmiş plazma spektrometresi gibi spektroskopik yöntemler kullanılarak eser miktarda ağır metallerin tayini yapılabilmektedir. Fakat bu yöntemler için karmaşık örnek hazırlama aşamaları ve sofistike cihazlar gerekmektedir. Oldukça pahalı ve zaman alıcı yöntemlerin tersine, yüksek analit duyarlılığı ve seçiciliği olan, daha kolay örnek hazırlama ve daha basit cihazlar gerektiren florojenik ve kromojenik yöntemler ile eser miktarda metal tayini yapmak iyi bir alternatif olabilir.

Bu yöntemlerde sinyal iletici olarak kullanılan çeşitli organik moleküller bulunmaktadır. Rodamin türevleri, florosein, kumarin ve BODIPY bu yapılardan sadece bir kaçıdır. Gerçekleştireceğimiz tez çalışmasında uzun dalga boyunda uyarılması/yayılması, yüksek molar absorpsiyon katsayısı ve floresans kuantum verimi, geniş pH aralığında çalışılabilir olması gibi diğer boya yapılarından oldukça üstün niteliklere sahip olması ve kolayca türevlendirilebilmesinden dolayı BODIPY yapısı sinyal iletici olarak seçilmiştir. Bu tez çalışmasındaki temel olarak amacımız BODIPY yapısını altın ve civa iyonlarına karşı yüksek seçicilik ve duyarlılık gösterebilecek reseptör gruplar ile türevlendirmektir. Aynı zamanda tasarladığımız sensör moleküllerinin hem sulu çözeltilerde hem de hücre içerisinde analit varlığında/yokluğunda foto-fiziksel değişimlerini incelemektir.

TABLE OF CONTENT

LIST OF FIGURES

Figure **Page**

LIST OF ABBREVIATIONS

BODIPY	4, 4-difluoro-4-bora-3a, 4a-diaza-s-indacene
DDQ	2,3-Dichloro-5,6-dicyano-1,4-benzoquinone
TFA	Trifluoroacetic Acid
PET	Photoinduced Electron Transfer
ICT	Intramolecular Charge Transfer
FRET	Fluorescence Resonance Energy Transfer
TBET	Through Bond Energy Transfer
CHEF	Chelation Enhanced Fluorescence
TICT	Twisted Intramolecular/Intermediate Charge Transfer
PICT	Planar Intramolecular Charge Transfer
HOMO	Highest Occupied Molecular Orbital
LUMO	Lowest Unoccupied Molecular Orbital
THF	Tetrahydrofuran
DCM	Dichloromethane
DMF	Dimethyl Formamide
DCE	Dichloroethane
RT	Room Temperature
EtOH	Ethanol
DAPI	4',6-diamidino-2-phenylindole

CHAPTER 1

INTRODUCTION

1.1. An Overview

Fluorescent molecular sensors have become popular during the last thirty years. Although the first fluorescent molecular sensors were invented in 1868 by Göppelsröder (Göppelsröder, 1868) they did not gain attention from scientists until the 1980s. Tsein put the spotlights on fluorescent molecular sensors with his report in which calcium ions were detected by gaining advantage of the changes in the fluorescence signals of a fluorophore molecule (Tsein, 1980). Since then, interest in the fluorescence sensing strategy has continuously increased. This approach has offered many advantages and has become an outstanding alternative to classical sensing systems such as inductively coupled plasma mass spectrometry, inductively coupled plasma atomic emission spectrometry, and cold vapour atomic absorption spectrometry (Clevenger et al., 1997; Powell et al., 1992). Classical methods require sophisticated instrumentation and time consuming sample preparation steps. However, the fluorescence sensing strategy offers a simple and cost-effective analysis of synthetic samples. Fluorescent dyes have also become an indispensable tool for biological systems. They are frequently used for biological applications such as the tracking of targeted analytes in living cells, the labeling of proteins, and the monitoring of biological processes.

The breakthrough invention of Frederich Herchel in 1845, which described the shining property of a water solution of quinoline salt under sunlight illumination, drew attention to fluorescent molecules (Herchel, 1845). Up until now, various fluorophores such as Rhodamine (Beija et al., 2009), Fluorescein (Baeyer, 1871), Coumarin (Perkin, 1868), Cyanine (Williams, 1856) etc. have been synthesized and their photophysical properties reported in details. Many of these molecules offer various advantages for different applications. OLED systems, bioimaging and labeling processes, and trace metal analysis applications are some important examples in which fluorescent molecules have been frequently used. Each application requries special conditions that create an urgent need for the development of florescent molecules that can be easily

modified. Among all the fluorescent molecules, BODIPY (4,4-difluoro-4-bora-3a, 4a-diaza-s-indacene) is one of the best fluorophore; it bears exceptional photophysical properties such as high photostability, high fluorescence quantum yield, robustness towards light and chemicals, and long emission/absorption wavelength. In addition to these advantages, BODIPY molecules have many reactive units that can be functionalized arbitrarily. (Boens et al., 2012).

A fluorescent sensor molecule is comprised of two parts: a fluorophore unit and a receptor unit. As mentioned above, a BODIPY core was chosen as the fluorophore unit because it has exceptional photophysical properties over other fluorophore molecules and also because it can be easily derivatized using well-known chemical reactions. Another crucial aspect of constructing a fluorescent molecular probe is designing a selective and sensitive receptor group. A receptor unit can be defined as an analyte-specific unit that translates the presence of a targeted analyte by way of coordination or reaction. If the sensing event takes place via reversible intearctions, the probe is called a chemosensor. If the receptor undergoes an irreversible change in the presence of the targeted analyte, the probe molecule is named a chemodosimeter (Culzoni et al., 2013).

Performing an analysis for the detection of trace amounts of metal ions in synthetic samples and living organisms is an important field of interest for scientists. Recent devolopments in industry and technology produce new sources of environmental pollutions, and a major part of these pollutions originate from chemical wastes from factories. The soil or drinking water may be contaminated from these wastes and may become a significant threat for human beings and other living organisms. Especially some of the transition metal ions such as Hg^{2+}, Cd^{2+}, Pb^{2+}, Au^{3+} and As^{3+}, which are present in chemical wastes, are very toxic and may cause irremediable damages to the human body. There is an urgent need for the detection of the above metal ions with fast, simple, and cost-effective methods. There are various molecular sensors that make the recognition of one or more of the above trace metal ions possible by way of changes in the fluorescence signal (Carter et al., 2014; Xu et al., 2014). However, the metal ions with a similar chemical nature, such as Hg^{2+} and Au^{3+}, make sensing events difficult for differential detection. In the literature, there are very few examples that differentiate metal ions sharing a similar nature (Maity and Govindaraju, 2012; Li et al., 2014; Dong et al., 2010). Clearly, the differentiation or selective detection of metal ions having similar chemical nature is seriously needed for the development of molecular sensors.

In this thesis, design and synthesis of new BODIPY-based fluorescent molecular sensors for the individual or differential detection of gold and mercury ions in synthetic samples and living organisms was aimed. Gold and mercury ions show high affinity to heteroatom containing molecules, especially sulfur-bearing compounds. Based on this reactivity, the accumulation of the above mentioned metal ions in the human body may cause disorders in cellular processes (Onyido et al., 2004; Nyarko et al., 2004). There are several fluorescent molecular sensors that benefit from this high affinity towards heteroatoms. In addition, both metal ions are very reactive towards unsaturated systems (possesing highly alkynophilic character), and this reactivity is used as another strategy to construct fluorescent sensor molecules. (Singha et al., 2015; Zhang et al., 2011; Yan et al., 2014; Chen et al., 2015; Kim et al., 2011). Although several attempts have been made, there are very few examples that can differentiate gold and mercury ions by using their alkynophilic character (Dong et al., 2010). The scope of this thesis encompasses new BODIPY-based sensors that benefit from alkynophilicity and the strong coordination ability of gold and mercury species. Also, new reactive motifs and strategies are designed and applied to detect targeted metal ions successfully.

1.2. Organic Fluorescent Molecules

The invention of Frederich Herchel in 1845 shed light on a new area of chemistry and drew attention to fluorescent molecules. Since this invention, scientists have made great efforts to discover new fluorescent molecules for various purposes. Fluorescein, Rhodamine, Coumarin, Cyanine, and BODIPY dyes are the most common fluorescent molecules that are used in applications such as metal ion, anion, or ROS/RNS sensors, protein labeling agents, and biological processes monitoring, etc. In this chapter, some of the characteristics and synthetic methods of important fluorophores are summarized briefly.

1.2.1. Fluorescein

Fluorescein is one of the first example of synthetic fluorescent dye, it was studied in 1871 by Adolph Von Baeyer (Baeyer, 1871). As shown in Figure 1.1, fluorescein dye can be obtained from the reaction of resorcinol and phthalic anhydride in the presence of a Lewis acid (Orndorff and Hemmer, 1927).

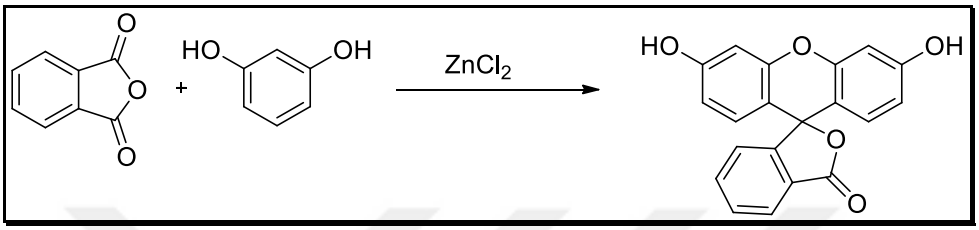

Figure 1.1. Synthesis of fluorescein fluorophore
(Source: Orndorff and Hemmer, 1927)

Fluorescein dyes have important photophysical properties such as high quantum yields and molar extinction coefficients. The most outstanding feature of fluoresceins is their high water solubilities, which make them excellent tools for labeling and bio-imaging applications. Also, the fluorescein core has been extensively used in sensor applications for synthetic samples and living cells (Li et al., 2013).

Although fluorescein molecules offer many advantages – especially water solubility- they have some limitations. The main disadvantage of this group of molecules is their pH dependency. At lower pH values, the fluorescence property of fluorescein dyes is significantly diminished, which makes them impractical in many applications. In addition, the high rate of photobleaching and the quenching tendency of these molecules restricts their use in many applications.

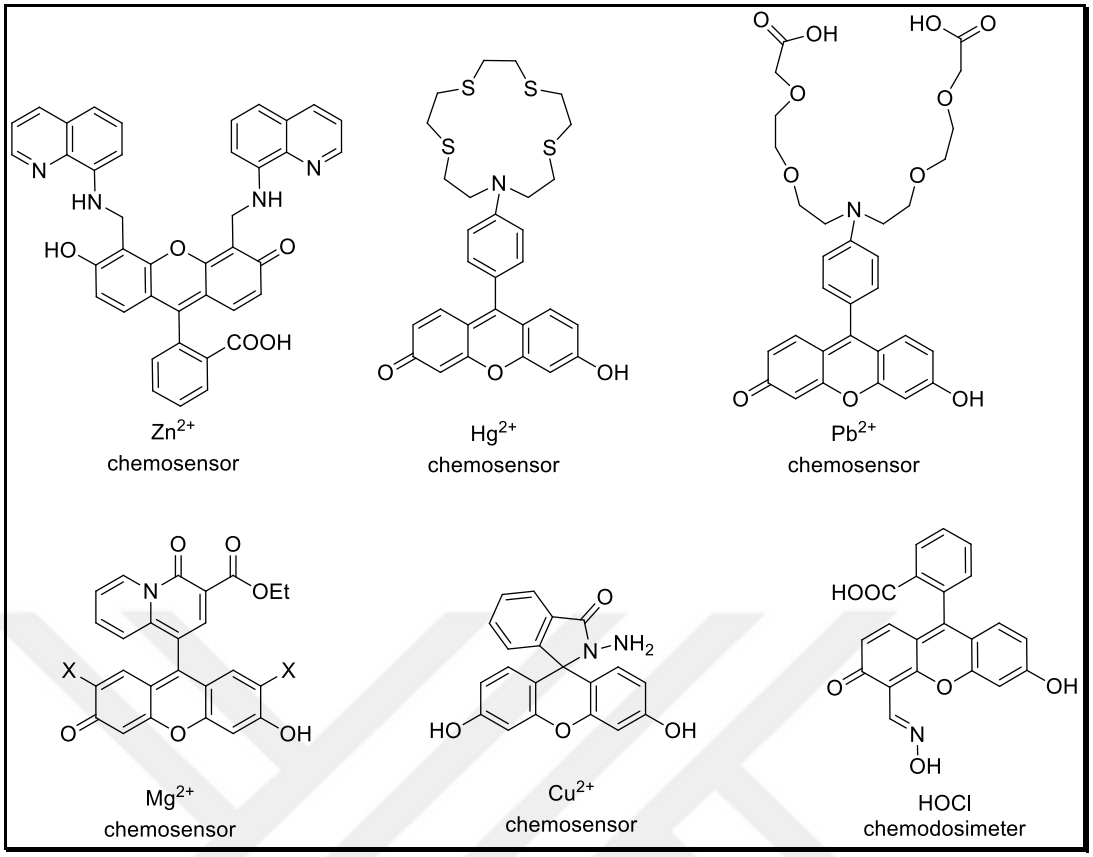

Figure 1.2. Fluorescein based sensors
(Source: Li et al., 2013)

1.2.2. Rhodamine

Rhodamine dyes are the other members of the xhanthene family that are synthesized from the reaction of *m*-aminophenol and phthalic anhydride in the presence of a Lewis acid (Noelting and Dziewoński, 1905).

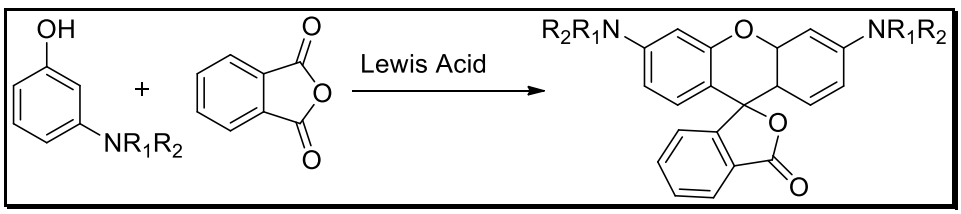

Figure 1.3. Synthetic scheme for Rhodamine core
(Source: Noelting and Dziewoński, 1905)

There are several derivatives of Rhodamine molecules such as Rhodamine B, Rhodamine 6G, and Rhodamine 101. Because of their elegant photophysical properties and high photostabilities, Rhodamine dyes are frequently used for many purposes such as laser dyes, fluorescence standards, and labeling agents. Moreover, Rhodamine derivatives have been used for the analysis of metal ions, anions, and biologically important species in both synthetic samples and living milieus (Beija et al., 2009).

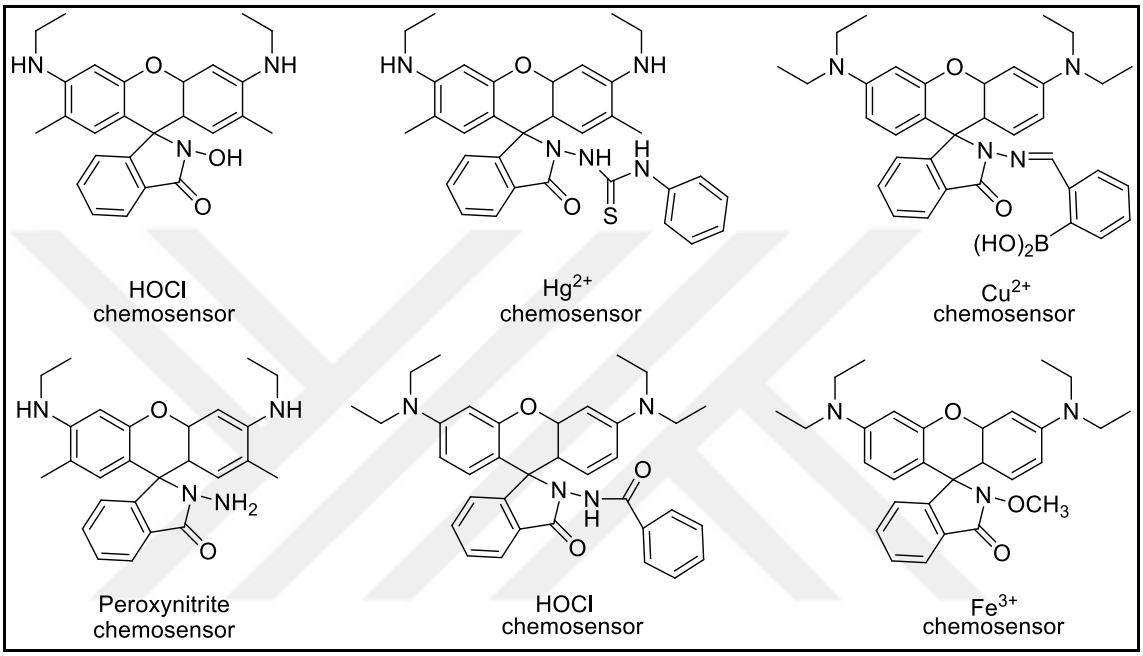

Figure 1.4. Rhodamine based chemosensors
(Source: Beija et al., 2009)

Although Rhodamine dyes exhibit subtantial advantages for sensor, labeling, and other applications, they have critical restrictions. Water solubility is the leading restriction of this group of dyes. Their protein conjugates have a strong tendency to precipitate and lose their fluorescence property. Another important limitation of Rhodamine dyes is their high sensitivity towards pH changes. There have been various Rhodamine-based chemosensors constructed to detect pH changes in solutions and living cells. However, their pH sensitivity may cause significant deficiencies for sensor applications.

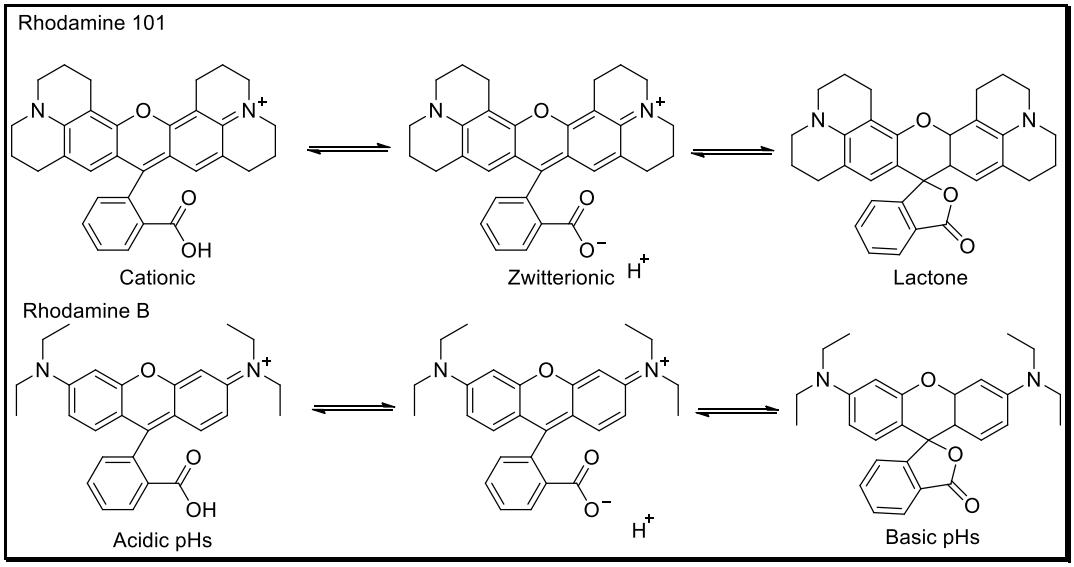

Figure 1.5. The structural forms of Rhodamine 101 and Rhodamine B in acidic and basic media (Source: Beija et al., 2009)

1.2.3. Coumarin

Benzo-α-pyrones, commonly called coumarins, are members of the Benzopyrone family. Coumarin is a naturally occurring compound that was first isolated from Tonka beans in 1820. The first synthesis of Coumarins in laboratory conditions was performed by W. H. Perkin, Sr. in 1868 from the reaction of salicylaldehyde with acetic anhydride and anhydrous sodium acetate with the aid of heating (Perkin, 1868). The reaction produces o-hydroxycinnamic acid derivative that automatically transforms into Coumarin. This methodology has frequently been used by many scientisits. However, there has been growing attention given to the discovery of new easy and efficient methods for the synthesis of the coumarin skeleton. There have been some new methodologies for the synthesis of coumarin derivatives such as the Pechmann reaction, Pechmann-Duisberg reaction, and Knoevenagel reaction (Trenor et al., 2004; Sethna and Shah, 1944).

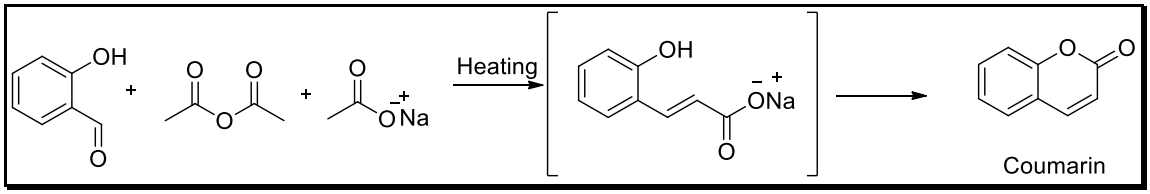

Figure 1.6. Synthesis of Coumarin structure by using Perkin reaction
(Source: Perkin, 1868)

There are thousands of naturally occurring Coumarin derivatives, and these molecules are used in various areas. Coumarins have fluorescence emission in the range of visible light that makes them useful for laser dye and organic light-emitting diode (OLED) applications. There are also several molecular sensors that benefit from the changes in fluorescence emission of the Coumarin core. In Figure 1.7, some of the coumarin-based fluorescent sensors are indicated (Liu et al., 2015; Aulsebrook et al., 2015; Hettie and Glass, 2016; Yan et al., 2016).

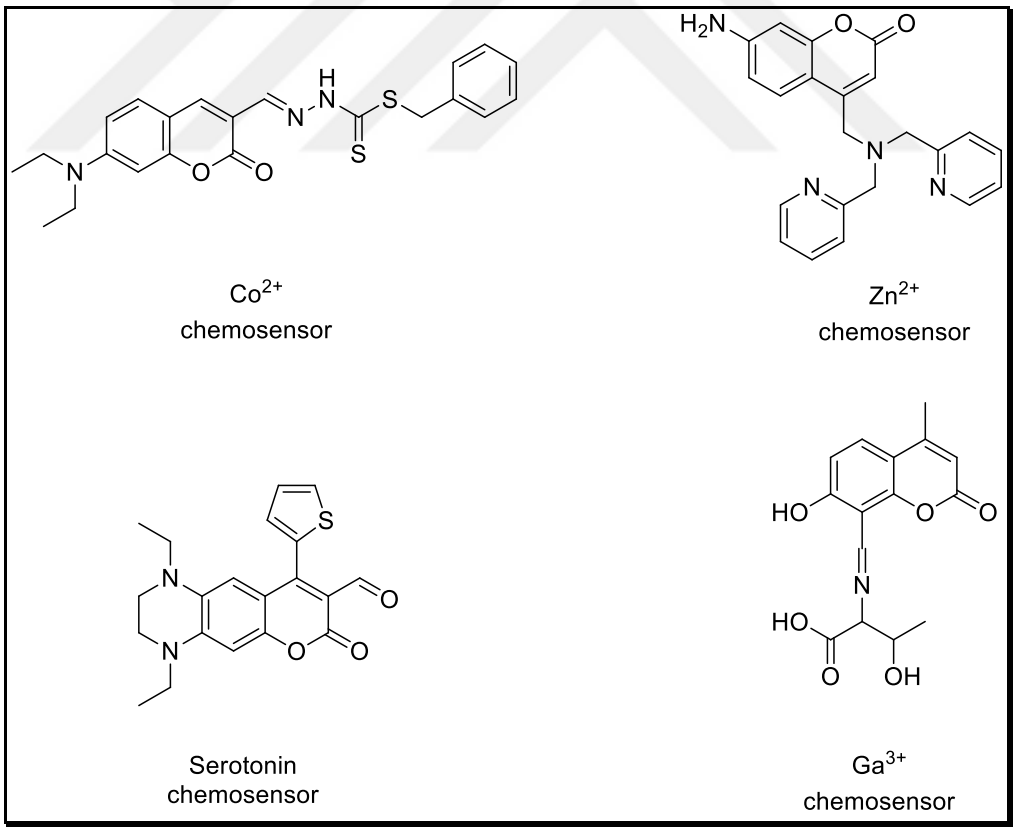

Figure 1.7. Coumarin based fluorescent sensors
(Source: Liu et al., 2015; Aulsebrook et al., 2015; Hettie and Glass, 2016; Yan et al., 2016)

The main drawback of coumarin-based molecular sensors is their short absorption and emission wavelengths, which make them impractical for living cell applications

1.2.4. Cyanine

The Cyanine dyes were first synthesized by C. H. G. Williams from the reaction of *N*-amyl quinolinium iodide and *N*-amyl lepidinium iodide in ammonia with strong heating, it generated a magnificient blue-colored compound. The usual approach to obtain hemicyanine dyes relies on the condensation reaction of 2,4-dimethyl quaternary salt of the base and an aromatic aldehyde with a proper base (Mishra et al., 2000). There has been an increasing interest in finding new methodologies to synthesize cyanine dyes in different patterns.

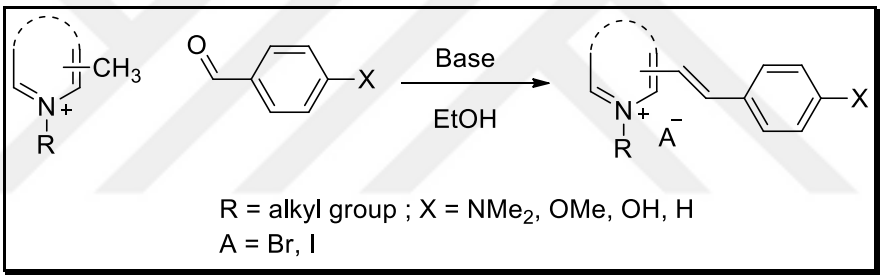

Figure 1.8. Synthetic scheme of cyanine dyes
(Source: Mishra et al., 2000)

Cyanine dyes have a cationic structure that is comprised of two heterocyclic rings that are connected to each other with a polymethine chain (Narayanan and Patonay, 1995) (Figure 1.9).

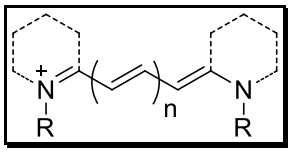

Figure 1.9. General structure of cyanine dyes
(Source: Narayanan and Patonay, 1995)

From its structure we know that cyanine dyes are near IR emitting dyes, and this property can easily be tuned by introducing double bonds to the polymethine chain. The near IR emitting nature indicates that cyanine dyes can be used for a wide range of applications. They are important candidates for biological processes such as DNA sequencing, in vivo imaging, and proteomics. Besides their biological utility, cyanine dyes are very powerful materials as fluorescent sensors. (Guo et al., 2012; Yin et al., 2015; Zhao et al., 2014).

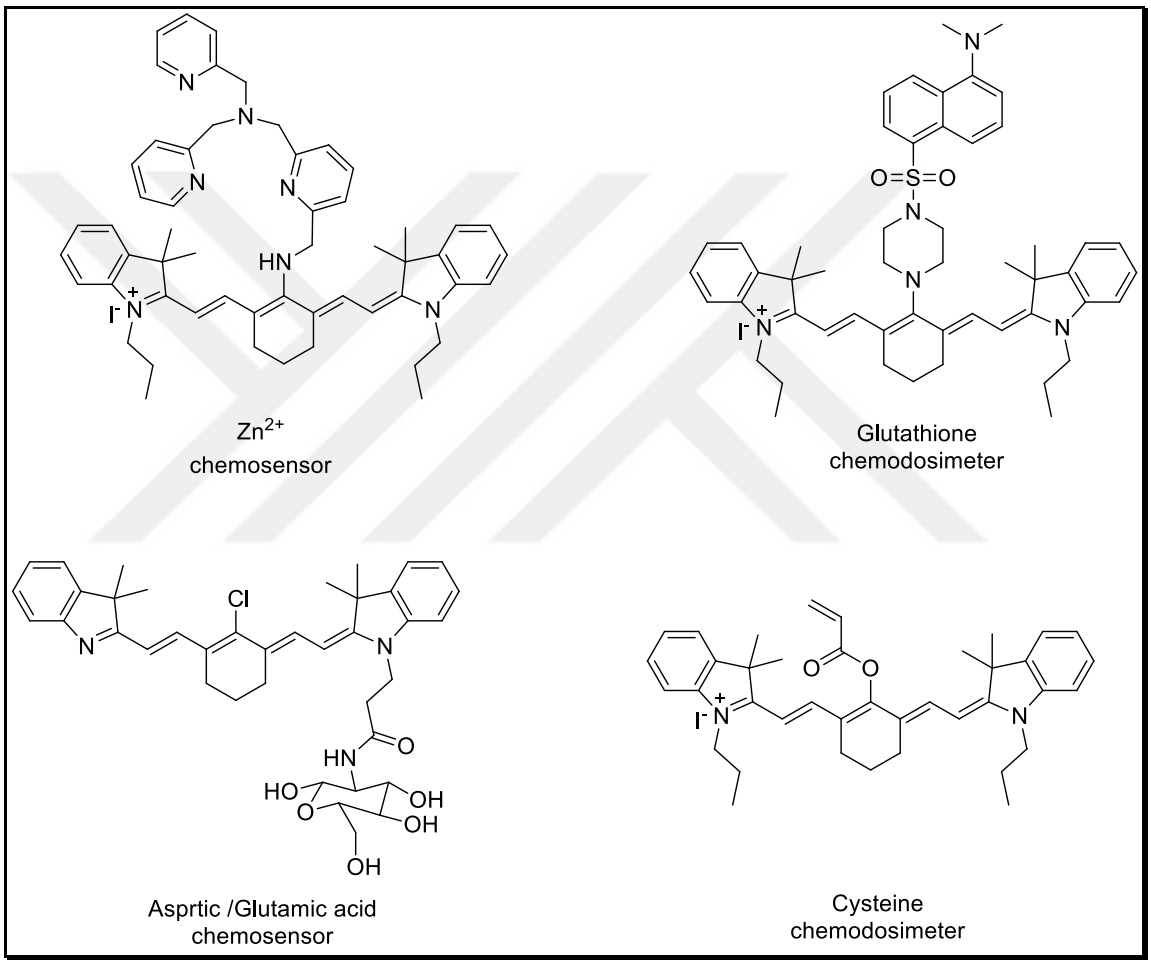

Figure 1.10. Cyanine based chemosensors and chemodosimeters
(Source: Guo et al., 2012; Yin et al., 2015; Zhao et al., 2014)

Despite the fact that cyanines possess impressive properties, they have some limitations in practice. Low fluorescence quantum yields and short lifetimes are the primary deficiencies of cyanine dyes. In addition, aggregation in aqueous solutions limits their usage in biological systems because of low fluorescence intensity.

1.2.5. BODIPY (4,4-difluoro-4-bora-3a,4a-diaza-s-indacene)

BODIPY (4,4-difluoro-4-bora-3a, 4a-diaza-s-indacene) fluorophore was serendipitously discovered by Treibs and Kreuzer in 1968 (Treibs and Kreuzer, 1968). The acylation of dimethylpyrrole with acetic anhydride in the presence of boron trifluoride yielded a highly fluorescent product instead of acetylated dimethylpyrrole. (Figure 1.11).

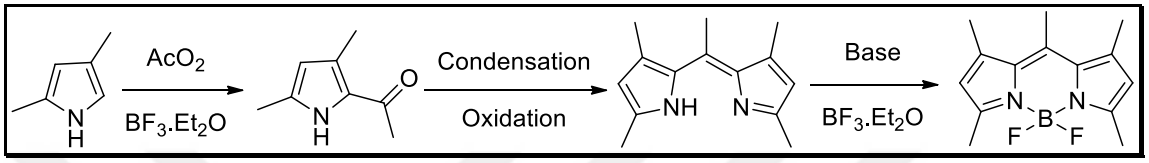

Figure 1.11. Serendipitioous discovery of BODIPY
(Source: Treibs and Kreuzer, 1968)

Although the BODIPY fluorophore has fascinating chemical and photophysical properties, scientists did not show any interest in this new class of fluorophore until the 1990s. Towards the end of the 1980s, BODIPY dyes started to be used in the labeling of proteins for biological applications (Monsma et al., 1989). Henceforward, new studies have been conducted based on the advanced properties of the BODIPY structure. Several uses of BODIPY-based compounds have been developed, for instance as photodynamic therapy agents (Awuah et al., 2012; Kamkaew et al., 2013), fluorescent molecular sensors for metal ions (Boens et al., 2012; Carter et al., 2014), anion (Fu et al., 2015; Sekhar et al., 2015) or biologically important species (Kowada et al., 2015; Zhou and Joon, 2013), solar cells (Li and Diau, 2013), light harvesting antennas (Benstead et al., 2011;), laser dyes (Wood and Thompson, 2007; Arbeloa et al., 2005) and labeling agents (Kowada et al., 2015).

Among other fluorescent molecules, BODIPY dyes bear exceptional photophysical properties such as high photostability, high fluorescence quantum yields, robustness towards light and chemicals, long emission/absorption wavelength in the visible spectral region, and narrow emission bandwidths (Boens et al., 2015; Ulrich et al., 2008). However, the nature of BODIPY dyes shows small Stoke's shifts that limit the usage of this class of molecules in flow cytometry and fluorescence microscopy.

Luckily, the spectroscopic properties of BODIPY dyes can be easily tuned by structural modifications. The BODIPY structure has many reactive sites that can be modified by using well-known chemical reactions. BODIPY compounds are numbered, as shown in Figure 1.12 in which the central C is indicated as *meso* carbon, the N adjacent C atoms are named as α carbons, and the other carbons (C-6 and C-7) are defined as β carbons according to the IUPAC numbering system. Each C atom on the molecule is highly reactive and allows the postmodification to achieve the desired properties. Also, the boron atom is reactive, and the fluorine atoms can be changed by using proper reaction conditions.

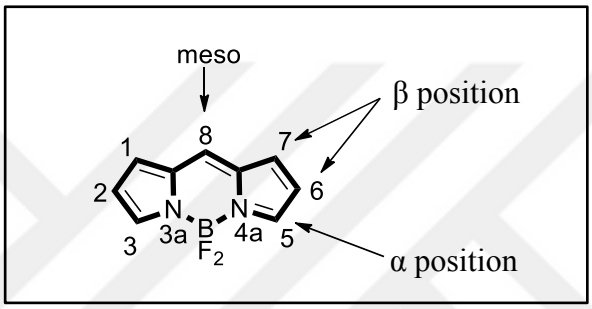

Figure 1.12. IUPAC numbering system of a boron dipyrrin compound
(Source: Wood and Thompson, 2007)

To obtain BODIPY structure, two distinct methodologies based upon porphyrin chemistry are used (Wood and Thompson, 2007). In the first approach, pyrrole undergoes acid catalysed condensation reaction with an aldehyde to yield dipyrromethane compound that will immediately oxidize to dipyrrin. *P*-chloranil and 2,3-Dichloro-5,6-dicyano-1,4-benzoquinone (DDQ) reagents are the most effective oxidizing agents for the oxidation of the dipyrromethane structures. Except for unsubstituted pyrroles, the condensation and oxidation reactions proceeded in the same reaction vassel. Because of the high sensitivity of the unsubstituted dipyrromethane compounds to light and air, some experimental modifications are required, for example, performing experiments with an excess amount of pyrrole (Littler et al., 1999). The final part of the synthesis includes the addition of $BF_3.Et_2O$ and an organic base (e.g., triethylamine, disopropylethylamine) to yield the BODIPY sutructure. (Figure 1.13).

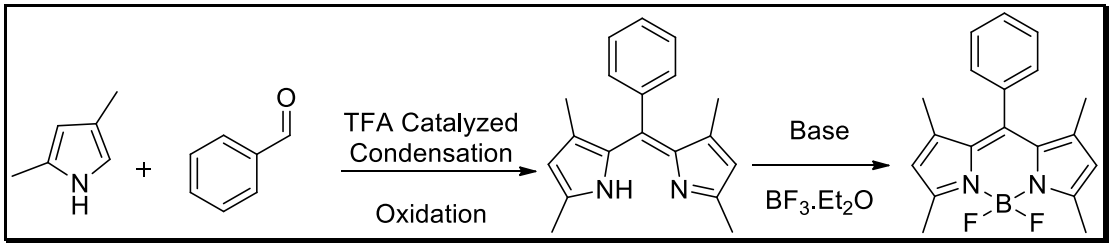

Figure 1.13. Acid catalyzed condensation of aromatic aldehydes with pyrroles (Source: Boens et al., 2012)

In another approach, the BODIPY structure can be obtained by the reaction of the pyrrole compound with an acyl halide (Shah et al., 1990), acid anhyride (Li et al., 2006), or an orthoester (Yakubovskyi et al., 2009) in which there is no need for any acid catalyst and oxidizing reagent. When the appropriate pyrrole and acyl halide reacts, the dipyrrin compound is obtained as a major product. Treatment of the dipyrrin compound with $BF_3.Et_2O$ and an organic base (e.g. triethylamine, diisopropylamine), the BODIPY sutructure is obtained within a moderate yield (Boens et al., 2012).

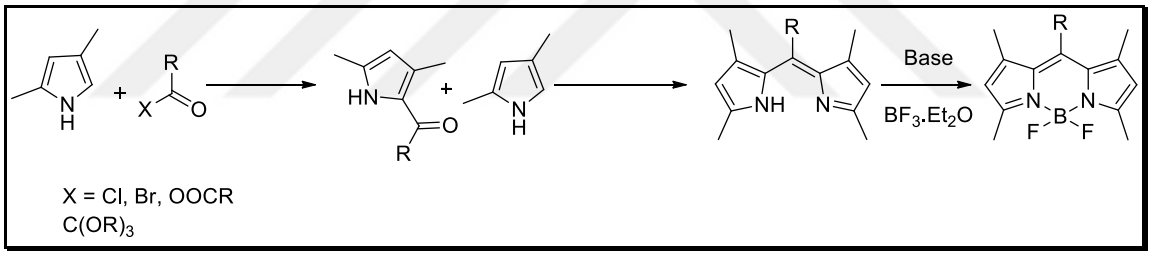

Figure 1.14. Synthesis of BODIPY dyes with the acylation of pyrrole followed by condensation and complexation (Source: Boens et al., 2012)

The second methodology offers a premodification opportunity to obtain derivatized BODIPY structure. When the acetylated pyrrole reacts with another pyrrole with a different substitution pattern, it is possible to obtain asymmetric BODIPY structures (Figure 1.14). These two approaches are mainly competetive methods, and the utility of the methodology strongly depends upon the nature of the functional group on the BODIPY core. However, in some cases they may act as complementary to each other (Ni and Wu, 2014; Boens et al., 2015).

As shown in Figure 1.15.a, to obtain thiolated BODIPY structure, it is impossible to achieve the final product with pre-modification methods. To obtain the final product, *meso* halogenated BODIPY has to be synthesized first. Then the reaction of methanthiolate produces the desired BODIPY derivative. On the other hand, Figure b indicates an important feature of the pre-modification approach in which the desired BODIPY structure is obtained starting with the premodified pyrrole as the key step. Both methods are important, based on the aim of the study. In some cases, it is possible to obtain the intended BODIPY structure by using both approaches. Figure 1.15.c is a significant example of this idea in which arylated BODIPY can be synthesized via pre- and post-modification approaches.

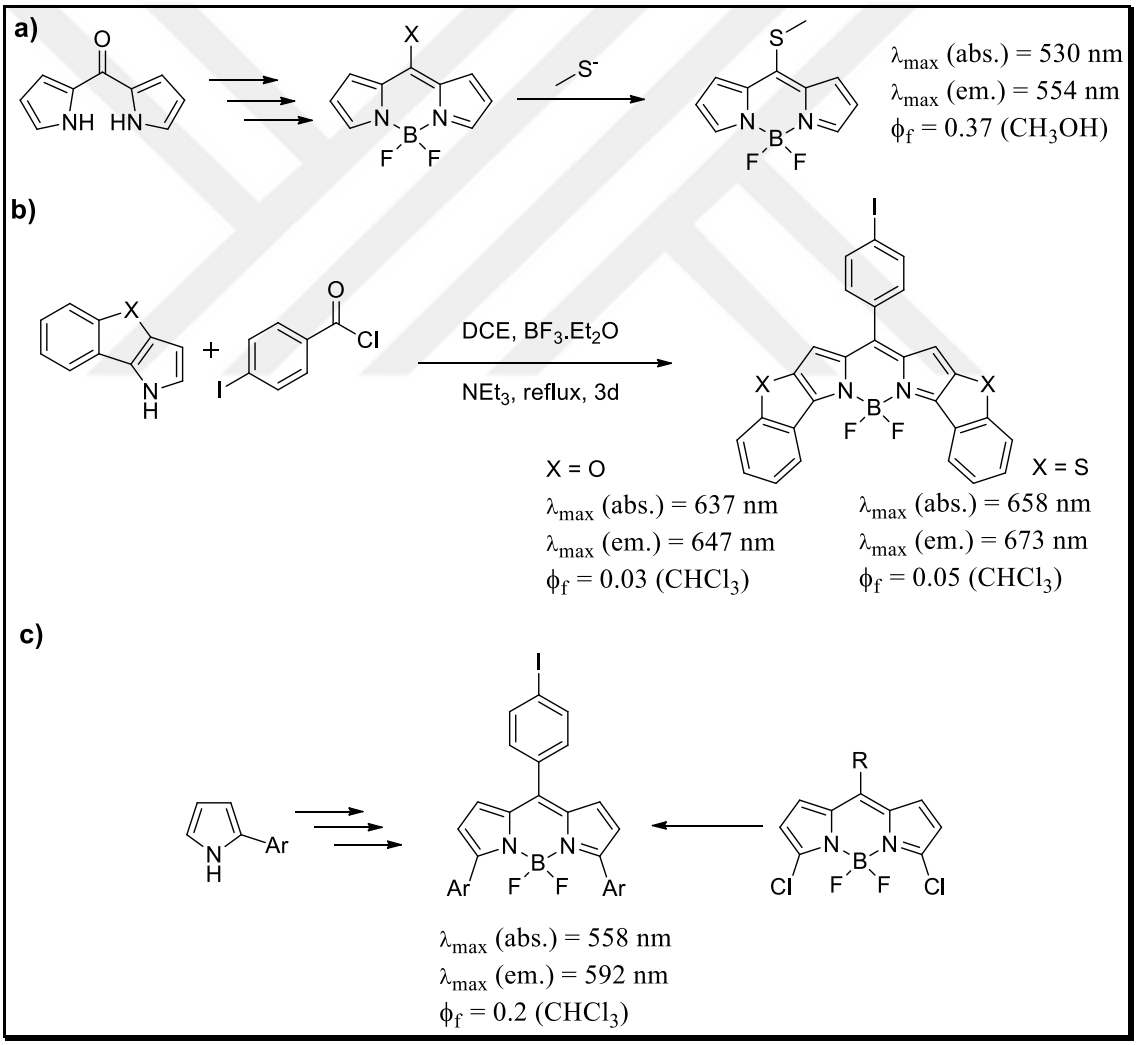

Figure 1.15. Synthetic pathways of BODIPY derivatives by using a) post-modification, b) premodification, and c) both methods. (Source: Ni and Wu, 2014; Boens et al., 2015)

Scientists have put great effort in developing new methodologies to synthesize the BODIPY structure in more efficient and cost-effective ways. In 2008, Wu and Burgess published an article in which the BODIPY compound was obtained by using the pyrrole compound without any aldehyde or other condensation reagent. This serendipitious discovery represents a new way for the synthesis of the dipyrrin structure by using phosphorus oxychloride as the condensation reagent.

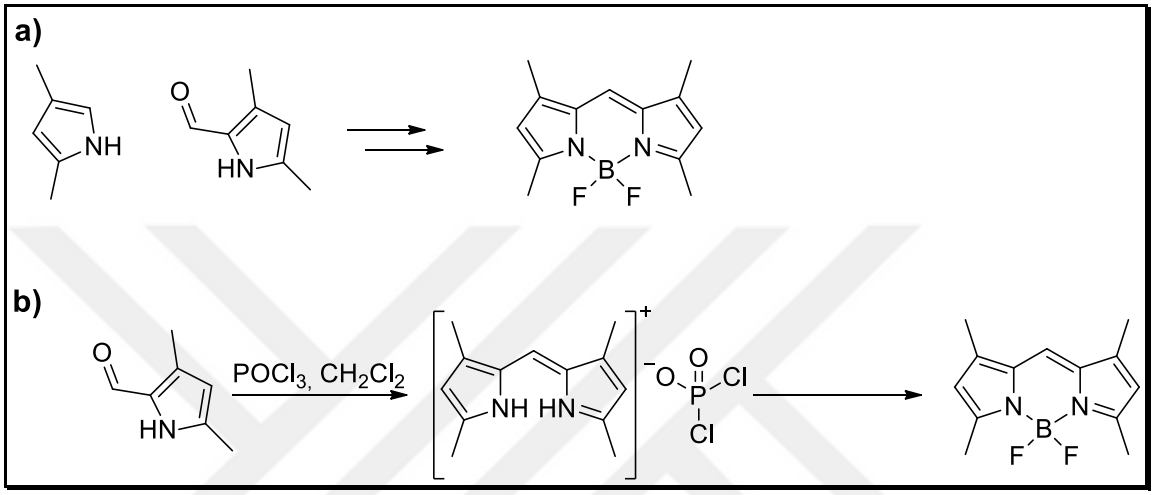

Figure 1.16. a) Conventional synthesis of tetramethyl-BODIPY and b) the new approach described (Source: Wu and Burgess, 2008)

The core structure of BODIPY dyes absorbs and emits relatively at lower wavelengths, about 450-500 nm. The substituent pattern on the core structure is strongly influences the photophysical properties of fluorophore. For example, the core structure without any substituent or bearing methyl groups on 1,3,5,7 carbon atoms shows similiar absorption/emission maxima and fluorescence quantum yields (φ_f=0.93, φ_f =0.80) (Schmitt et al., 2009). However, the addition of the phenyl group to the meso position strongly diminishes the fluorescence quantum yield because of free rotation of the phenyl group (Leen et al., 2011). The restriction of free rotation of the phenyl group results in an increase in the quantum yield of the core structure (Gabe et al., 2004).

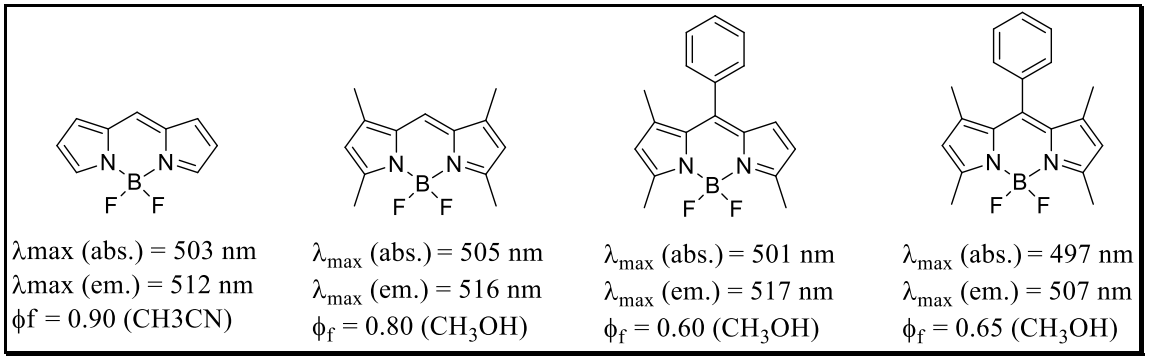

Figure 1.17. Influence of alkyl and meso aryl substituents on the spectroscopic properties (Source: Ni and Wu, 2014)

To tune the wavelength of the BODIPY structure, several pre- or post-modifications can be done easily. As mentioned above, the BODIPY core has many reactive positions that undergo several types of reaction. In Figure 1.18, most of the popular reactions are summarized briefly.

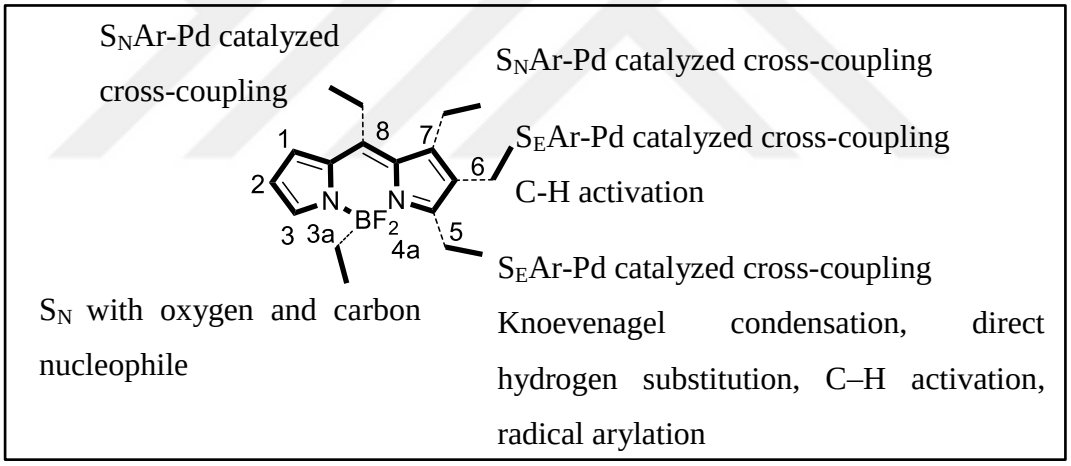

Figure 1.18. Possible post-functionalization sites of BODIPY structure (Source: Boens et al., 2015)

Increasing the conjugation of the core structure with double or triple bonds results in red shifts that vary up to 800 nm. Another way to obtain red-shifted BODIPY structures is to use a premodification approach in which unsaturated bond or aryl-attached or aryl-fused pyrroles are used as the starting material. In Figure 1.19, some examples that are synthesized via both pre- and post-modification approaches are given.

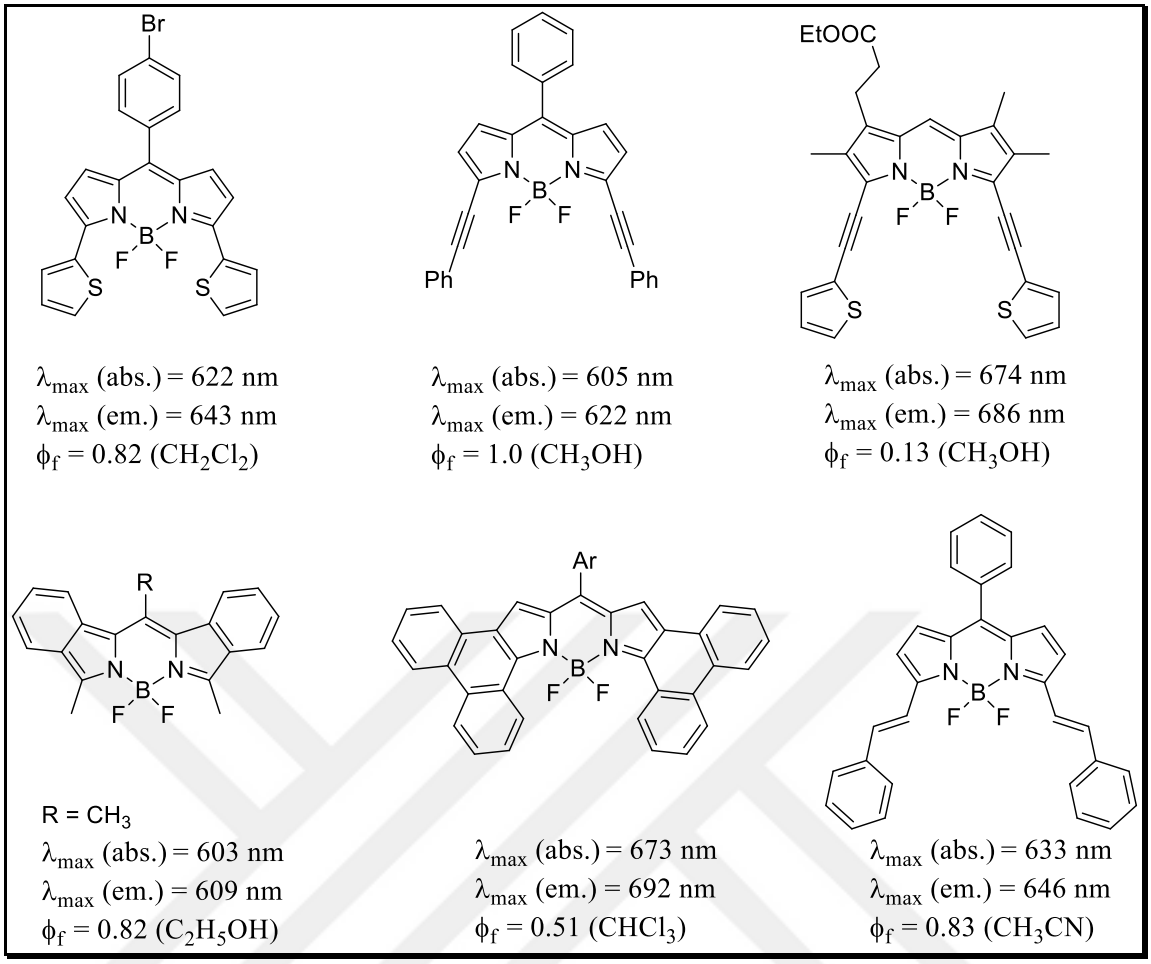

Figure 1.19. BODIPY structures with extented conjugation
(Source: Ni and Wu, 2014)

Besides its tunable nature of absorption/emission wavelength, the ease of functionalization of the BODIPY core also offers many advantages in constructing fluorescent molecular sensors. For many sensing applications, red-shifted molecular sensors are the main choice, especially for in vivo and in vitro studies. As mentioned above, a molecular fluorescent sensor requires two main compartments, the fluorophore and the receptor units. Many of the other fluorophore units have limited active sites that allow the integration of a analyte sensitive group. Due to the ease of functionalization, BODIPY core also offers substantial advantages to integrate receptor unit. Some examples of synthetic routes for derivatizing fluorescent molecular sensors that are functionalized in different positions are summarized below.

♦ ***Functionilazion of the BODIPY core from the meso position:***

The *meso* position of the BODIPY core can be altered by starting with an appropriate aromatic aldehyde bearing functional groups on it, such as alcohol, nitro, carboxylic acid, or ester. The robustness of the BODIPY structure allows the postmodifications and desired receptor units to easily integrate on these functional groups (Figure 1.20).

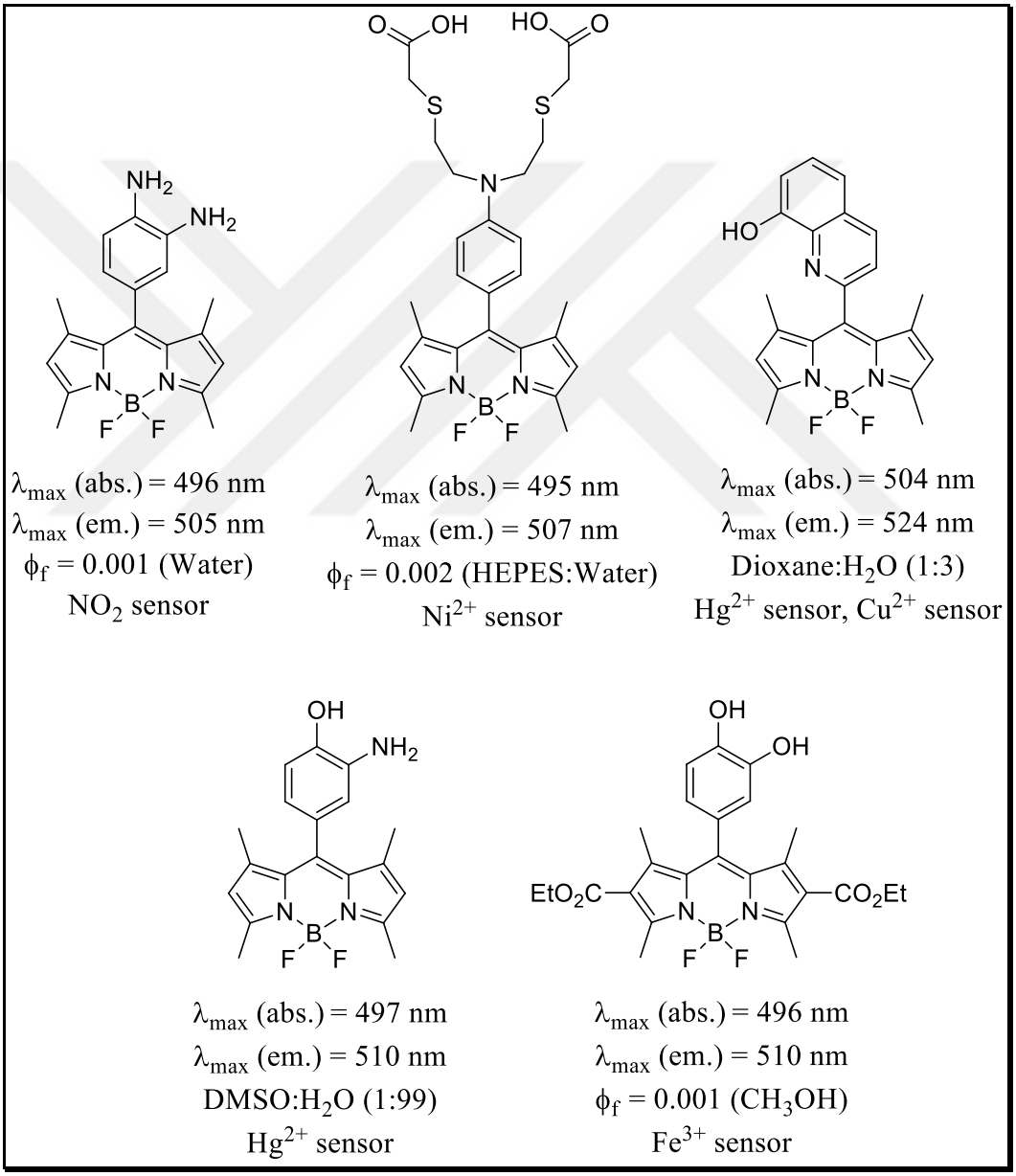

Figure 1.20. BODIPY based sensors synthesized from aldehyde derivative (Source: Boens et al., 2012)

Another approach to *meso* derivatization is the synthesis of the BODIPY core with halogen substituent at the *meso* position. To achieve a *meso* halogenated product, the starting material must be in dipyrrile ketone structure. The deoxygenative substitution reaction produces halogenated dipyrrine structure, which is further converted to a BODIPY through treatment with a suitable base and BF_3EtO_2 (Leen et al., 2012).

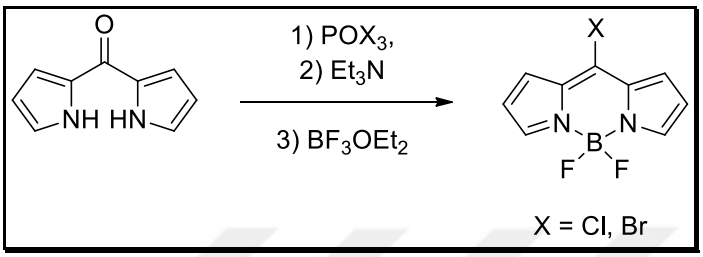

Figure 1.21. Synthesis of *meso*-halogenated BODIPY
(Source: Leen et al., 2012)

The *meso* halogenated BODIPYs are very useful tools for designing molecular probes because they are highly reactive towards palladium catalyzed coupling reactions (e.g., Suzuki coupling, Sonagashira coupling). In addition, this site is very reactive toward nucleophilic addition reactions. In the presence of a relatively strong nucleophile (e.g., R-SH, R-NH_2, or R-OH), replacement of halogen with nucleophile takes place under mild reaction conditions (Zhao et al., 2015; Leen et al., 2012).

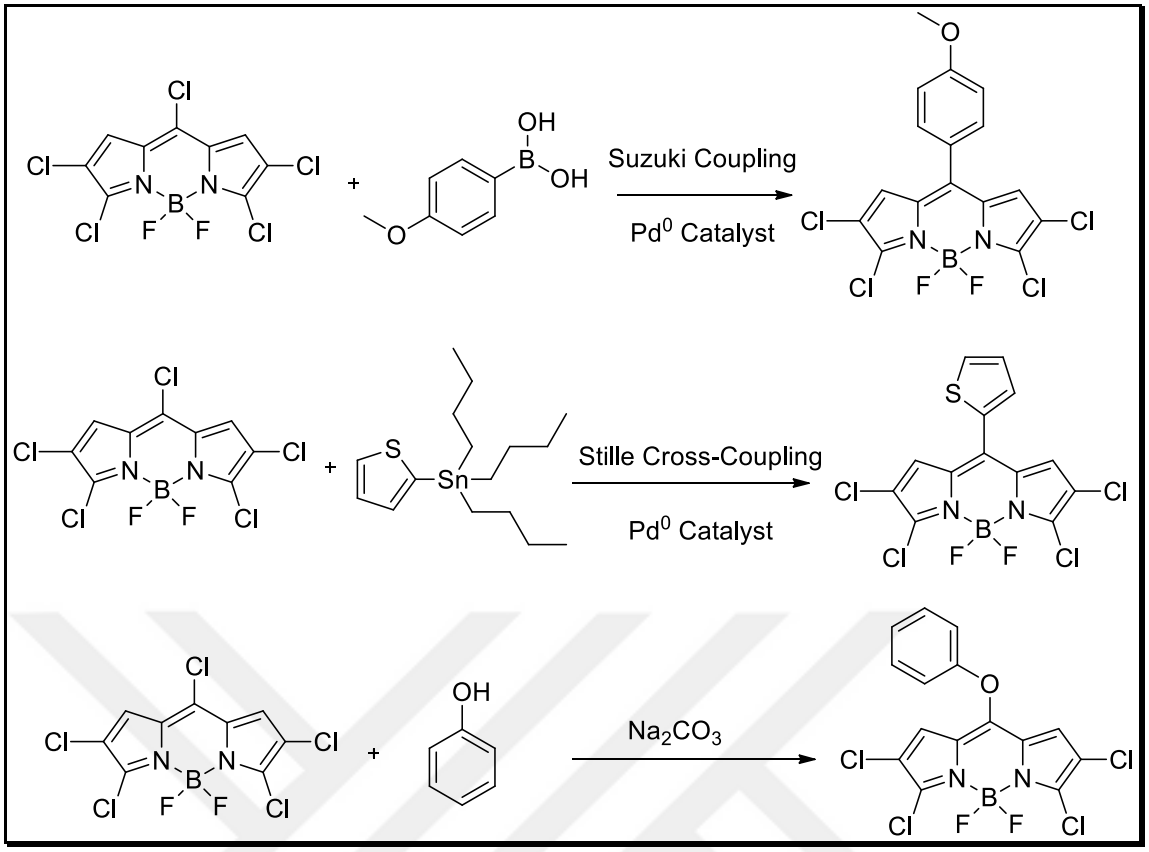

Figure 1.22. Examples of reactions of *meso* halogenated BODIPYs
(Source: Zhao et al., 2015)

♦ ***Functionalization of the BODIPY core from the 3- and 3,5- positions:***

The 3- and 3,5- positions of the BODIPY core are frequently used for the construction of molecular sensors. The strategy of design is mainly based on halogenation of the 3- and 3,5- positions of the BODIPY core by using proper halogenation agents. The experimental strategy is summarized in the figure below. To obtain halogenated BODIPY structure, the same methodology is applied in which a dipyrromethane compound is achieved from the reaction of an excess amount of pyrrole with appropriate aldehyde in the presence of a catalytic amount of trifluoroacetic acid. Halogenation protocol is applied at this stage by using an *N*-halosuccinimide reagent with a proper solvent at very low reaction temperatures (-78^{o}C) to obtain a dihalogenated product. Further stages are the same, with usual synthesis protocol in which oxidation is achieved by *p*-chloranil or DDQ followed by the addition of an organic base and BF_3Et_2O (Lakshmi et al., 2015).

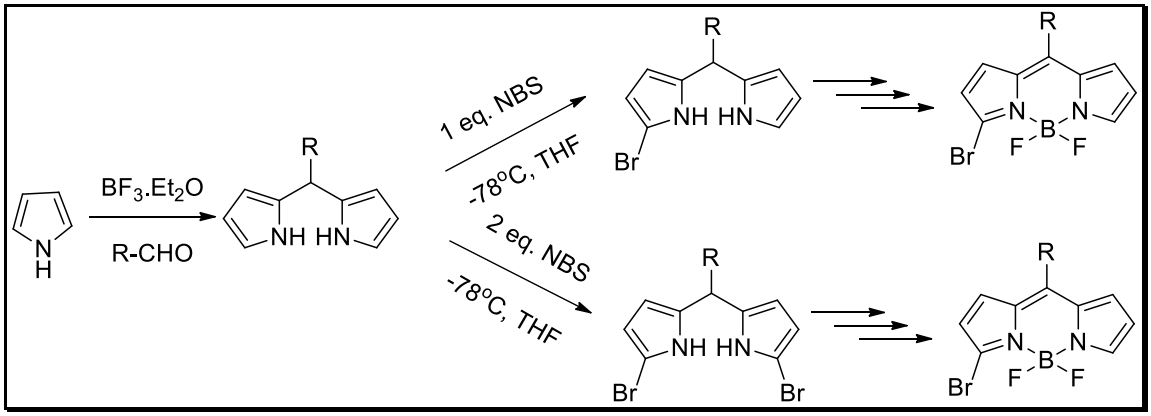

Figure 1.23. Synthesis of 3- and 3,5-bis- halogenated BODIPYs
(Source: Lakshmi et al., 2015)

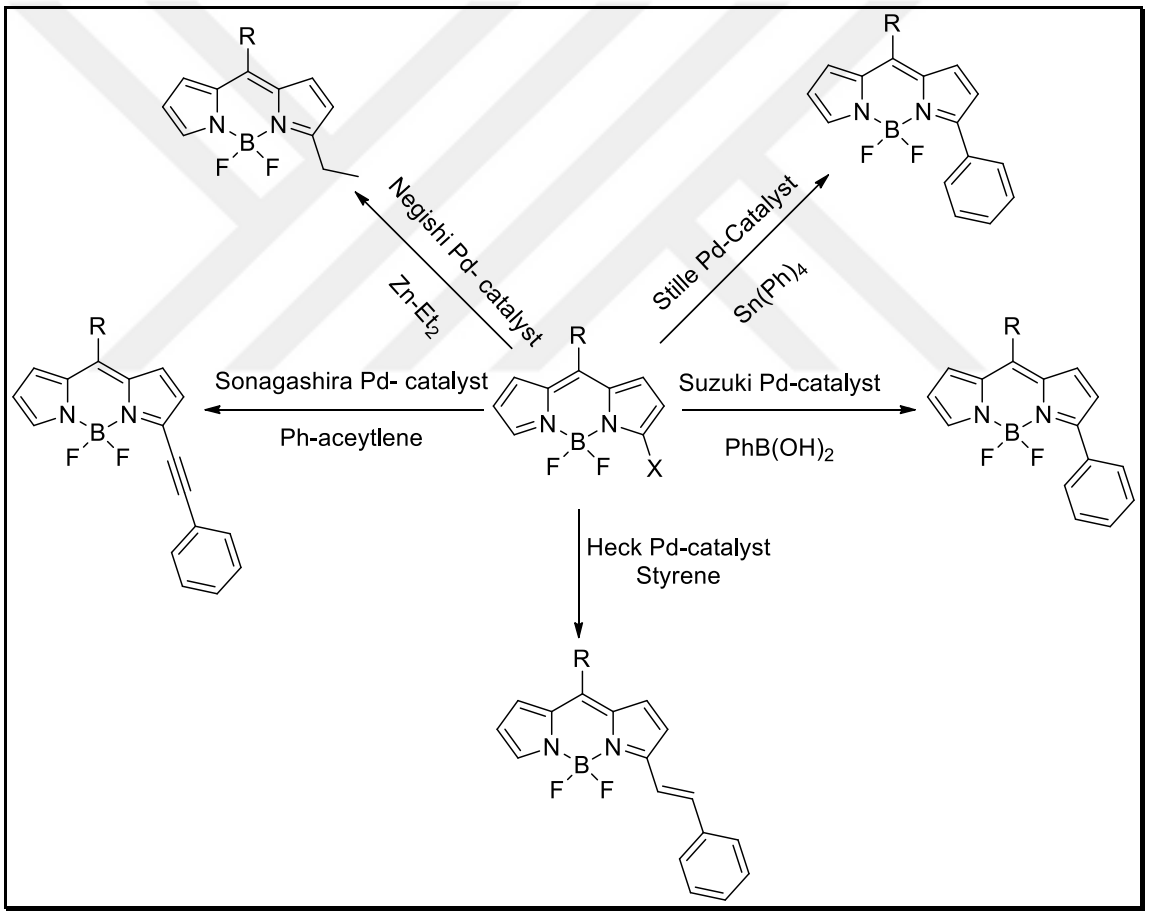

Figure 1.24. Pd catalyzed derivatization of BODIPYs from 3- and 3,5- positions
(Source: Lakshmi et al., 2015)

To get a monohalogenated product, the obtained dihalogenated BODIPY structure is further reacted with one equivalent of sodium methoxide in methanol at room temperature. These synthesized mono- and di-halogenated BODIPY compounds are versatile candidates for further modifications to construct new molecular sensors. Halo-BODIPYs are highly reactive towards many well-known reactions such as nucleophilic aromatic substitution (S_NAr) (e.g., R-SH, R-NH_2, R-$C:^-$, or R-OH) and transition metal catalyzed C–C bond formation reactions (e.g., Suzuki coupling, Sonagashira coupling).

Halogenation methodology also makes it possible to construct BODIPYs which are unfeasible when using premodification methods. Some examples of molecular fluorescent sensors that were synthesized via the halogenation of 3- and 3,5- positions of the BODIPY core are given below.

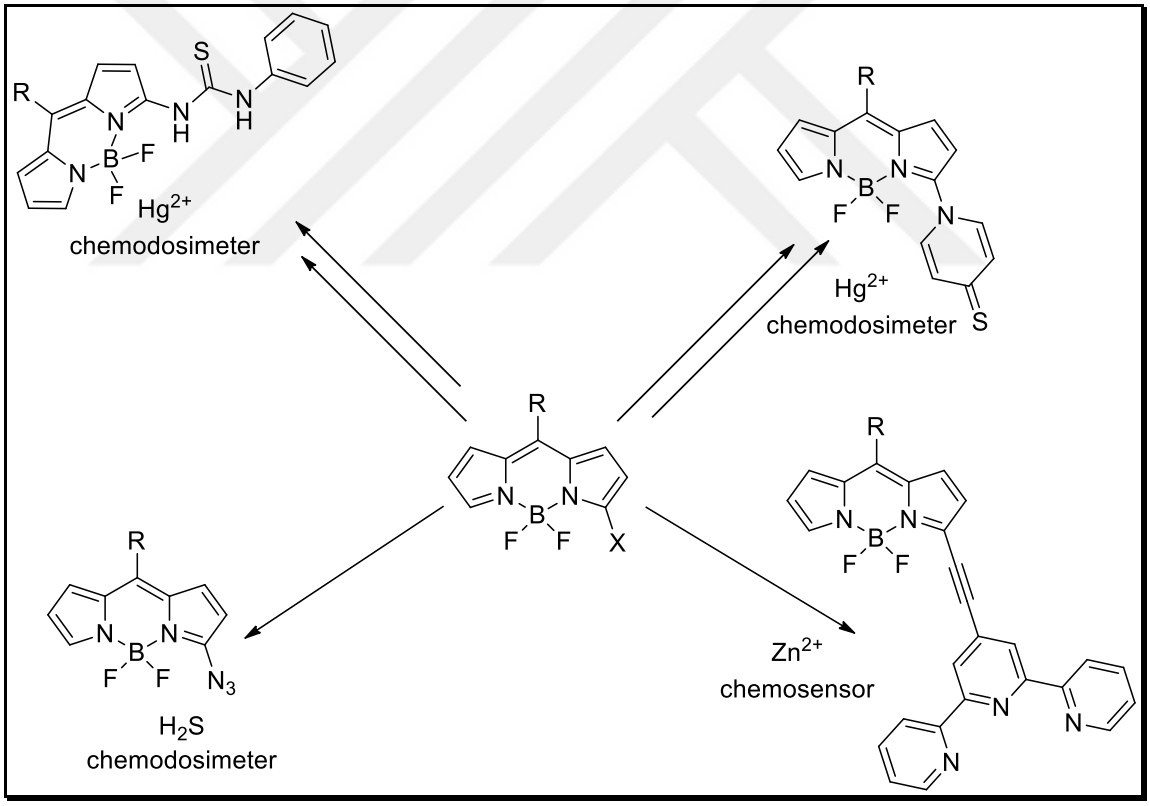

Figure 1.25. BODIPY based sensors functionalized from 3- position
(Source: Lakshmi et al., 2015)

Another way to functionalize BODIPY compounds from the 3- and 3,5-positions is to use the well-known Knoevenagel condensation reaction. This reaction was first introduced by Knoevenagel in 1894 as the condensation reaction of an aldehyde with another aldeyhde or ketone that bears active methylene groups in the presence of amine derivative as a catalyst. To gain insight into the working principle of this type of reaction, the mechanism of the reaction between malonate ester and benzaldehyde in the presence of the piperidine catalyst is given in Figure 1.26. The reaction is first initiated by the deprotonation of active hydrogen of the methylene group with piperidine. The formed carbanion attacks the partially positive site of carbonyl followed by a proton transfer that produces a typical aldol addition product. This step regenerates the active catalyst, which undergoes the further deprotonation reaction with the addition product because of the high acidity of the hydrogen of the addition product. The final steps of the reaction yields the condensation product (Knoevenagel, 1898).

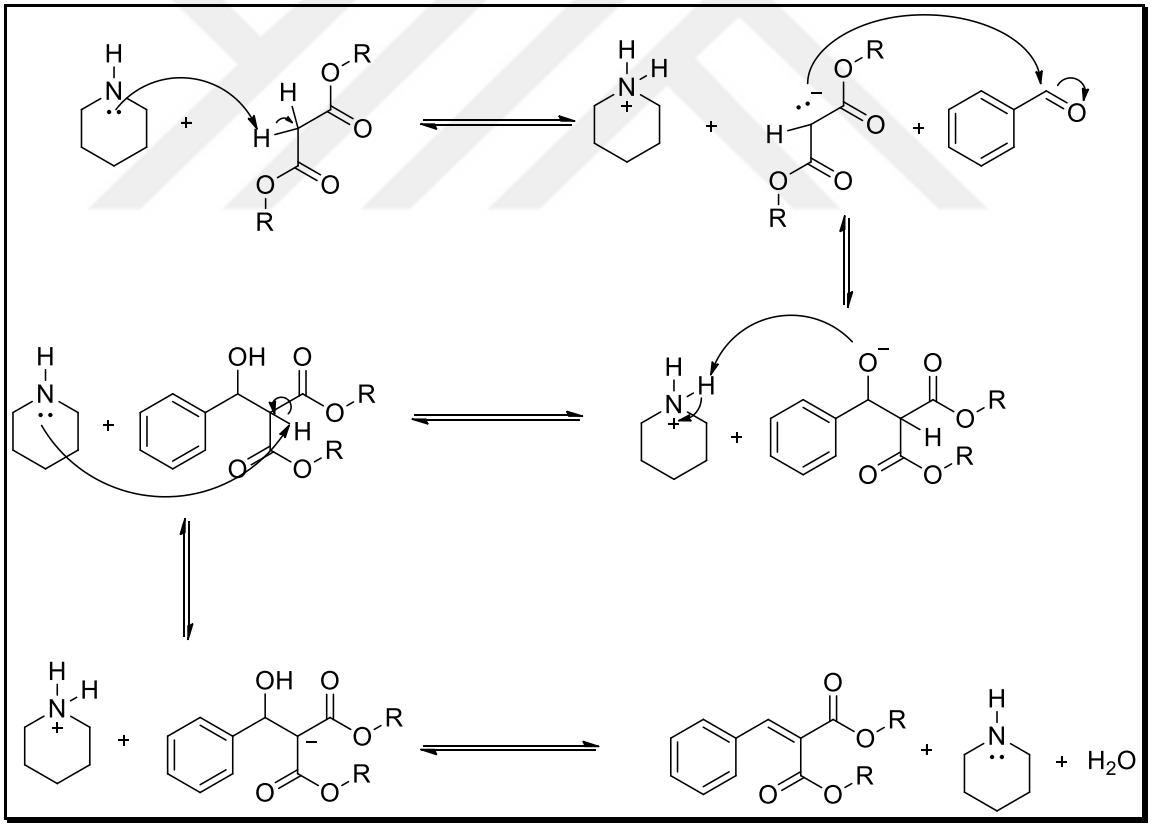

Figure 1.26. Reaction mechanism of Knoevenagel Condensation
(Source: Knoevenagel, 1898)

The same reaction mechanism is feasible for BODIPY structure. The first attempt to apply Knoevenagel reaction to the BODIPY structure was presented by Haugland and Kang in 1988. They described the reaction of 1,3,5,7-tetramethyl-substituted BODIPY with 4-(dimethylamino)benzaldehyde in the presence of piperidine catalyst in an alcoholic solvent at reflux temperature, and they successfully produced the 3-monostyryl derivative as a major product (Haugland and Kang, 1988).

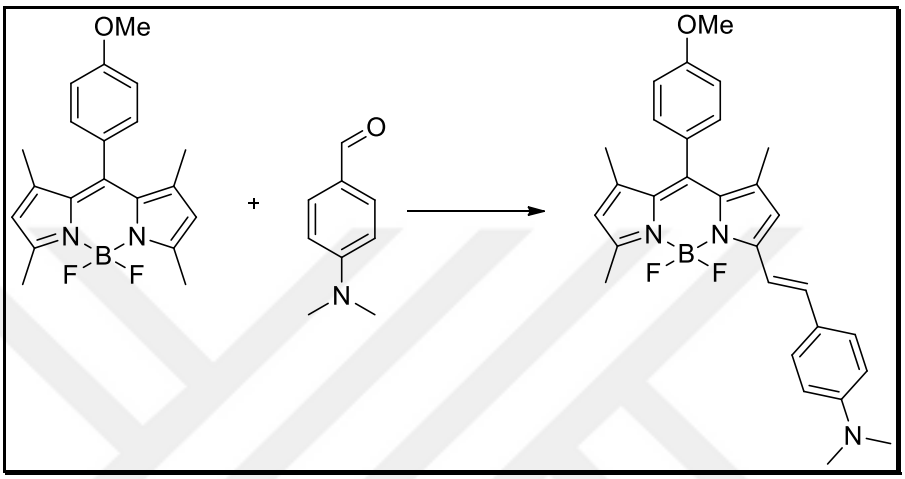

Figure 1.27. 3-monostyryl derivative of BODIPY
(Source: Haugland and Kang, 1988)

The methyl groups at 3- and 3,5- positions of the BODIPY are highly acidic in character because of the electron withdrawing nature of the core structure. The near IR emitting derivative of BODIPY can be synthesized by the condensation of 3-methyl-BODIPY structure with an aldehyde in the presence of a amine catalyst. In addition, a Knoevenagel-type reaction offers the addition of mono-, di-, tri- and tetrastyrene groups to the core structure, which results in a large red shift in spectrum (Figure 1.28) (Ni and Wu, 2014).

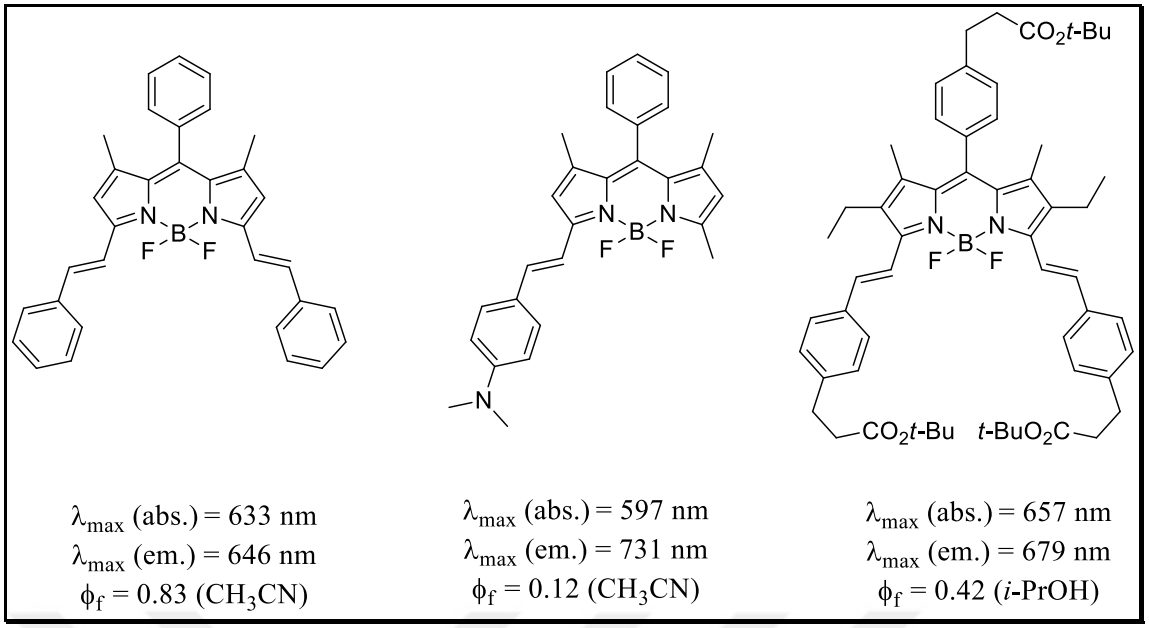

Figure 1.28. BODIPY structures synthesized via Knoevenagel condensation.
(Source: Ni and Wu, 2014)

♦ ***Functionalization of the BODIPY core from the 1,7- positions:***

The functionalization of the BODIPY core from the 1,7- positions is only possible with pre-modifications of the starting pyrrole. The halogenation strategy is also feasible if other reactive sites of the compound are blocked. As shown in Figure 1.29, the halogenated pyrrole carbaldehyde is converted to BODIPY structure by using the Burgess method.

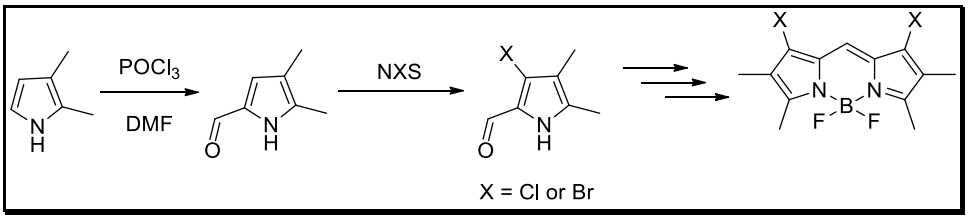

Figure 1.29. Synthesis route of 1,7-bis-halogenated BODIPYs.
(Source: Boens et al., 2015)

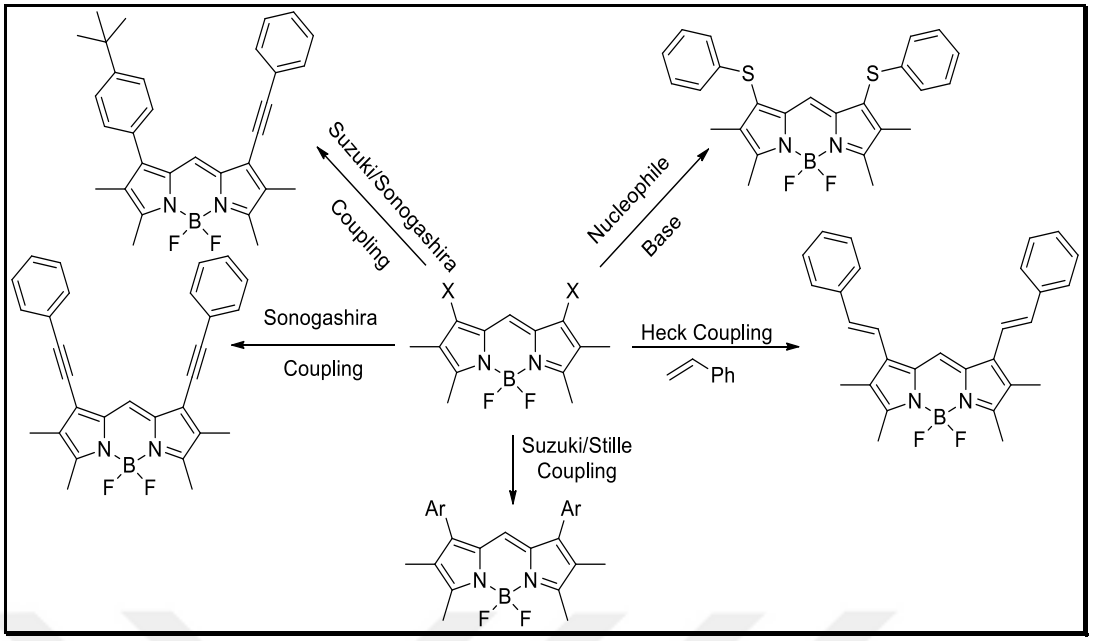

Figure 1.30. Reactions of BODIPY core halogenated from 1,7- positions
(Source: Lakshmi et al., 2015)

The halogenated BODIPYs are very important precursors to post-modifications because of their high reactivity towards palladium-catalyzed reactions such as Stille, Suzuki, Heck, and Sonogashira couplings. However, 1,7-bis-halogenated compounds have a lower tendency toward nucleophilic substitution reactions than 3,5-bis-halogenated ones. These compounds undergo nucleophilic substitution reactions only with thiolate anions that have strong nucleophilic character.

♦ ***Functionalization of the BODIPY core from the 2,6- positions:***

The 2,6- positions are the electron-rich parts of the BODIPY core with respect to resonance theory, which makes them highly available for electrophilic addition reactions. There are several ways to functionalize this part of the compound such as halogenation, formylation, sulfonation, and nitration. Among these approaches, halogenation is the most important one. It can generate mono- and di-halogenated products with regard to reaction conditions. There are different methods to obtain halogenated product. One of them is using *N*-halosuccinimide reagent in an inert solvent at low reaction temperatures. For example, while the reaction of 1,3,5,7-tetramethyl-8-phenyl-4,4'-difluoro-bora-3a,4a-diaza-s-indacene and 1 equivalent of *N*-

iodossuccinamide produces mono-iodinated BODIPY, the addition of 4 equivalents of *N*-iodossuccinamide yields di-iodinated BODIPY as a single product. Another important protocol for iodination of the BODIPY compound is the treatment of the core structure with iodine and iodic acid in proper reaction conditions (Figure 1.31) (Çakmak and Akkaya, 2009; Yogo et al., 2005).

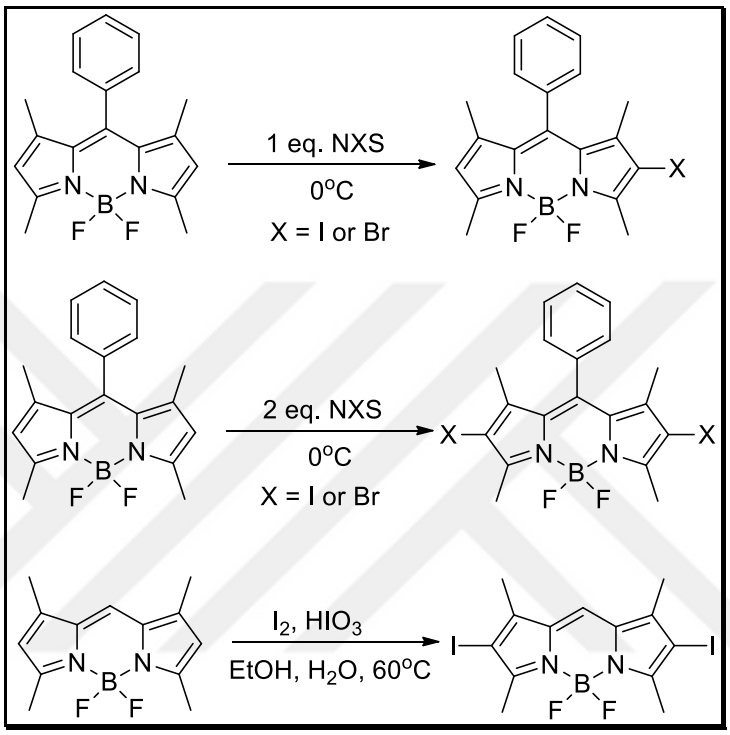

Figure 1.31. Halogenation of BODIPY compound from 2,6- position.
(Source: Çakmak and Akkaya, 2009; Yogo et al., 2005)

The halogenated BODIPYs are versatile precursors to the post-modifications to construct molecular sensors. They are highly reactive towards transition metal catalyzed C–C bond formation reactions (Stille, Suzuki, Heck, and Sonogashira couplings). Because of the increasing conjugation, red-shifted dye structures can easily be achieved with the aid of these types of reactions (Lakshmi et al., 2015).

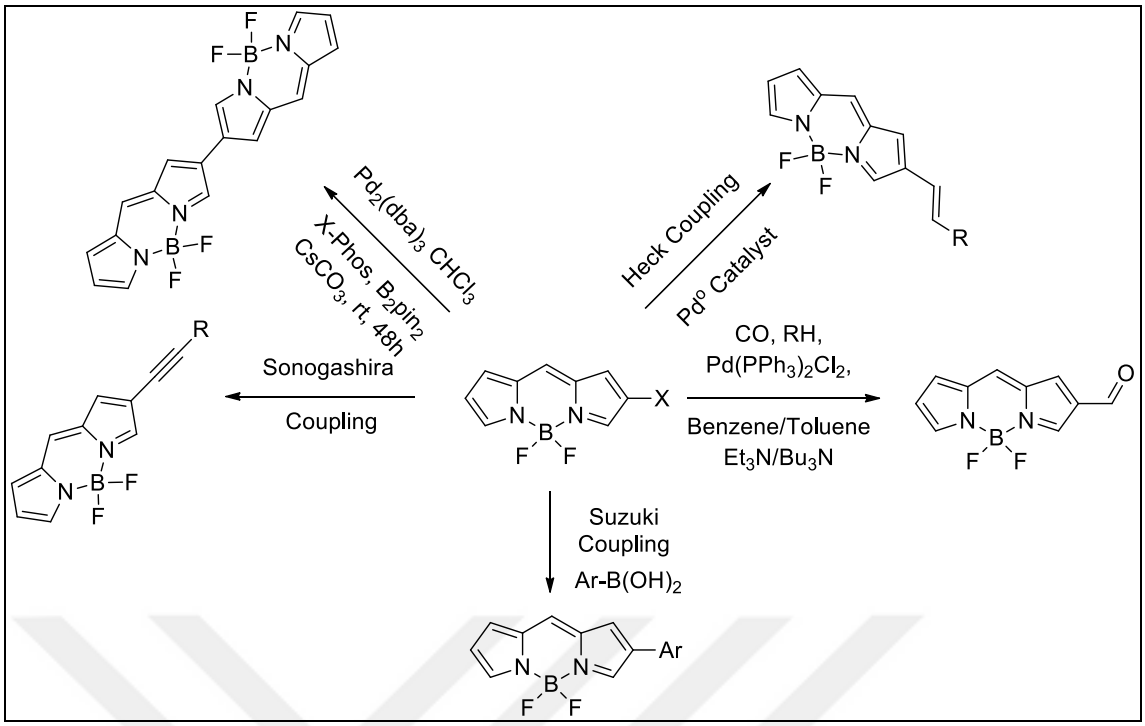

Figure 1.32. Reactions of BODIPY core halogenated from 2,6- positions
(Source: Lakshmi et al., 2015)

One of the most important feature of BODIPY dyes is their reactivity towards formylation reactions. To get mono- or di-formylated BODIPYs, the well-known Vismeier Haack's reaction is applied. To gain insight into the formation of formylated compounds, the mechanism of BODIPY reaction is summarized in Figure 1.33. The reaction is first started with the reaction of DMF (dimethylformamide) and phosphorus oxychloride to get the Vilsmeier reagent. The electrophilic aromatic substitution reaction proceeds via the attack of the electron rich aryl to the iminium ion with a concomitant loss of aromaticity. In the following step, the aromaticity is regenerated with deprotonation, and the second iminium ion is obtained. The iminium structure is hydrolized via the addition of water, which produces the formylated compound as a major product.

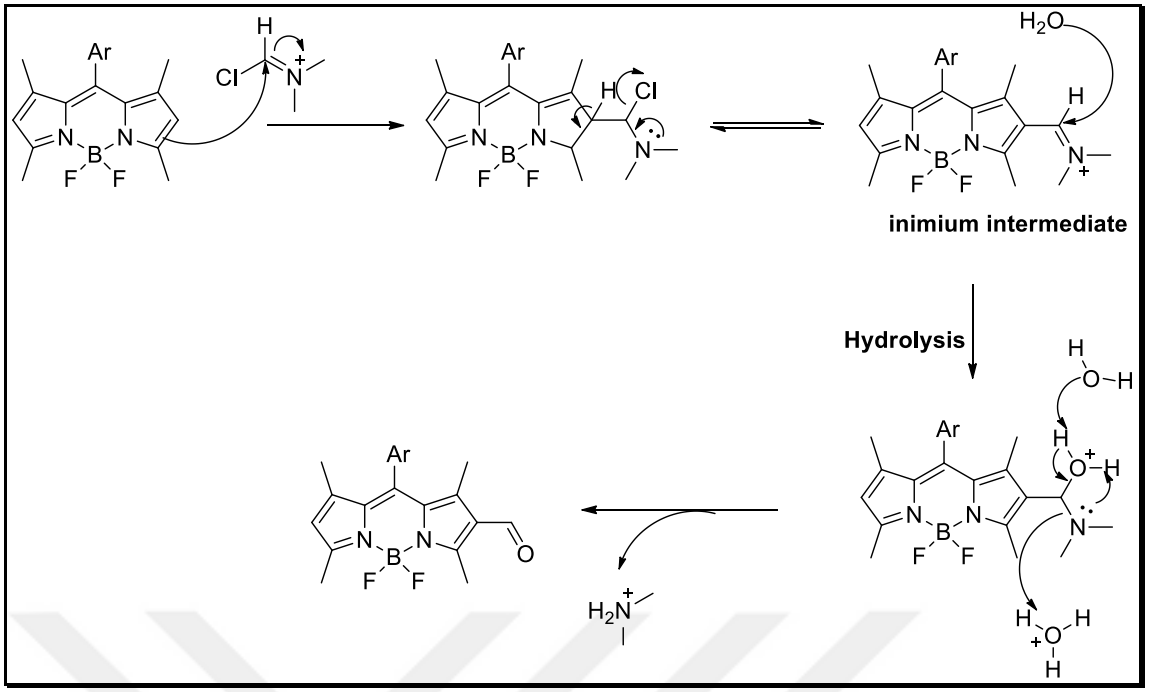

Figure 1.33. Reaction mechanism of Vilsmeier Haack's Formylation
(Source: Jiao et al., 2009)

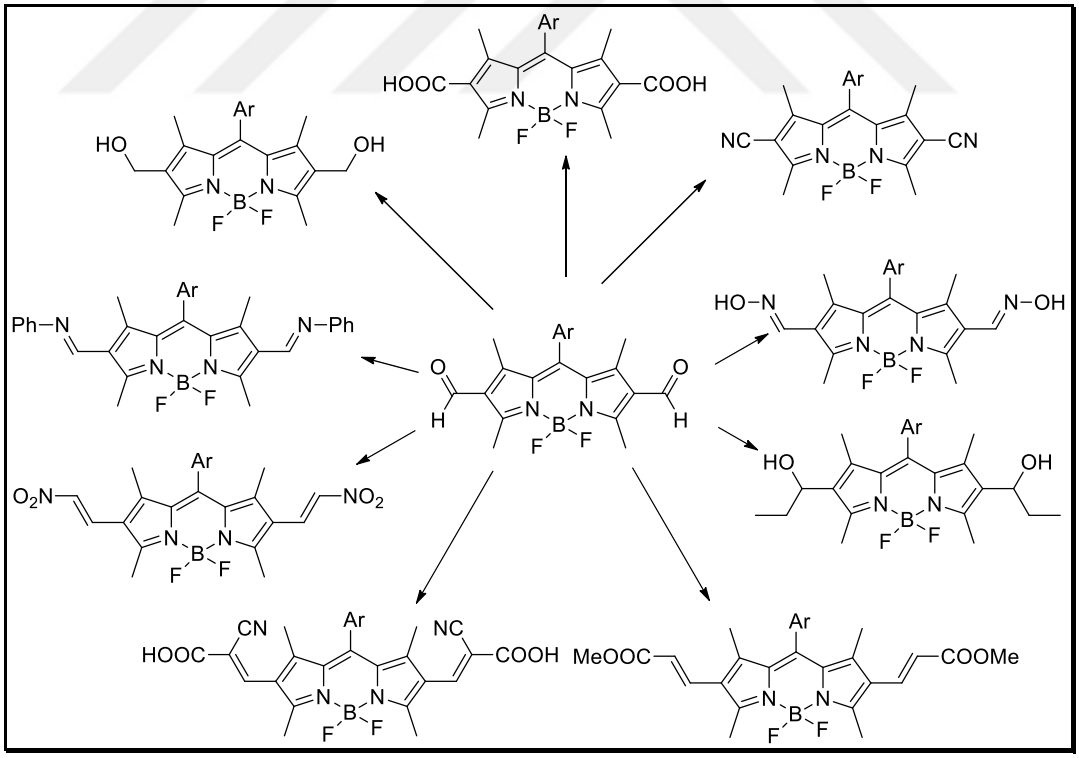

Figure 1.34. Derivatization possibilities of 2,6- formylated BODPYs
(Source: Zu et al., 2013)

The formylated BODIPYs are valuable tools for designing the new skeleton to construct fluorescent molecular sensors. Formyl groups are susceptible towards various types of reaction (e.g., redox, elimination, addition, and rearrangement) under mild conditions. As shown in Figure 1.34, formylated BODIPYs offer numerous post-modification opportunities to design and synthesize new molecules.

Halogenation and formylation reactions are frequently used in BODIPY chemistry. The functionalization of the 2,6- positions by sulfonation and nitration reactions are also important types of reactions. However, these types of functionalizations do not offer many advantages to post-modifications. The only advantage of sulfonation is high water solubility of its product (Wories et al., 1985; Esnal et al., 2013).

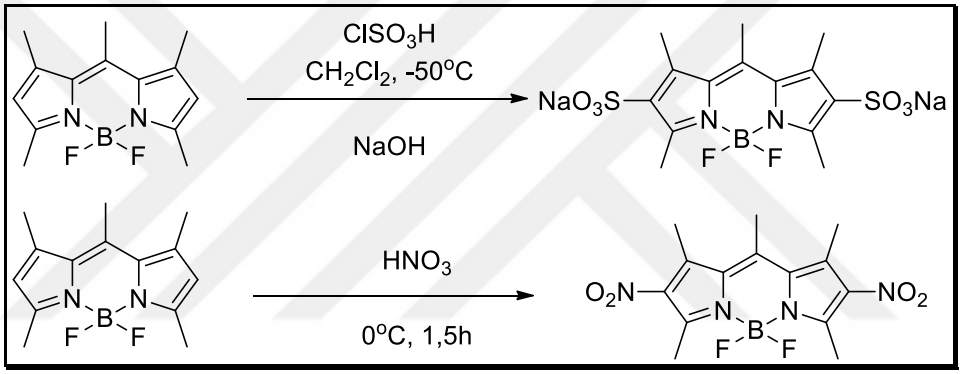

Figure 1.35. Sulfonation and nitration reactions of BODIPY from 2,6- positions (Source: Wories et al., 1985; Esnal et al., 2013)

♦ ***Functionalization of the BODIPY core from the Boron atom:***

The functionalization of BOIPY dyes from the boron center by replacing the fluorine atom with aryl, alkl, and alkynyl groups or alkoxylates and carboxyltes is possible by using strong nucleophiles of these compounds. The nucleophilic subtitution reaction of BODIPY core with strong nucleophiles such as Grignard reagent, alkynyl lithium, or alkoxide reagents produce B-C bonded BODIPY structure with improved features (e.g., quantum yield), except for absorption/emission wavelength. Because boron has tetrahedral geometry in core structure the attached groups are in out of the conjugation pattern. In Figure 1.36, some of the examples of post-modification reactions of BODIPYs from boron center are represented (Ulrich et al., 2008).

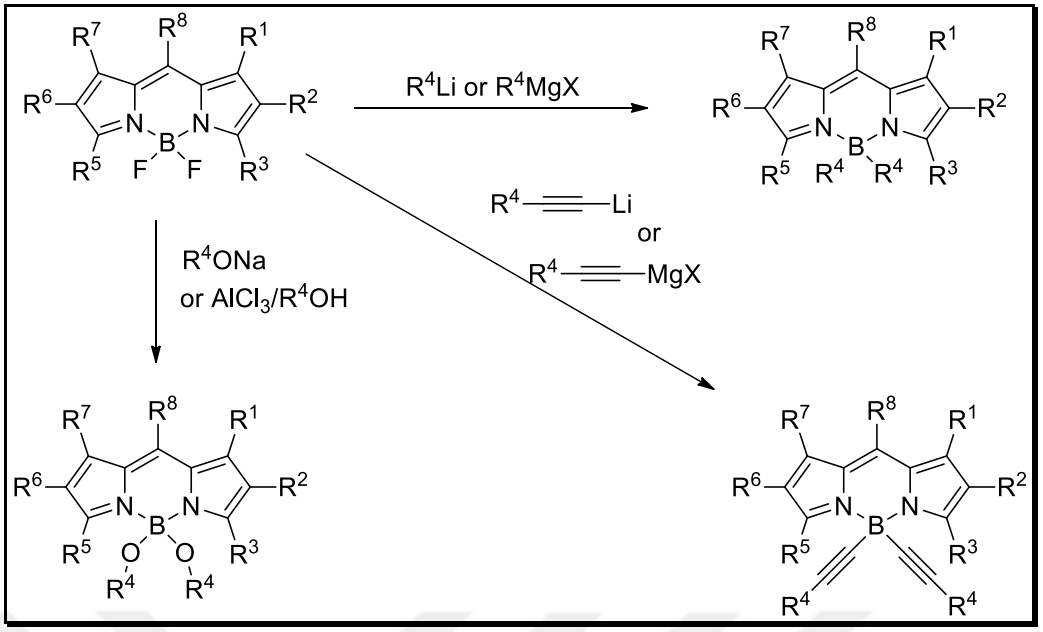

Figure 1.36. Reactions of BODIPY core from boron center
(Source: Ulrich et al., 2008)

1.3. Sensing Strategies

A fluorescent molecular sensor is a versatile tool for analyzing trace amounts of analytes such as metal ions, anions, and biological species by using the advantages of photo-physical changes of fluorophore. A classical sensor molecule is comprised of two or three units, including fluorophore, spacer, and recognition parts (Figure 1.37) (Das et al., 2013).

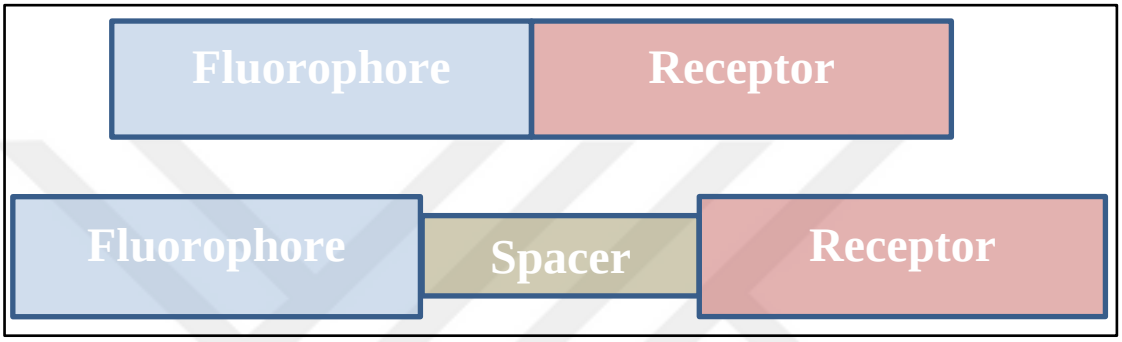

Figure1.37. Structural design of a fluorescent sensor.
(Source: Das et al., 2013)

The design strategy mainly depends upon the structural availibility of the fluorophore and receptor units. In addition, there have been different photo-physical mechanisms that have to be considered during the skeletonazation of fluorescent molecular sensors. The response of a fluorogenic/chromogenic sensor is measured as the changes in absorbance, fluorescence, or fluorescence lifetimes. The changes in these properties occur when the analyte affects the present photophysical mechanism. Examples are ICT (intramolecular charge transfer), PET (photo-induced electron transfer), CHEF (chelation enhanced fluorescence), FRET (fluorescence resonance energy transfer), TICT (twisted intramolecular/intermediate charge transfer), and PICT (planar intramolecular charge transfer). (Das et al., 2013; Wu et al., 2015).

There are different strategies to construct a fluorescent molecular sensor. The reactivity of the receptor unit is of key importance for the analysis of the targeted analyte. In the first approach, the chosen receptor unit undergoes an irreversible reaction with the targeted analyte in which the molecular and electronic structure of the sensor

changes and produces a computable signal to understand the presence of investigated species.

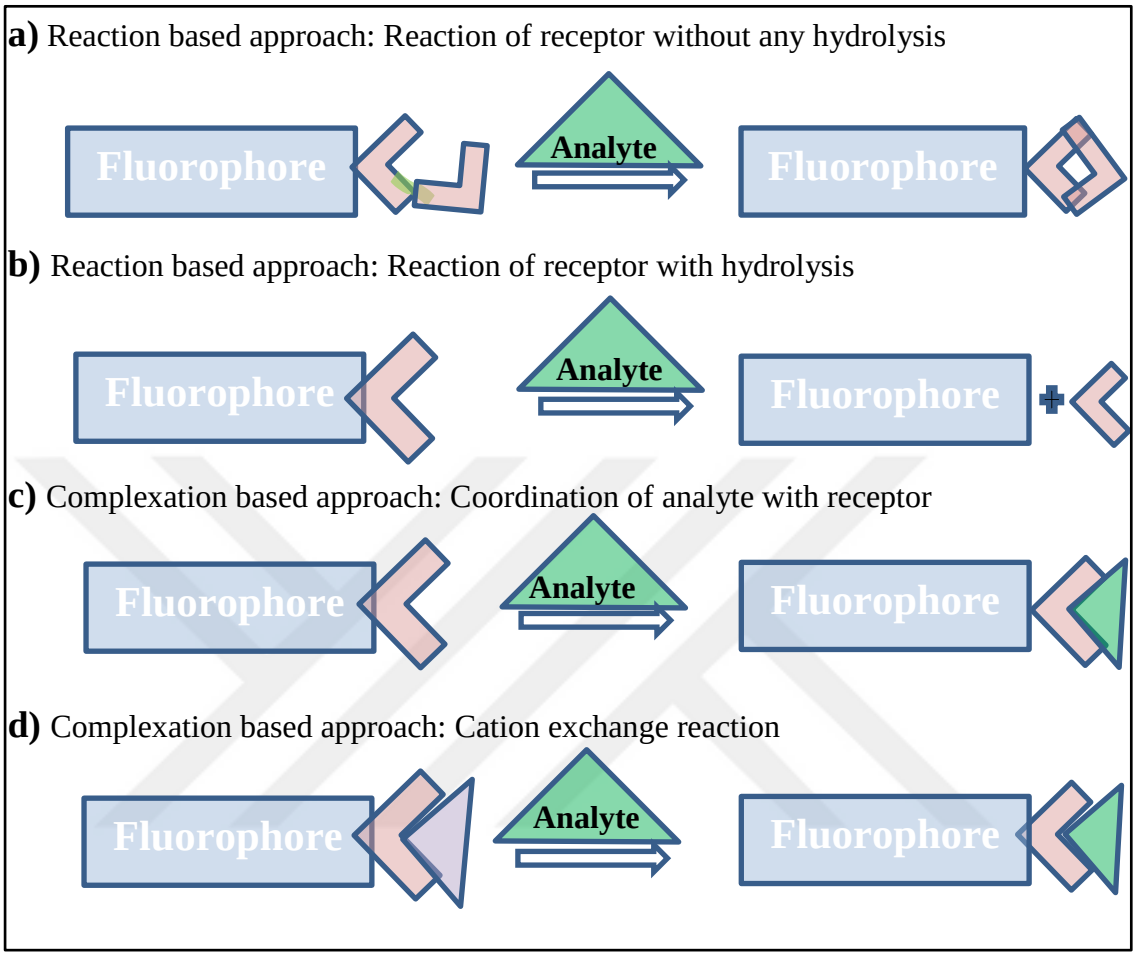

Figure 1.38. Sensing approaches to construct molecular sensors
(Source: Patil et al., 2012; Cheng et al., 2015)

Figure 1.38 indicates the most popular sensing approaches that offer many advantages to sense targeted analytes in synthetic samples and living milieu. For designing a sensor molecule, there are some important features of receptor and fluorophore units that have to be taken into consideration. These are:

- High selectivity and sensitivity of receptor to analyte
- Long absorption and emission wavelength of fluorophore unit that will not be influenced from any interference coming from the sensing environment
- Low detection limit
- High water solubility (especially for living cell studies)
- Robustness toward pH changes, light, and chemicals

The sensing approaches are summarized below.

- ***Reaction based approach: Reaction of receptor without any hydrolysis:***

In this sensing strategy, the molecular probe integrates with a reactive unit which undergoes an irreversible reaction in the presence of a targeted analyte without elimination of any group. Scientists have paid a great deal of attention to develope molecular sensors benefiting from this strategy (Zhou and Joon, 2012; Kowada et al., 2015).

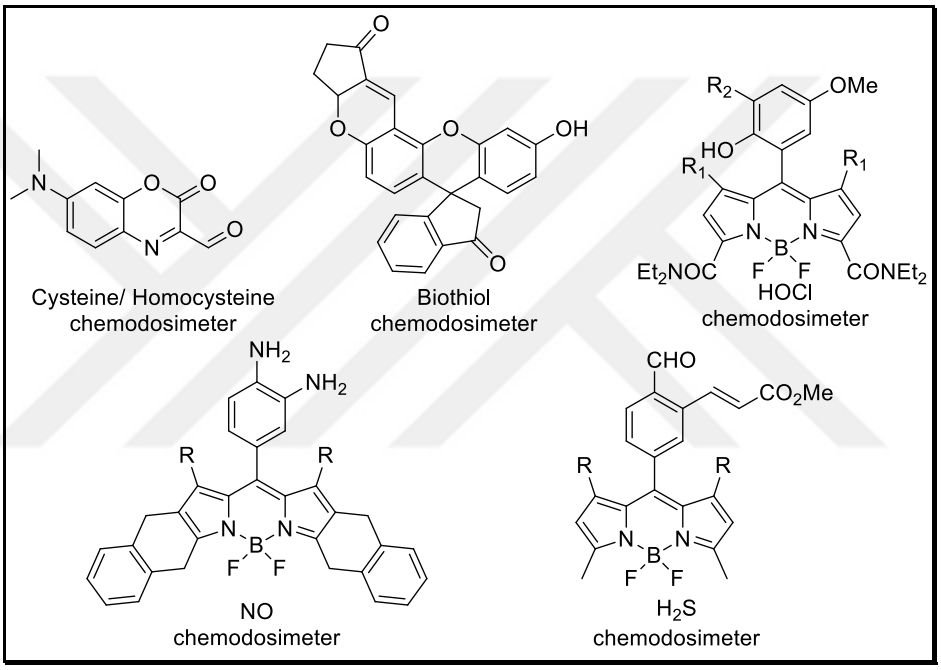

Figure 1.39. Fluorescent molecular sensors working via reaction based approach (Source: Zhou and Joon, 2012; Kowada et al., 2015)

♦ ***<u>Reaction-based approach: Reaction of receptor with hydrolysis</u>***

The second strategy differs from the first approach only in the outcome of the sensing event. In this approach, the receptor unit and analyte undergo an irreversible reaction via the production of a hydrolysis product. There have been several studies built on this hydrolysis mechanism. The frequently used fluorophore units contain hydroxyl or amine groups that functionalize with a receptor unit via the reaction of an alkyl derivative of receptor and fluorophore in the presence of a base (Figure 1.40) (Aron et al., 2015; Manjare et al., 2014; Karakuş et al., 2016).

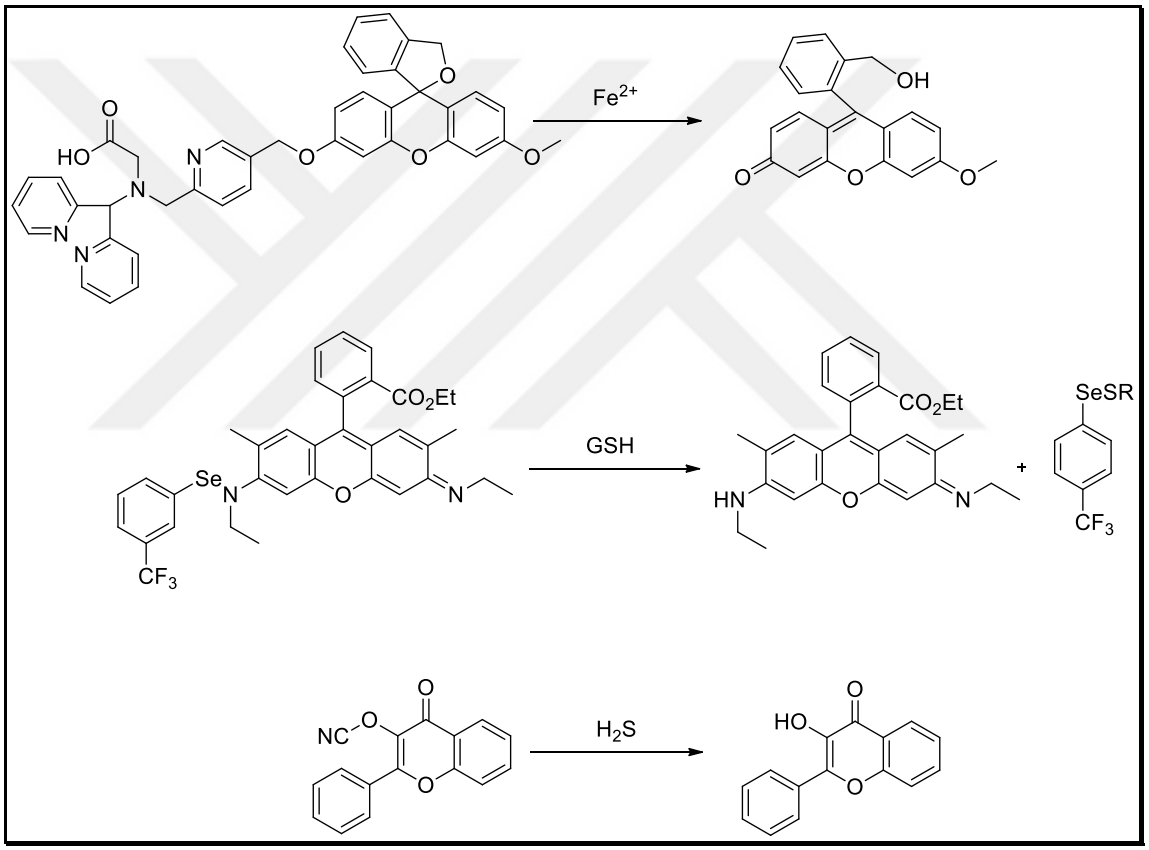

Figure 1.40. Fluorescent molecular sensors work via hydrolysis mechanism (Source: Aron et al., 2015; Manjare et al., 2014; Karakuş et al., 2016)

♦ ***Complexation-based approach: Coordination of analyte with receptor***

The complexation-based approach is constructed on the noncovalent interactions between receptor unit and targeted analyte, which can be reversed by using a specific reagent that has a higher affinity to the analyte than to the receptor unit. These supramolecular interactions consist of hydrophobic and hydrophilic interactions and electrostatic, van der Waals, π–π stacking, and hyrogen-bonding interactions. Besides these interactions, there are some important concepts that have to be considered, such as hard-soft acid/base theory and coordination chemistry. Because of the Lewis acidic character of many of the transition metal cations, the coordination ability of metal ions has to be kept in mind during the development of a metal ion selective chemosensor. Although there are various examples of complexation-based chemosensors, the cross-affinity of other metal ions with similar chemical characteristics limit the usability of this approach dramatically. Some examples of complexation-based fluorescent sensors are summarized in Figure 1.41 (Joung and Joon, 2012; Das et al., 2013; Wu et al., 2015).

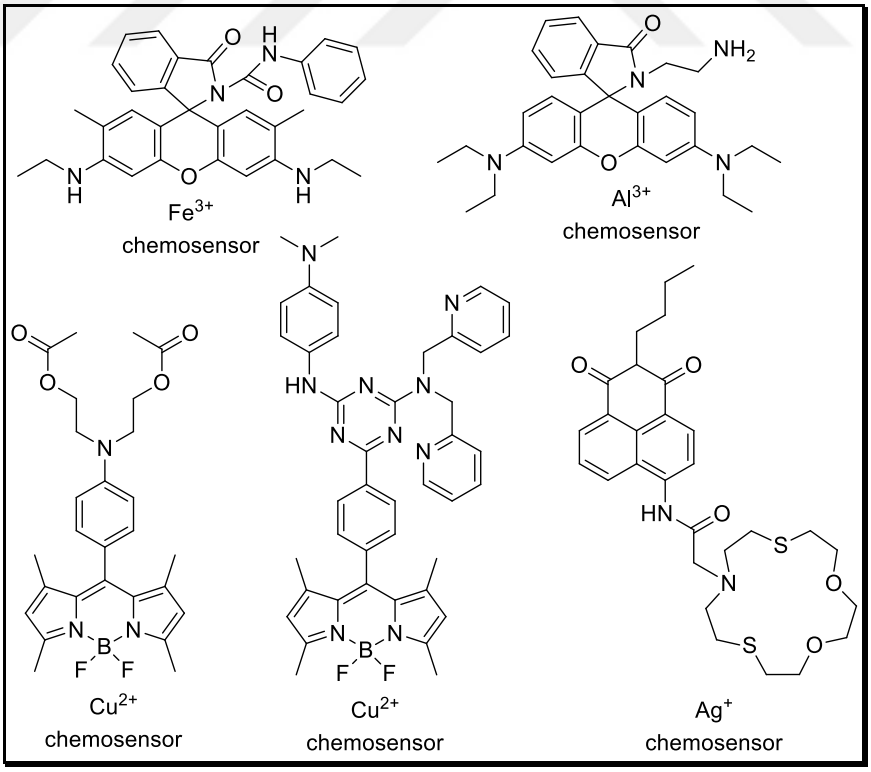

Figure 1.41. Examples of comlexation based fluorescent sensors
(Source: Joung and Joon, 2012; Das et al., 2013; Wu et al., 2015)

- ***Complexation based approach: Cation exchange reaction:***

This approach may be considered the subtopic of designing a coordination-based chemosensor and bears major improvements. The main drawback of a traditional type of chemosensor is the cross-affinity of competitive metal ions towards the receptor unit. To eliminate this problem, complexation-based chemosensors – working via cation exchange reactions – have become very popular in the field of fluorescence sensing. The shielding function of a metal ion improves the selectivity. The shielding effect can only be removed in the presence of a specific metal ion that forms a thermodynamically favoured complex structure. Another beneficial side of this approach is the possibility of constructing a turn-on fluorescent chemosensor. Metal ions (Cu^{2+}, Fe^{3+}) with a paramagnetic nature quench the fluorescence of a fluorophore molecule and make it non-emissive so that it can be used as a turn-on chemosensor for thermodynamically favoured metal cations. In addition, metal complexes of many other fluorophores have distinct fluorescence emissions that make them usaful to construct a turn-off or ratiometric fluorescent chemosensor (Cheng et al., 2015; Wu et al., 2015). Examples of fluorescent molecular chemosensors that working via cation exchange reaction are given in Figure 1.42.

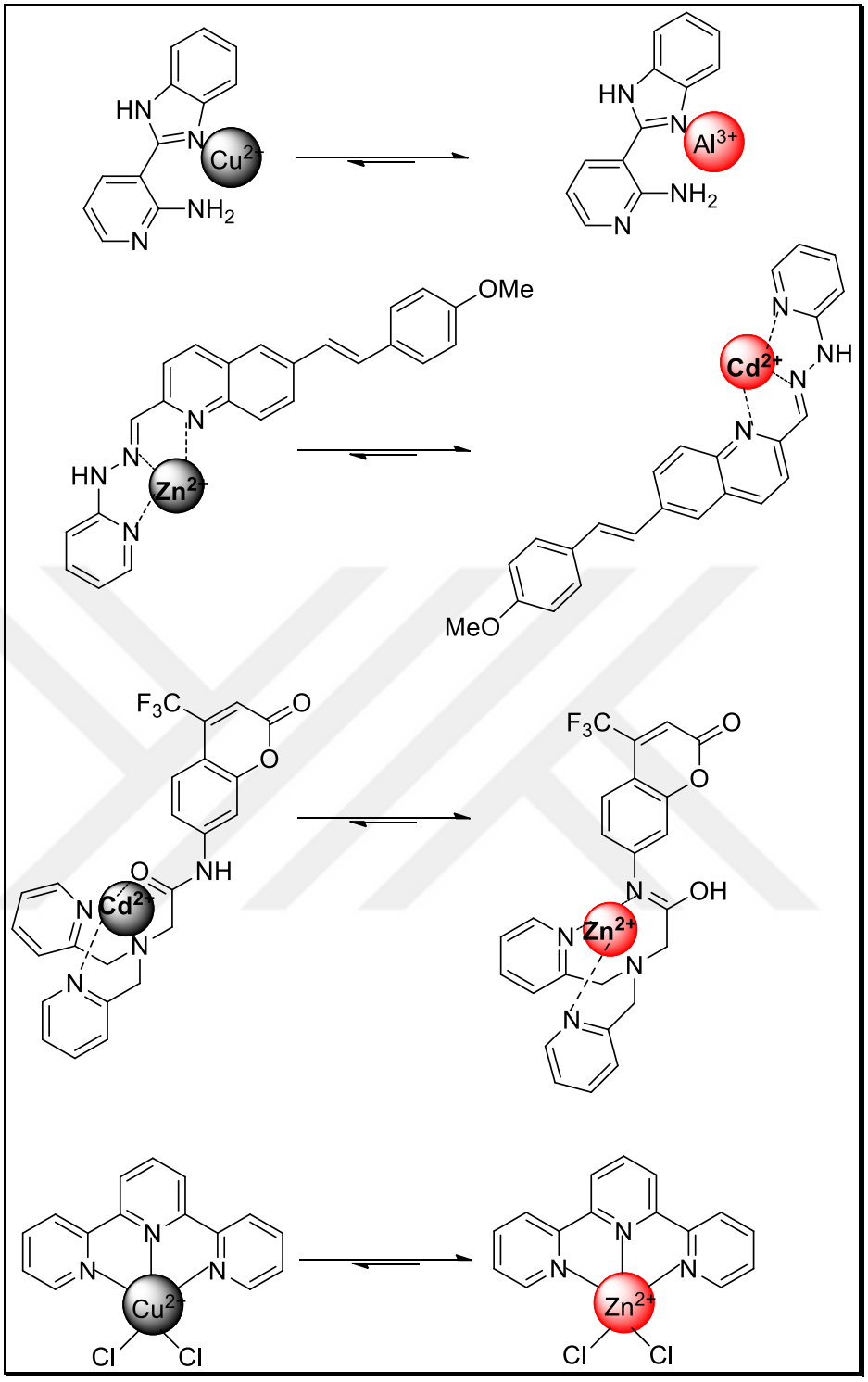

Figure 1.42. Examples of chemosensors working via cation exchange reaction (Source: Cheng et al., 2015)

1.4. Fluorescence Sensing Mechanisms

The photophysical sensing mechanism for the above mentioned sensing strategies are photo-induced electron transfer (PET), intramolecular charge transfer (ICT), fluorescence resonance energy transfer (FRET), through-bond energy transfer (TBET), chelation enhanced fluorescence (CHEF), planar intramolecular charge transfer (PICT), and twisted intramolecular/intermediate charge transfer (TICT). Brief descriptions of the most frequently used mechanisms (PET, ICT, and FRET) are summarized below.

1.4.1. Photo-induced electron transfer (PET)

In general, a fluorescent sensor that works via a photo-induced electron transfer mechanism is constructed from a fluorophore and receptor unit connected with a spacer.

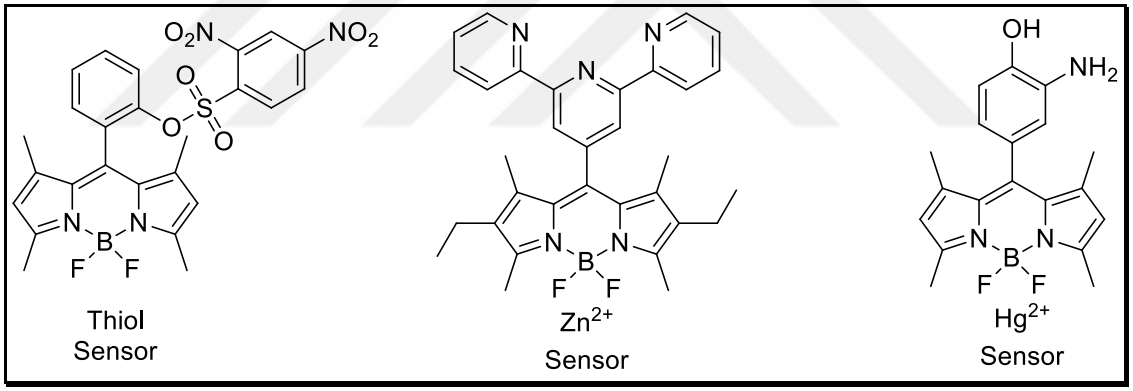

Figure 1.43. Examples of PET based sensors
(Source: Boens et al., 2012)

The PET sensors include a heteroatom -bearing a nonbonding electron pair- that quenches the fluorescence of the fluorophore unit by transferring it to the excited fluorophore. As shown in figure 1.45, the HOMO energy level of the receptor unit lies between the HOMO and LUMO energy levels of the fluorophore. When the fluorophore unit is excited, an electron from the HOMO level of the free receptor is transferred to the empty HOMO level of the fluorophore that prohibits the turn-back of the excited electron with a concomitant emission. Coordination of an analyte to the lone-pair electrons of the receptor unit increases its redox potential, which results in a decrease in

energy at the HOMO level. These newly formed HOMO and LUMO levels cause the turn back of the excited electrons to the ground state with a fluorescence emission. In this way, the PET process is canceled, and the analyte is recognized via a turn-on system (Das et al., 2013).

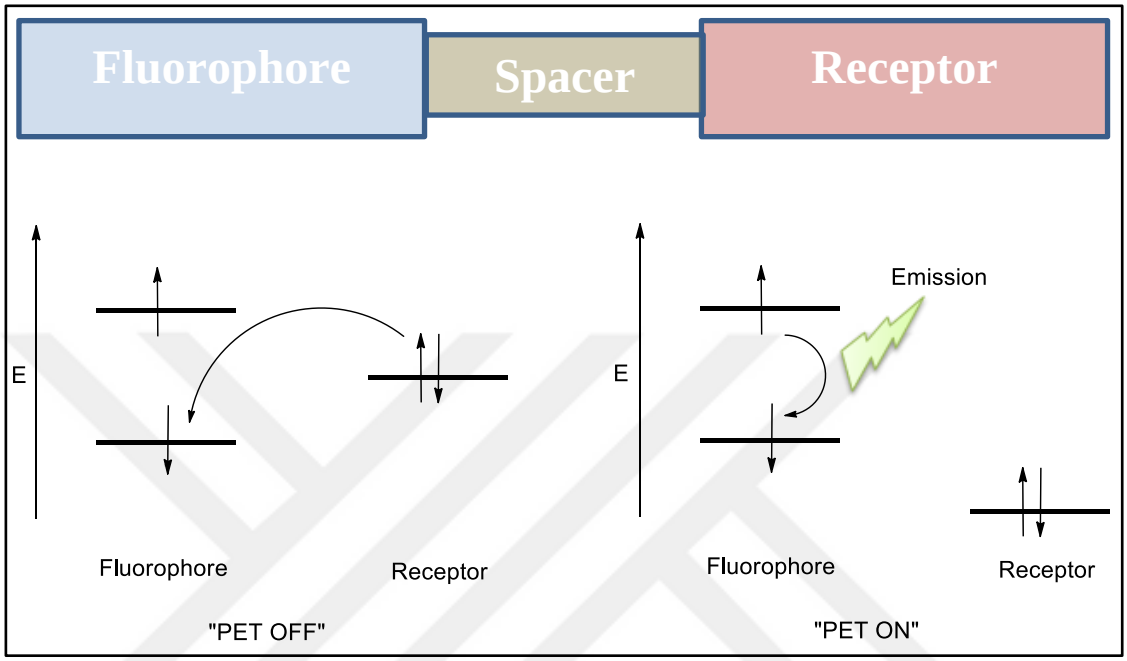

Figure 1.44. Photo-induced electron transfer mechanism
(Source: Das et al., 2013)

1.4.2. Intramolecular charge transfer (ICT)

ICT-based sensors involve a fluorophore and a receptor unit that are directly connected to each other without any spacer. The electronic structure is constructed based on a push-pull effect, which means that the sensor molecule includes an electron-rich terminal (donor) and an electron-poor terminal (acceptor). The changes in the electron flow between these two terminus result in a change in the position of the fluorescence emission (ratiometric response). For instance, the interaction of a cation with a donor part decreases its electron-donating character, which results in a blue shift in the elecromagnetic spectrum. On the other hand, the interaction of a cation with an acceptor unit increases the strength of the push-pull effect, which produces a red shift in the absorption spectrum. The interactions of donor/acceptor units with a cation also

affect the fluorescence quantum yield and the lifetime of the sensor (Das et al., 2013; Lee et al., 2015).

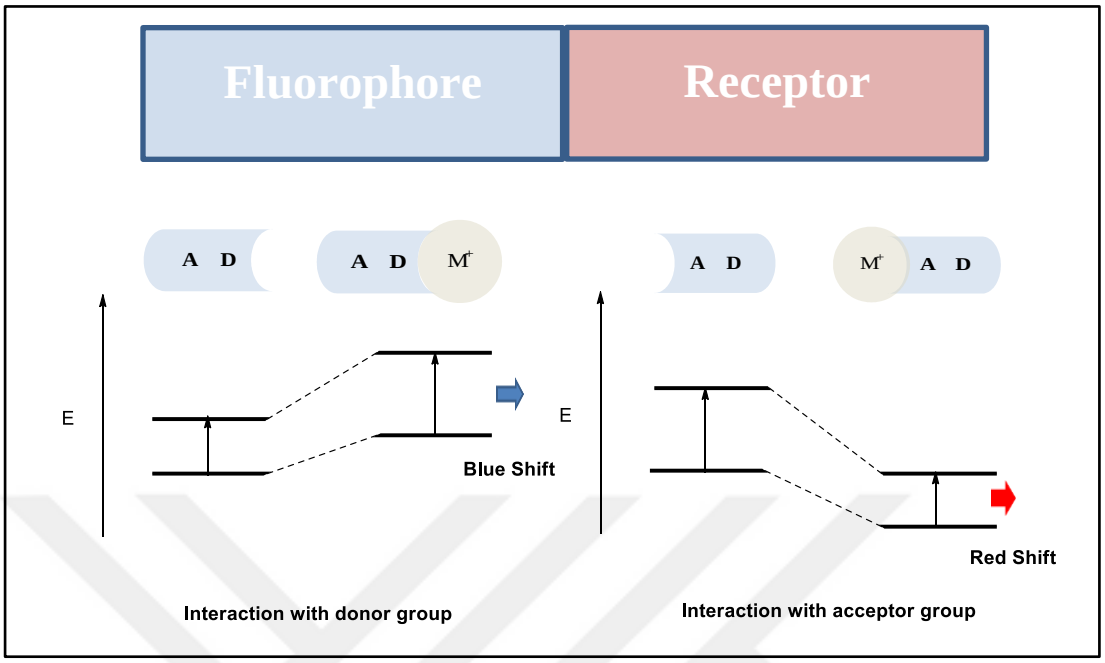

Figure 1.45. Intramolecular charge transfer mechanism
(Source: Das et al., 2013; Lee et al., 2015)

There are many examples of chemosensors that benefit from the changes of the donor and acceptor properties in the presence of an analyte (Figure 1.46).

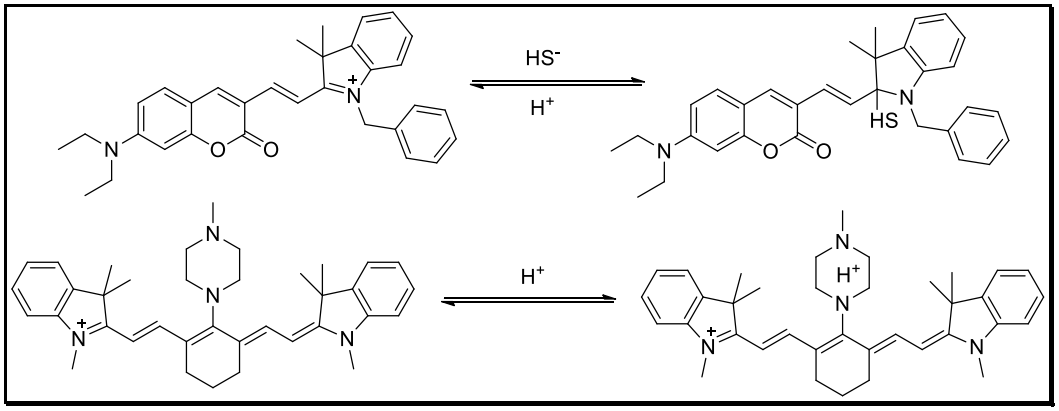

Figure 1.46. Examples of ICT based sensors
(Source: Lee et al., 2015)

1.4.3. Fluorescence Resonance Energy Transfer (FRET) and Through Bond Energy Transfer (TBET)

In a FRET or TBET system, two or more fluorophores are connected to the each other via a spacer. The only difference between these two models is the type of spacer structure. While a FRET system includes a nonconjugated spacer, a TBET has an electronically conjugated spacer. In a typical FRET system, the fluorophore having shorter fluorescence emission wavelength donates its energy to the other fluorophore that has an absorption spectrum matching the emission of the former fluorophore. The efficiency of a FRET system strongly depends on the degree of spectral overlap of the fluorescence emission spectrum of the donor and acceptor absorption spectrum. In addition to the spectral overlap, the distance between two fluorophore units is also critically important for an efficient FRET system. The optimal distance between donor and acceptor units lies within a 1 and 10 nm range. This property makes it a spectroscopic ruler to measure the distances in DNA, proteins, and function analyses (Das et al., 2013; Lee et al., 2015).

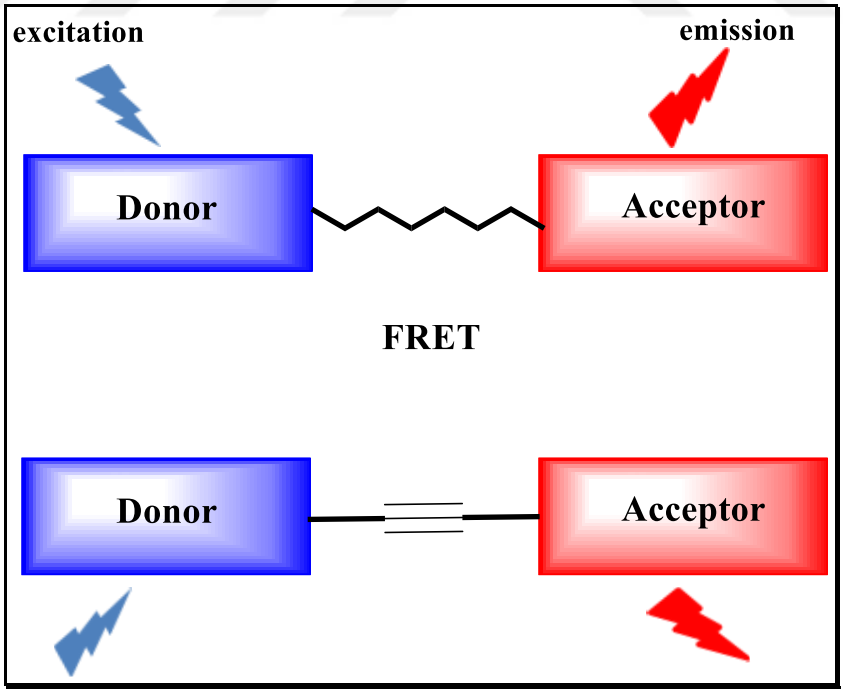

Figure 1.47. Schematic representation of FRET and TBET systems
(Source: Das et al., 2013; Lee et al., 2015)

In a trough-bond energy transfer system, two fluorophores are connected to each other via an electronically conjugated spacer. The conjugation prevents the planarization of the two fluorophores and provides energy transfer from donor to acceptor without any spectral overlap (Das et al., 2013; Lee et al., 2015).

CHAPTER 2

FLUORESCENT MOLECULAR SENSORS FOR GOLD ION DETECTION

2.1. An Overwiev

Gold was discovered as shining yellow nuggets and is undoubtedly the first metal known to early civilizations. Gold have been used in many area in people's lives such as coins, goods and jewelry for ages. Besides its utility in daily life, the chemistry of gold has also attracted a special attention in chemistry, medicine, and biology recently. During the last 50 years, the catalytic properties of gold have attracted a surge of attention in the field of synthetic chemistry (Alcaide and Almendros, 2014; Braun et al., 2013; Krause and Winter, 2011). In addition to their ability to catalyse chemical transformations in organic synthesis, gold species have significant impacts on human health. Due to high biocompatibility, functionalized gold nanoparticles have been extensively employed as drug and gene delivery systems, biosensors, and bio-imaging materials. For a long time, certain drugs based on various gold ion complexes have been used in the treatment of diseases including rheumatic arthritis, cancer, asthma, and HIV (Shaw III, 1999; Ott, 2009; Navarro, 2009). In contrast to gold's elemental form, its ionic forms (i.e., Au^{+} and Au^{3+}) are sensitive, extremely reactive. Although they have beneficial roles in disease treatment, the intake of gold ions can also dramatically cause toxicity to the living organisms because of the possibility to interact with biomolecules such as enzymes and DNA. Numerous scientific studies have established the detrimental effects of gold species on vital human organs. For instance, the intake of $AuCl_3$ causes damage to kidneys, liver, and the peripheral nervous system (Goodman et al., 2004; Habib and Tabata, 2004).

Considering the deleterious effects of gold species on living organisms and their increasing role as catalysts in the chemical industry, it is crucial for researchers to be able to assess the levels of gold species in certain chemical, environmental, and biological samples.

Nowadays trace metal analysis relying on fluorescence techniques are very popular and become an important alternative to classical methods (Li et al., 2014; Chen et al., 2014; Su and Aprahamian, 2014). In contrast to the traditional instrumental techniques, fluorescence based techniques have many preferable advantages such as low cost, simplicity, high sensitivity and reproducibility. Several gold ion selective molecular sensors utilizing various fluorophore units -including rhodamine, BODIPY, fluorescein, naphthalimide, and coumarin dyes- have been developed over the last years (Singha et al., 2015; Zhang et al., 2011).

The great majority of those sensors present in the literature are based on irreversible chemical events, which take advantage of the alkynophilic behaviour of gold species. In general, the fluorophore core being integrated with a gold ion specific reactive unit (i.e. alkyne), transforms the action of gold ions into a fluorescent signal output either through a change in fluorescence wavelength or a change in fluorescence intensity. Notably, the major drawback in reaction- based gold ion sensing is the interference of the fluorescent signal with other alkynophilic metal species such as Pd^{2+}, Ag^{+} and Hg^{2+}. To avoid this handicap, new sensing strategies utilizing alternative recognition motifs are urgently sought.

In this thesis development of new BODIPY derivatives bearing novel receptor units that overcomes the main drawbacks of present literature studies was aimed. To this end, a novel receptor unit relying on hydrolysis of **C=N** bond in the presensce of gold ions is achieved to literature. In addition, another molecular sensor was designed to detect gold ions by taking advantage of the alkynophilic behaviour of gold species. Another important drawback in the area of gold ion sensing is the rare presence of reversible chemosensor. In the field of this area, we developed a novel turn-on type fluorescent chemosensor that allows both Au^{3+} and H_3O^{+} ions to be detected on the basis of reversible ion- dipole interactions.

2.2. Literature Study

Gold has a chemically silent nature and due to its quenching property of fluorophore units (heavy atom effect), its fluorometric detection had not become possible until 2009. The study of Yang and co-workers is the first example of molecular fluorescent sensor enables to detect gold ions in solution and living cells (Yang et al., 2009). The strategy was constructed on the alkynophilicity of gold ions. An alkyne unit was integrated to the rhodamine fluorophore having no fluorescence emission in spirocyclic form. The concomitant addition of gold(III) ions resulted in appearance of an emission band by the aid of turn on signal quantification of gold(III) ions became possible. The most excited feature of this new alternative sensing methodology is its applicability to living cells. Tea and co-workers were also demonstrated imaging study of gold ions in HeLa cell lines (Yang et al., 2009).

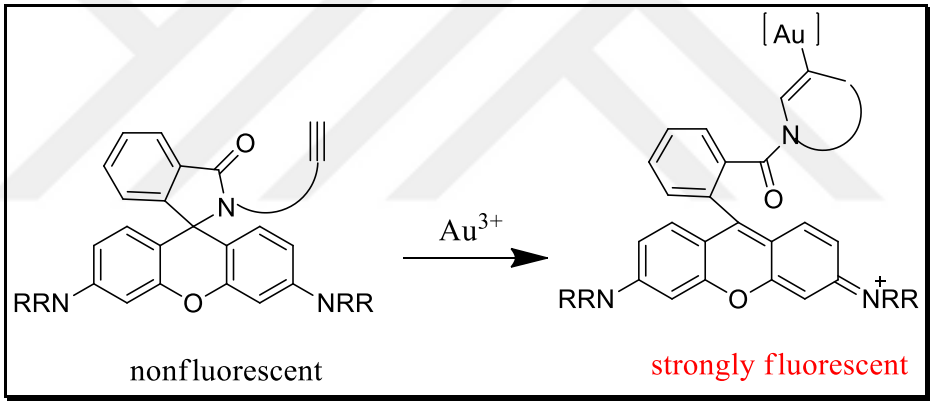

Figure 2.1. First example of gold ion sensors
(Source: Yang et al, 2009)

The study of Tae and co-workers became a milestone in the area of fluorescent molecular sensors for gold ion detection (Yang et al., 2009). Up to now there have been increasing interests for the development of molecular tools for the detection of gold ions in synhetic samples and living organisms.

After the work of Tae, two independent groups –Joon's and Ahn's groups- published their works separately in which the structure of chemodosimeter bearing the same skeleton (Jou et al., 2009; Egorova et al., 2010). The sensor molecule synthesized via the reaction of rhodamine B and propargyl amide with a modarate yield.

The only difference of these two studies was the media of sensing system. In Joon's work Au^{3+} ions were detected in EtOH/HEPES (1/1 (v/v), pH = 7.4) system, on the other hand, the same molecule was capable of sensing both Au^{3+} and Au^{+} in CH_3CN/PBS buffer (1/1 (v/v), pH = 7.2). These studies obviously demonstrated the effect of sensing media to analyte selectivity. Also, as shown in Figure 2.2, the color of solution was affected from the identity of sensing system.

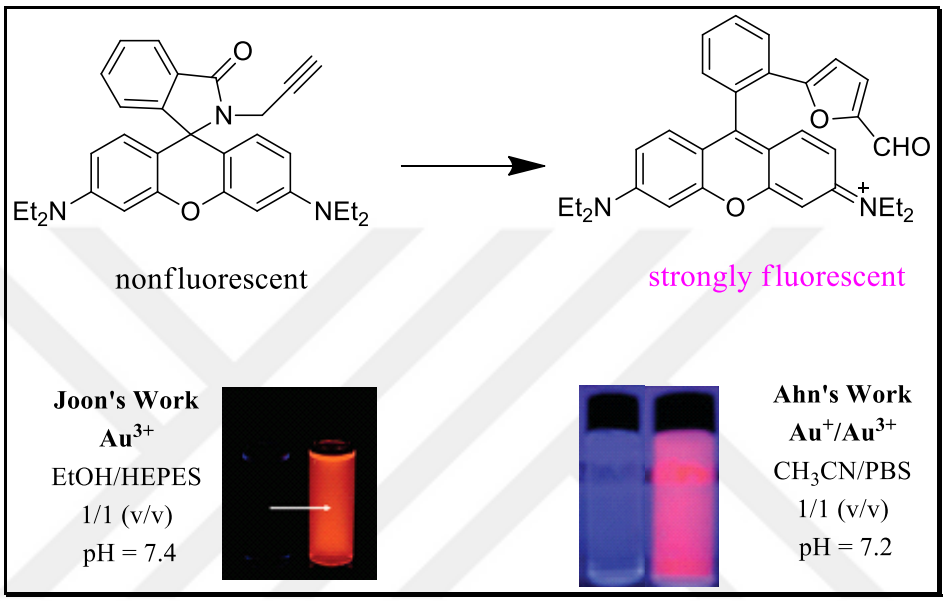

Figure 2.2. Rhodamine-propargylamide based fluorescent sensor for gold ions (Source: Jou et al., 2009; Egorova et al., 2010)

Soon after above works, a ratiometric fluorescent molecular sensor was improved by Dong et al. (Dong et al., 2010). The probe's design was based on 1,8-naphtalimide and alkyne scaffold and made differentiation of the two metal ions (Au^{3+} and Hg^{2+} sharing similar chemical nature) possible by only changing the solvent system and pH of the sensing media. The mechanism proceeds via Kucherov reaction which starts with activation of triple bond with mercury or gold ions. The second step includes the formation of vinyl gold or oxymercuryration intermediate that is responsible for the blue shift in fluorescence spectrum (Dong et al., 2010).

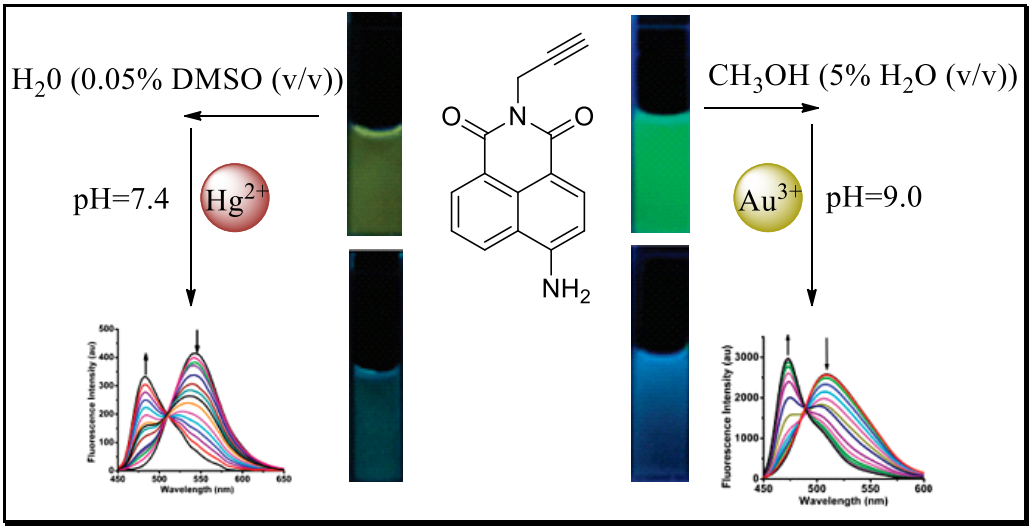

Figure 2.3. A ratiometric probe for gold and mercury ions
(Source: Dong et al., 2010)

In 2010, a rare example of fluorescent sensor was demonstrated by Do et al. (Do et al., 2010). In this approach, a non-fluorophore compound reacted with gold(III) ions and underwent a gold-ion mediated hydroarylation reaction, thereby yielding a fluorescent coumarine derivative. With the aid of fluorescence enhancement, gold (III) ions could be monitored in solutions and living cells (HaCaT cells).

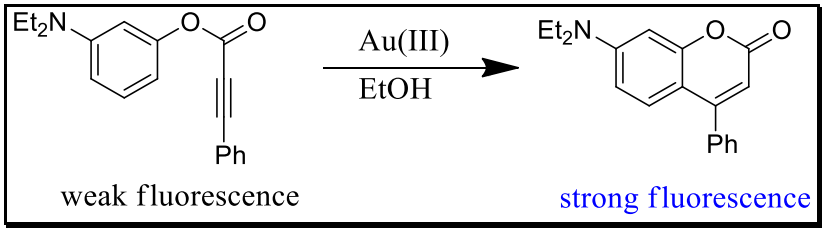

Figure 2.4. Reaction based fluorescent sensor for gold(III) ion
(Source: Do et al., 2010)

Up to now, several molecular fluorescent sensors have been devoloped by taking advantage of alkynophilic chracter of gold ions. Figure 2.5. summarizes the gold ion selective fluorescent sensors bearing alkyne moiety in their receptor unit (Seo et al., 2012; Patil et al., 2012; Cao et al., 2011; Choi et al., 2013; Wang et al., 2012; Wang et al. 2013).

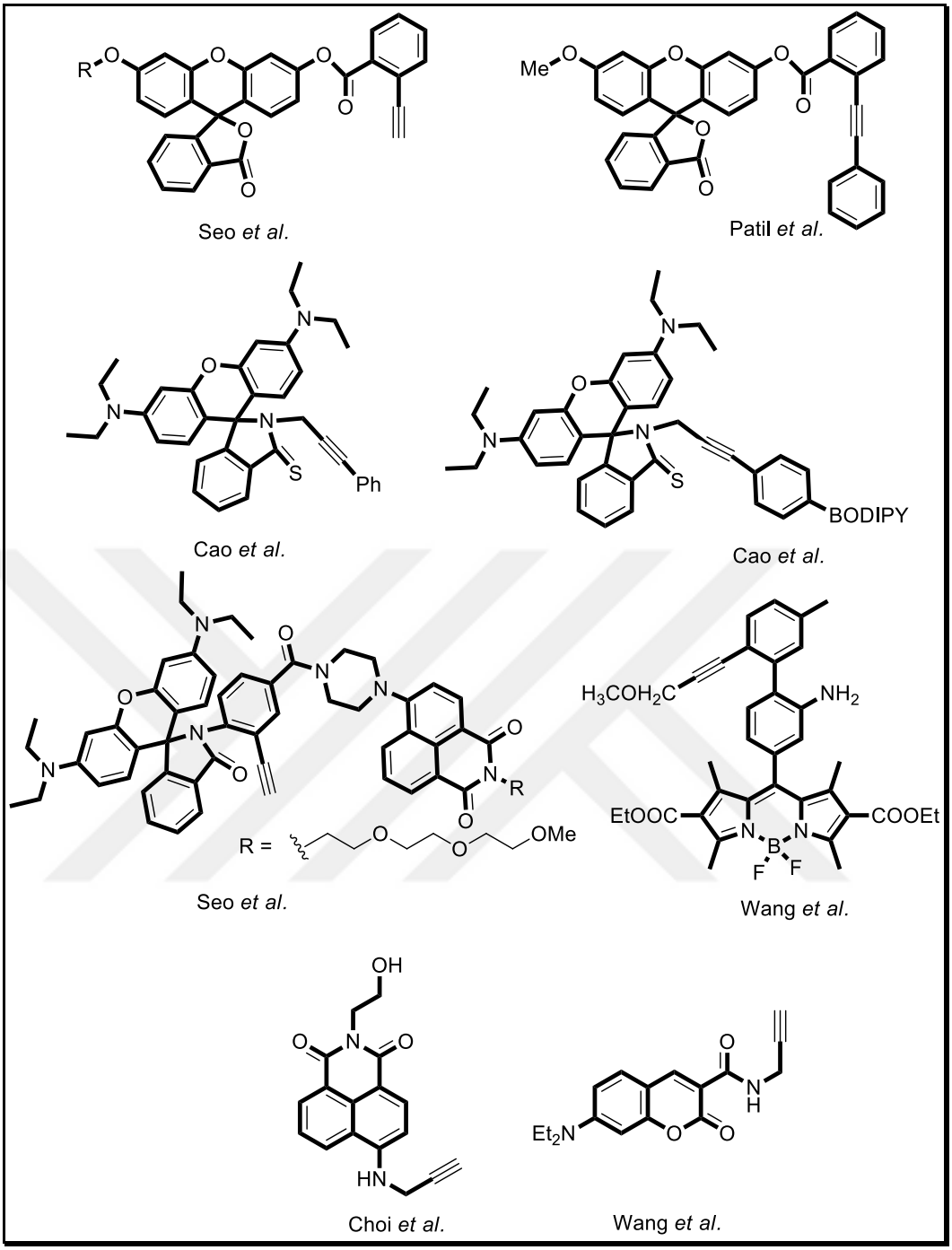

Figure 2.5. Gold ion sensor based on alkyne moiety.
(Source: Singha et al., 2015)

In addition to above molecules, -as a part of ongoing studies- our research group also developed a turn on fluorescent molecular sensor for the detection of gold ions in sythetic samples and living cells (HTC-116 cell lines). The rhodamine derivative, which contains a reactive alkyne moiety highly specific for Au^{+} and Au^{3+} ions, was

synthesized by reacting rhodamine-B hydrazide with 2-alkynylbenzaldehyde in ethanol at reflux temperature (Emrullahoglu et al., 2013).

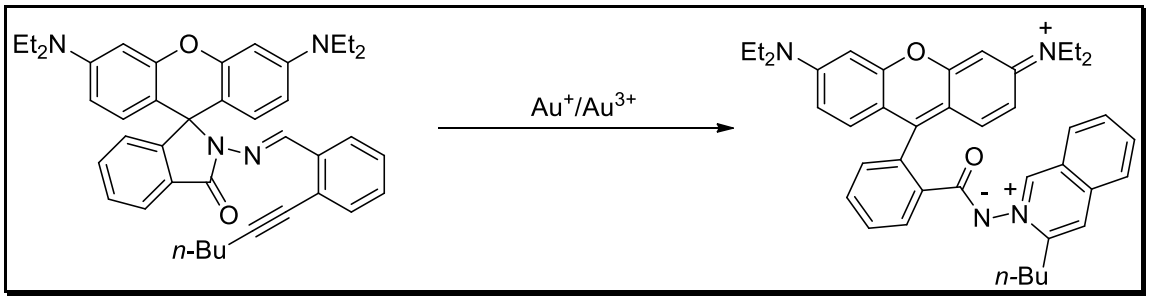

Figure 2.6. Rhodamine based gold ion sensor developed by Emrullahoglu research group (Source: Emrullahoglu et al., 2013)

The colorless solution of sensor molecule showed no absorption in the visible region and was nonfluorescent, indicating that spirocyclic form of the dye was predominant. Addition of Au^{3+} ions initiated the gold-ion mediated cyclization reaction that triggered ring opening reaction of spirocyclic rhodamine derivative. As it had colorless and nonfluorescent solution in sleep mode, upon direct addition of gold ions the resulting solution immediately became pink in color and started to fluoresce under UV light. The spectroscopic change in the fluorescence emission provides the detection of gold ions.

There has been limited number of reaction based fluorescent molecular sensors bearing reactive recognition motif without alkyne moiety. In 2011, a gold ion selective turn on fluorescent sensor integrated with an acylsemicarbazide unit was demonstrated by Yuan et al. (Yuan et al., 2011).

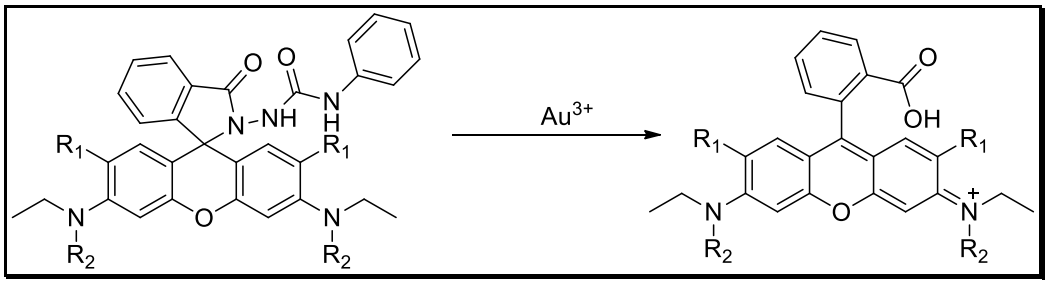

Figure 2.7. Fluorescent molecular sensor works via hydrolysis of acylsemicarbazide (Source: Yuan et al., 2011)

The unexpected hydrolysis of acylsemicarbazide moiety to a carboxylic acid derivative in the presence of gold ions produced fluorescence enhancement within the seconds. In addition to applicability to monitoring gold ions in the living cells, the probe molecule was also usaful for quantification of residual gold ions in synthetic samples.

Another interesting strategy was applied by Park et al. in 2012 constructed on BODIPY structure (Park et al., 2012). The metodology built on an indirect sensing protocol in which Au^{3+} ions first converted into the gold nanoparticles in HEPES solution then, the generated nanoparticles broke the C-I bond by yielding a turn on response. Cleavage of C-X bond via nanoparticles is an interesting approach and the examples of this type of chemodosimeters are fairly seldom.

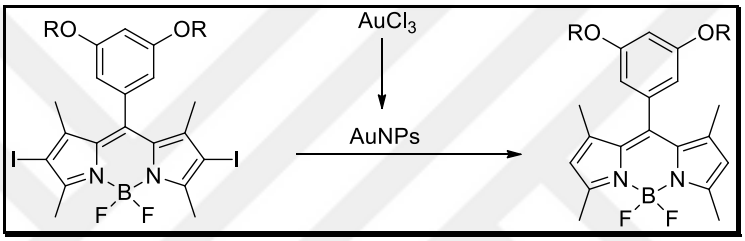

Figure 2.8. Detection of Au^{3+} ions via C-I bond cleavage
(Source: Park et al., 2012)

In general desulfation reactions have used for mercury ion sensing strategies. Interestingly, Park et al. published an article that enable the detect Au^{3+} ions via a desulfation of thiocoumarin derivative. While thiocoumarin derivative had no fluorescence emission direct addition of Au^{3+} ions generated a turn on response in fluorescence spectrum (Park et al., 2012).

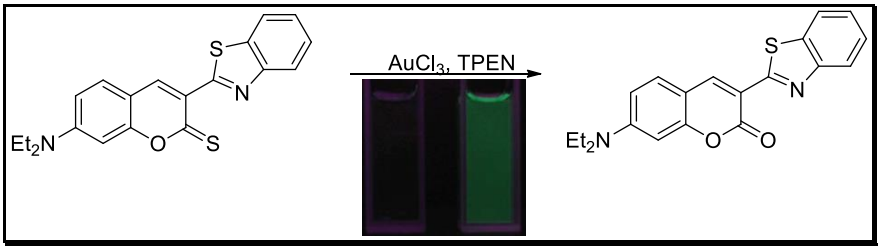

Figure 2.9. Detection of Au^{3+} ions via desulfation reaction
(Source: Park et al., 2012)

Along with the sensing systems based upon a chemical reaction, coordination based sensors have also prevailed in constructing molecular sensors. Although complexation based chemosensors are in common, a few examples of gold ions selective chemosensors have been demonstrated yet.

The gold complexes are very helpful for many transformations in organic synthesis. Most of these complexes include gold – heteroatom interactions. On the basis of gold heteroatom interactions, reversible gold ion sensors have started to draw interests of scientists.

The first example of a reversible Au^{3+} ion sensor was demonstrated by Wang et al. in 2011 (Wang et al., 2011). The molecule was synthesized from the reaction of rhodamine 6G hydrazide and 8-hydroxyquinoline-2-carbaldehyde followed by the zinc mediated reduction in acetic acid. As shown in figure 2.10 rhodamine based chemosensor included several hetoroatoms that possibly underwent reversible interactions with Au^{3+} ions. These interactions triggered the ring openning reaction of spirocyclic rhodamine compound resulting with an increase in fluorescence emission. The reversiblty of sensing event was also surveyed by the addition of excess amount of CN^- ions. After addition of CN^- ions fluorescence intensity of probe molecule was sagaciously decreased. With the aid of this observation the reversibility of sensing event has been proven.

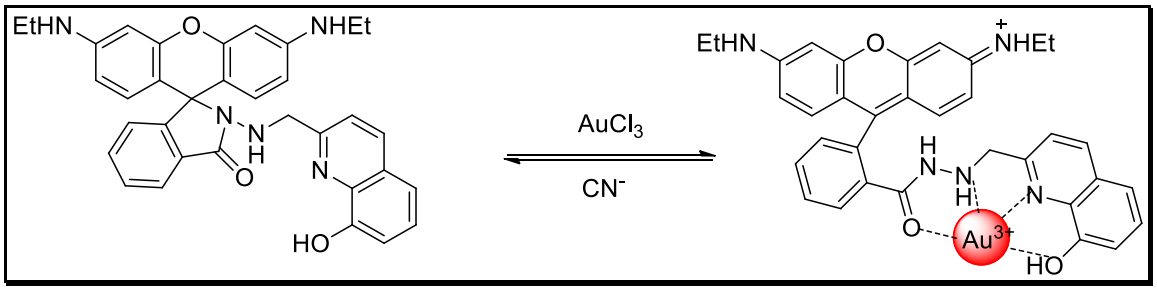

Figure 2.10. The first example of reversible Au^{3+} ions sensor
(Source: Wang et al., 2011)

In literature, the design of all gold ion sensors is based upon the enhancement or ratiometric change of fluorescent signal. Unusual examples of gold ion sensors were developed by Öztaş et al. and Yang et al. in 2013. In both studies the fluorescent signal of free dye molecules were started to quench with the gradual addition of gold ions (Öztaş et al., 2013; Yang et al., 2013). The binding stoichiometry of sensing events was

also established by using Job's plot analysis and mass analysis. In both sensing strategy formation of 1:1 complex between Au^{3+} and probe molecules were proved.

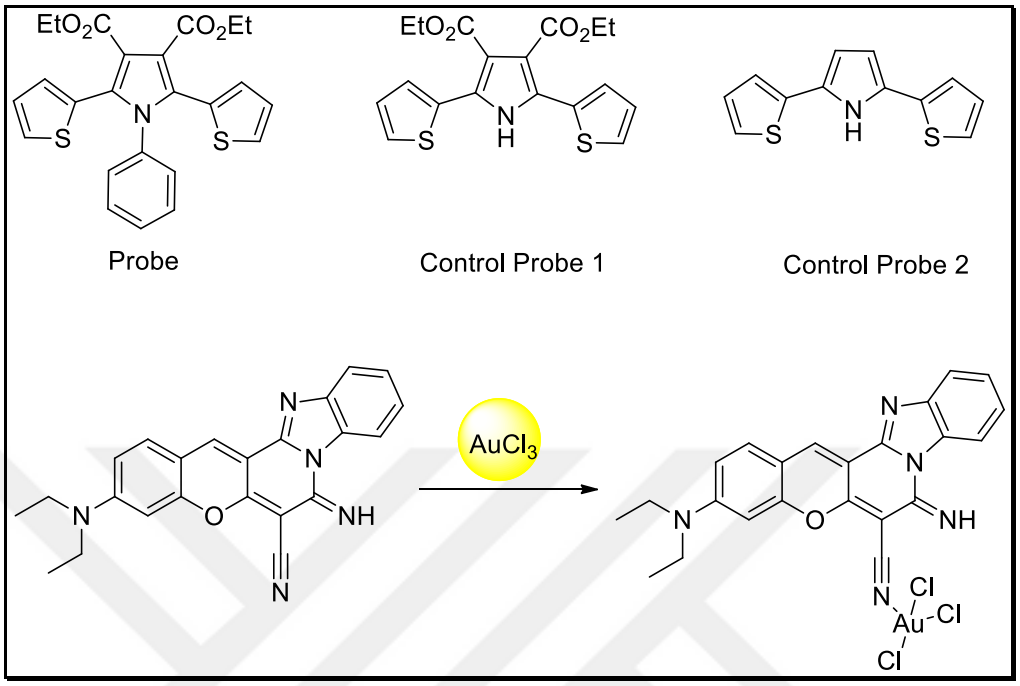

Figure 2.11. Non-reaction based Au^{3+} ion sensors
(Source: Öztaş et al., 2013; Yang et al., 2013)

Last example of reversible chemosensor was published in 2015 by Chinapang et al. The sensor molecule included a ferrocenyl unit that quenched the fluorescence of naphthalimide moiety via the PET mechanism. The coordination of gold ions to the alkyne and ferrocenyl units blocked the PET mechanism and dye molecule started to fluoresce (Chinapang et al., 2015).

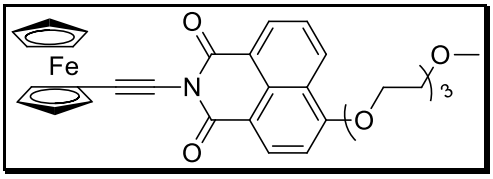

Figure 2.12. Reversible gold ion senser based on Ferrocenyl- naphthalimide scaffold
(Chinapang et al., 2015)

2.3. BODIPY Based Fluorescent Sensors for Gold Ions

In the subject of this thesis, six novel fluorescent sensor based on BODIPY skeleton were designed, synthesized, characterized and their analyte sensitivities and selectivities were carefully investigated (Figure 2.13).

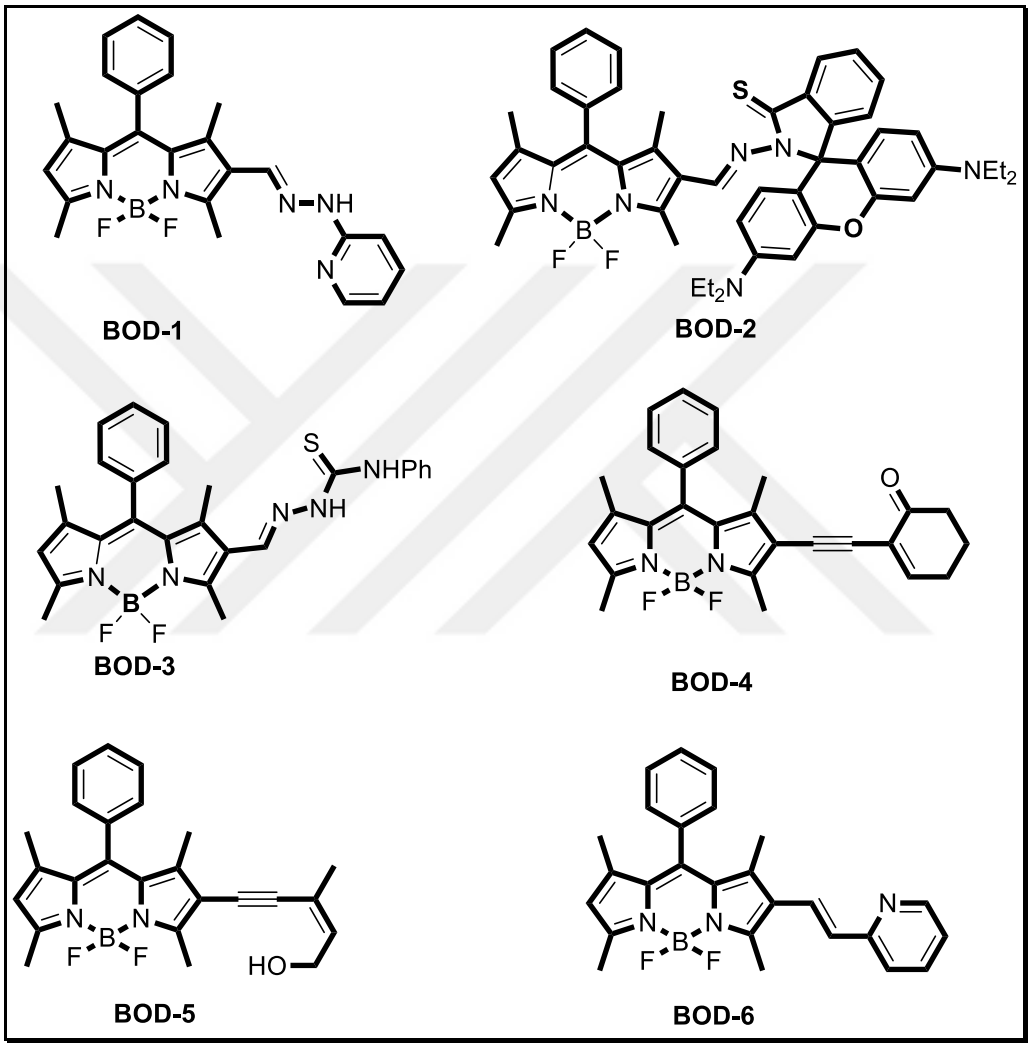

Figure 2.13. BODIPY based gold and mercury ions selective sensors.

2.3.1. Gold Ion Sensing Properties of BOD-1

As indicated above there have been very limited number of gold ion sensing strategies and presented strategies have many disadvantages mainly cross-affinity of other metal ions with similar chemical nature (e.g. Hg^{2+}, Pd^{2+}, Ag^{+}). To avoid this handicap, new sensing strategies utilizing alternative recognition motifs are urgently sought.

To overcome these problems, a novel reactive motive was presented that only shows reactivity to gold ions, if properly designed have no response to other competitive cations. In the first design, a BODIPY based fluorecent chemodosimeter bearing **C=N** functionality that diminishes the fluorescence of probe molecule based upon the **C=N** bond isomerization phenomena was developed and its spectral properties towards addition of various metal ions was investigated.

BOD-1 was synthesized by the synthetic route outlined in Figure 2.14, and structure of the sensor was confirmed by ^{1}H-NMR and ^{13}C-NMR analysis. In the first step, mono-formylated BODIPY (**BODIPY-ALD**) was synthesized via Vilsmeier Haack's Formylation of the non-modified BODIPY (Işık et al., 2015). In the second step, (**BODIPY-ALD**) was treated with 2-hydrazinopyridine in the presence of catalytic amount of glacial acetic acid to afford the title compound, **BOD-1**, in a good yield (76%).

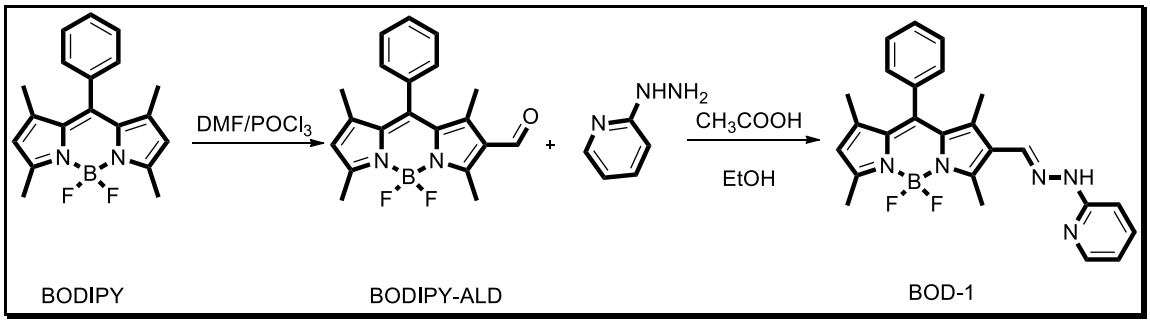

Figure 2.14. Synthetic route to **BOD-1**

Importantly, **BOD-1**, was designed in such a way that the BODIPY fluorophore is non-emissive before the addition of any metal species. As displayed in Figure 2.15, the **C=N** functional group incorporated into the fluorophore diminishes the fluorescence emission because of a non-radiative deactivation process of the excited state via

isomerization of the **C=N** group. It was envisioned that either blocking the isomerization of **C=N** bond by metal binding or directly hydrolysing it with a metal species would allow for the recovery of the BODIPY emission.

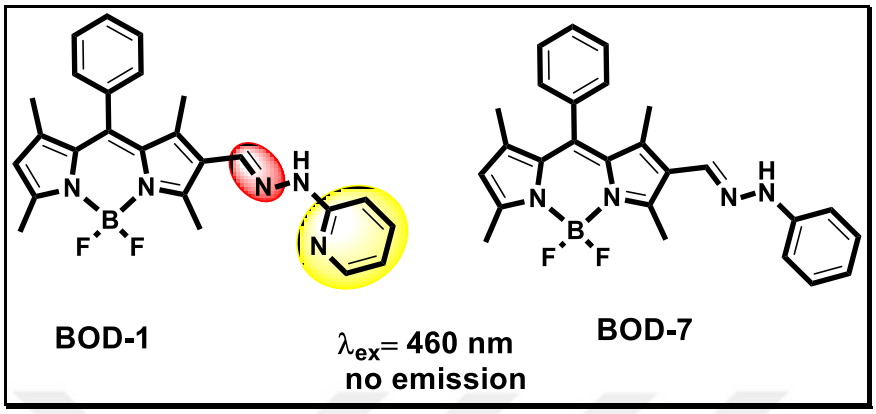

Figure 2.15. Structure of **BOD-1** and control probe **BOD-7**

The investigation was commenced by first determining the optimum conditions for the recognition of Au^{3+} ions. The effect of variations of solvent ratio and water content were investigated carefully. Eventually, the optimum condition for the sensing process was established as 0.1 M phosphate buffer/EtOH (pH 7.0, v/v, 1:1) with 10 µM dye concentration.

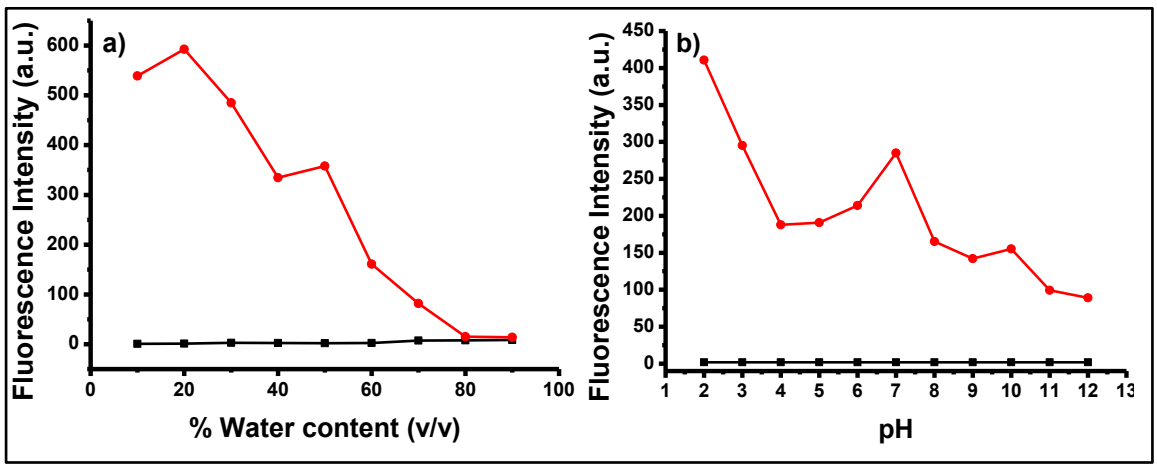

Figure 2.16. a) Effect of fraction of water (in 0.1M potassium phosphate buffer pH 7.0/EtOH) and b) Effect of pH (in 0.1M potassium phosphate buffer pH/EtOH (v/v, 1:1)) on the interaction of **BOD-1** (10 µM) (black line) with Au^{3+} (200 µM, 20 equiv.) (red line), (λ_{ex}: 460 nm, λ_{em}= 512 nm at 25 ^{o}C).

The fluorescence-sensing behaviour of **BOD-1** towards addition of Au^{3+} was comprehensively surveyed upon excitation at 460 nm. As shown in Figure 2.17.a, metal-free **BOD-1** was non-emissive due to a non-radiative deactivation process. As envisioned, the addition of $AuCl_3$ (20 μM, 2 equiv.) to the probe solution (0.1 M phosphate buffer pH 7.0/EtOH, v/v, 1:1) resulted in a significant increase of the emission band centred at 512 nm. The emission intensity reached its maximum when 20 equiv. of Au^{3+} was added, with an enhancement factor over 300 fold.

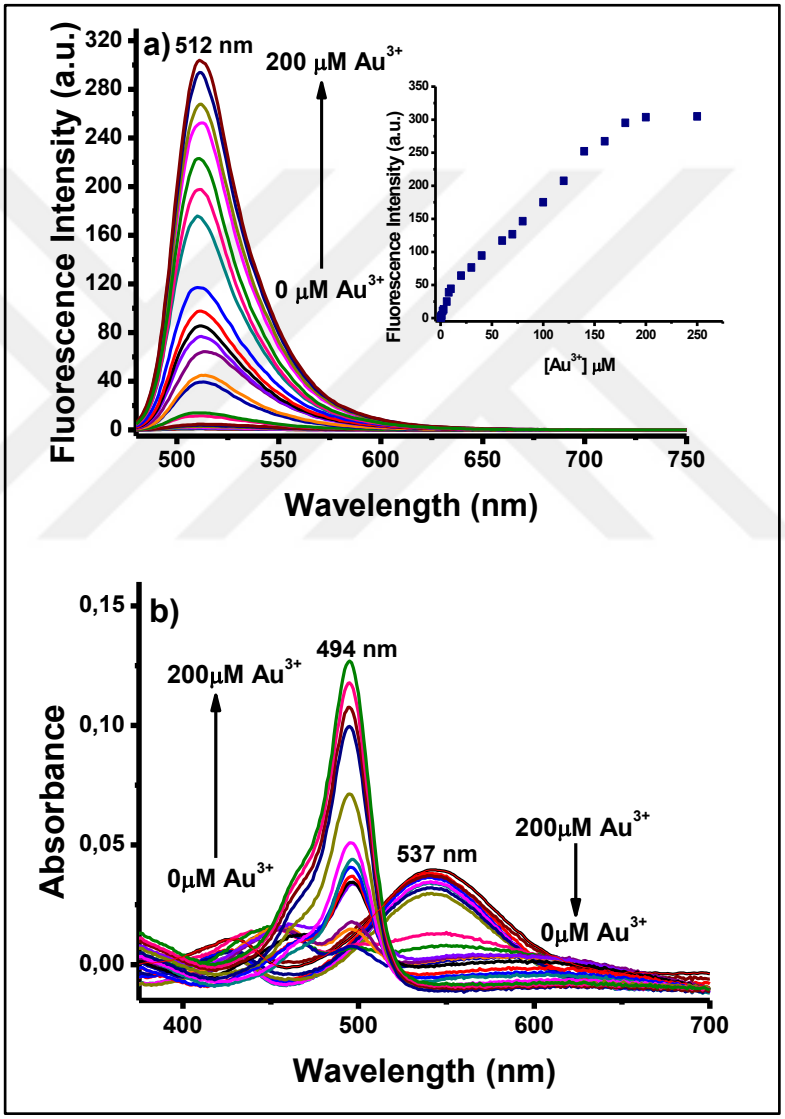

Figure 2.17. a) Fluorescence and b) Absorbance spectra of **BOD-1** (10μM) in the presence of increasing amount of Au^{3+} (0-200 μM) 0.1 M phosphate buffer/EtOH (pH 7.0, v/v, 1:1).Inset: Calibration curve. (λ_{ex}: 460 nm at 25 ^{o}C).

The UV-Vis spectra of **BOD-1** displayed a similar sensing behaviour towards the addition of $AuCl_3$. The absorbance spectrum of metal-free **BOD-1** displayed one single absorption band at 537 nm belonging to the BODIPY core. In response to the addition of Au^{3+}, this band disappeared concomitantly with the appearance of a new absorption band at 494 nm indicating a possible structural change of the BODIPY core. The blue shift of absorption wavelength is reflected in a change in the colour of the solution from red to light orange. All spectral changes were easily detectable by the naked eye under visible light and the UV lamp.

To evaluate the detection limit of **BOD-1** towards Au^{3+} a careful titration experiment was performed. The increase in the emission intensity was proportional to the amount of Au^{3+} with a good linear correlation and the minimum amount of Au^{3+} that can be detected under these conditions was evaluated to be 44 nm based on S/N = 3.

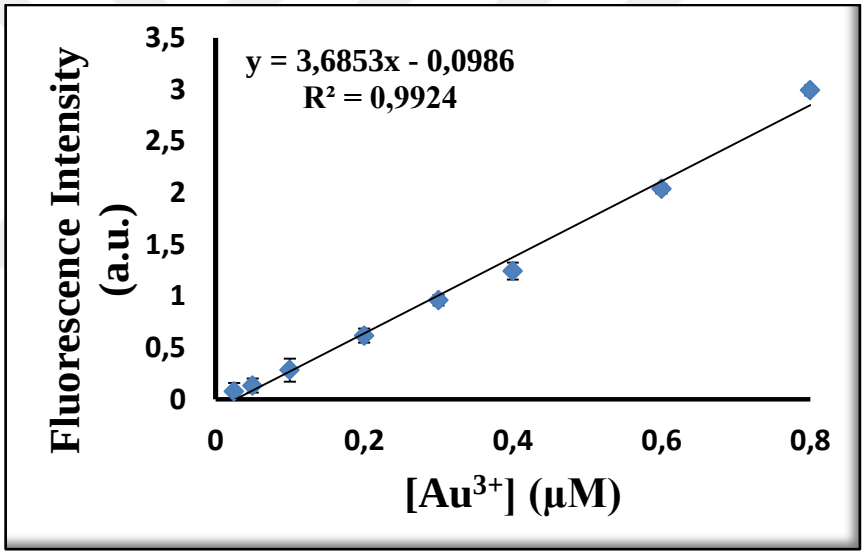

Figure 2.18. Fluorescence changes of **BOD-1** (10.0 µM) upon addition of Au^{3+} (0,025 to 0,8 µM, 0. 025 to 0.08 equiv.) in 0.1 M potassium phosphate buffer, pH 7.0/EtOH (v/v, 1:1) (λ_{ex}: 460 nm, λ_{em}= 512 nm at 25 ^{o}C).

The reaction time profile of sensing event was surveyed by the addition of various concentrations of Au^{3+} to the sensing media. Notably, the spectroscopic response was fast and saturation of the emission intensity was observed within minutes (Figure 2.19).

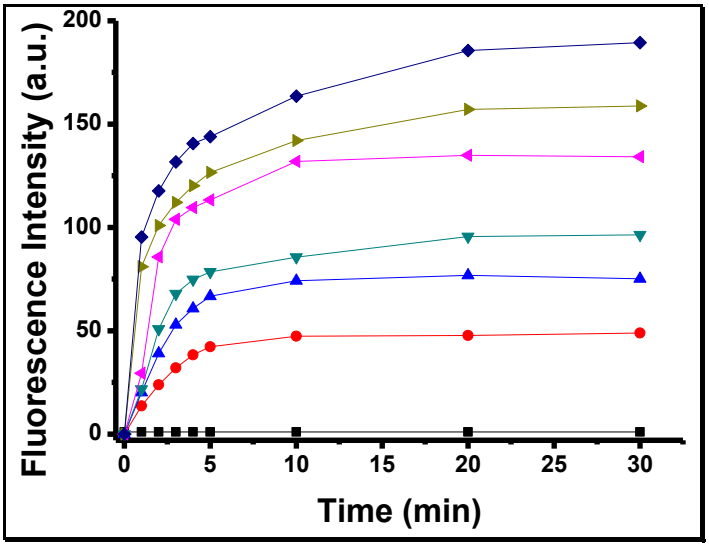

Figure 2.19. Reaction time profiles of **BOD-1** (10 μM) in the absence (■) or presence of Au^{3+} [10 (●), 30(▲), 50(▼), 100 (◀), 150(▶), 200(♦) μM.]. The fluorescence intensities at 512 nm were continuously monitored at time intervals in 0.1 M phosphate buffer/EtOH (pH 7.0, v/v, 1:1) (λ_{exc}=460 nm, λ_{em}= 512 nm at 25 ^{o}C).

The sensitivity and selectivity of **BOD-1** towards other metal ions were further explored. To our delight, no significant spectral changes could be detected for the competing alkynophilic metal species such as Ag^{+}, Ni^{2+}, Pd^{2+}, Hg^{2+}, Cu^{2+}, and for the other metal species such as Mg^{2+}, Mn^{2+}, Pb^{2+}, Zn^{2+}, Cd^{2+}, Fe^{3+}, K^{+}, Li^{+}, Ba^{2+}, Ca^{2+}. Especially notable was the observed selectivity for Au^{3+} over Au^{+}, which can be hardly seen for other gold ion responsive molecular sensors (Figure 2.20.a).

Interference of other metal ions to the selectivity of **BOD-1** was also explored. The spectral response induced by Au^{3+} ions was not affected in the presence of any other metal species (Figure 2.20.b). These results indicated that **BOD-1** could properly detect Au^{3+} ions in the mixtures of other related species.

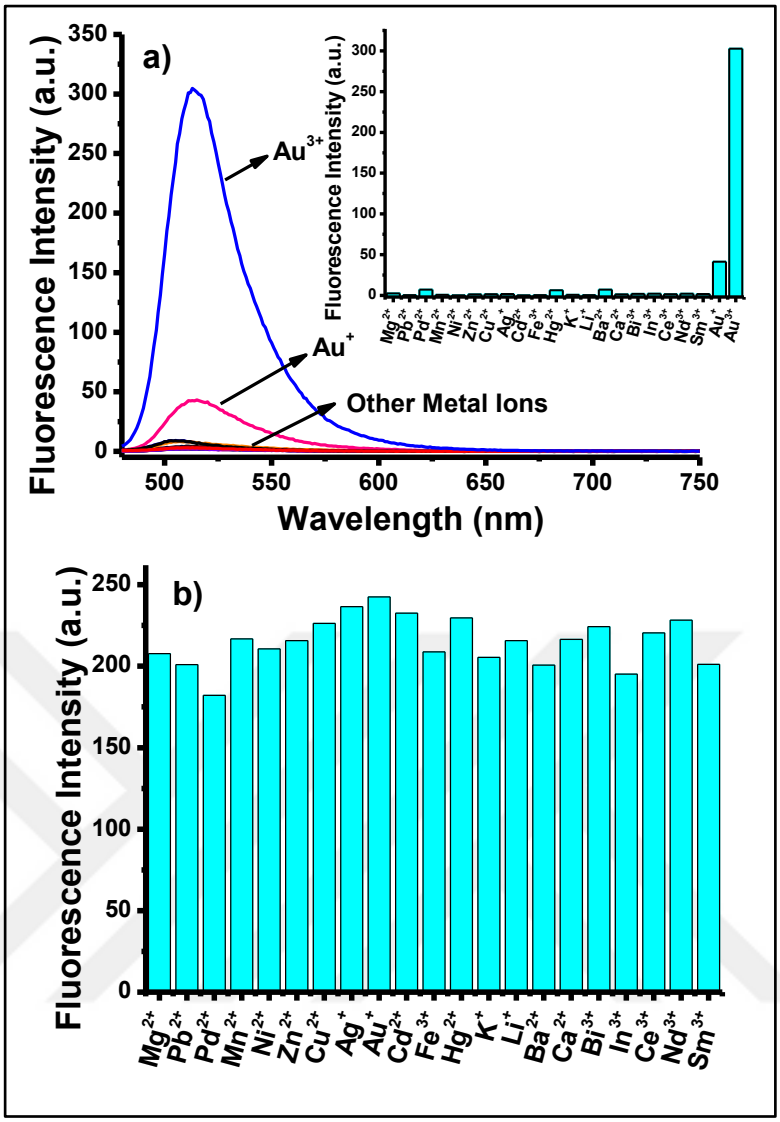

Figure 2.20. Fluorescence of a) selectivity b) competition experiments of **BOD-1** (10 μM) + Au^{3+} (200 μM, 20 equiv.), **BOD-1** (10 μM) + other metal ions (200 μM, 20 equiv.) in 0.1M potassium phosphate buffer, pH 7.0/EtOH (v/v, 1:1) (λ_{ex}: 460 nm, at 25 ^{o}C). Inset: Bar graph notation.

The sensing mechanism of **BOD-1** was invesigated carefully. To get insight into whether the sensing process reversible or not, excess amount of Bu_4NCN was added to the sensing media. However, there was no observable change in the emission pattern indicating the sensing process to be irreversible in nature and based on a chemical reaction. To understand the mechanism of irreversible reaction the outcome of the sensing event was tried to isolate. The process was monitored by TLC and a new green fluorescing spot was observed as a strong evidence for the formation of a new BODIPY derivate. By the aid of NMR spectroscopy, the structure of this new compound was easily confirmed to be the hydrolysis product (**BODIPY-ALD**) of **BOD-1**.

The sensing mechanism, as illustrated in Figure 2.21, is proposed to proceed via coordination of Au^{3+} to both pyridyl and imine nitrogen atoms forming an intermediate (**BOD-1**–Au^{3+}), which rapidly hydrolysed by the attack of water. Optimization experiments revealed that the content of water in the sensing media has a dramatic role in the sensing efficiency. While there were no spectral changes in pure organic solvent (i.e., ethanol), increasing the content of water to some extent (H_2O/EtOH, v/v, 1:1) dramatically enhanced the response of the probe towards Au^{3+}, which established the obvious need of water for the hydrolysis step. However, it is worth noting that, at higher percentages of water (e.g. H_2O/EtOH, v/v, 9:1), the catalyst species loses its activity by forming aggregates in the solution.

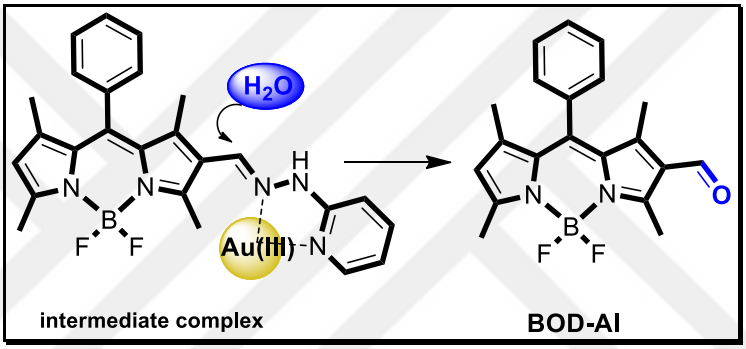

Figure 2.21. Gold mediated hydrolysis of **BOD-1**

A BODIPY derivative, **BOD-7**, lacking a pyridyl nitrogen atom on the phenyl ring, was prepared as an control probe to **BOD-1** and to clarify the nature of the sensing process. Surprisingly, under the same sensing conditions probe **BOD-7**, even in the absence of any metal species, was not stable and hydrolysed rapidly to the corresponding aldehyde (Figure 2.22). Given its instability, **BOD-7**, could not be used further as a probe for gold analysis. Eventually, it turned out that the pyridyl nitrogen atom plays a superior role in selective binding of Au^{3+} ions and also, in improving the overall efficiency of the sensing process.

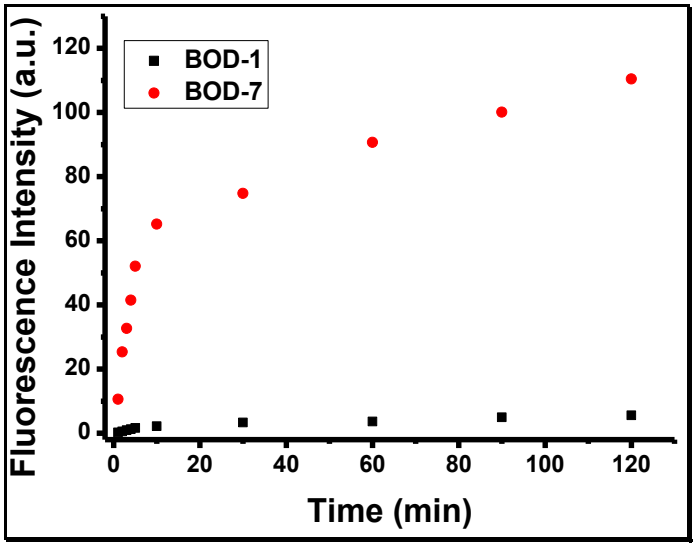

Figure 2.22. Fluorescence responses of **BOD-1** (10 μM) and **BOD-7** (10 μM) in reaction conditions (0.1 M phosphate buffer/EtOH (pH 7.0, v/v, 1:1) without addititon of Au^{3+}. (λ_{exc}=460 nm, λ_{em}= 512 nm at 25 ^{o}C).

Applicability to living cells is an important aspect of a fluorescent sensor. In this regard, we investigated its potential for tracking Au^{3+} ions in living cells. A549 Human Lung Adenocarcinoma cells were incubated at 37^{o}C first with **BOD-1** (5.0 μM) for 20 min, followed by the addition of Au^{3+} (10 μM) and incubation for another 20 min. Then, the cells were stained with a nucleus staining dye (DAPI (1.0 mM)) for another 10 min. With the aid of fluorescence microscopy, the turn-on response towards Au^{3+} was clearly monitored in the cells (Figure 2.23). The fluorescence images of cells taken before and after the addition of Au^{3+} displayed a distinct fluorescence enhancement consistent with the results observed in the solution. Importantly, throughout the cell imaging process the cells were intact and showed healthy spread and adherent morphology. This preliminary cell imaging study suggested that **BOD-1** is cell-membrane permeable and can be efficiently used for in vitro imaging of Au^{3+} in living cells.

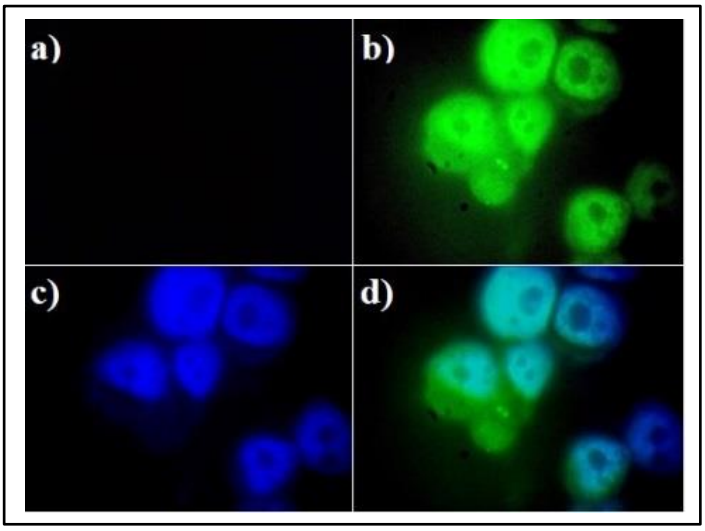

Figure 2.23 Fluorescence images of Human Lung Adenocarcinoma cells (A549). a) Fluorescence image of A549 cells treated with only **BOD-1** (5 μM); b) Fluorescence image of cells treated with **BOD-1** (5 μM) and Au^{3+} (10 μM) (λ_{ex}=460 nm); c) Fluorescence image of cells treated with DAPI (control); d) merged images of frames b and c.

In this part of thesis study, a novel sensing methodology was demonstrated based on the gold mediated hydrolysis of **C=N** bond. This new strategy offers highly selective and sensitive detection of Au^{3+} without any interference of competitive metal ions. To further improve this new methodology other fluorescent sensors bearing **C=N** functionality were also designed.

2.3.2. Gold Ion Sensing Properties of BOD-2

To date a large number of molecular sensors have been designed and developed, and the majority of which are single-ion responsive and present no great challenge to researchers. Compared to single-ion responsive molecular sensors, however, the construction of multi-ion responsive molecular sensors with different emission modes is extremely challenging (Xue et al., 2009; Komatsu et al., 2005; Yuan et al., 2008).

The challenge of multiple analyte recognition presents several detection strategies. Incorporating multiple binding motifs onto a single sensing molecule, or alternatively, combining different transducing units (chromophore/fluorophore), allows for rapid access to molecular sensors with multiple emission modes.

In this respect the design, synthesis, spectral properties, and cell imaging studies of **BOD-2** presented, a new "turn-on" multi-fluorescent probe that allows the Hg^{2+} and Au^{3+} species to be differentiated on the basis of distinct fluorescence responses. **BOD-2** constitutes a boron-dipyrromethene dye (BODIPY) and a spirocyclic rhodamine dye covalently attached to each other. **BOD-2** is prepared in a reasonable yield (25%, overall) by the synthetic route outlined in Figure 2.24.

.

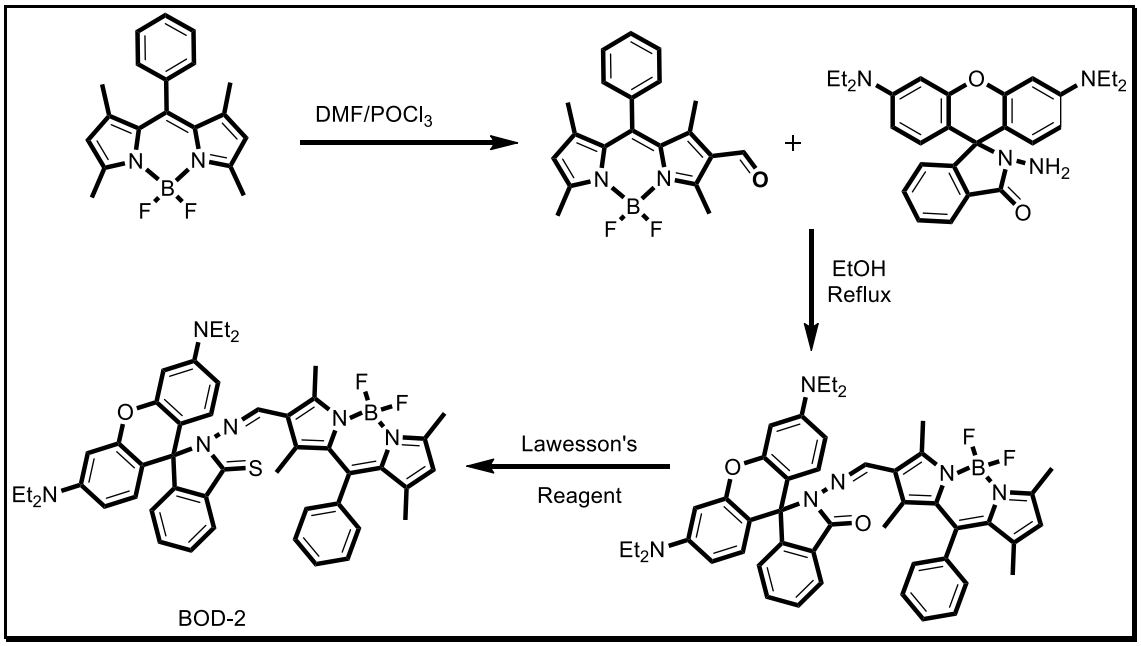

Figure 2.24. Synthetic route to **BOD-2**

Importantly, the novel molecular sensor, **BOD-2**, was designed in such a way that both of the fluorophore units are non-emissive before the addition of any metal species. As can be seen from the structure of the probe shown in Figure 2.25, the **C=N** functionality on the BODIPY core diminishes the BODIPY emission potentially because of a non-radiative decay process of the excited state through rapid isomerization of the **C=N** group. Likewise, the rhodamine fluorophore is non-emissive because the rhodamine dye exists in the ring closed isomeric form.

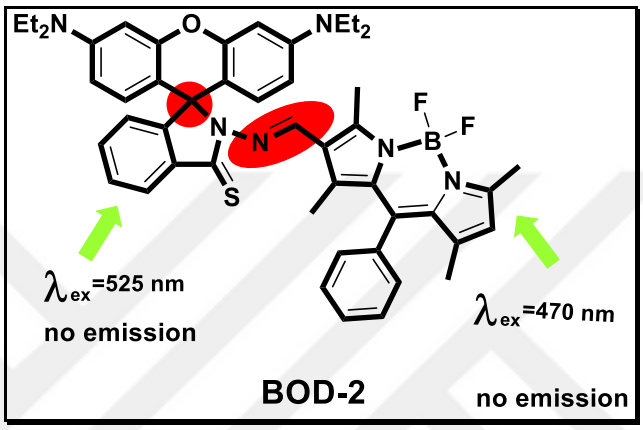

Figure 2.25. Structure of **BOD-2**

The investigations for the determination of optimal sensing media for gold ions were started by screening several sensing conditions (e.g. solvent system, water ratio, pH). Eventually, the optimum condition for the sensing process was established as CH_3CN/HEPES (pH 7.0, v/v, 1:1) with 5 μM dye concentration.

The sensing behavior of **BOD-2** towards the addition of Au^{3+} ions was studied by using UV-Vis and fluorescence spectroscopy. As shown in Figure 2.26, the UV/Vis spectrum of free **BOD-2** (CH_3CN/HEPES 1:1, pH 7.0) exhibits a single absorption band at 527 nm, which belongs to BODIPY core. As the rhodamine core is in the ring closed isomeric form, no absorption bands was expected for the rhodamine derivate. Upon the addition of Au^{3+}, two new absorption bands appeared in absorption spectrum they belong to the ring opened form of rhodamine and BODIPY derivatives. In addition, the non-emissive probe solution immediately turned to a strong green emissive solution that could be easily monitored by the naked eye under the UV lamp. A green emission was a clear evidence for the existence of an emissive BODIPY derivative. The formation of the green emissive compound could be easily monitored from the spots on the TLC

plate. As in the case of previos study, the reaction of **BOD-2** and Au^{3+} produced the hydrolysis products –formylated bodipy and ring opened rhodamine derivative- that was also confirmed by NMR analysis.

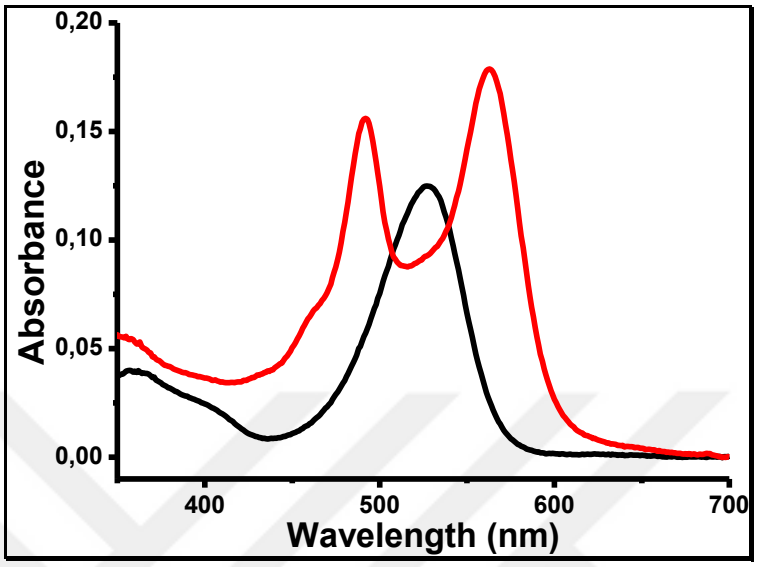

Figure 2.26. Absorption spectra of **BOD-2** (5 μM) and Au^{3+} (1 equiv.) in 1:1 CH_3CN/HEPES buffer at pH = 7.0; (λ_{ex}: 470 nm, at 25 ^{o}C).

The fluorescence sensing behavior of **BOD-2** towards Au^{3+} was comprehensively surveyed upon excitation at 470 nm and 525 nm. As shown in Figure 2.27, the fluorescence spectrum of (**BOD-2**/Au^{3+}) displays an emission band at 506 nm when excited at 470 nm, a characteristic emission band of a BODIPY fluorophore. On the other hand, the same probe solution (**BOD-2**/Au^{3+}) when exited at 525 nm displays a different emission band at 585 nm, which is supposed to belong to the ring opened isomer of the rhodamine core.

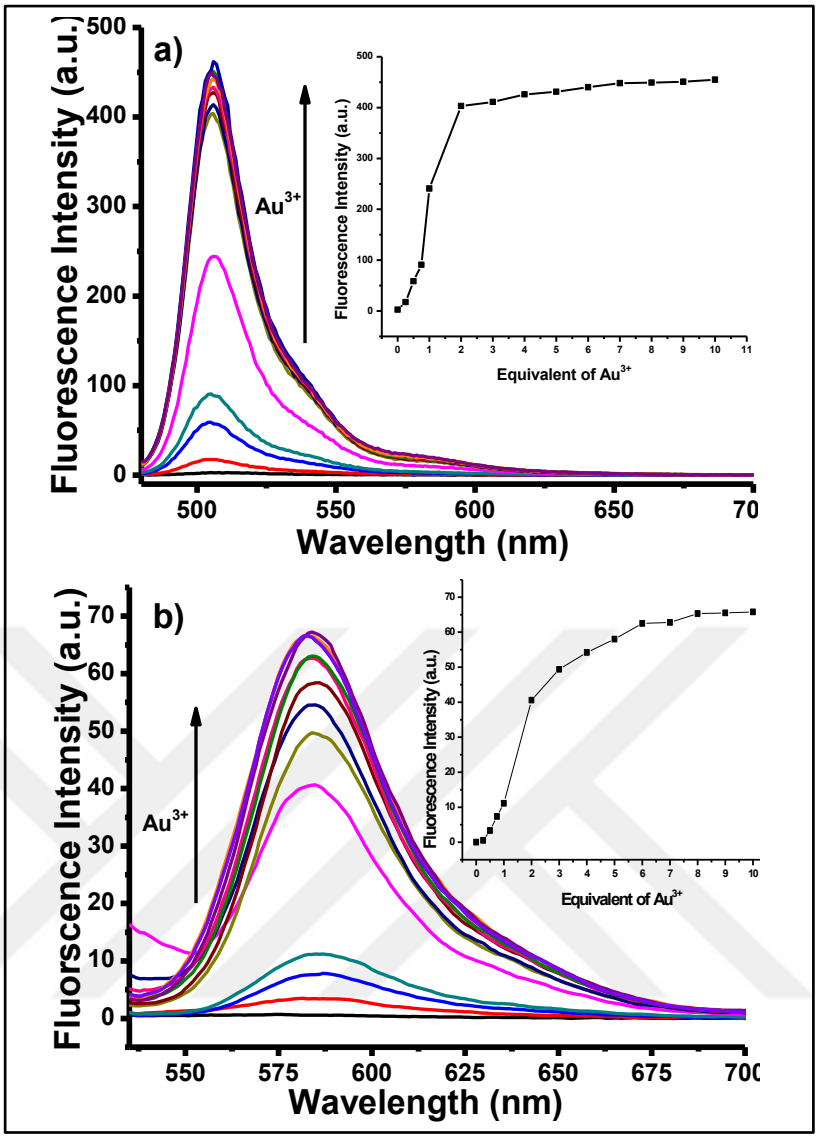

Figure 2.27. Fluorescence spectra of **BOD-2** (5 μM) in 1:1 CH_3CN/HEPES buffer at pH = 7.0 in the presence of Au^{3+} (mole equivalents = 0.25 - 10.0) a) λ_{exc}= 470 nm, b) λ_{exc}= 525 nm.

The fluorescence emission intensity at both wavelengths increased linearly with an increasing concentration of Au^{3+} over a wide concentration range (Figure 2.27). The response of **BOD-2** towards Au^{3+} was fast (<1 min.) and the emission intensity became saturated when 2 equiv. of Au^{3+} was added. The detection limit measured at both wavelengths was at nM level ((a) 10 nM, λ_{em}=506 nm and ((b) 65 nM, λ_{em}=585 nm).

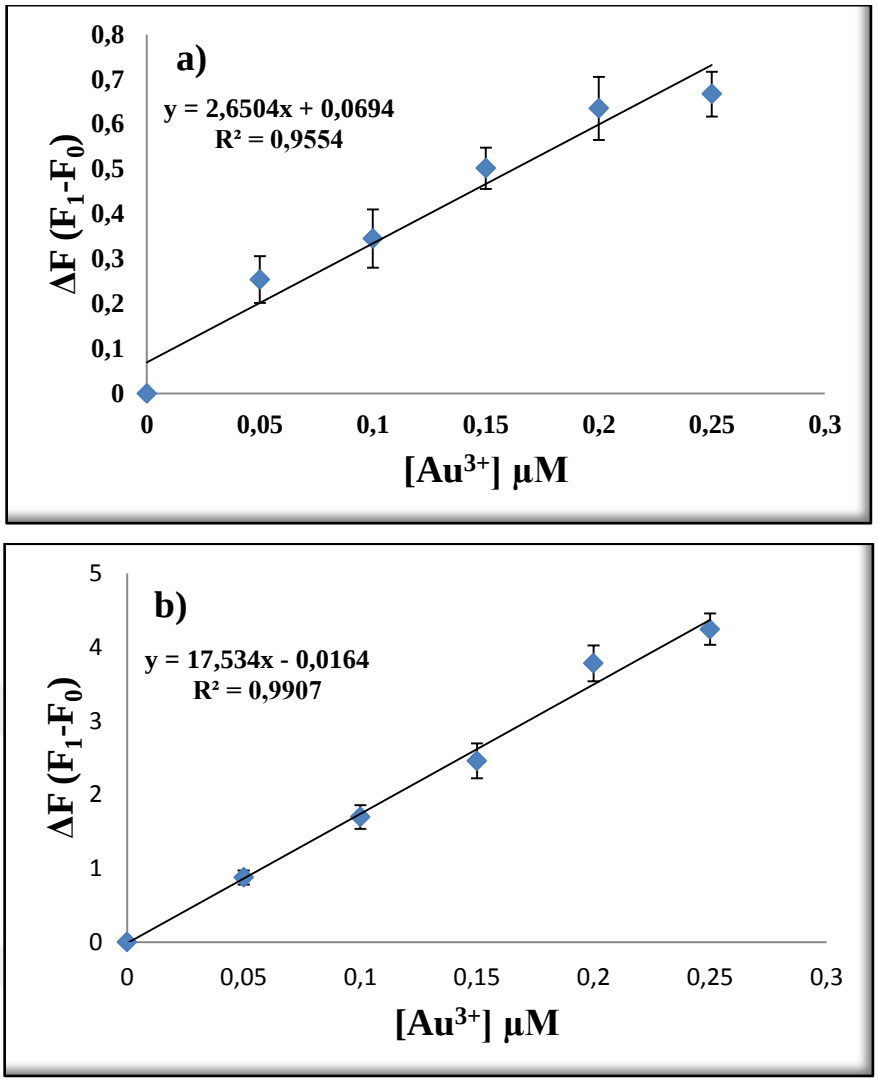

Figure 2.28. Detection limit of **BOD-2** towards addition of Au^{3+} ions a) λ_{em}=506 nm and b) λ_{em}=585 nm

The selectivity profile of **BOD-2** was further investigated in response to other metal ions. For all other metal cations, such as Cu^{2+}, Ag^{+}, Zn^{2+}, Pb^{2+}, Ni^{2+}, Na^{+}, Mg^{2+}, Li^{+}, K^{+}, Pd^{2+}, Fe^{2+}, Co^{2+}, Cd^{2+}, Ca^{2+}, Ba^{2+}, Fe^{3+} and Cr^{3+}, no detectable change in the emission intensity for **BOD-2** were observed (Figure 2.29). The probe was highly selective towards Au^{3+} and showed no spectral response to any other metals ions, except for Hg^{2+} ions. **BOD-2** showed high affinity towards mercury ions in which the fluorescence intensity of probe increased with the direct addition (λ_{em}=585 nm). However, addition of mercury ions had no effect on the fluorescence emission at 506 nm.

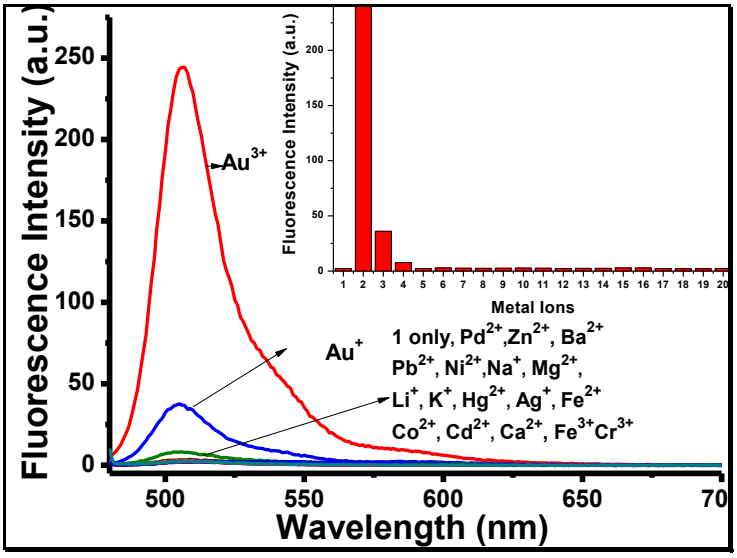

Figure 2.29. Fluorescence intensities of **BOD-2** (5 μM) in 1:1 CH_3CN/HEPES buffer at pH = 7.0 at λ_{max}: 505 nm in the presence of 10.0 equivalent of the cations interest.

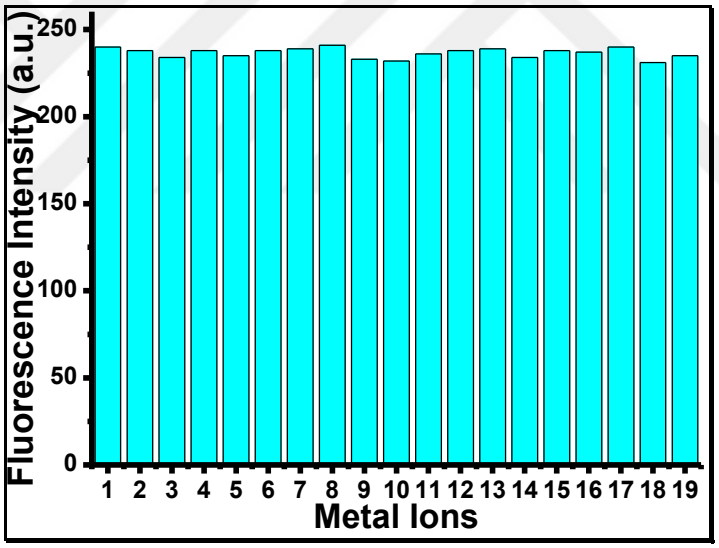

Figure 2.30. Fluorescence intensities of **BOD-2** (5 μM) in 1:1 CH_3CN/HEPES buffer at pH = 7.0 at λ_{max}: 505 nm in the presence Au^{3+} (1.0 equiv.) and 10.0 equiv. of the following metal ions: 1, none; 2, Au^{+}; 3, Cu^{2+}; 4, Zn^{2+}; 5, Pb^{2+}; 6, Ni^{2+}; 7, Na^{+}; 8, Mg^{2+}; 9, Li^{+}; 10, K^{+}, 11, Pd^{2+}; 12, Fe^{2+}; 13, Co^{2+}; 14, Cd^{2+}; 15, Ca^{2+}; 16, Ba^{2+} 17, Ag^{+}; 18, Cr^{3+}; 19, Fe^{3+}

The fluorescence response of **BOD-2** toward Au^{3+} (1 equiv.) in the presence of the other metal ions (10 equiv.) was explored in order to assess the possible interference by other metal ions. As shown in Figure 2.30, the tested metal ions displayed no interference with the detection of Au^{3+} ions.

The **BOD-2** showed high selectivity towards Au^{3+} and Hg^{2+} ions via different emission modes. The detailed information for Hg^{2+} sensing event will be discussed in the following chapter. With this in mind, the addition of Hg^{2+} to **BOD-2** triggers a spiro-ring opening reaction and results in the formation of a highly emissive rhodamine derivative. Notably, the addition of Hg^{2+} to **BOD-2**, the BODIPY core continued to be non-emissive because the **C=N** moiety was preserved. However, the addition of Au^{3+} to the probe solution pre-treated with Hg^{2+} (**BOD-2**/Hg^{2+}) resulted in an immediate change in the emission color from orange to green. Evidently, in the presence of Hg^{2+} and Au^{3+}, **BOD-2** hydrolyzes to give the green emissive **BODIPY-ALD** that dominates the emission color of the probe solution (Figure 2.31).

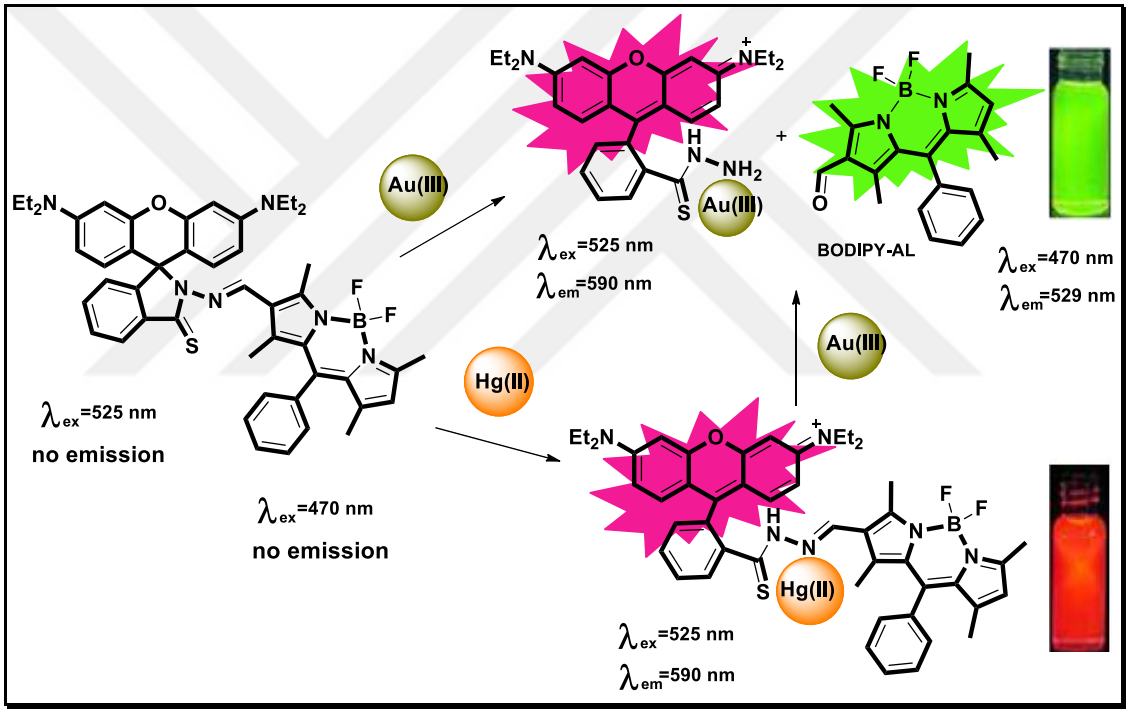

Figure 2.31. Response of **BOD-2** towards the addition of Au^{3+} and Hg^{2+}

To clarify the sensing mechanism the BODIPY derivative bearing oxygen functionality on its rhodamine core instead of sulphur (**BOD-8**) was synthesized. Under the same sensing conditions, **BOD-8** displayed no response towards any metal species, indicating the indispensable role of the sulfur functionality in the detection of both metal species.

Taken together, the sensing mechanism was established as the detection of Hg^{2+} relies on a reversible metal-ligand coordination which triggers a rhodamine spiro-ring

opening reaction. On the other hand, the detection of Au^{3+} is based on an Au^{3+} mediated **C=N** hydrolysis reaction which affords two highly emissive compounds that emit at two distinct wavelengths.

As shown in above Figure, gold mediated hydrolysis produced two fluorophore units, one is formylated BODIPY that has the dominant color in solution and the other is the gold comlex of rhodamine derivative. To access to information about complex structure Job's plot experiment was performed and 1:1 rhodamine derivative: Au^{3+} complex was established (Figure 2.32).

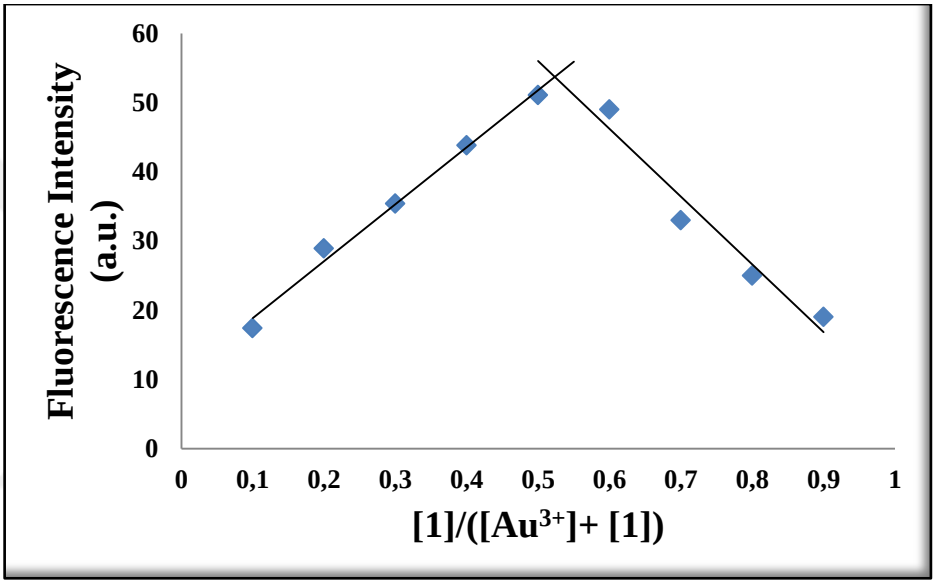

Figure 2.32. Job's plot for the rhodamine derivative and Au^{3+} in 1:1 CH_3CN/HEPES solution at λ_{ex}: 525 nm

The ability of **BOD-2** to operate in living organisms was next assessed. To our delight, **BOD-2** showed the same sensing behavior in living cells. Human Lung Adenocarcinoma (A549) cell lines were incubated with the probe (5 μM) for 40 min. and then followed by the addition of metal species. With the aid of fluorescence microscopy, the differential turn-on response towards Au^{3+} and Hg^{2+} was clearly monitored in the cells. The images taken before and after the addition of the metal species displayed a distinct fluorescence change consistent with the results observed in the solution.

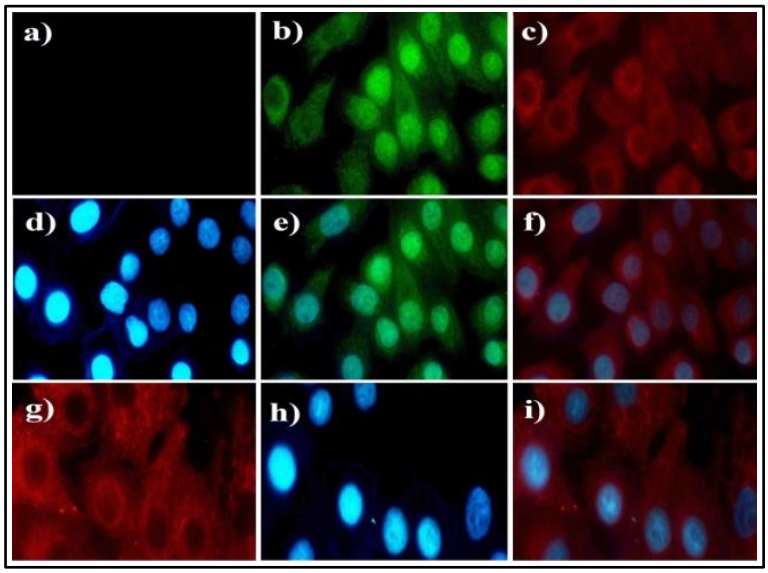

Figure 2.33. a) Fluorescence image of A549 cells treated with only **BOD-2** (5μM); b) Image of cells treated with Au^{3+} (5μM) and probe (5μM) (λ_{ex}=470 nm); c) Cells treated with Au^{3+} (5μM) and probe (5μM) (λ_{ex}=525 nm); d and h) Cells treated with DAPI for 15 min (control); d) Merged image of frame b and d; f) merged image of frame c and d; g) Cells treated with Hg^{2+} (5μM) and probe (5μM) (λ_{ex}=525 nm); l) merged image of frame g and h.

In this part of thesis, the synthesis, spectral properties, and biological application of **BOD-2** was presented. This new sensing strategy offers the detection of Hg^{2+} and Au^{3+}, differentially. Detection of Hg^{2+} and Au^{3+} is realized through two distinct fluorescence changes resulting from Hg^{+2}/ligand coordination or from the Au^{3+} catalyzed hydrolysis of the **C=N** moiety.

2.3.3. Gold Ion Sensing Properties of BOD-3

As in the subject of previous study development of fluorescent molecular sensor enable to differentiate two or more metal ions via different emission modes remains a big challange for scientific community. In previous study an important example of fluorescent probe (**BOD-2**) that allowed the differantiaton of Hg^{2+} and Au^{3+} was demostrated. Notably, the primary weakness of previous investigation is the requirement of two individual fluorophore units to construct the sensor that could elicit a dual signal output.

In this part of the thesis, a new molecular sensor with a single fluorophore core appended with semithiocarbazone functionality as the metal ion recognition motif was designed. The fluorophore core, based on a BODIPY dye, is designed to be inactive (i.e., non-emissive) in its initial state yet expected to become active in response to the metal species (Figure 2.34). The second generation molecular sensor, **BOD-3**, displays a differential signal output for detecting Hg^{2+} and Au^{3+} ions that relies on different modulation mechanisms.

The title compound, **BOD-3**, was prepared (40% overall) by the synthetic route outlined in Figure 2.34. The structure of **BOD-3** was unambiguously confirmed by ^{1}H-NMR, ^{13}C-NMR, and HRMS spectroscopy.

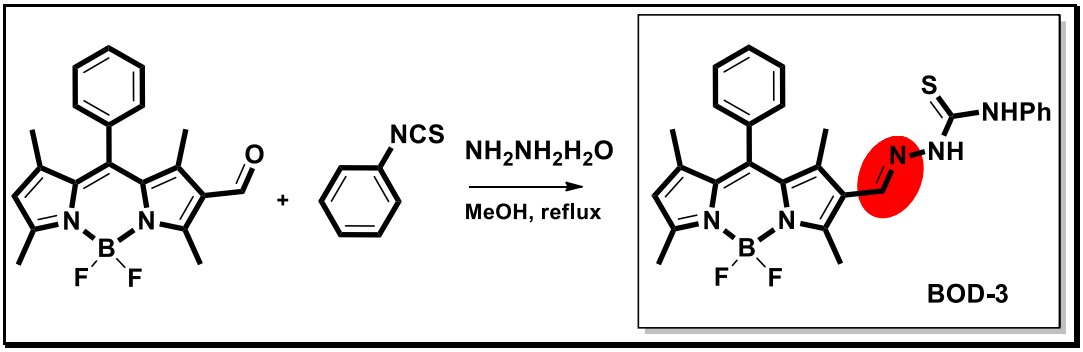

Figure 2.34. Synthesis route of **BOD-3**.

The sensing behaviour of **BOD-3** toward the addition of a range of metal ion species was studied by UV/Vis and fluorescence spectroscopy. The investigation was commenced for the determination of optimal sensing media. Various combinations of solvent systems were first surveyed (EtOH/Phosphate buffer solution (v/v, 1:1, pH =

7.0), CH_3CN/HEPES buffer solution (v/v, 1:1, pH = 7.0) and DMSO/Phosphate buffer solution (v/v, 1:100, pH = 7.0)) and the best results were obtained in EtOH/Phosphate buffer system. The effects of water content and pH changes were further examined, carefully. To close, the optimum sensing media was chosen as 0.1 M phosphate buffer/EtOH (pH 7.0, v/v, 1:4) with 10 μM dye concentration.

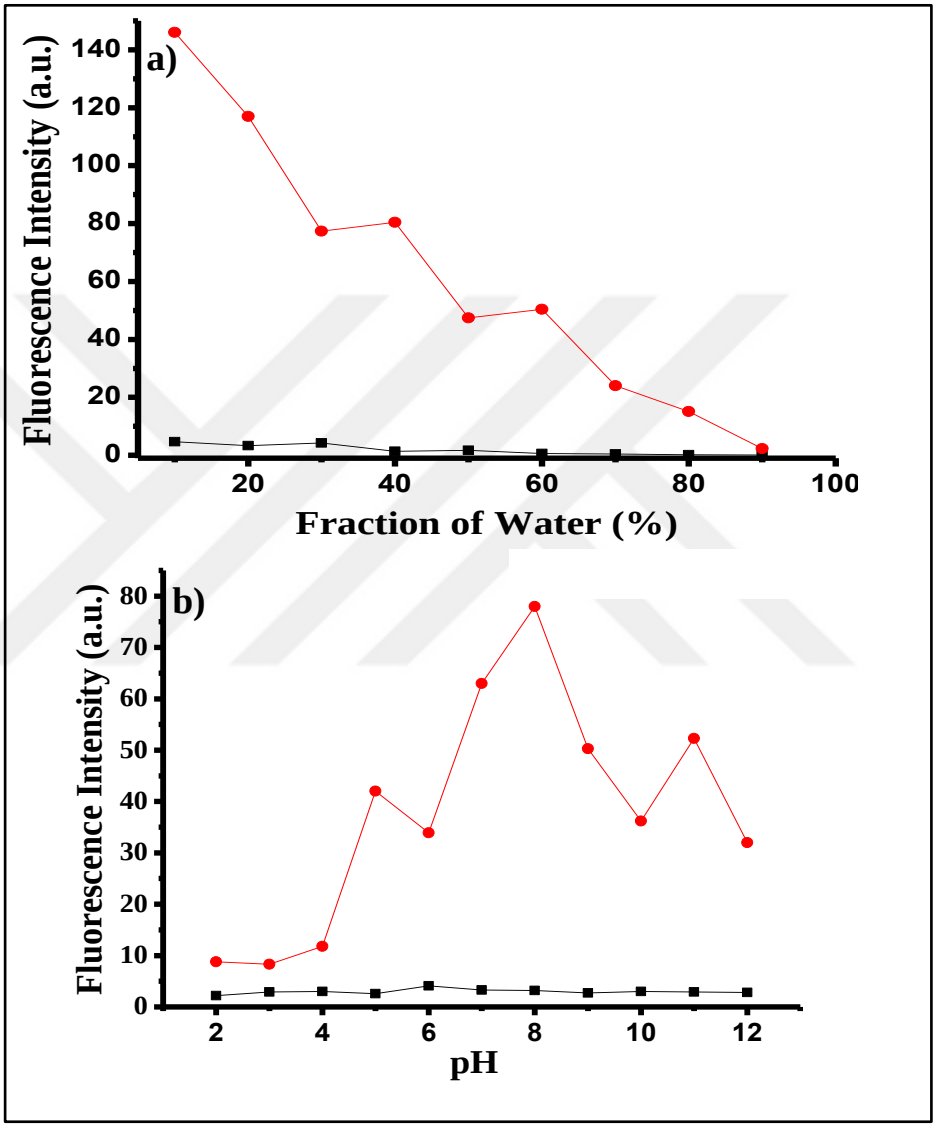

Figure 2.35. a) Effect of fraction of water (pH 7.0/EtOH) and b) Effect of pH (pH/EtOH (v/v, 1:4)) on the interaction of **BOD-3** (10 μM) (black line) with Au^{3+} (200 μM, 20 equiv.) (red line) in 0.1M potassium phosphate buffer, (λ_{ex}: 460 nm, λ_{em}= 512 nm at 25 ^{o}C).

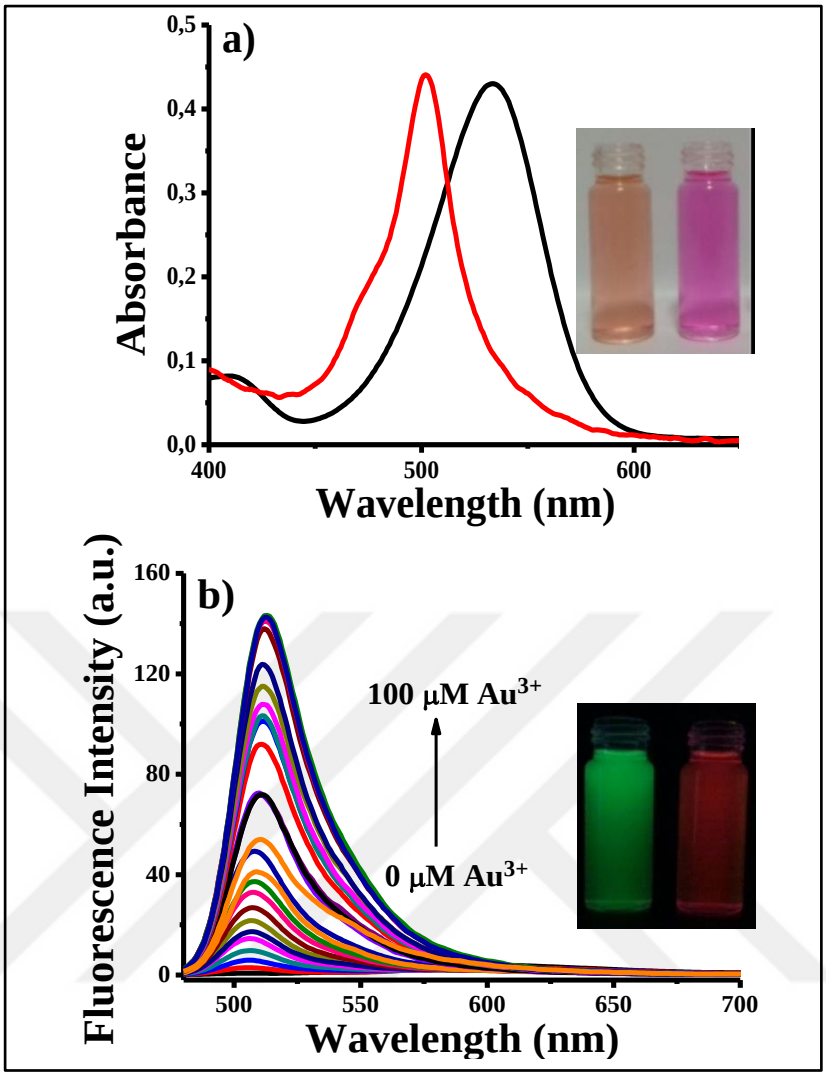

Figure 2.36. a) Absorbance spectra of **BOD-3** (10 μM) in the absence (black line) and presence (red line) of 10 equiv. (100 μM) of Au^{3+}; b) Fluorescence titration spectra of **BOD-3** (10 μM) + Au^{3+} (0.1 to 100 μM, 0.01 to 10 equiv.) in 0.1 M phosphate buffer / EtOH (pH 7.0, v/v, 1:4) (25°C, λ_{ex}=460 nm).

Investigations were begun with the evaluation of the optical behaviour of **BOD-3** in response to the addition of Au^{3+} ions (e.g., $AuCl_3$). The addition of Au^{3+} (1 equiv.) to **BOD-3** prompted the appearance of a new emission band at 512 nm that was assigned to the formation of a new BODIPY derivative (Figure 2.36.b). The appearance of this new band was accompanied with a distinct change in the solution's emission colour; the red-emitting probe solution became distinctly green, as was clearly visible to the naked eye.

A systematic titration of **BOD-3** with Au^{3+} reveals that emission band intensity increases linearly with the increase in concentration of Au^{3+} in the range of 0.1–100

μM. Moreover, the minimum amount of detectable Au^{3+} was evaluated to be 128.0 nM based on the signal-to-noise ratio (S/N=3) (Figure 2.37).

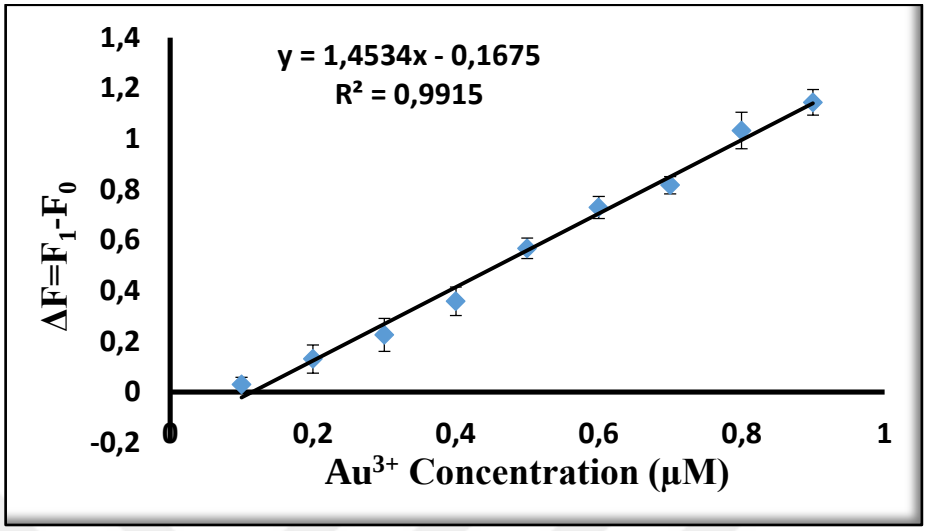

Figure 2.37. Fluorescence changes of **BOD-3** (10 μM) in 0.1 M phosphate buffer/EtOH (pH = 7.0, v/v, 1:4) upon the addition of Au^{3+} (0.01 to 0.1 equiv.) (0.1-1 μM) (25°C, λ_{ex}=460 nm).

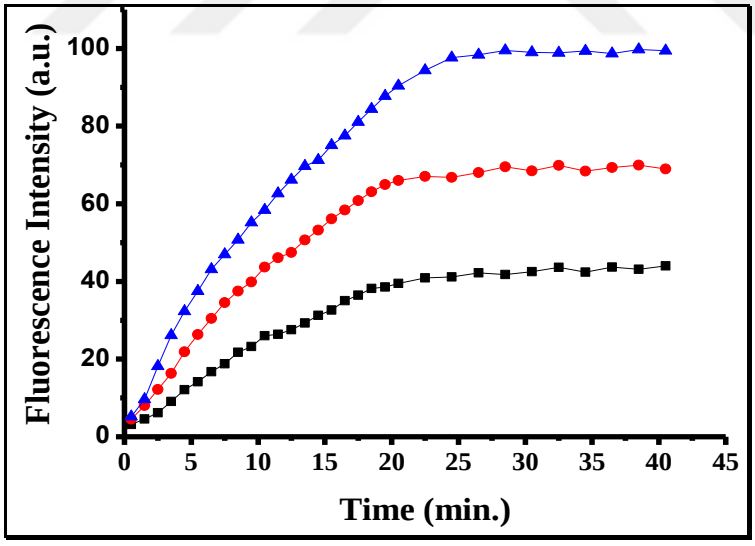

Figure 2.38 Time-dependent fluorescence change of **BOD-3** (10 μM) in the presence of 1.0 (■), 3.0 (●) and 5.0 (▲) equiv. (10, 30 and 50 μM) of $AuCl_3$ measured in 0.1 M phosphate buffer/EtOH (pH = 7.0, v/v, 1:4) (λ_{ex} = 460 nm, λ_{em} = 512 nm).

To get idea about the saturation time of sensing event, the kinetic study was performed and showed that the spectral response toward the addition of Au^{3+} was rapid (<1 min) and that the emission intensity plateaued within 20 min. due to the addition of Au^{3+} in different concentrations, which thereby enhanced intensity by over 200-fold (Figure 2.39).

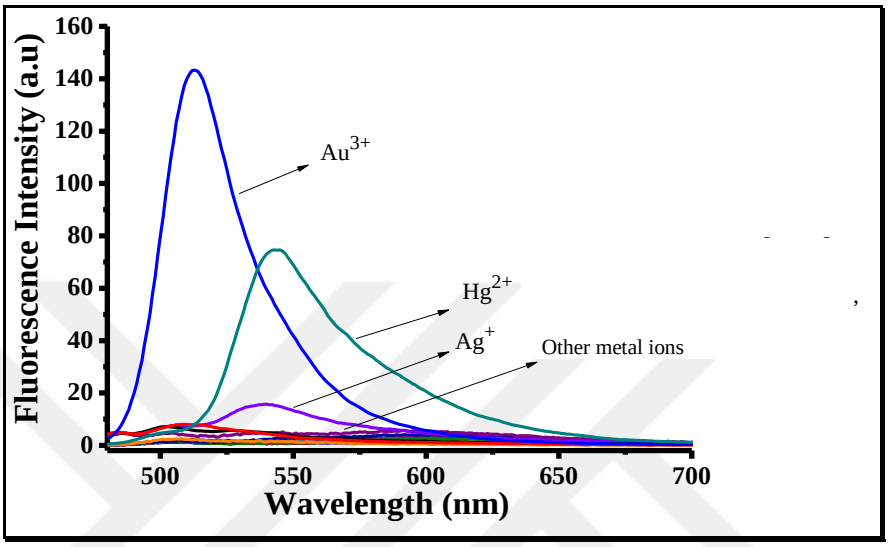

Figure 2.39. Fluorescence intensities of **BOD-3** (10 μM) in 0.1 M phosphate buffer/EtOH (pH = 7.0, v/v, 1:4) in the presence of 20.0 equiv. (200 μM) of the cations of interest: **BOD-3** only , Au^{+} , Ba^{2+}, Ca^{2+}, Cd^{2+}, Cr^{3+}, Cu^{2+}, Fe^{3+}, F^{-}, I^{-}, Li^{+}, Mg^{2+}, Ni^{2+}, Pb^{2+}, Zn^{2+} (λ_{ex} = 460 nm, λ_{em} = 512 nm).

Furthermore, the selectivity profile of **BOD-3** in response to other metal species was investigated. The probe proved to be highly specific for Au^{3+} ions, since no change was detected in the spectrum when Au^{+} ions were present. Furthermore, **BOD-3** showed no spectral response to other metal ions such as Cu^{2+}, Ag^{+}, Zn^{2+}, Pb^{2+}, Ni^{2+}, Na^{+}, Mg^{2+}, Li^{+}, K^{+}, Pd^{2+}, Co^{2+}, Cd^{2+}, Ca^{2+}, Ba^{2+}, Fe^{3+}, and Cr^{3+}, except for Hg^{2+}.

In addition, the fluorescence response of **BOD-3** toward Au^{3+} in the presence of the other metal ions (20 equiv.) was explored in order to assess the possible interference by other metal ions. As shown in Figure 2.40 the tested metal ions displayed no interference with the detection of Au^{3+} ions.

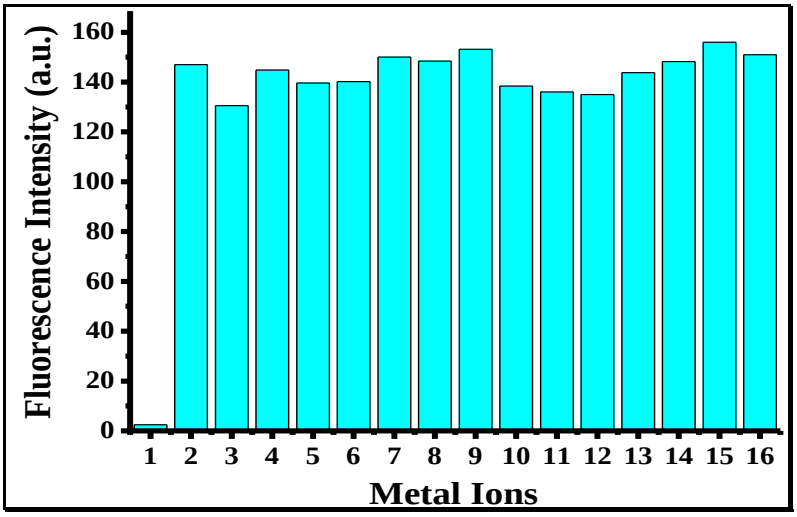

Figure 2.40. Fluorescence intensities of **BOD-3** (10 μM) in 0.1 M phosphate buffer/EtOH (pH = 7.0, v/v, 1:4) in the presence of Au^{3+} and 20.0 equiv. (200 μM) of the cations interest: 1, **BOD-3** only; 2, Au^{3+}; 3, Au^{+} ; 4, Ba^{2+}; 5, Ca^{2+}; 6, Cd^{2+}; 7, Cr^{3+}; 8, Cu^{2+}; 9, Fe^{3+}; 10, K^{+}; 11, Li^{+}; 12, Mg^{2+}; 13, Ni^{2+}; 14, Zn^{2+}; 15, Ag^{+}; 16, F^{-} (λ_{ex} = 460 nm, λ_{em} = 480 nm).

The mechanistic study indicated us the sensing event proceeds via the same **C=N** hydrolysis mechanism to produce formylated BODIPY derivative as in the case of previous studies. The outcome of the study was monitored by TLC and characterized with spectroscopic methods (Figure 2.41).

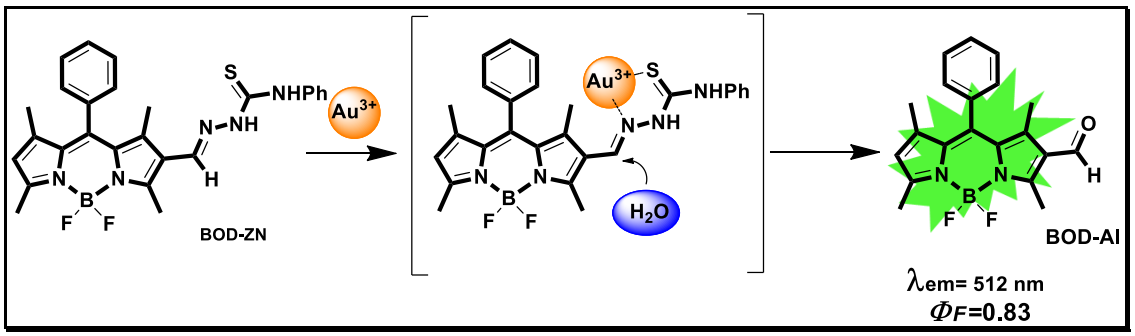

Figure 2.41. Hydrolysis mechanism of **BOD-3** in the presence of Au^{3+} ions.

Relying on the impressive sensing properties of **BOD-3**, its capacity for imaging Hg^{2+} and Au^{3+} ions in living cells were next investigated. As shown in Figure 42.a and 42.a', the images of Human Lung Adenocarcinoma (A549) cells incubated with **BOD-3** did not display any fluorescence until the addition of the metal species. However, upon incubation with Au^{3+} or Hg^{2+}, the cells started to emit a distinct fluorescence emission

consistent with results obtained in the solution. Based on the nucleus staining experiment using DAPI as the staining dye, it was concluded that the probe passes through the cell membrane and detects both metal species from within the cell. This preliminary cell imaging study suggested that **BOD-3** can be used efficiently for the in vitro imaging of Au^{3+} and Hg^{2+} species in living cells.

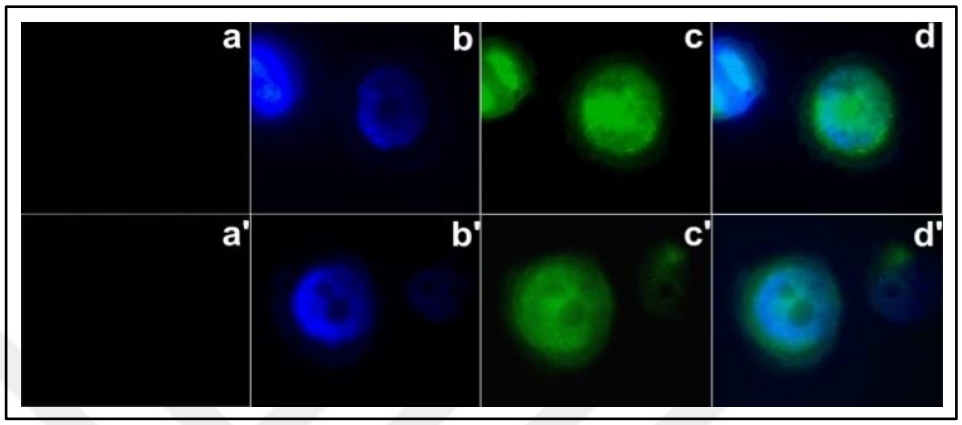

Figure 2.42. Fluorescence images of Human Lung Adenocarcinoma cells (A549). a,a') Fluorescence image of A549 cells treated with only **BOD-3** (10 μM); b, b') Fluorescence image of cells treated with DAPI (control); c, c') Fluorescence image of cells treated with **BOD-3** (10 μM) and Au^{3+} (10 μM) or Hg^{2+} (10 μM) (λ_{ex} = 460 nm); d, d') merged images of frames b-c or b'-c'.

All in all, the study offers the advantage of differential detection of Au^{3+} and Hg^{2+} ions with a single fluorophore via two distinct emission modes. Also, the **BOD-3** is able to detect gold and mercury ions in A549 cells. This strategy opened a new era for Au^{3+} ion sensing with a new receptor unit being a pioneering study.

2.3.4. Gold Ion Sensing Properties of BOD-4

As indicated above, most of the existing gold ion sensors are based on specific chemical reactions that exploit the exceptional catalytic behaviour of gold species. In general, the optical signal is recognized as either an increase ("turn-on") or a decrease ("turn-off") in emission intensity without any noticeable change in emission wavelength. Importantly, measurements based on intensity changes are easily influenced by a host of environmental factors, including concentration variations and intensity of excitation.

By contrast, measuring optical signals as intensity ratios at two different wavelengths provides a built-in correction for the environmental effects and may assuage many of the problems associated with intensity-based sensors. Interestingly, the ratiometric recognition of gold ions by a single fluorescent probe structure is currently uncommon. Two of those examples in recent literature are smart extensions of intensity-based sensors that benefit from the FRET (i.e., fluorescence resonance energy transfer) principle to achieve ratiometric response (Seo et al., 2012; Cao et al., 2011).

In response, here the design, synthesis, spectral behaviour, and living cell application of a fluorescent probe, **BOD-4**, which displays a sensitive, highly selective ratiometric response to gold ions and, surprisingly, Hg^{2+} ions as well, was presented.

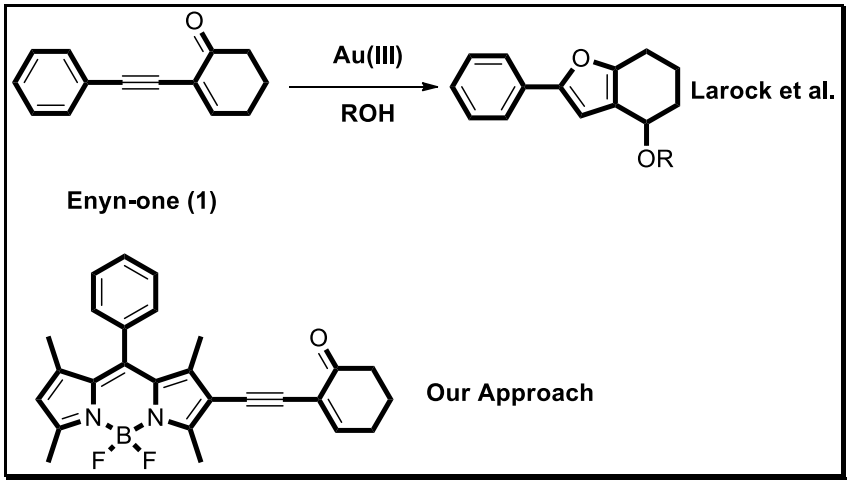

Figure 2.43. Work of both our and the Larock group.

In this sensing approach, we drew inspiration from a gold-catalysed intramolecular cyclization reaction presented years ago by Larock et al. (Figure 2.43) (Yao et al., 2004). It was reported that Enyn-one (1) transforms rapidly into a new furan (2) derivative in the presence of a catalytic amount of $AuCl_3$. By extension, our attention focused chiefly on exploiting this unique chemical transformation as a signal-transducing event for the recognition of gold ions.

The title compound **BOD-4** investigated in this study was prepared according to the synthetic route outlined in Figure 2.44. Following a Sonogashira coupling protocol, the acetylene derivative of BODIPY (**BODIPY-ACET**) prepared in three individual steps was coupled with 2-iodocyclohex-2-enone to give the desired probe structure in a moderate yield. The structure of the probe was clearly confirmed by NMR and HRMS analysis.

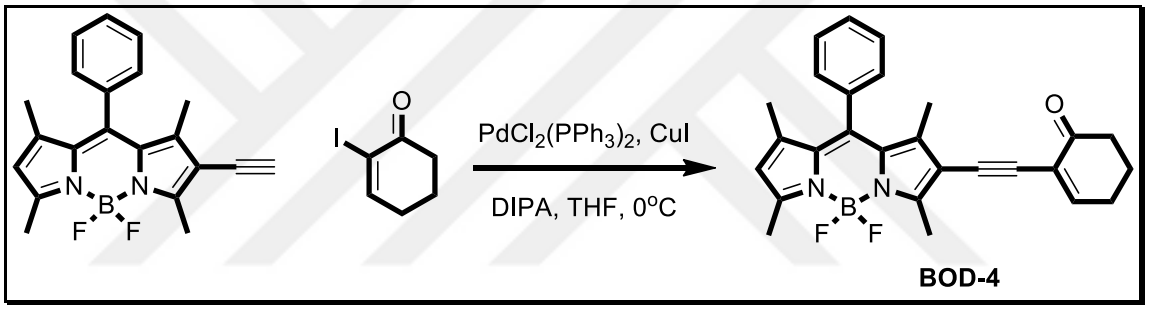

Figure 2.44. Synthesis route of **BOD-4**

The most appropriate sensing condition towards Au^{3+} ions was investigated by screening various parameters such as solvent system, water content and pH of media. The optimal condition was determined as 0.1M phosphate buffer:ethanol 6:4 (v/v), pH 7.0 with 5μM dye concentration.

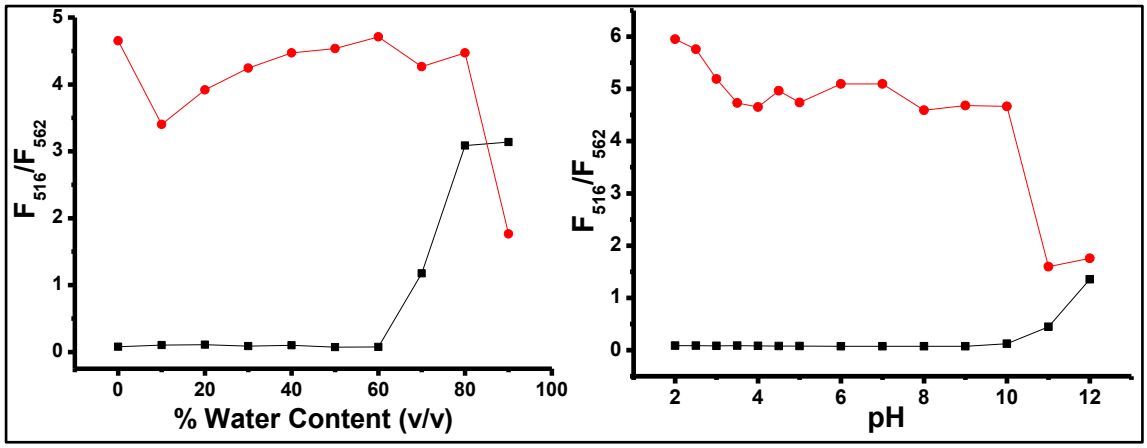

Figure 2.45. a) Effect of fraction of water (in 0.1M potassium phosphate buffer pH 7.0/EtOH) and b) Effect of pH (in 0.1M potassium phosphate buffer pH/EtOH (v/v, 6:4)) on the interaction of **BOD-4** (5 μM) (black line) with Au^{3+} (10 μM, 2 equiv.) (red line), (λ_{ex}: 460 nm, λ_{em}= 516 nm at 25 ^{o}C).

The probe's spectroscopic behaviour towards the added metal species was systematically investigated with the aid of UV-Vis and fluorescence spectroscopy. As depicted in Figure 2.46.a, the absorbance spectrum of free **BOD-4** (phosphate buffer:ethanol 6:4, pH 7.0) displays a maximum absorption band at 526 nm, while its fluorescence spectrum collected upon excitation at 460 nm exhibits an intense emission band at 562 nm, which belongs to the BODIPY chromophore.

Our investigation resumed with an evaluation of the optical behaviour of **BOD-4** in response to the addition of Au^{3+} ions (e.g., $AuCl_3$). The spectral changes of the probe in the absence and presence of Au^{3+} ions appear in Figure 2.46. As shown there, the addition of Au^{3+} (2 equiv.) to **BOD-4** prompted the appearance of a new emission band at 516 nm, with a concomitant decrease in the emission band at 562 nm. As anticipated, when the probe solution was treated with $AuCl_3$, the orange-emitting probe solution became distinctly green, as was clearly visible to the naked eye. The dramatic change in colour of the solution was attributed to a change of the BODIPY dye structure. Moreover, green emission was evidence of the existence of a non-conjugated BODIPY derivative.

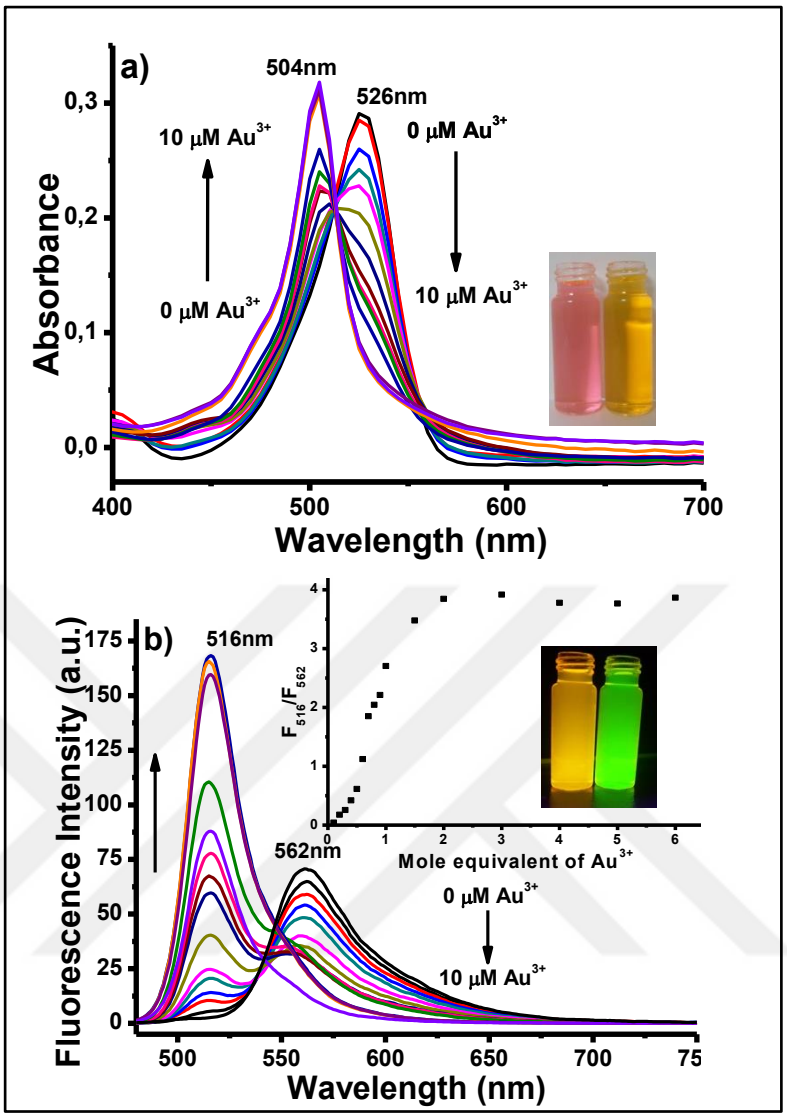

Figure 2.46. a) Absorbance and b) Fluorescence titration spectra of **BOD-4** (5 μM) + Au^{3+} (0.005 to 10 μM), 0.001 to 2 equiv.) in 0.1 M phosphate buffer / EtOH (pH 7.0, v/v, 6:4).Inset: Calibration curve.

This suggestion was supported by the outcome of the reaction of **BOD-4** mediated by Au^{3+}, controlled by using TLC. The green emissive compound, clearly followed on the TLC plate, was isolated and further characterized by NMR and HRMS as **BODIPY-FUR**, the cyclization product of **BOD-4** (Figure 2.47). Evidently, the recognition of Au^{3+} was achieved by an Au^{3+}-mediated cyclization reaction that resulted in the formation of a highly emissive BODIPY-furane derivative (**BODIPY-FUR**).

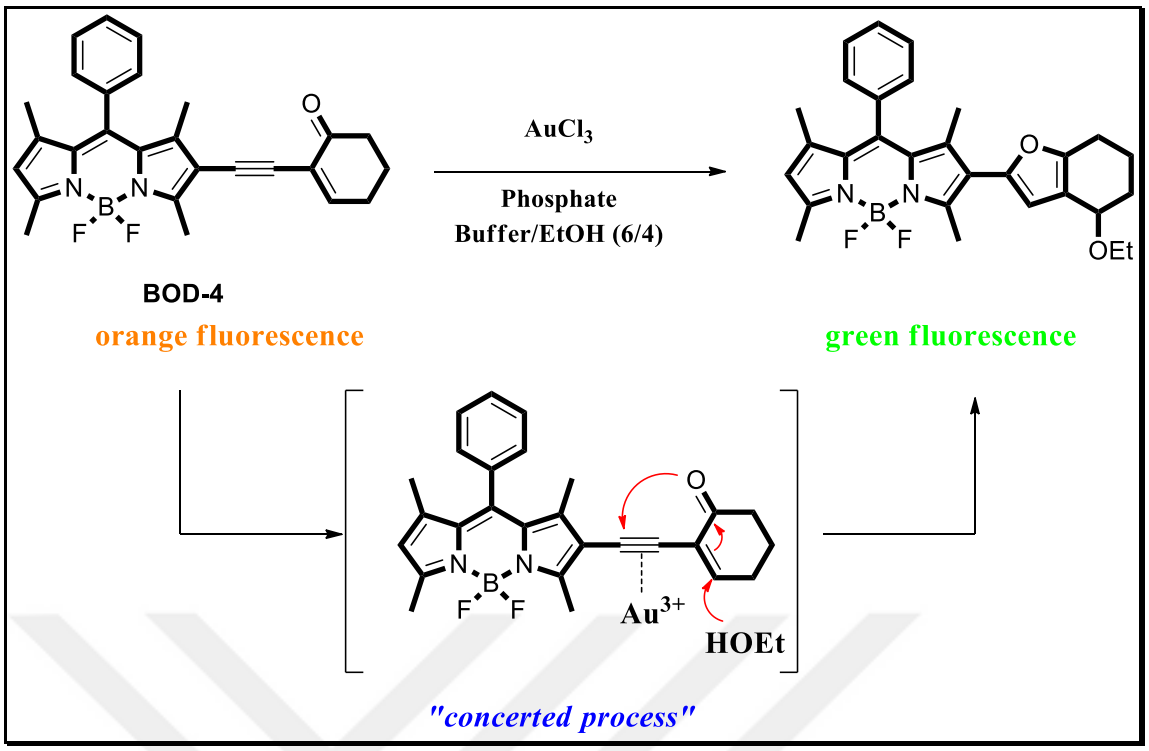

Figure 2.47. Proposed reaction mechanism for the detection of gold ions

As consistent with findings reported in the literature, the recognition of Au^{3+} is suggested to proceed via a concerted process initiated by the activation of the triple bond by the metal species. This process follows a conjugate addition of oxygen nucleophile that promotes intramolecular cyclization and yields a new BODIPY structure appended with a furan motive, which displays the distinct colour and emission in the solution.

The systematic titration of **BOD-4** with Au^{3+} revealed that the ratiometric change of emission intensities at both wavelengths linearly correlated with the increased concentration of Au^{3+} in the range of 0.005–10 μM. Moreover, the minimum amount of Au^{3+} detectable was evaluated to be 8 nM, one of the lowest detection limits reported in fluorescence-based gold ion sensing. Meanwhile, a similar spectral trend was observed in the presence of Au^{+} species, revealing that the probe operates efficiently for both oxidation states of gold in a non-discriminative manner.

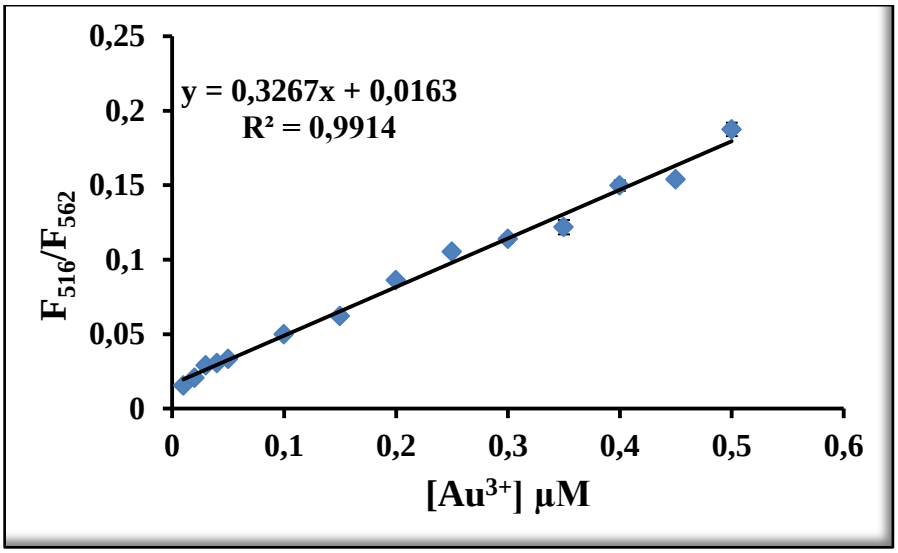

Figure 2.48. Fluorescence changes of **BOD-4** (5.0 µM) upon addition of Au^{3+} (0,005 to 0,5 µM, 0. 001 to 0.1 equiv.) in 0.1M potassium phosphate buffer, pH 7.0/EtOH (v/v, 6:4) (λ_{ex}: 460 nm, at 25 ^{o}C).

At the same time, kinetic study showed that the spectral response towards the addition of Au^{3+} was rapid (<1 min) and that emission intensity at 516 nm plateaued within 40 min due to the addition of 2 equiv. of Au^{3+}, which thereby enhanced intensity at 516 nm by more than 70-fold.

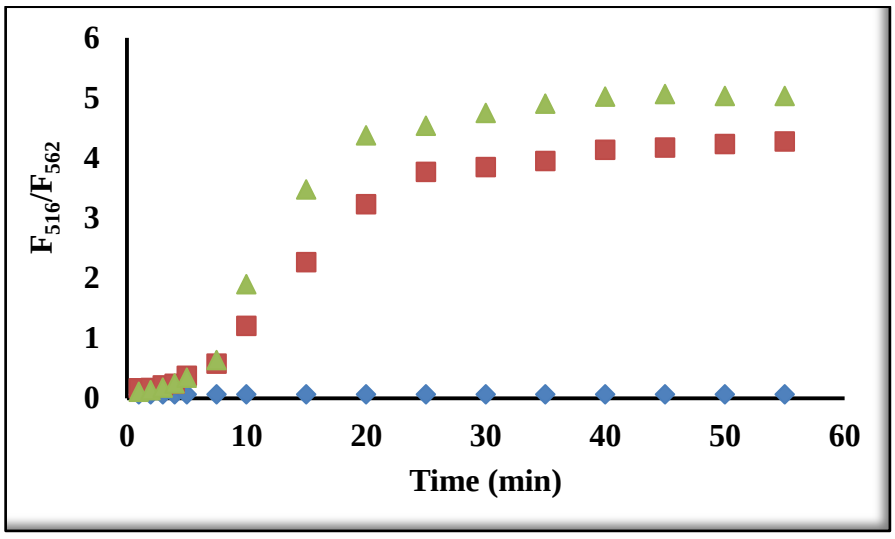

Figure 2.49. Reaction time profiles of **BOD-4** (5 µM) in the absence (♦) or presence of Au^{3+} [5 (■), 10(▲) µM]. The fluorescence intensities were continuously monitored at time intervals in 0.1 M phosphate buffer/EtOH (pH 7.0, v/v, 6:4) (λ_{exc}=460 nm at 25 ^{o}C).

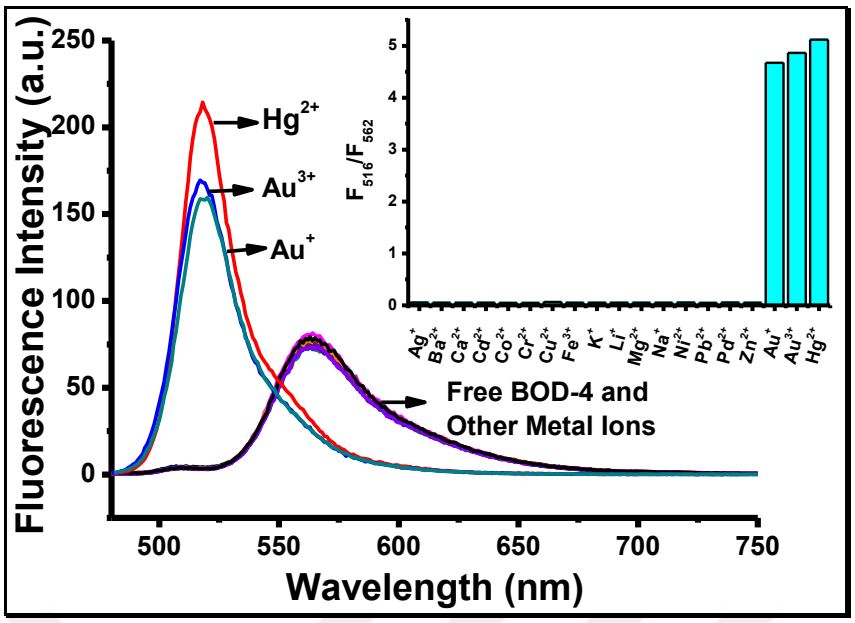

Figure 2.50. Fluorescence intensities of **BOD-4** (5 μM), **BOD-4** (5 μM) + Au^{3+} (25 μM, 5 equiv.), **BOD-4** (5 μM) + other metal ions (50 μM, 10 equiv.) in 0.1M potassium phosphate buffer, pH 7.0/EtOH (v/v, 6:4) (λ_{ex}: 460 nm, at 25 ^{o}C). Inset: Bar graph notation.

The selectivity profile of **BOD-4** was surveyed by screening the spectral response towards metal species, including Zn^{2+}, Cd^{2+}, Ba^{2+}, Cu^{2+}, Li^{+}, K^{+}, Ni^{2+}, Cr^{2+}, Mg^{2+}, Fe^{3+}, Pb^{2+}, Hg^{2+}, Co^{2+}, and Ag^{+} (Figure 2.50). Surprisingly, in the presence of Hg^{2+} ions the probe displayed the exact sensing behaviour as in the detection of gold species. Similar to the gold ion sensing event, with the addition of Hg^{2+} a new peak band appeared at 516 nm, while the band at 562 nm decreased with an increased concentration of Hg^{2+} ions. This unexpected observation was reasonable, for Hg^{2+} ions similar to Au^{3+} species are known to have high affinities to alkynes.

Having clarified the nature of detecting both metal species, the possible interference of other metal species in the detection of Au^{3+} was next assessed. As shown in Figure 2.51, the response of **BOD-4** towards gold species remained unaffected in the presence of other competitive metal species.

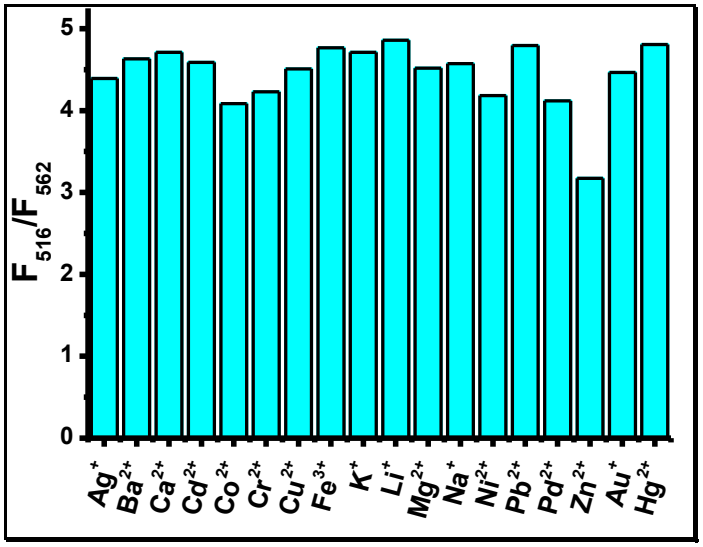

Figure 2.51. Fluorescence intensities of **BOD-4** (5 μM) in the presence of Au^{3+} (10 μM, 2 equiv.) and 10 equiv. of other metal ions in 0.1 M phosphate buffer/EtOH (pH 7.0, v/v, 6:4) (λ_{exc}=460 nm at 25 ^{o}C)

Since **BOD-4** constitutes all of the desirable features necessary for tracking species in a living milieu, its sensing capacity in living cells was assessed. To this end, Human Lung Adenocarcinoma cells (A-549) were incubated first with the probe (10 μM), to which was added Au^{3+} or Hg^{2+} (10μM) to be incubated for another 60 min. The cells were also stained with a nucleus-staining dye (DAPI) for another 10 min. With the aid of fluorescence microscopy, the fluorescence images of the cells were taken before and after the addition of the metal species. As Figure 2.52 clearly shows, the cells incubated with **BOD-4** emitted a red fluorescence in the absence of the metal species, while following Hg^{2+} or Au^{3+} accumulation they emitted a characteristic green BODIPY emission, which agrees well with the spectral response obtained in the solution phase. Based on the nucleus counter-stain experiment and from the distinct change in cell fluorescence emission, we conclude that the probe passes through the cell membrane and detects Au^{3+} and Hg^{2+} from within the cell, particularly in the cytosol.

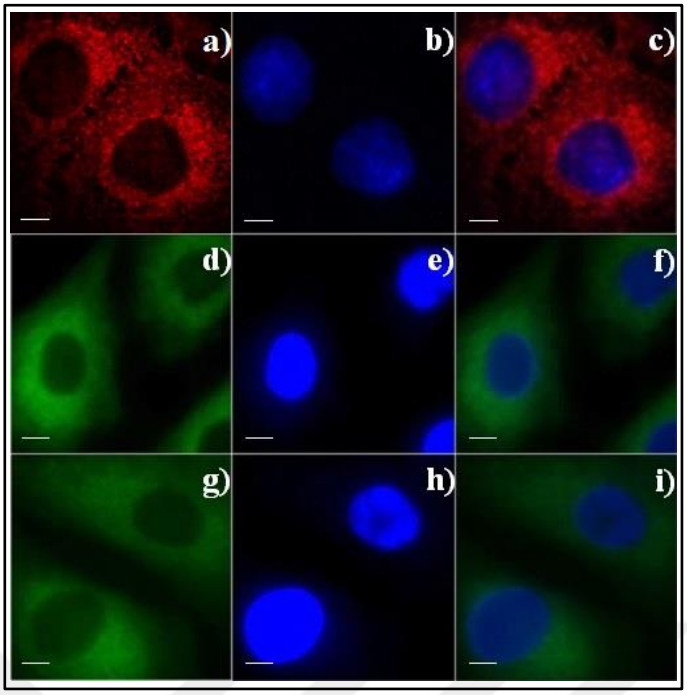

Figure 2.52. Fluorescence images of Human Lung Adenocarcinoma cells (A549). a) Fluorescence image of A549 cells treated with only **BOD-4** (10 μM); b, e, h) Fluorescence image of cells treated with DAPI (control); d, g) Fluorescence image of cells treated with **BOD-4** (10 μM) and Au^{3+} (10 μM), Hg^{2+} (10 μM); c, f, i) merged images of frames a-b, d-e and g-h (λ_{ex} = 460 nm). Scale bar represents 10 μm.

To close, in this part of thesis a molecular sensor bearing Enyn-one functionality was constructed and its sensor ability towards addition of gold and mercury ions was surveyed. Unfortunately, the probe did not offer differential detection but if the conditions fixed properly, probe able to detect mercury (II) ions selectively that will be mentioned into the next chapter.

2.3.5. Gold Ion Sensing Properties of BOD-5

Up to now, examples of fluorescent probes based on the ratiometric detection of gold ions are still inadequate, which is due to the absence of effective strategies and guidelines for the design of ratiometric fluorescent molecules. In previous episode of chapter the significancy of constructing new ratiometric probes was elucidated briefly. The major drawback of **BOD-4** was its cross affinity towards Hg^{2+} ions that have the similar chemical nature and reactivity. In this context, a new strategy for the ratiometric sensing of gold ions, drawing upon a gold ion triggered transformation of a highly conjugated probe structure into non-conjugated one, thereby, enabling recognition of gold species as a ratio of two distinct emission wavelengths selectively was introduced.

The extent of π-conjugation within the fluorophore/chromorphore structure has a dramatic effect on the frontier orbital energy levels (HOMO/LUMO) of the molecules. More specifically, extending the conjugation of fluorescent dye decreases the energy difference between the frontier orbitals, this most often results in a red shift of absorption and emission wavelengths.

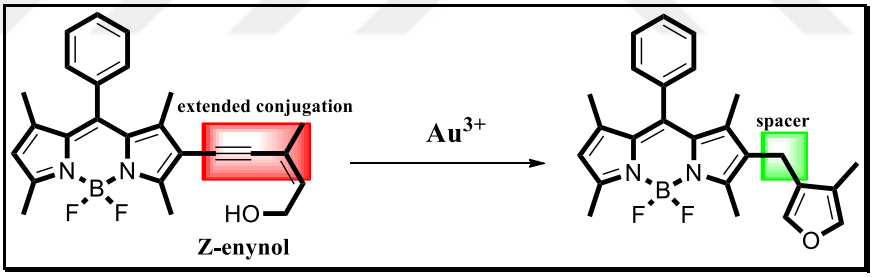

Figure 2.53. The rationale of ratiometric sensing

Based on these considerations, **BOD-5** was designed and constructed by integrating a *Z*-enynol motif to a BODIPY-based fluorophore scaffold with the expectation of generating a highly π-conjugated BODIPY derivative emitting at a wavelength distinctly longer than its unmodified scaffold (Figure 2.53).

The fluorescent probe, **BOD-5**, was prepared through a straightforward synthetic pathway as outlined in Figure 2.54. Mono-iodo derivative of BODIPY (**BODIPY-I**), which was prepared individually, was coupled with *Z*-enynol ((*Z*)-3-methylpent-2-en-4-yn-1-ol) according to a Sonogashira coupling protocol to give the desired probe structure in a moderate yield. The identity of the title compound, purified after

chromatographic techniques, was clearly confirmed by NMR spectroscopy and mass spectrometry. Furthermore, based on the same synthetic route **BOD-9**, the *E*-enynol isomer of the probe, was also prepared in order to comparatively investigate the mechanism of gold ion detecting.

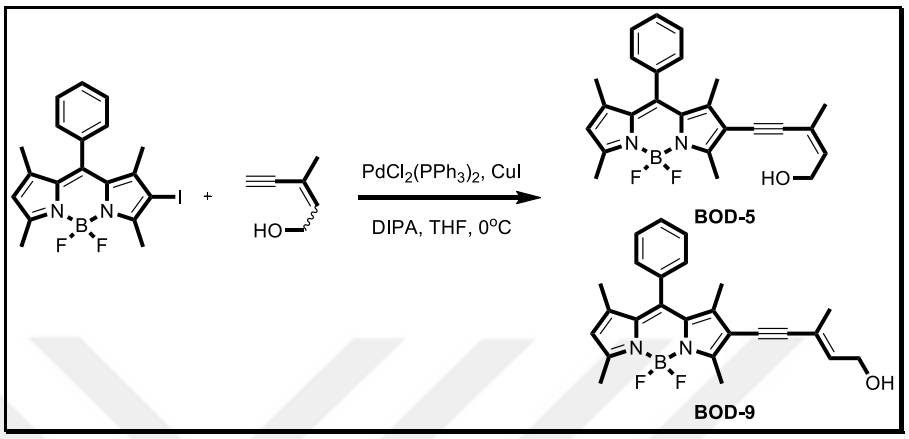

Figure 2.54. Synthesis route of **BOD-5** and **BOD-9**

The spectral investigation began with screening the optical behaviour of the probe in response to addition of gold ions. Various sensing environments were screened to obtain most proper sensing conditions for gold ions. The optimal condition was determined as 0.1 M potassium phosphate buffer pH/EtOH (v/v, 7:3) with 10 μM dye concentration.

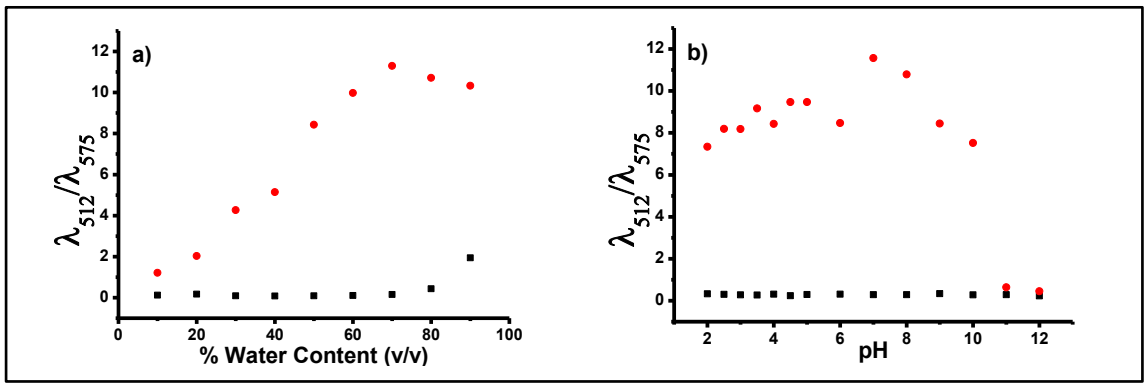

Figure 2.55. a) Effect of fraction of water (in 0.1M potassium phosphate buffer pH 7.0/EtOH) and b) Effect of pH (in 0.1M potassium phosphate buffer pH/EtOH (v/v, 7:3)) on the interaction of **BOD-5** (10 μM) (black line) with Au^{3+} (200 μM, 20 equiv.) (red line), (λ_{ex}: 460 nm, emission wavelengths: λ_{512}/ λ_{575} at 25 ^{o}C).

In the absence of any analyte species, **BOD-5** displays a single absorption band at 532 nm (Figure 2.56.a). Meanwhile, in the fluorescence spectrum of **BOD-5**, collected upon excitation at 460 nm, a long wavelength emission band at 575 nm can be clearly monitored. As proposed, upon addition of $AuCl_3$ (20 equiv.) a new emission band at 512 nm appeared, with a concomitant sharp decrease in the emission band intensity at 575 nm (Figure 2.56.b). The response of the probe towards gold was clearly visible to the naked eye. Namely, in the presence of gold species the orange-emitting probe solution became distinctly green, which was attributed to a structural modification of the dye structure.

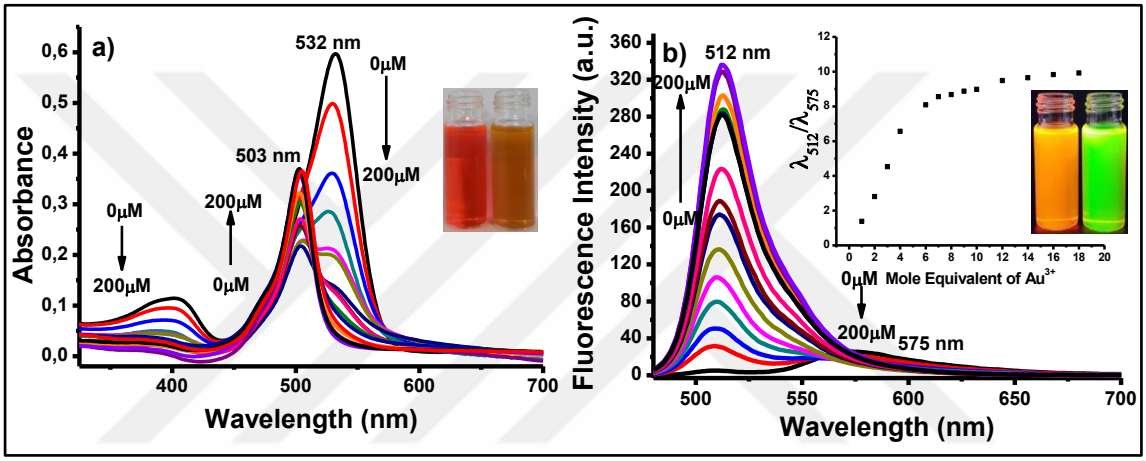

Figure 2.56. a) Absorbance and b) Fluorescence titration spectra of **BOD-5** (10 μM) + Au^{3+} (1 to 200 μM), 0.1 to 20 equiv.) in 0.1 M phosphate buffer / EtOH (pH 7.0, v/v, 7:3). Inset: Calibration curve.

The investigations were continued with the systematic addition of the gold ions to the probe solution. Upon addition of Au^{3+} ions (0–20 equiv.) the absorption band at 532 nm decreased gradually, with a concomitant and linear increase of a new absorbance band at 503 nm. A similar trend was observed in its fluorescence emission behaviour. With an increasing concentration of Au^{3+} across a wide concentration range the intensity of fluorescence emission at 512 nm increased linearly. Under the optimum sensing conditions, the detection limit of **BOD-5** for detecting Au^{3+} was evaluated to be 293 nM, based on the signal-to-noise ratio (S/N=3).

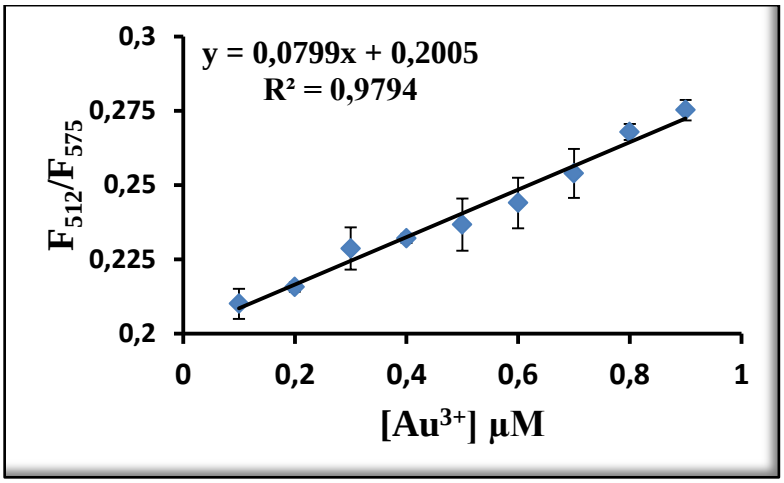

Figure 2.57. Fluorescence changes of **BOD-5** (10.0 µM) upon addition of Au^{3+} (0. 1 to 0.9 µM, 0.01 to 0.09 equiv.) in 0.1M potassium phosphate buffer, pH 7.0/EtOH (v/v, 7:3) (λ_{ex}: 460 nm, emission wavelengths: λ_{512}/ λ_{575} at 25 ^{o}C).

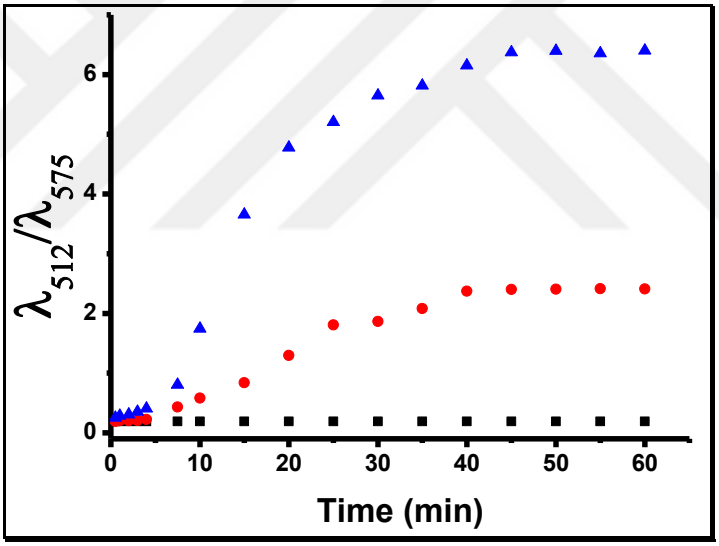

Figure 2.58. Reaction time profiles of **BOD-5** (10 µM) in the absence (■) or presence of Au^{3+} [10 (●), 30(▲) µM.]. The fluorescence intensities at 512 nm and 575 nm were continuously monitored at time intervals in 0.1 M phosphate buffer/EtOH (pH 7.0, v/v, 7:3) (λ_{ex}: 460 nm, emission wavelengths: λ_{512}/ λ_{575} at 25 ^{o}C).

The response of **BOD-5** to Au^{3+} was exceptionally fast (<5 min) and within a couple of minutes the enhancement of the emission intensity (>75 fold) became completely saturated. A 57-fold enhancement (from 0.23 to 13.15) in emission ratio was achieved when 20 equiv. of gold was introduced.

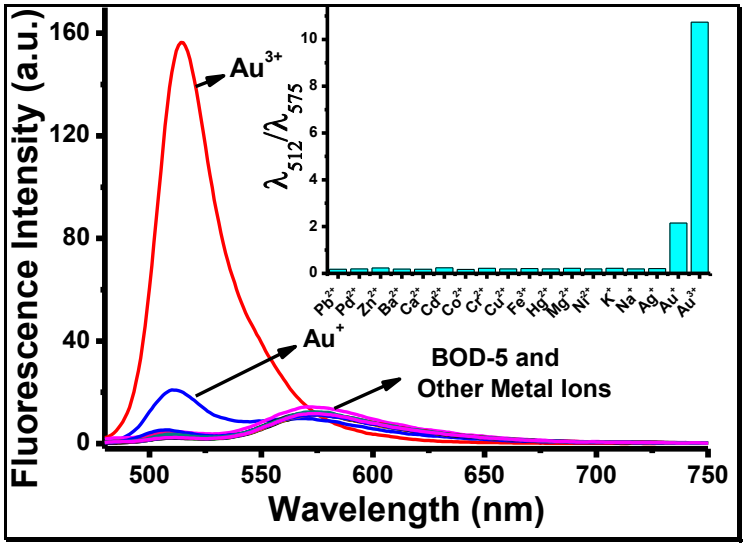

Figure 2.59. Fluorescence intensities of **BOD-5** (10 μM), **BOD-5** (10 μM) + Au^{3+} (100 μM, 10 equiv.), **BOD-5** (10 μM) + other metal ions (200 μM, 20 equiv.) in 0.1M potassium phosphate buffer, pH 7.0/EtOH (v/v, 7:3) (λ_{ex}: 460 nm, at 25 ^{o}C). Inset: Bar graph notation.

Moreover, no obvious spectral changes were noticed for the competing alkynophlic metal species such as Ag^{+}, Ni^{2+}, Pd^{2+}, Hg^{2+}, Cu^{2+}, and for other metal species such as Mg^{2+}, Mn^{2+}, Pb^{2+}, Zn^{2+}, Cd^{2+}, Fe^{3+}, K^{+}, Li^{+}, Ba^{2+}, Ca^{2+}. Delightfully, other metal ions did not interfere with detection of gold ions. Namely, the spectral response induced by Au^{3+} ions was not affected in the presence of any of these metal species. These results indicated that **BOD-5** could properly detect Au^{3+} ions in the mixtures of other related species.

To get information about the mechanism of the sensing event, the outcome of reaction of **BOD-5** and Au^{3+} ions was isolated. A new green emissive compound was monitored on the TLC (Thin Layer Chromotography) plate that indicated us the formation of a new non-conjugated BODIPY derivative. After chromatographic purification the structure of this new BODIPY derivative was confirmed by NMR Spectroscopy and High Resolution Mass Spectrometry (ESI-TOF) as **BODIPY-FUR**; the intramolecular cyclization product of **BOD-5**.

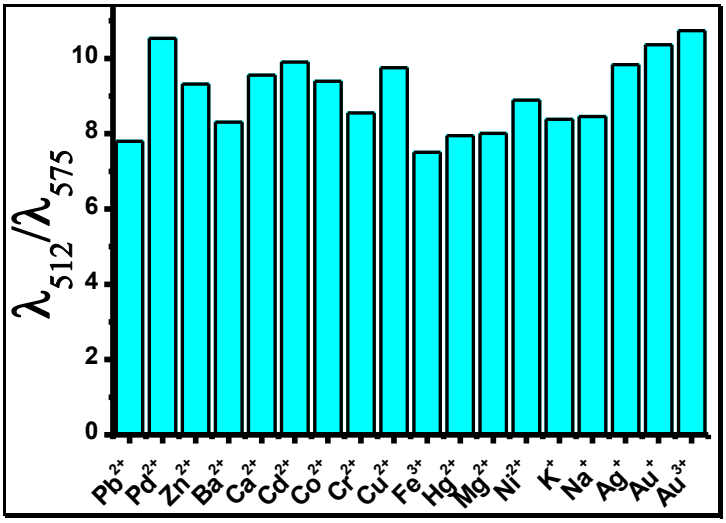

Figure 2.60. Fluorescence intensities of **BOD-5** (10 μM) in the presence of Au^{3+} (200 μM, 20 equiv.) and 20 equiv. of other metal ions in 0.1 M phosphate buffer pH 7.0/EtOH (v/v, 7:3) (λ_{ex}: 460 nm, emission wavelengths: λ_{512}/ λ_{575} at 25 °C).

The sensing mechanism, analogous to what has been previously reported in the literature, is proposed to proceed via activation of triple bond by Au^{3+} and subsequent intramolecular 5-*exo-dig* cyclization from hydroxyl group to the triple bond forming a vinylgold intermediate, which through a rapid isomerization and protonolysis pathway, affords the BODIPY-furan structure (**BODIPY-FUR**).

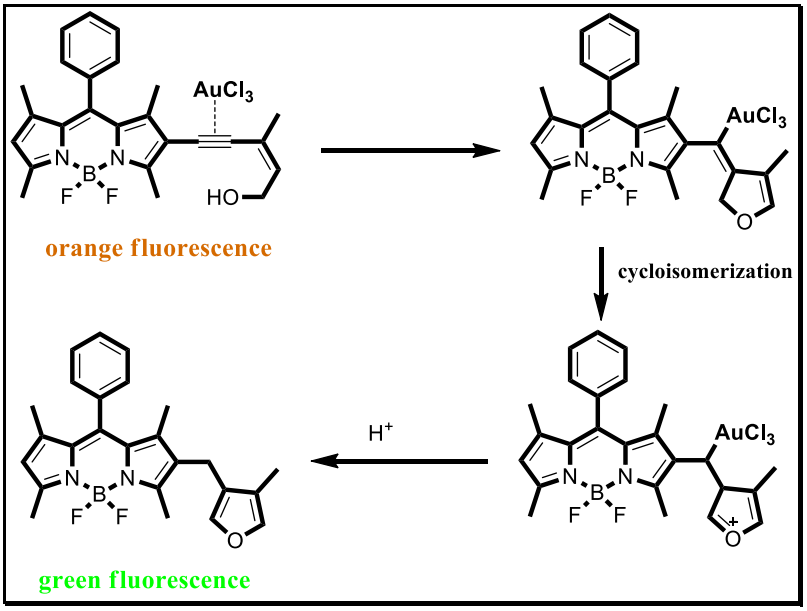

Figure 2.61. Proposed mechanism for Au^{3+} triggered intramolecular cyclization

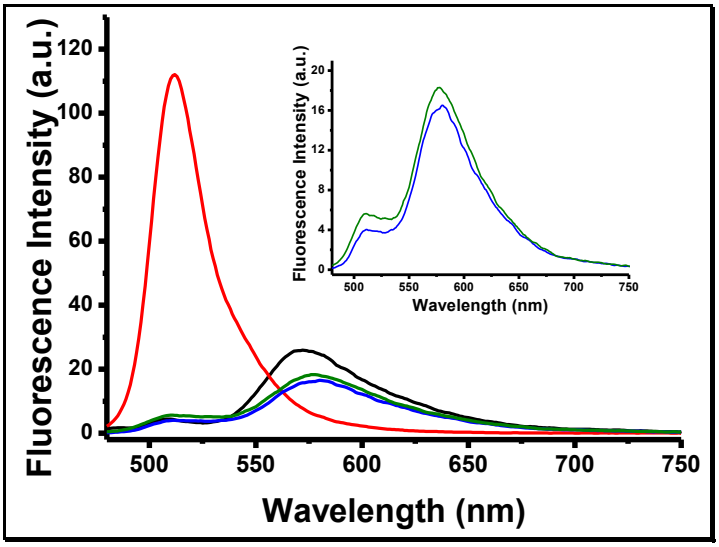

Figure 2.62. Fluorescence responses of **BOD-5** (10 μM) and **BOD-9** (10 μM) in reaction conditions (0.1 M phosphate buffer/EtOH (pH 7.0, v/v, 7:3) (λ_{exc}=460 nm at 25 ^{o}C). [(**BOD-5):** black line, (**BOD-5**+ Au^{3+} (100 μM)): red line, (**BOD-9**): blue line and (**BOD-9** + Au^{3+} (100 μM)): green line]

In sharp contrast to **BOD-5**, the *E*-stereoisomer of the probe, **BOD-9**, under identical sensing conditions was inert towards gold as well as to other metal species. Consistent with the proposed mechanism and in agreement with literature reports, the addition of Au^{3+} could not alter the emission pattern of **BOD-9** indicating the sensing process to be highly stereo-selective in nature.

Relying on the promising photo-chemical/physical properties of **BOD-5**, including fast response time, unique gold ion specificity, exceptionally low detection limit, high fold ratiometric change, etc., its potential for tracking Au^{3+} ions in living cells was next evaluated. To this end, A549 Human Lung Adenocarcinoma cells were incubated with **BOD-5** (10 μM) for 20 min, followed by incubation with Au^{3+} (20 μM) for another 20 min. Using fluorescence microscopy, the sensing behaviour of the probe towards Au^{3+} was clearly monitored in the cells (Figure 2.63). In consistent with the results observed in the solution, after incubation with Au^{3+} the orange emissive cells turned immediately into to green emissive ones, unambiguously proving that **BOD-5** is cell-membrane permeable and has a great potential to be used for in vitro imaging of Au^{3+} in living cells.

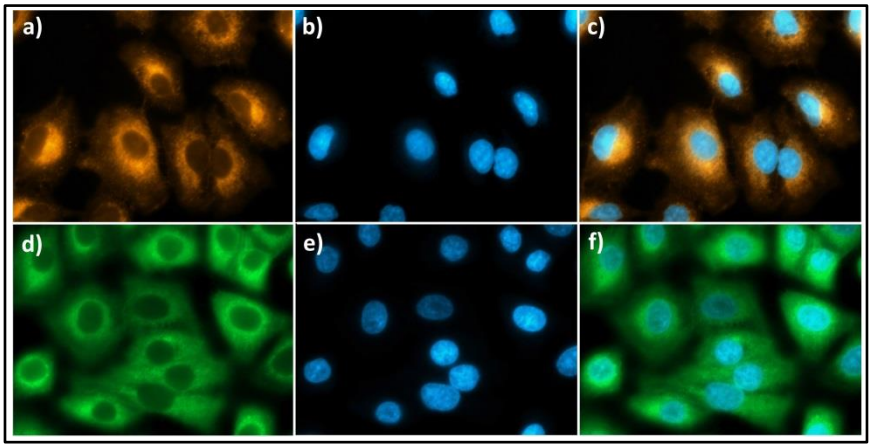

Figure 2.63. Fluorescence images of Human Lung Adenocarcinoma cells (A549). a) Fluorescence image of A549 cells treated with only **BOD-5** (5 μM); b, e) Fluorescence image of cells treated with DAPI (control); d) Fluorescence image of cells treated with **BOD-5** (10 μM) and Au^{3+} (20 μM); c, f) merged images of frames a-b and d-e (λ_{ex} = 460 nm).

Herewith, a fluorescent molecular sensor was developed by taking advantage of alkynophilicity of gold ions. Luckily, the BODIPY-Enyn-ol scaffold was selectively detect gold ions via an intramolecular 5-*exo*-*dig* cyclization path, the high-wavelength emitting conjugated probe structure transforms into a low-wavelength emitting non-conjugated BODIPY structure.

2.3.6. Gold Ion Sensing Properties of BOD-6

As indicated above there have been lots of fluorescent molecular sensors selectively detect gold ions in solution and living cells. The great majority of those sensors present in the literature are based on irreversible chemical events, which take advantage of the alkynophilic behaviour of gold species. In general, the fluorophore core being integrated with a gold ion specific reactive unit (i.e. alkyne), transforms the action of gold ions into a fluorescent signal output either through a change in fluorescence wavelength or a change in fluorescence intensity. Notably, one chronic issue in reaction-based gold ion sensing is the potential of other alkynophilic metal species to interfere with detection of gold ions. Thus, new sensing strategies utilizing alternative recognition events are needed to be developed in order to improve the general shortcomings of reaction based sensing strategies.

In this regard, molecular sensors relying on reversible ion-dipole interactions appear as good alternatives to reaction-based molecular sensors. Interestingly, however, molecular sensors operating reversibly towards gold ions are extremely scarce, most predominantly due to the challenge in design and synthesis.

In this part of the thesis study, the design, synthesis and spectral properties of **BOD-6**, a novel turn-on type fluorescent chemosensor was presented that allows Au^{3+} ions to be detected on the basis of reversible ion-dipole interactions. Knowing the capability of pyridine to act as a ligand for ionic gold species, we envisioned that a pyridine motif, when integrated to a fluorophore core, could act as a specific recognition motif for gold ions. Several Bodipy-pyridine conjugates have already been reported in the literature which mainly responds to changes in pH and to certain metal species such as Cu^{2+} and Hg^{2+} (Deniz et al., 2008; Wagner et al., 2012; Zhou et al., 2013).

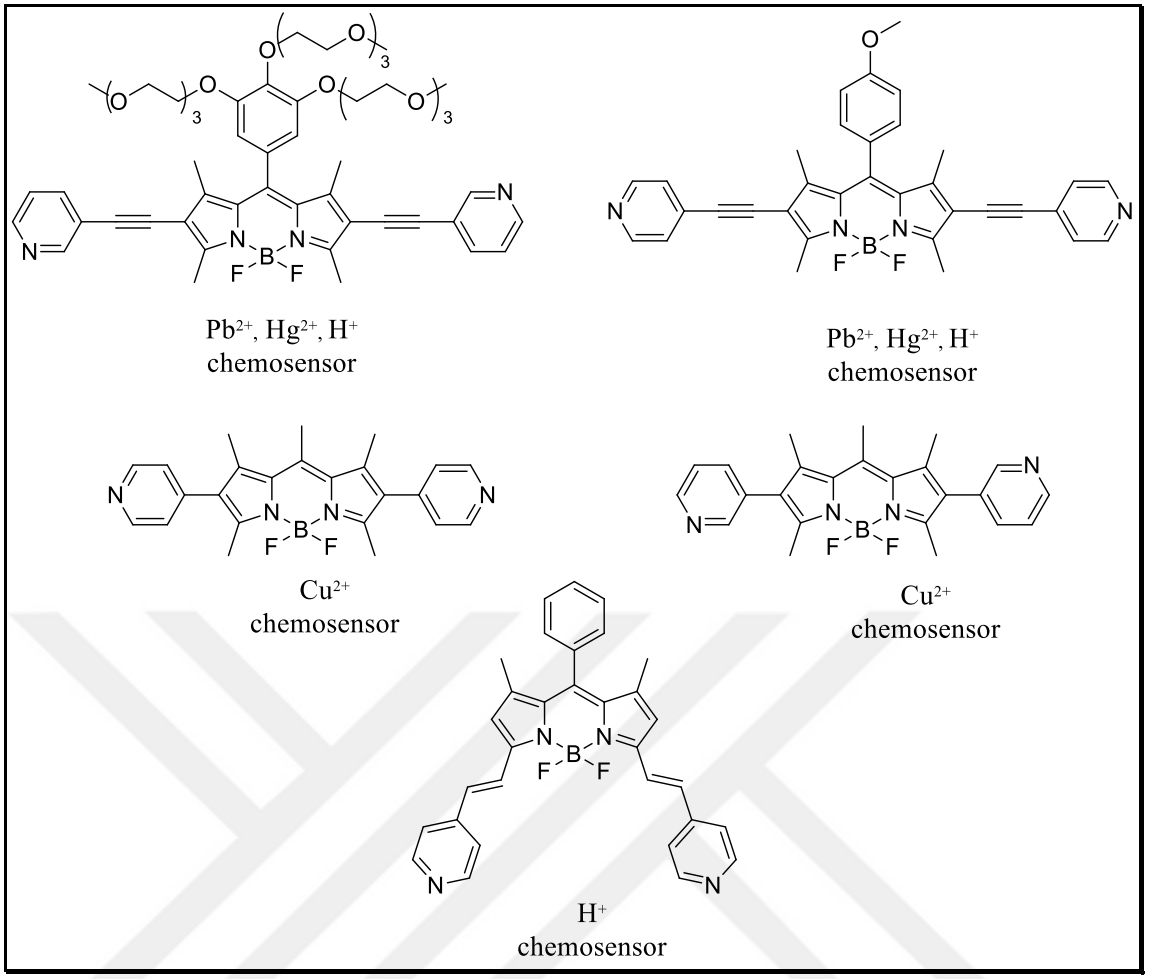

Figure 2.64. Literature examples of pyridine bearing fluorophores (Source: Deniz et al., 2008; Wagner et al., 2012; Zhou et al., 2013)

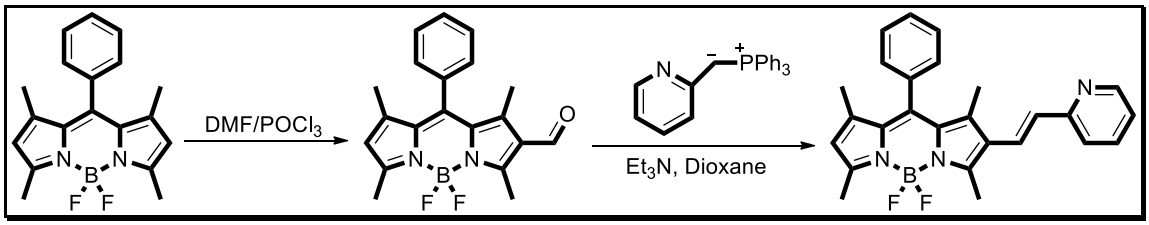

Figure 2.65. Synthesis route of BOD-6

With all these in mind, a molecular structure was designed which comprises a BODIPY dye as a fluorophore unit and a pyridylethenyl motif as the recognition site. **BOD-6** was prepared by the synthetic route outlined in Figure 2.65. First, a Vilsmeier Haack's formylation reaction of **BODIPY-3** gave **BODIPY-ALD**, which in the final step was treated with an appropriate Wittig reagent to give the title compound in a

reasonable yield of ca. 56% (Buynak et al., 1997). The chemical structure of **BOD-6** was clearly confirmed by performing NMR spectroscopy and HRMS analysis.

The photophysical behaviour of **BOD-6** in response to a series of metal species was carried out by both UV–vis absorption and fluorescence spectroscopy. Investigations were commenced by first determining the optimum conditions for the recognition of Au^{3+} ions. A variety of solvent combinations involving EtOH-H_2O, DMF-H_2O, and CH_3CN-H_2O were screened. Furthermore, the ratio of water in the semi-aqueous environment and the effect of pH on the sensing process were carefully investigated. Eventually, the optimum condition for the sensing process was established as 0.1 M phosphate buffer/EtOH (pH 7.0, v/v, 1:1) with 10 μM dye concentration.

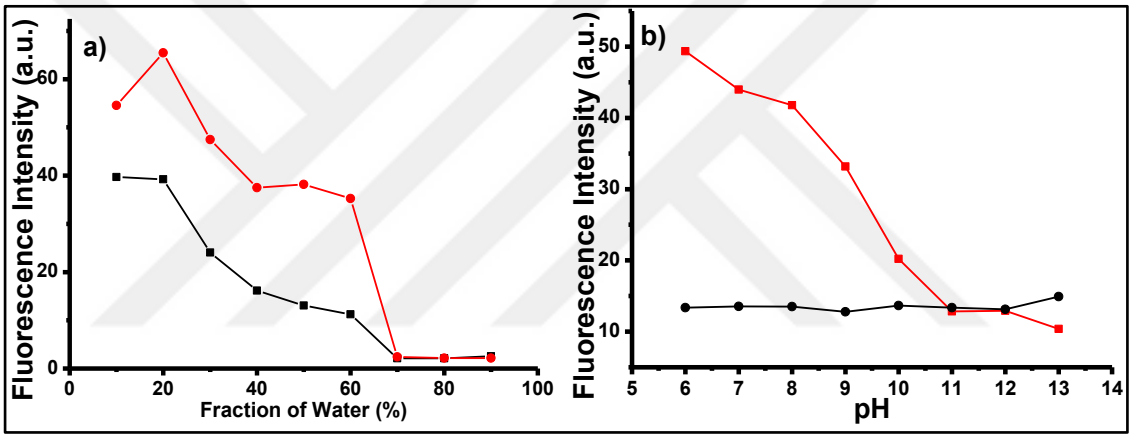

Figure 2.66. **a)** Effect of fraction of water (in 0.1M potassium phosphate buffer pH 7.0/EtOH) and **b)** Effect of pH (in 0.1M potassium phosphate buffer pH/EtOH (v/v, 1:1)) on the interaction of **BOD-6** (10 μM) (black line) with Au^{3+} (200 μM, 20 equiv.) (red line), (λ_{ex}: 460 nm, λ_{em}= 577 at 25 ^{o}C).

The spectral changes of **BOD-6** in the absence and presence of Au^{3+} ions are displayed in Figure 2.67. As shown, free **BOD-6** exhibits a faint fluorescence emission cantered at 591 nm. (Φ_F=0.044). However, the addition of Au^{3+} (6 equiv.) to **BOD-6** results in an observable enhancement of the emission intensity together with a slight blue shift in the emission wavelength (λ_{em}=577 nm) in a very short time (100 sec.) (Figure 2.68). This spectral behaviour of **BOD-6** was suggested to be due to the complexation of $AuCl_3$ with the lone pair electrons of the pyridylethenyl unit which terminates the overall quenching process.

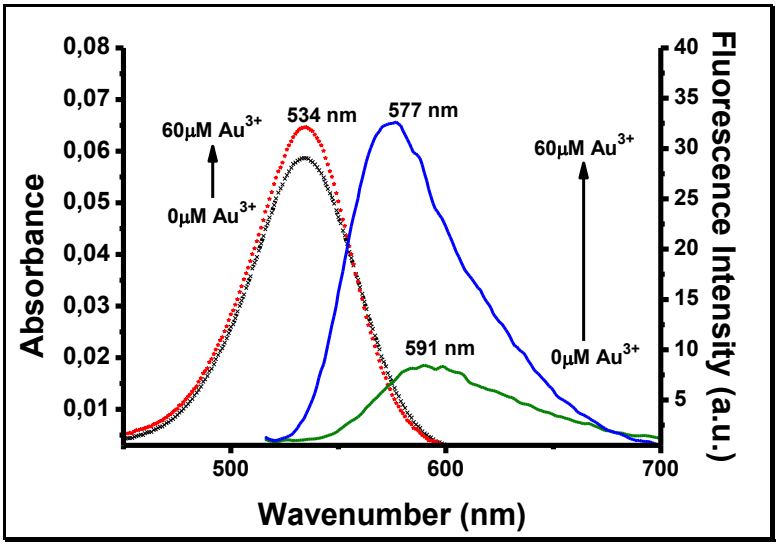

Figure 2.67. Absorbance spectra of **BOD-6** (10μM) in the absence (black dot-line) and presence (red dot-line) of 6 equiv. (60μM) of Au^{3+} and fluorescence spectra of **BOD-6** (10μM) in the absence (green line) and presence (blue line) of 6 equiv. (60μM) of Au^{3+} in 0.1 M phosphate buffer/EtOH (pH 7.0, v/v, 1:1).

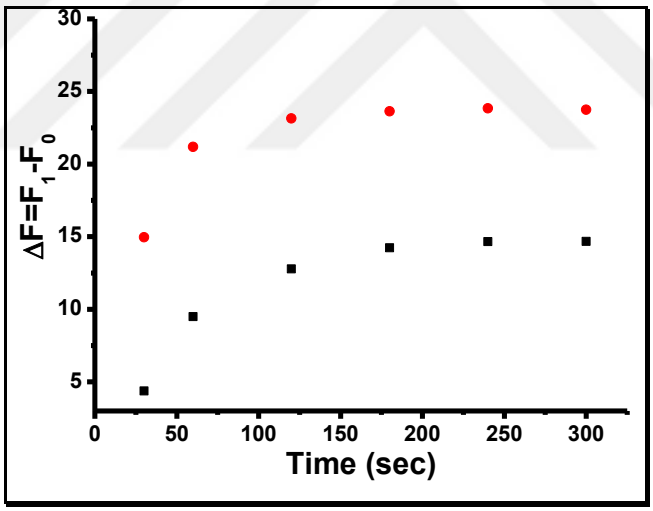

Figure 2.68. Reaction time profiles of **BOD-6** (10.0 μM) in the presence of Au^{3+} [30 (■) and 60 (●) μM.]. The fluorescence intensities at 577 nm were continuously monitored at time intervals in 0.1 M phosphate buffer/EtOH (pH 7.0, v/v, 1:1) (λ_{ex}: 500 nm, λ_{em}= 577 nm at 25 ^{o}C).

The selectivity profile of **BOD-6** was surveyed by screening the spectral response towards metal species including Zn^{2+}, Cd^{2+}, Ba^{2+}, Cu^{2+}, Li^{+}, K^{+}, Ni^{2+}, Cr^{2+}, Mg^{2+}, Fe^{3+}, Pb^{2+}, Hg^{2+}, Co^{2+}, Ag^{+} and Au^{+}. Delightfully, no significant changes were measured in the presence of other metal species. Only the addition of Au^{3+} and, to a

lesser extent the addition of Au^{+} resulted in an increase of fluorescence at 577 nm, which obviously implied the high selectivity of **BOD-6** to gold ions (Figure 2.69). Fortunately, Hg^{2+} and Pd^{2+}, being the most competitive metal ions in the detection of gold species did not result in any spectral change.

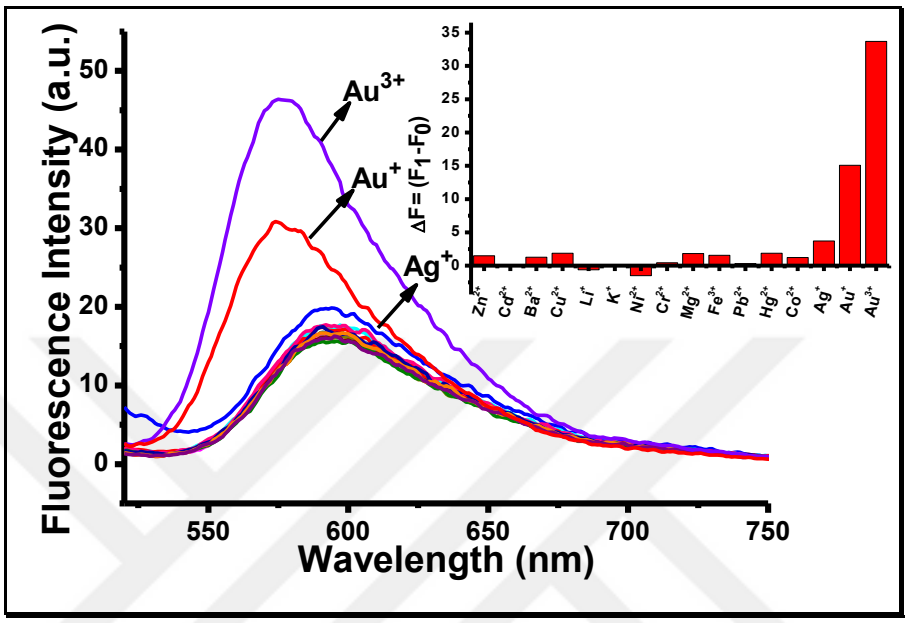

Figure 2.69. Fluorescence intensities of **BOD-6** (10.0μM), **BOD-6** (10.0μM) + Au^{3+} (60 μM, 6 equiv.), **BOD-6** (10.0μM) + other ions (250μM, 25 equiv.) in 0.1M potassium phosphate buffer, pH 7.0/EtOH (v/v, 1:1) (λ_{ex}:500 nm, at 25 ^{o}C). Inset: Bar graph notation.

In order to assess the interference of other metal ions the fluorescence response was explored in the presence of other metal ions. As shown in Figure 2.70, the response of **BOD-6** towards Au^{3+} ions was not affected in the presence of other competitive metal species. These results established that **BOD-6** can properly detect gold ions in the mixtures of other related species.

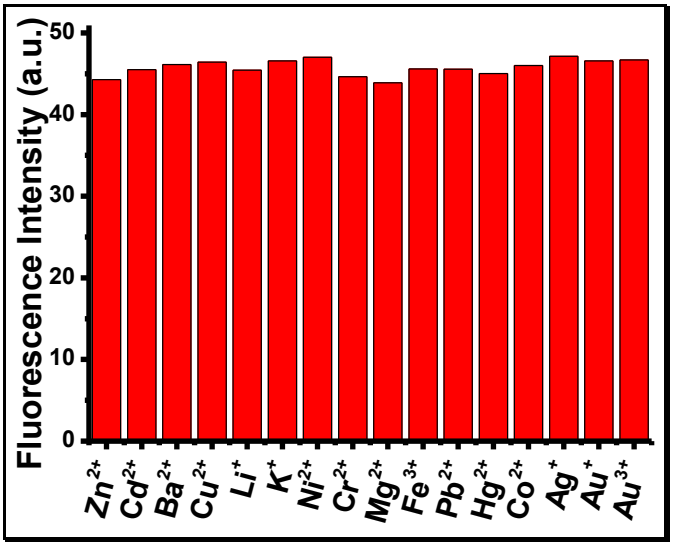

Figure 2.70. Fluorescence intensities of **BOD-6** (10μM) in the presence of Au^{3+} (6 equiv.) and 10 equiv. of other metal ions in 0.1 M phosphate buffer/EtOH (pH 7.0, v/v, 1:1) (λ_{exc}=500 nm, λ_{em}= 577 nm at 25 ^{o}C).

The fluorescence titration experiment was performed to get idea about the saturation concentration and minimum amount of detectable gold ions. Notably, emission intensity reached its maximum when 6 equiv. of Au^{3+} ions was added. In addition, there was a good linear relationship between fluorescence intensity and the equivalency of Au^{3+} ions (0.2 to 0.7 equivalent of Au^{3+}) (Figure 2.71). From this data the detection limit of **BOD-6** was evaluated as 4.0 μM.

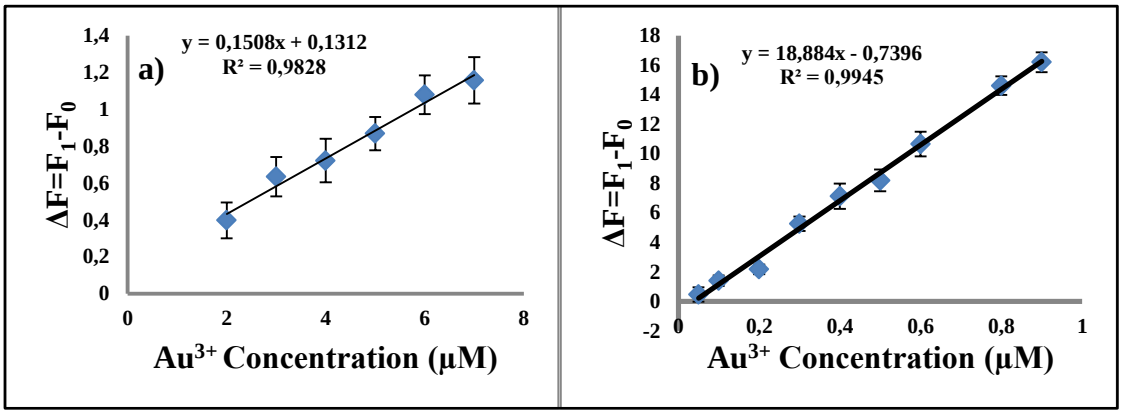

Figure 2.71. Fluorescence changes of **BOD-6** (10 μM) upon addition of Au^{3+} a) (2 to 7 μM, 0. 2 to 0.7 equiv.) in 0.1M potassium phosphate buffer, pH 7.0/EtOH (v/v, 1:1) b) (0.05 to 1.0 μM, 0.005 to 0.1 equiv.) in dichloroethane (λ_{ex}: 500 nm, λ_{em}= 577 nm at 25 ^{o}C).

The binding ability of **BOD-6** to Au^{3+} ions was further investigated by performing a fluorescence titration experiment (Figure 2.72). The emission intensity reached its maximum when 6 equiv. of Au^{3+} was added and the stoichiometry of the sensing event was established by following the Benesi-Hildebrand method and Job's plot analysis. A straight line was obtained from the plot of $\ln[(F-F_0)/(F_{max}-F)]$ against $\ln[Au^{3+}]$ and the related binding constant was determined as 4.9 x 10^4 M^{-2}. Moreover, the Job's plot analysis supported a 2:1 stoichiometry for the complexation (Figure 2.73).

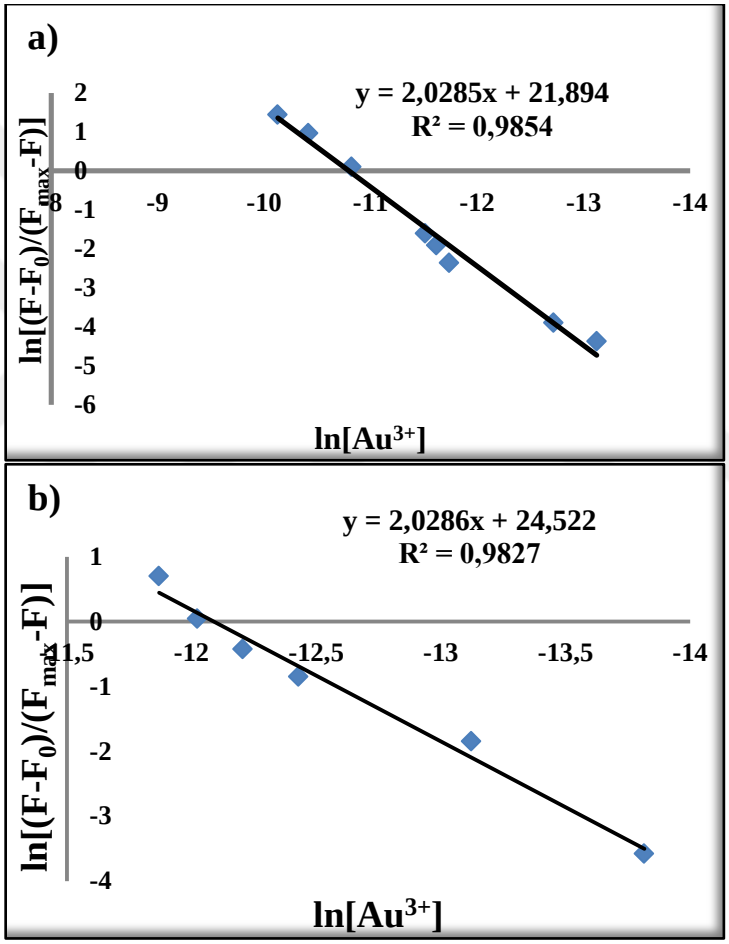

Figure 2.72. Binding ability of **BOD-6** to Au^{3+} a) in EtOH n 0.1M potassium phosphate buffer, pH 7.0/EtOH (v/v, 1:1) b) in dichloroethane (λ_{exc}=500 nm, λ_{em}= 577 nm at 25 ^oC).

Further experiments revealed that the binding ability of **BOD-6** to Au^{3+} could be dramatically improved in a non-aqueous sensing media. For example in

DCE the binding constant was evaluated to be 1.8 x 10^5 M^{-2} which was visibly greater than that measured in the aqueous media.

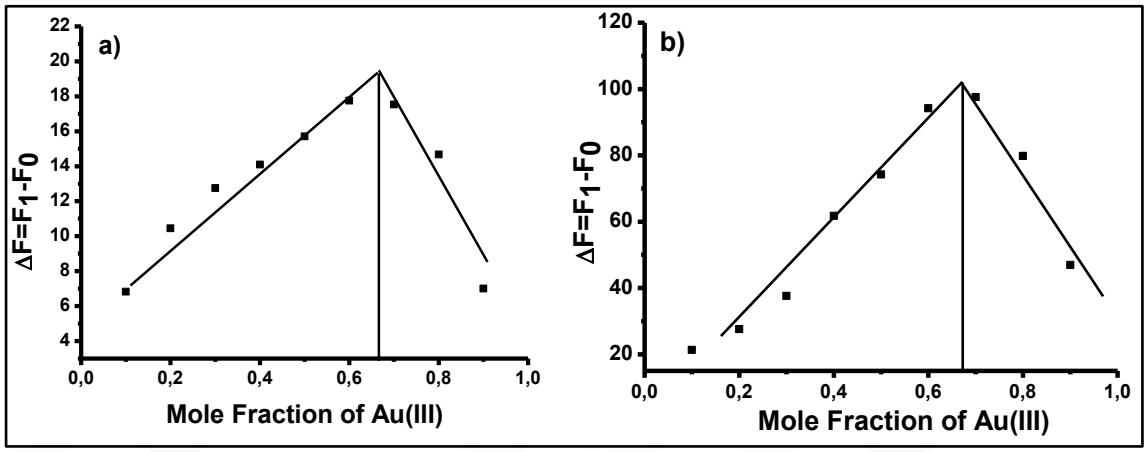

Figure 2.73. The Job's plot analysis between **BOD-6** and Au^{3+} (a) in 0.1 M phosphate buffer/EtOH (pH 7.0, v/v, 1:1) (b) in ethanol. The total concentration of **BOD-6** and Au^{3+} was kept constant at 20 μM (λ_{exc}=500 nm, λ_{em}= 577 nm at 25 ^oC).

In a non-aqueous sensing media, where the effect of solvation is minimized, the complexation of Au^{3+} to the Bodipy-pyridine conjugate gave a 20-fold fluorescence enhancement, which is visibly greater than the fluorescence increase observed in aqueous media (Figure 2.74). Similar to the measurements carried out in aqueous conditions, the fluorescence titration profile of **BOD-6** with Au^{3+} in non-aqueous media showed a linear relationship for a concentration range of 0.05-1.0 μM. Notably, the detection limit of **BOD-6** was significantly improved to nanomolar levels (63 nm, S/N > 3). However, it is worth mentioning here that, despite the improved sensitivity, the selectivity towards Au^{3+} dramatically decreased in non-aqueous media.

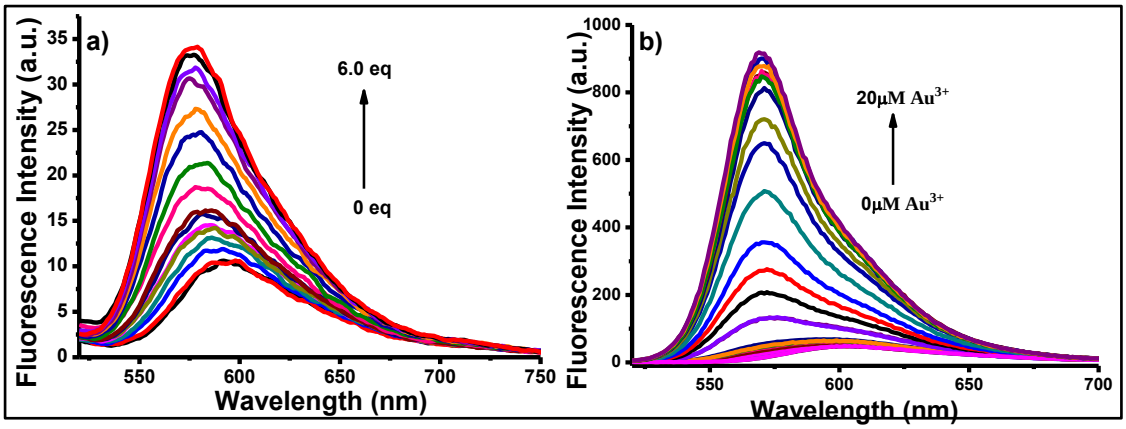

Figure 2.74. Fluorescence spectra of **BOD-6** (10μM) in the presence of increasing concentrations of Au^{3+} a) (0-60 μM, 0-6 equiv.) in 0.1 M phosphate buffer/EtOH (pH 7.0, v/v, 1:1) (λ_{exc}=500 nm at 25°C) and b) (0-20μM, 0-2 equiv.) in DCE.

The sensing mechanism of the probe was envisioned to be reversible. To get insight into whether the sensing mechanism is reversible or not, an excess amount of CN^- ions were introduced into the solution including 10 μM dye and 6.0 equivalents of Au^{3+} (0.1 M phosphate buffer/EtOH (pH 7.0, v/v, 1:1). As shown in Figure 2.75, the fluorescence intensity of the probe solution was immediately reduced by the addition of CN^- which proofs the reversibility of recognition process.

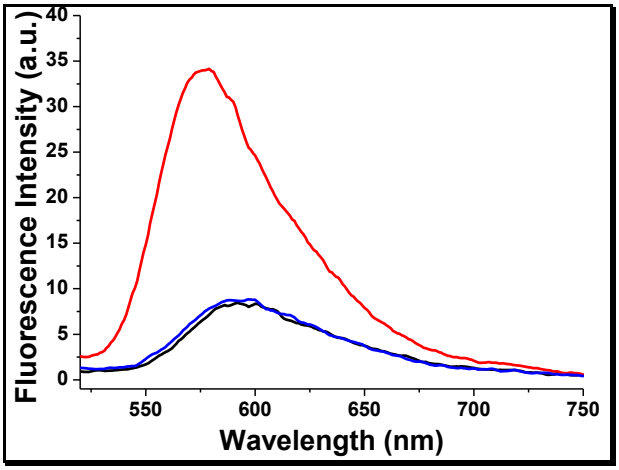

Figure 2.75. Fluorescence intensities of **BOD-6** (10 μM) (black), **BOD-6** (10 μM) + Au^{3+} (red), **BOD-6** (10.0μM) + Au^{3+} + excess amount of CN^- (blue), in 0.1M potassium phosphate buffer, pH 7.0/EtOH (v/v, 1:1) (λ_{ex}: 500 nm, at 25 ^oC).

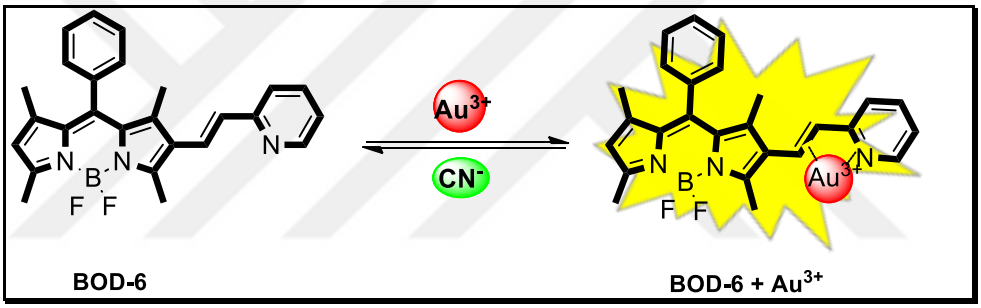

Figure 2.76. Proposed interaction mechanism of **BOD-6** and Au^{3+}

The specific binding of Au^{3+} to the pyridine ligand was clearly followed by the aid of ^{1}H-NMR spectroscopy (Figure 2.77). Upon the binding of $AuCl_3$ with **BOD-6**, the pyridine ring protons (H_b, H_c and H_d) of the binding complex were dramatically shifted to a higher frequency (downfield shift), consistent with the coordination of nitrogen to $AuCl_3$.

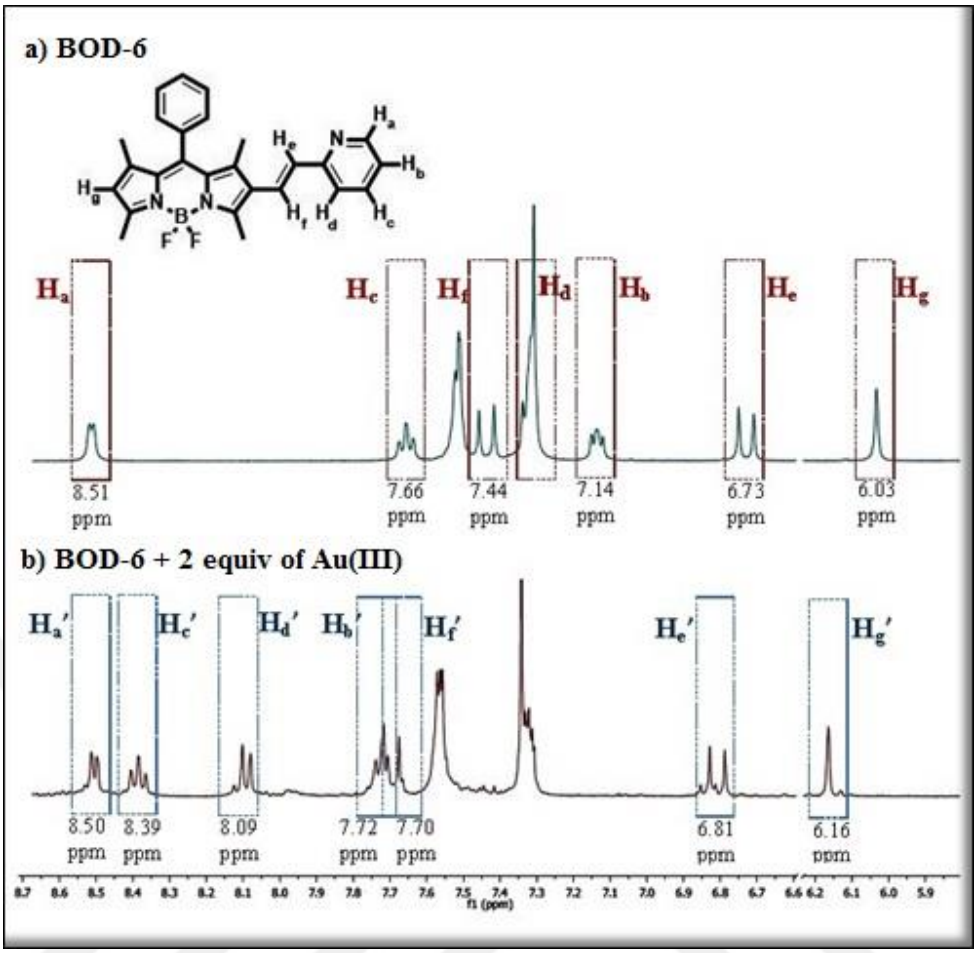

Figure 2.77. a) Partial ^{1}H NMR spectra of **BOD-6** and b) **BOD-6** + $AuCl_3$ (2 equiv.) in $CDCl_3$.

One of the important aims of thesis was to detect residual Au^{3+} ions in synthetic samples. In order to assess whether **BOD-6** could be applied to monitoring residual Au^{3+} ions in a synthetic end-product a known chemical transformation utilizing $AuCl_3$ as the active catalyst was performed. To this end, a propargylic amide derivative in dichloromethane was rapidly transformed to its Oxazole derivative under the catalysis of $AuCl_3$ (10 mol%) (Figure 2.78).

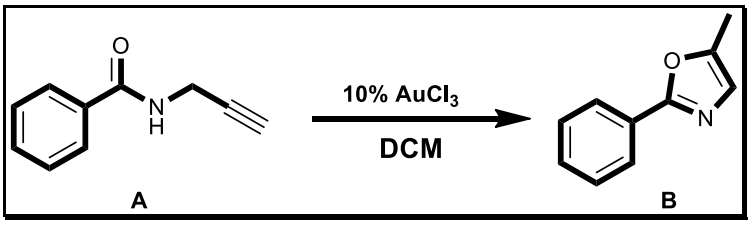

Figure 2.78. $AuCl_3$ catalysed cyclization reaction of propargyl amide

The crude product of the chemical reaction was subjected to chromatographic purification using silica as the stationary phase and dichloromethane as an eluent. A defined amount of the purified sample (2 mg) was added to the solution of **BOD-6** (10 μM in 0.1 M phosphate buffer/EtOH (pH 7.0, v/v, 1:1). Immediately, a distinct change in colour and fluorescence could be monitored in the probe solution indicating the presence of gold species in the solution. This observation was in consistent with literature reports, which have proven a synthetic end product may still contain residues of the metal catalyst even after chromatographic purification.

By the aid of fluorescence measurements the gold content in the sample solution was measured to be 1.8 x 10^{-8} mol mg^{-1} based on a standard calibration curve (Figure 2.79). This result was also consistent with that obtained by inductively coupled plasma-mass spectrometry (ICP-MS) analysis (1.27 x 10^{-8} mol mg^{-1}). With this experiment the viability of **BOD-6** for quantitative gold analysis was unambiguously confirmed.

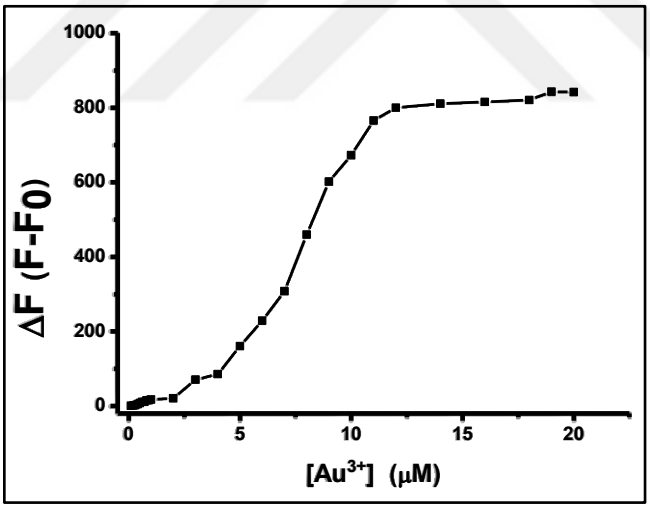

Figure 2.79. Calibration curve of **BOD-6** (10μM) in the presence of increasing concentrations of Au^{3+} (0-20μM, 0-2 equiv.) in dichloroethane (λ_{exc}=500 nm, λ_{em}= 570 nm at 25 ^{o}C).

In addition to being exceptionally selective towards Au^{3+} ions, **BOD-6** is also sensitive to changes in pH within the acidic pH range. Free **BOD-6**, which exhibits a faint fluorescence emission at 591 nm in pH range of 7-12, gave immediately a strong emission band at 564 nm upon protonation of

pyridylethenyl moiety (Figure 2.80). As the pH of solution decreased from 7.0 to 2.0, concomitantly the emission intensity increased by 18-fold. The quantum yield of **BOD-6** at pH=2.0, was determined to be 0.39 by using rhodamine 6G (Φ_F=0.95 in ethanol) as a standard dye.

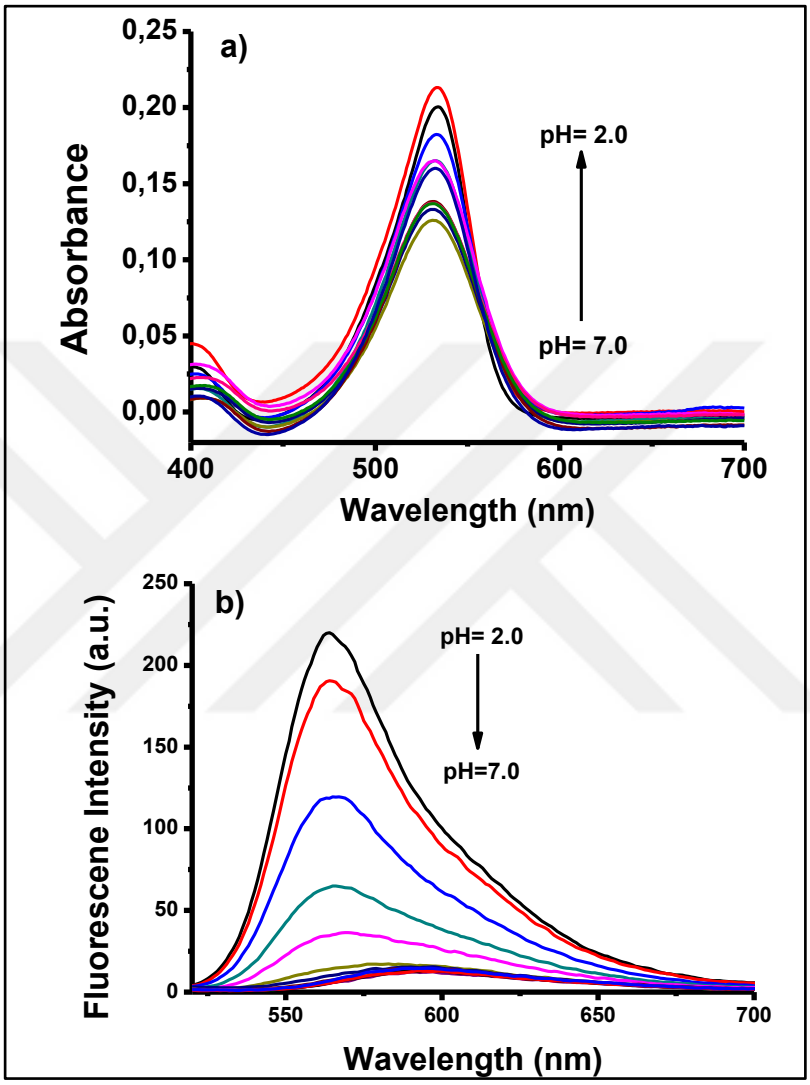

Figure 2.80. a) Absorbance and b) Fluorescence spectra of **BOD-6** (10 μM) in 0.1 M phosphate buffer/EtOH (v/v, 1:1) at various pH values (2.0-7.0) (λ_{exc}=500 nm, 25 ^{o}C).

To close, in this part of thesis, a dual responsive fluorescent chemosensor was constructed for the rapid detection of gold species and, also for monitoring the changes in acidity (pH=2-7). This novel chemosensor (**BOD-6**) comprises a pyridylethenyl unit as a recognition site and a BODIPY core as a fluorophore unit. The sensing mechanism of **BOD-6** is based on selective binding of gold ions

to the pyridyl-nitrogen atom which is recognized by a distinct change in the emission intensity. Importantly, **BOD-6** represents a rare example of a fluorescent probe that operates “reversibly” towards gold species. As a practical application the utility of **BOD-6** for the quantification of gold ion residues in synthetic chemicals that were prepared via gold catalysis was successfully documented.

CHAPTER 3

FLUORESCENT MOLECULAR SENSORS FOR MERCURY ION DETECTION

3.1. An Overwiev

In recent years, the fast growing industry and modern agriculture have lead an unpreventable environmetal pollution because of the increasing usage of heavy metals in these areas. To prevent environmental contamination the European Union's Restriction on Hazardous Substances (RoHS) banned the usage of hazardous heavy metal ions (e.g. lead, mercury and cadmium) in electrical and electronic devices (Kim et al., 2012). Among these heavy metal ions mercury is one of the most important sources of danger for ecosystem (Tchounwou et al., 2003; De Vries et al., 2007). Although its usage in some areas of industry restricted by international organizations there are several sources of mercury in nature. The main sources of mercury contaminations in nature can be examplified as oceanic and volcanic eruptions, coal plants, thermometers, caustic soda, gold production, and mercury lamps (Chen et al., 2015; Kim et al., 2011). The major threat of mercury is its nonbiodegredable nature because of its high toxicity and strong affinity to biomolecules such as proteins and DNA. In literature there has been great number of studies that reported the diseases caused from the accumulation of mercury in human body such as brain damage, kidney failure, and various cognitive and motion disorders. The World Health Organization (WHO) has estimated a tolerable concentration of elemental mercury vapour to be 0.2 $\mu g/m^3$ for long-term inhalation and a tolerable intake of total mercury to be 2 μg/kg body weight per day. At the same time, the US Environmental Protection Agency (EPA) and US Food and Drug Administration (FDA) have set a limit of 2 parts inorganic mercury per billion in drinking water posing no other lethal adverse health effects (Johnson, 1997; Diez-Gil et al., 2011).

As in the case of gold sensing mercury ions can also be detected by using classical analytical techniques such as inductively coupled plasma mass spectrometry, inductively coupled plasma atomic emission spectrometry, cold vapour atomic absorption spectrometry, neutron activation analysis, X-ray fluorescence spectrometry,

and atomic fluorescence spectrometry (Clevenger et al., 1997; Powell et al., 1992). Again requirements of above methods create an urgent need for development of new methodologies to sense mercury ions in trace. Since 1992, there have been intensive attentions to upgrade sensing methodologies for mercury ions in various environmets such as synthetic samples and living cells. Fluoregenic and chromogenic methods have become very popular during tha last two-three decades. The idea of sensing event via fluorogenic and chromogenic methods has majorly focused on mercury ions because of their extremely high toxcicity.

In this thesis study, we benefited from the high alkynophiliciy and strong thiol affinity of mercury ions for the design and development of BODIPY based fluorescent molecular sensors.

3.2. Literature Studies

Performing trace metal (metal ion) analysis with the aid of fluoreogenic and chromogenic methods have gained substantial attention during the last two-three decades. Fluoreogenic and chromogenic methods offer important advantages to tracking targeted analyte in various environments such as living organisims *in vivo* and *in vitro* and synthetic samples. However, the applicability of methods have sometimes restricted due to the chemical nature of targeted analyte. For example metal ions with having paramagnetic nature such as Hg^{2+}, Pb^{2+}, Cu^{2+} and Fe^{3+} make difficult to perform sensing event because of their quenching effect on the fluorescence (Fabbrizzi et al., 1994). Based on this information design and development of mercury ion sensor requires a special attention and the strategy have to be thought on several counts.

The first example of fluorescent molecular sensor for mercury ions that enable to overcome quenching effect was developed by Czarnik and Chae in 1992 (Chae and Czarnik, 1992). In their approach, the anthracene unit was functionalized with a thioamide receptor in which the thioamide structure isomerizes the thiolate form that causes quenching of fluorescence property of anthracene unit via PET mechanism. As it is well known, mercury ions have high affinity to sulphur and undergo a reversible coordination or an irreversible reaction with sulphur bearing compounds. In this situation, the desulfation reaction took place between mercury ions and probe molecule. Because of the predominant form of newly obtained probe was in amide structure the PET mechanism canceled and probe started to fluoresce. With the aid of fluorescence enhancement mercury ions could easily monitored. In addition to becoming a touchstone in mercury sensing, the study contributed to scientific community the term chemodosimeter.

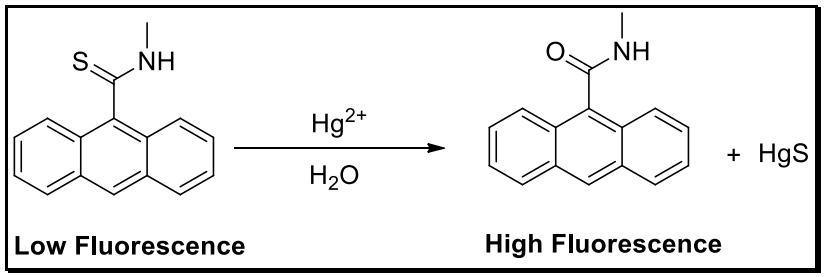

Figure 3.1. Response of the developed probe with the addition of Hg^{2+}
(Source: Chae and Czarnik, 1992)

After the pioneering invention of Chae and Czarnik, hundereds of examples for mercury ion sensing have been developed by using various reactive units. Mercury has similar chemical character with gold ions. As in the case of gold, mercury ions show high reactivity towards unsaturated bonds and there are numerous examples of sensors benefited from this property. In addition mercury ions have high affinity to heteroatoms especially to thiols, and in design of receptor unit the thiophilic nature of mercury have frequently used.

In 2001 Sancenon et al. demonstrated an example of chromogenic sensor that enable to detect mercury ions by using changes in absorption specturum. The polyether receptor unit was first time used for mercury sensing event (Sancenon et al., 2001). In this strategy, mercury ions coordinated to the polyether receptor unit by 1:1 molar ratio.

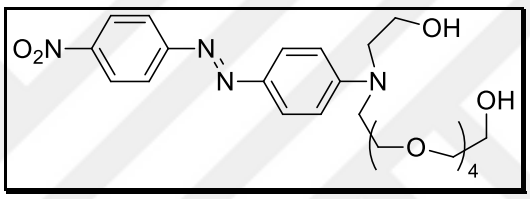

Figure 3.2. Chromogenic sensor for Hg2+ ions
(Source: Sancenon et al., 2001)

Usage of polyether is a ubiquitous approach for designing mercury ion selective sensors. Li and co-workers published an article in which mercury ions sensitive water soluble molecular sensor constructed based on hemicyanine-polyether scaffold. The coordination of mercury ions to the polyether structure resulted in a change on electronic structure and a ratiometric response obtained with a blue shift (Li et al., 2011).

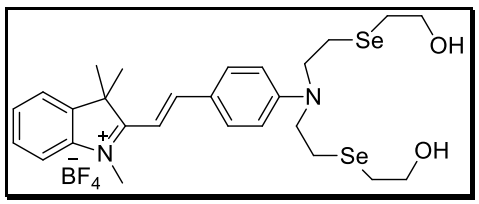

Figure 3.3. Hemicyanine based chemosensor for Hg^{2+}
(Source: Li et al., 2011)

In addition, polyether receptor unit have also appended to the BODIPY structure for designing a mercury ion selective chemosensor. BODIPY fluorophore was derivatized from *meso*- and 3- positions with cyclic polyether functionality having high coordination ability towards mercury ions by Yuan et al. in 2007. The molecule had two reactive units and the sensing event constructed on two photophsical mechanism. The addition mercury ions cancelled the PET mechanism and molecule produced a turn on respose. In addition to cancelling PET, further addition of mercury resulted in a blue shift on fluorescence spectrum because of the ICT mechanism (Yuan et al., 2007).

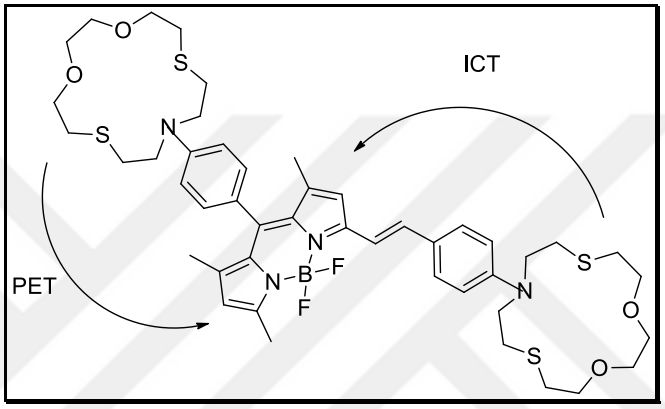

Figure 3.4. BODIPY based chemosensor for Hg^{2+}
(Source: Yuan et al., 2007)

In 2010, above strategy was used by Akkaya research group in their design. The BODIPY based sensor functionalized with cyclic polyether structure from 3- position by using Knoevenagel condensation reaction. With the aid of the same reaction main core structure was also functionalized from 5- position and another fluorophore appended by Huisgen type click reaction for energy transfer event. Because of the integration of two doube bonds into the conjugation the main core of the sensor molecule emited at red/near IR region. While molecule had two emission wavelengths in its initial state addition of mercury ions to the dye solution decreased the emission of lower wavelenth peak and caused a blue shift on higher wavelength peak. The blue shift was also increased the efficiency of energy transfer because of the increase in spectral overlap (Figure 3.5).

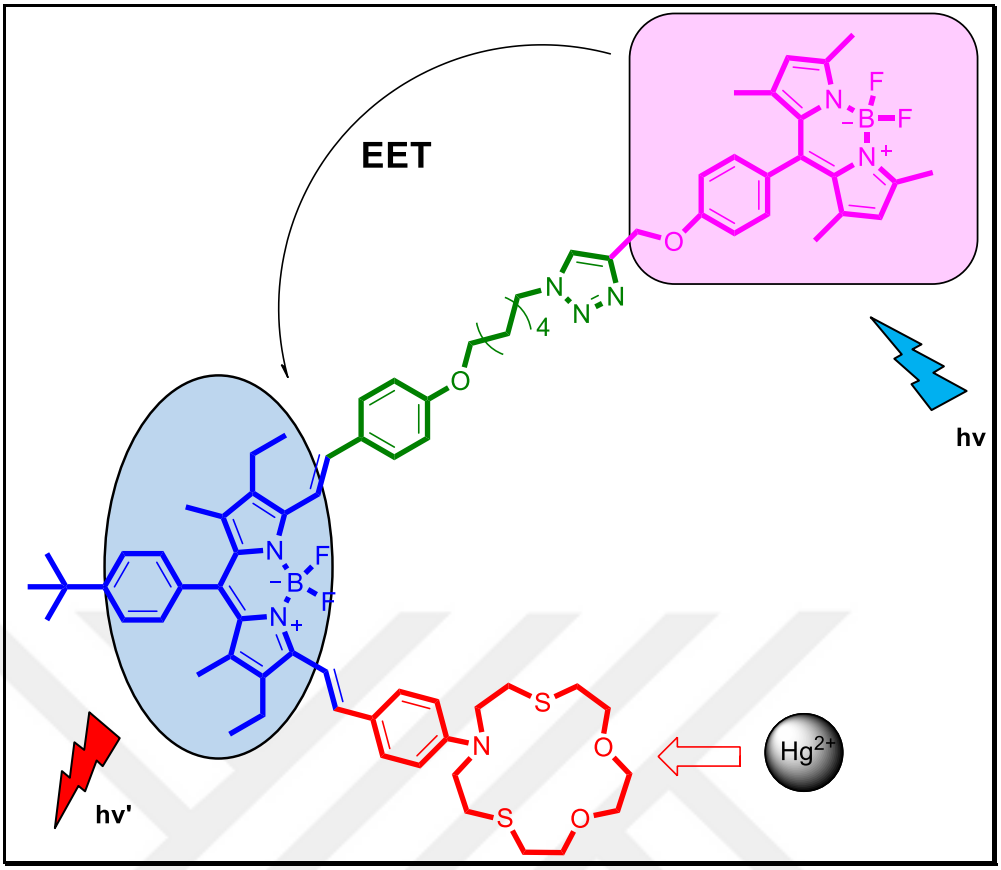

Figure 3.5. Selective Hg^{2+} sensing by coupling the internal charge transfer to excitation energy transfer (Source: Atılgan et al., 2010)

In addition to the cyclic polyether functionality, receptor units bearing oxygen and nitrogen atoms in their structure have also in demand for designing fluorogenic and chromogenic molecular sensors. For this sensing strategy Rhodamine dyes have frequently used in which coordination of mercury ions to the heteroatoms triggers the ring openning reaction and resulted in hydrolysis of receptor unit. In design of many sensor molecules the receptor unit have constructed on known literature reactions. For example, in 1972 Abley et al. demostrated the mercury mediated irreversible hysrolysis of isopropenyl acetate in the presence of mercury ions (Abley et al., 1972). After forty years, Du et al. used this strategy to construct a mercury ion sensor in 2010. They appended the known reactive motif to the rhodamine core which hydrolyzed in the presence of mercury ions. An interesting feature of the study is the applicability of strategy to the real samples such as sea water, tap water and pool water (Du et al., 2010).

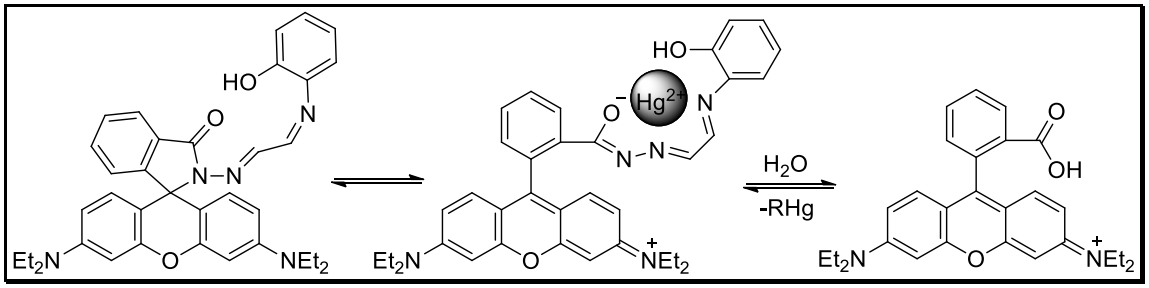

Figure 3.6. Hg^{2+} mediated hydrolysis of Rhodamine derivative
(Source: Du et al., 2010)

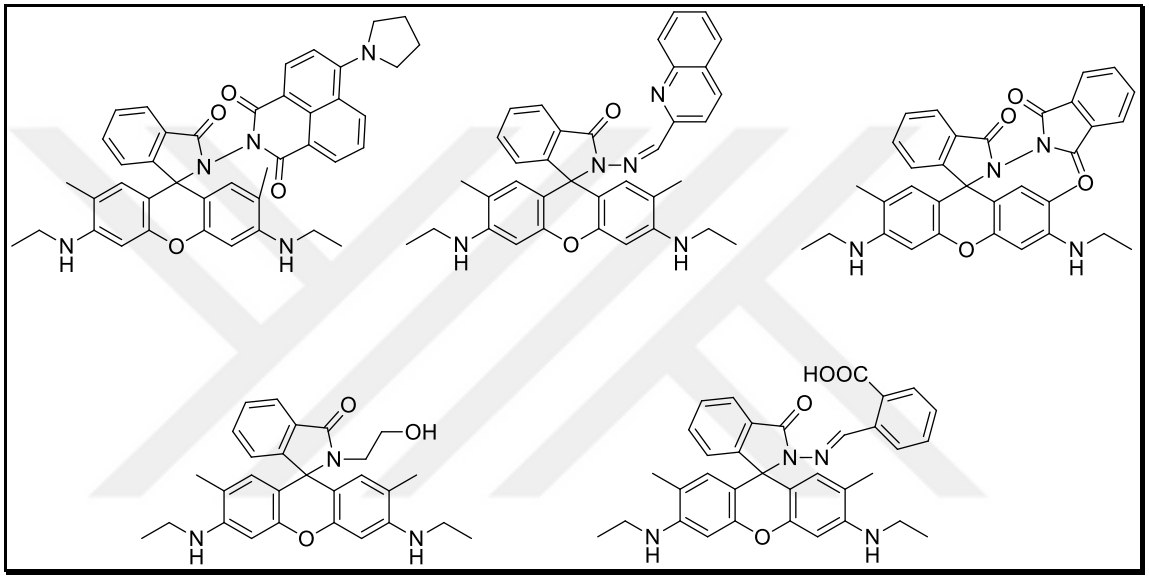

Figure 3.7. Rhodamine based chemosensors for Hg^{2+}
(Source: Chen et al., 2015)

Besides chemodosimeters, heteroatom containing molecular chemosensors that working via coordination chemistry have presented. The examples of rhodamine derivatives having "turn-on" response towards mercury ions were represented in Figure 3.7 (Chen et al., 2015).

Akkaya research group designed an aza-BODIPY structure bearing two 2-pyridyl units at 2,7- positions enable to detect mercury ions via a ratiometric response (Coskun et al., 2007). In their strategy, the BODIPY structure have emission band at relatively longer wavelength (682 nm). The addition of mercury ions to the sensing solution resulted in a decrease at emission band at 682 nm and a red shifted band appeared at 719 nm. The binding stoichiometry of probe molecule was investigated with

a systematic titration experiment and 1:1 binding stoichiomety was established (Figure 3.8).

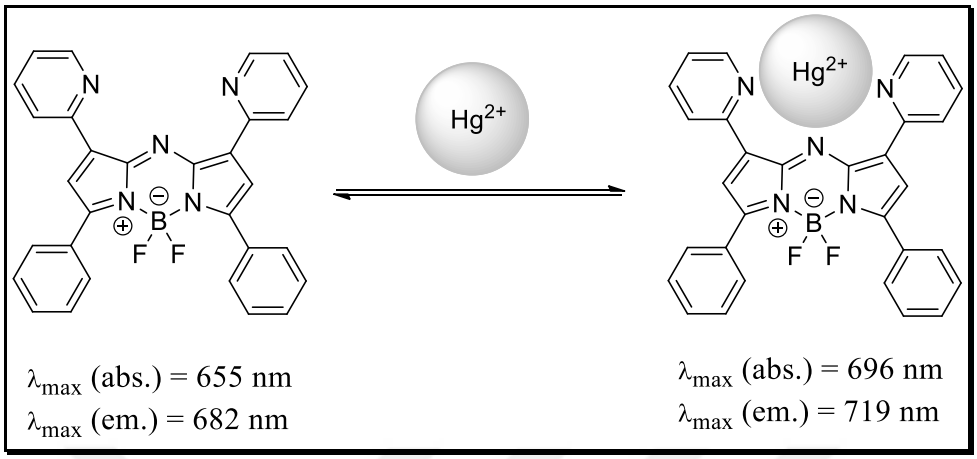

Figure 3.8. Hg^{2+}-induced response of modified boratriazaindacene
(Source: Coskun et al., 2007)

Another interesting study was reported by Fan's group. In their work, the sensor molecule included a BODIPY structure bearing 2-amino phenol moiety at *meso* position. Because of PET mechanism the chemosensor was of in its initial state. Addition of Hg^{2+} to sensing solution (EtOH/HEPES) the molecule produced a turn on response. An impressive feature of probe was its ability to detect mercury ions in the presence of thiol species (Fan et al., 2012).

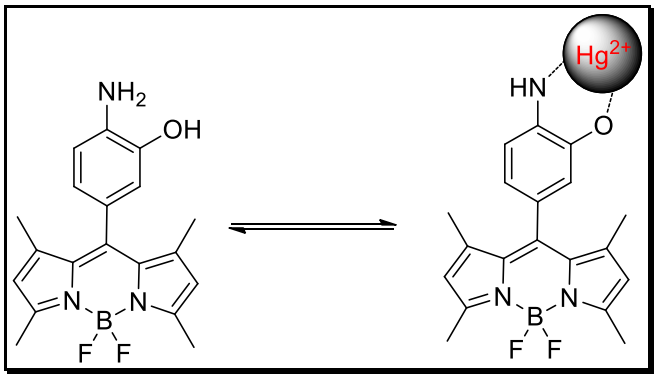

Figure 3.9. A reversible molecular sensor for Hg^{2+}
(Source: Fan et al., 2012)

Other examples of mercury ions sensors based on BODIPY scaffold demonstrated in Figure 3.10 (Chang et al., 2015).

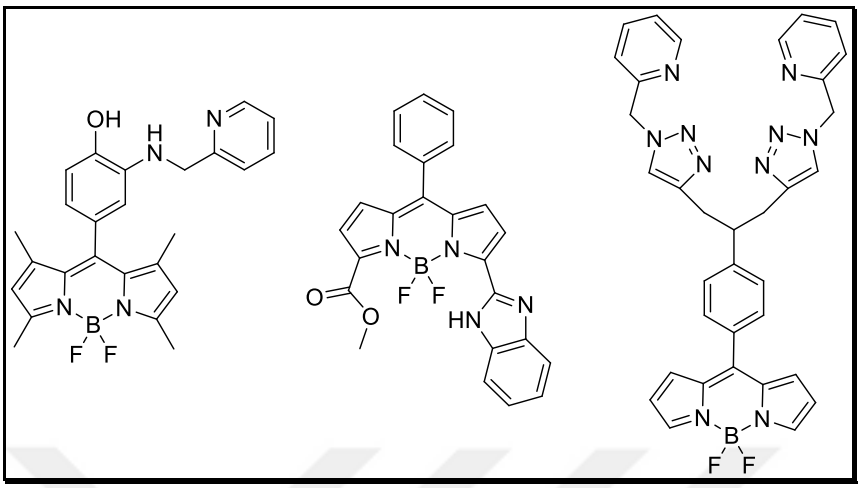

Figure 3.10. BODIPY based chemosensors for Hg^{2+} ions
(Source: Chang et al., 2015)

As indicated above, several strategies have presented for designing receptor units for mercury sensing event. The most prominent strategy is the usage of sulphur containing molecules in receptor units.

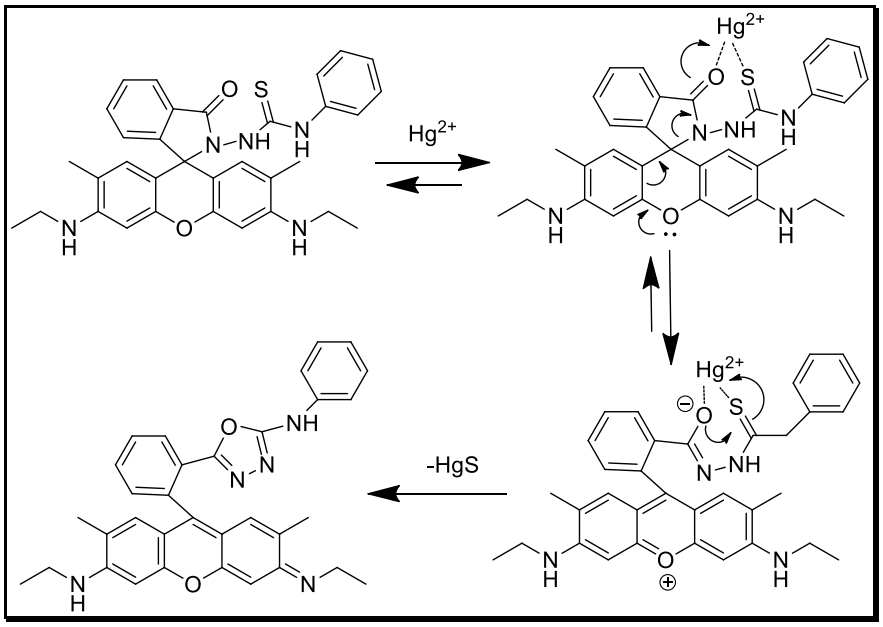

Figure 3.11. Hg^{2+}-induced ring opening and cyclization of the designed rhodamine derivative (Source: Yang et al., 2005)

In 2005, Tae and co-workers developed a rhodamine based chemodosimeter including thiosemicarbazide functionality in its structure (Yang et al., 2005). As indicated in Figure 3.11, mercury ions coordinated the sulphur and oxygen atoms on sensor molecule that triggered the mercury mediated cyclization reaction. The outcome of the reaction had a fluorescence band in emission spectrum. With the aid of this intensity enhancement, the Hg^{2+} ions were detected sensitively in ppb levels.

Just after this publication a similar approach was demonstrated by Wu et al. in 2007 for designing Hg^{2+} selective turn on chemodosimeter. They appended the thiourea moiety to spirocyclic rhodamine dye with an ethylene spacer. The probe molecule was off in its initial state. The sensing strategy established based on a well known mercury mediated cyclization reaction in which the thiourea structure converted to a guanidium moiety in the presence of mercury ions. The desulfation reaction took place with the addition of mercury ions and concomitant ring opening reaction produce fluorescence on response. In addition, the system also produces a colorimetric response that offered the monitoring mercury ions with naked eye.

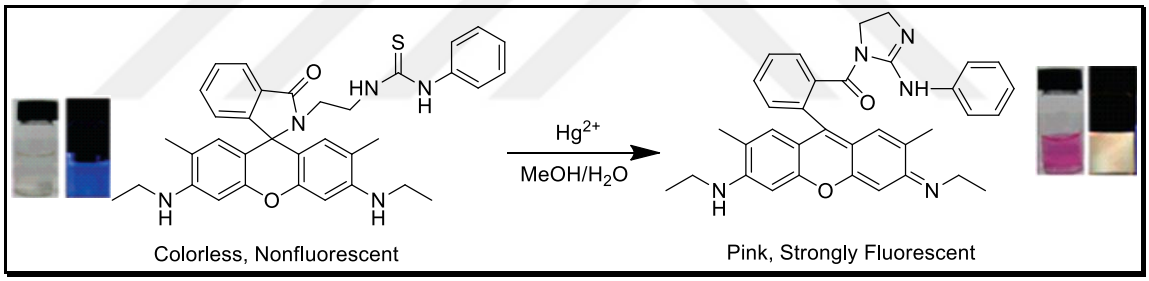

Figure 3.12. Response of the developed probe to the addition of Hg^{2+} ions (Source: Wu et al., 2007)

Desulfation reactions are also applicable for energy transfer systems. The design of Shang et al. represented the construction of a FRET sensor in which rhodamine and fluorescein derivatives attached to each other with a thiourea structure. While one of the fluorophores was in spirocyclic form (off mode) other one is in ring opened form (on mode) in their initial state. Excitation of fluorophore system from the lower wavelength produced a green fluorescence belonged to fluorescein structure. Addition of Hg^{2+} to the sensing solution triggeres ring oppening reaction of rhodamine dye followed by desulfation and cyclization processes and the green emission of fluorescein transferred to the rhodamine dye.

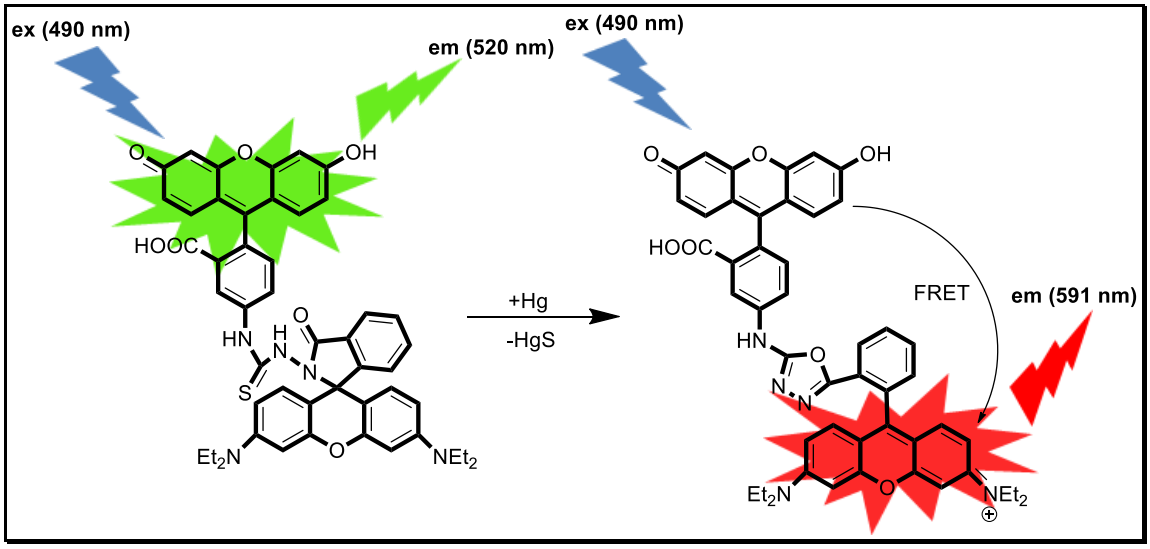

Figure 3.13. A FRET probe based on fluorescein-rhodamine scaffold
(Source: Shang et al., 2008)

The similar methodology was used by Srivastava et al. in 2013. The only difference of these two methodologies was the photophysical sensing mechanisims. In Shang's work sensing event proceeded via FRET mechanism. However, in this design combination of PET, ICT and FRET mechanisms were dominant (Srivastava et al., 2013).

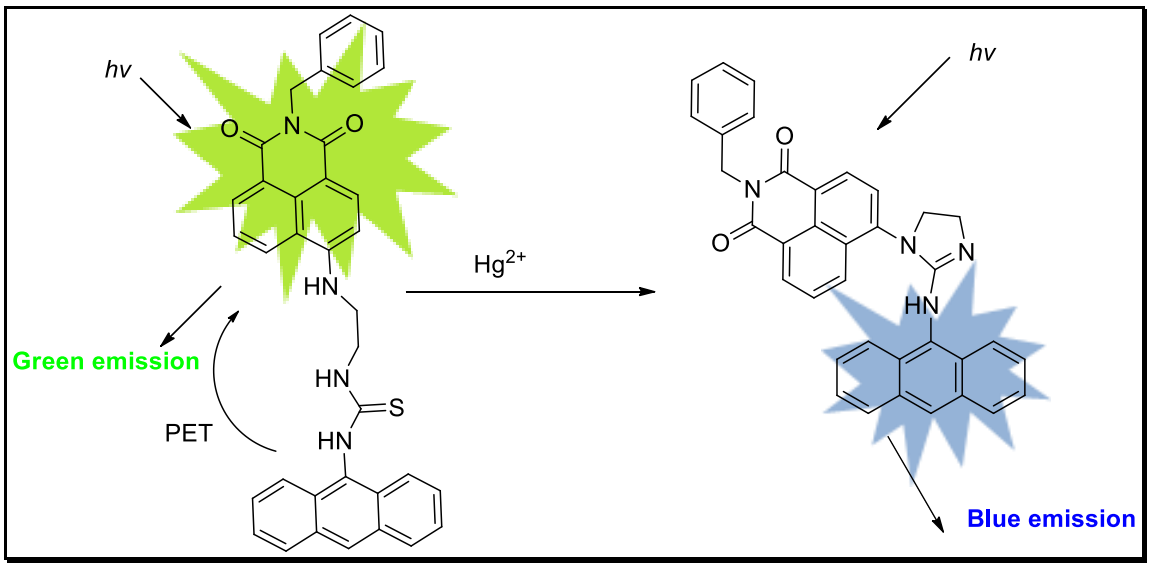

Figure 3.14. A FRET probe based on napthalimide-anthracene scaffold.
(Source: Srivastava et al., 2013)

The critical examples of fluorescent probes that enable to detect Hg^{2+} ions were summarized in Figure 3.15 (Yang et al., 2013).

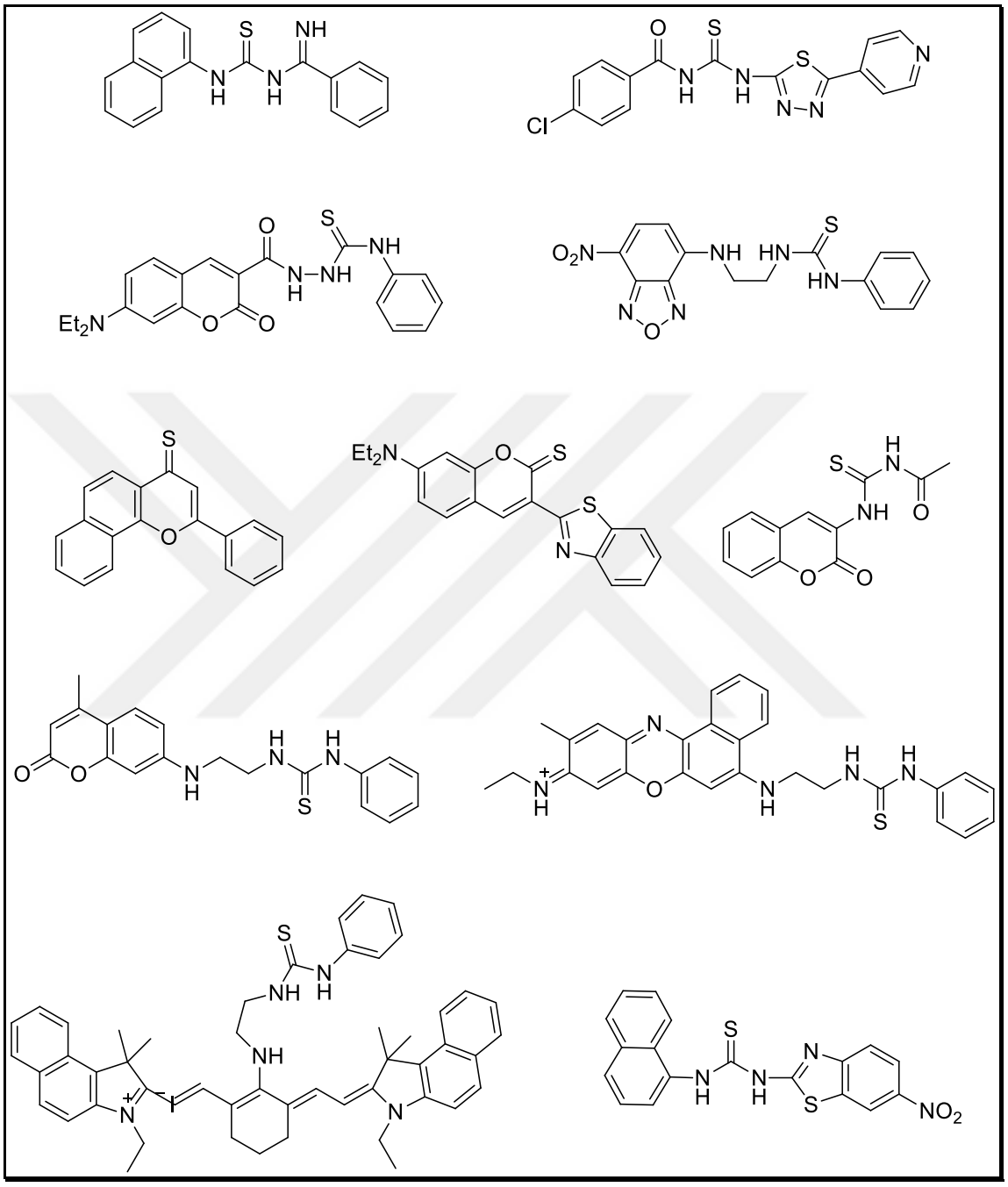

Figure 3.15. Fluorescent sensors for Hg^{2+} working via desulfation reaction (Source:Yang et al., 2013)

Other reactive units towards mercury ions are thioethers that are commonly used as protecting groups. The Hg^{2+} mediated hydrolysis of the thioethers produce the aldehyde structure. This reactivity provides a good opportunity to desing new fluorescent molecular sensors.

In 2012, Zhang et al. reported a study in which 2-formylated BODIPY protected with 1,3-propanedithiol –a mercury reactive group- was used as Hg^{2+} sensor. The addition of mercury ions to the sensing solution resulted in a distinct color chage and enhancement in fluorescence intensity with a small blue shift. To prove the formation of an aldehyde derivative at the end of the sensing event, the outcome of reaction was subjected to HPLC analysis and hydrolysis mechanism was proved (Zhang et al., 2012). The same motif was also used by Saha et al. in 2013. The only difference of this study was the combination of sensory system with a biologically benign β-cyclodextrin structure that enhances the water solubility of dye molecule (Saha et al., 2013).

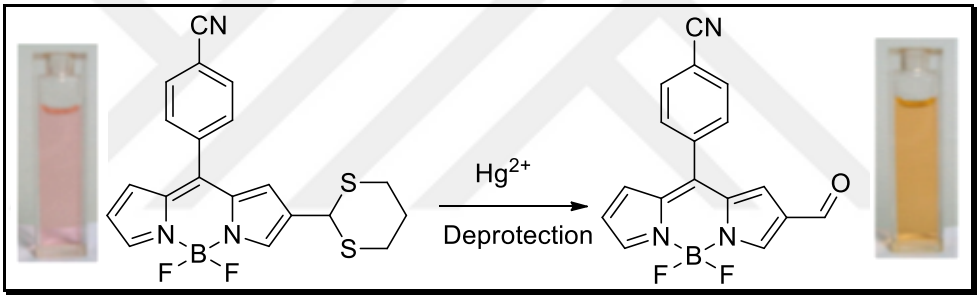

Figure 3.16. BODIPY based chemodosimeter working via deprotection mechanism (Source: Zhang et al., 2012)

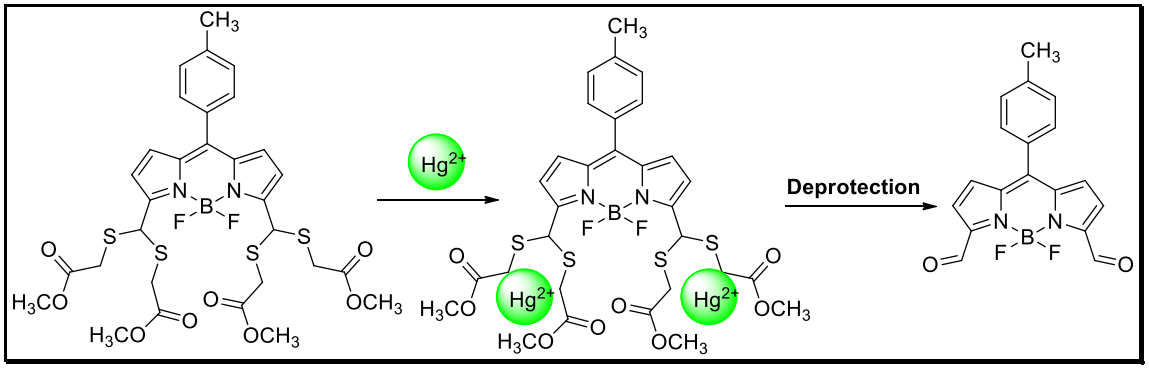

Figure 3.17. BODIPY based chemodosimeter working via deprotection mechanism (Source: Madhu et al., 2012)

Another example of BODIPY based chemodosimeter integrated with dithioacetal protecting groups from 3,5 positions was reported by Madhu (Madhu et al. 2014). Addition of mercury ions to the dye solution ended up with a fluorescence enhancement due to the Hg^{2+} promoted deprotection of dithioacetal groups. To clarify the reaction mechanism, NMR titration experiment was performed and the occurrence of an aldehyde peak -resonated at 10.5 ppm in ^{1}H NMR spectrum of end product- proved the deprotection mechanism.

Although desulfation approach is an effective and common, there are some important problems in real. Many of sensing environments especially living systems include sulphur containing compounds and that may interfere the sensing process. To overcome this handicap development of new sensing strategies are always in demand. As it mentioned before, Hg^{2+} ions share similar chamical nature with gold ions. The high alkynophilicity of mercury ions have frequently used in synthetic organic chemistry. Based on this reactivity, unsaturated bonds have intensively used in the design of mercury ion sensitive molecular sensors. The main drawback of molecular probes bearing unsaturated bond functionality in their structure is the cross affinity of competitive metal ions such as Au^{3+}, Pd^{2+}, Ag^{+}. However, there have been lots of chemodosimeters that specifically respond toward mercury ions.

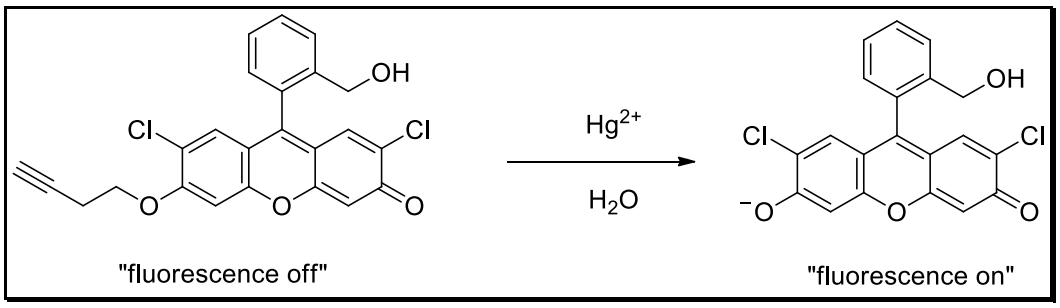

Figure 3.18. First example of Hg^{2+} sensor bearing alkyne moiety
(Source: Song et al., 2008)

Koide and co-workers have made a respectable contribution to the area of mercury ion sensing. The first example of fluorescent molecular sensor for mercury ions bearing an alkyne structure in its skeleton was demonstraed by them (Song et al., 2008). In their strategy, the fluorescein dye that derivatized from oxygen atom with an alkyne moiety was subjected to mercury ions. The sensor molecule was nonemissive in its

initial state. Addition of Hg^{2+} to the sensing solution resulted in an enhancement of fluorescence emission due to the formation of a new fluorescein derivative. Mercury ions promotes the oxymercuration reaction that followed by elimination of alkyne ether structure from the fluorescein dye. Besides being first example of Hg^{2+} sensor bearing alkyne moiety in its structure, the probe molecule also allowed the detection of Hg^{2+} ions in Salmon tissue and dental amalgam.

The high reactivity of Hg^{2+} towards alkyne groups was also used by Lee and Kim in 2011. They developed a ratiometric fluorescent probe based on coumarin structure. Addition of mercury ions to the sensing media produces an oxazole derivative of coumarine in the presence of water. The reaction is known as Kuscheroff reaction. While the sensor molecule had emission at 469 nm addition of Hg^{2+} to the sensing media caused a small red shift in fluorescence spectrum (492 nm).

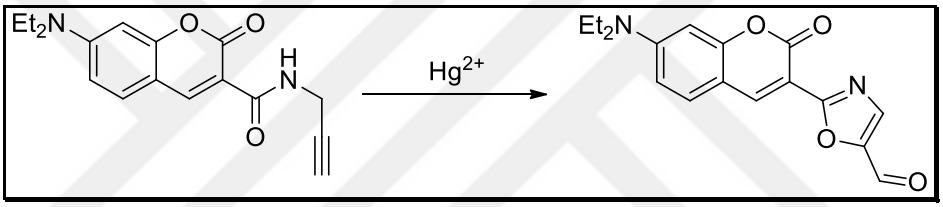

Figure 3.19. Hg^{2+} mediated transformation of amide to oxazole
(Source: Lee and Kim, 2011)

Vinyl ether functionality was also highly reactive towards Hg^{2+} ions and intensively used in design of new sensing methodologies. Ahn and co-workers demonstrated the usage of fluorescein fluorophore coupled with a vinyl ether structure from oxygen atom that underwent an irreversible hydrolysis reaction in the presence of mercury ions. The probe showed high reactivity towards organomercury and inorganic mercury ions. In addition the cell and zebrafish imaging studies were performed in the subject of study (Santra et al., 2009).

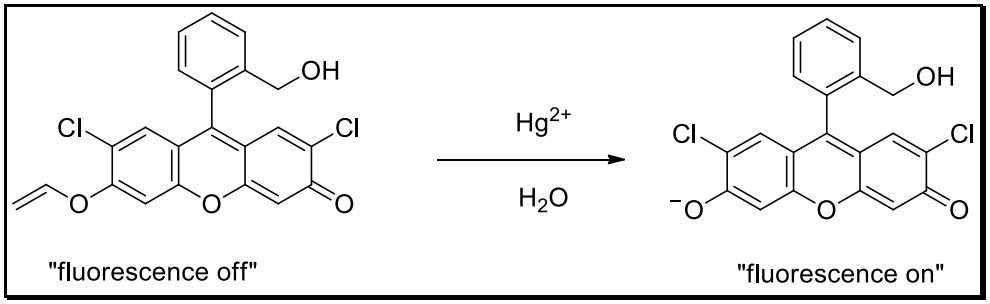

Figure 3.20. Hg^{2+} selective turn on sensor bearing viny ether structure (Source: Santra et al., 2009)

Ahn research group continued their study on the designing molecular probes bearing vinyl ether structure (Figure 3.21) (Santra et al., 2011; Cho and Ahn, 2010).

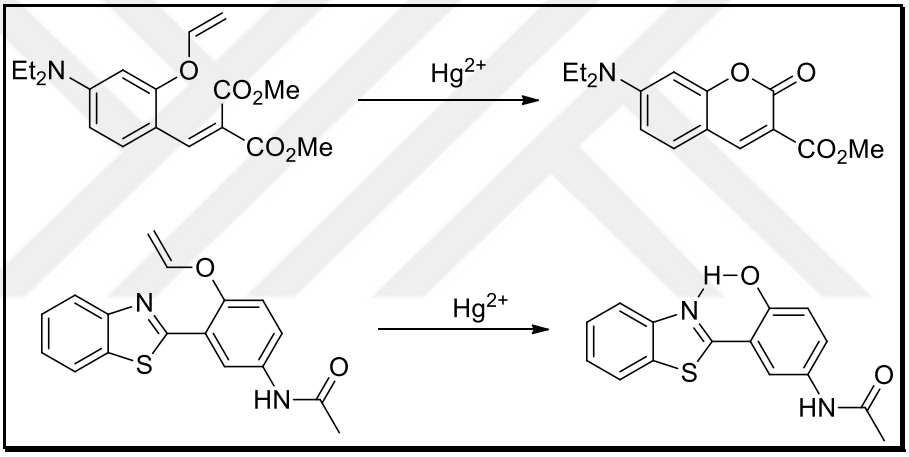

Figure 3.21. Hg^{2+} selective sensors bearing viny ether structure developed by Ahn group (Source: Santra et al, 2011; Cho and Ahn, 2010)

In 2010, Lin et al. demonstrated a mercury ion selective molecular fluorescent sensor including both thiol and alkyne functionality in its structure (Lin et al., 2010).

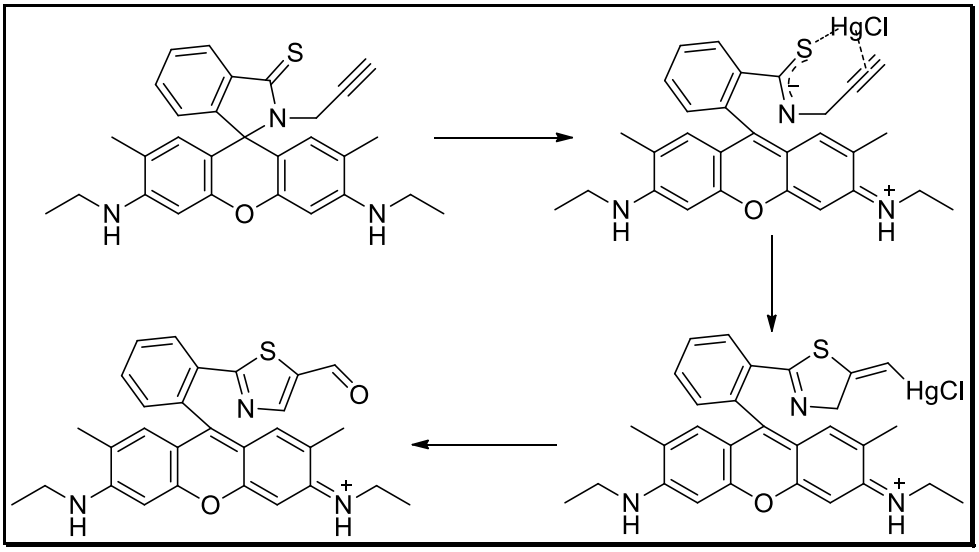

Figure 3.22. The proposed reaction mechanism of Rhodamine based probe with Hg^{2+} (Source: Lin et al., 2010)

The spirocyclic form of rhodamine dye was non-emissive in its initial form. The addition of mercury triggered the cyclization reaction and concomitant ring opening reaction took place. Hg^{2+} ions first coordinated to the thiol and alkyne moiety and produced an organomercury intermediate. Presence of water in sensing media generated the thioazol structure on rhodamine core with an increase in emission spectrum.

3.3. BODIPY Based Fluorescent Sensors for Mercury Ions

This thesis aimed the design, synthesis and investigation of sensory abilities of probe molecules towards addition of metal ions. The gold ion sensing abilities were mentioned in previous study. The subject of this chapter is the investigation of mercury ion sensitivity and selectivity of designed probe molecules. The mercury ion sensitive probes are given in Figure 3.23.

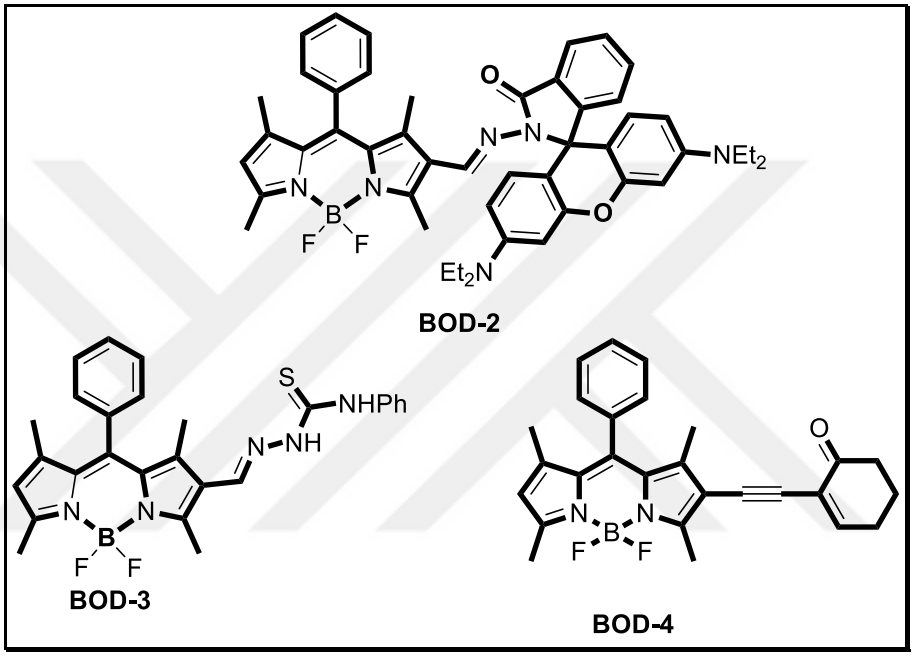

Figure 3.23. BODIPY based sensors detects both gold and mercury ions selectively.

3.3.1. Mercury Ion Sensing Properties of BOD-2

To device a molecular sensor enable to detect multiple ions with different signal outputs have a big challenge for scientists. The major drawback of design of multiple analyte sensors are the similar chemical nature of most of targeted analytes. As mentioned in previous chapter, we developed new generation molecular sensors that capable to differentiate gold and mercury ions.

A molecular sensor (**BOD-2**) was constructed by conjugated BODIPY and Rhodamine fluorophores via **C=N** spacer. As it mentioned, the novel sensing strategy for gold ions was first time developed by our research group. The discrimination of two competitive metal ions (Hg^{2+} and Au^{3+}) became possible by combining this novel approach with thiophilic nature of mercury ions.

After complete characterization of synthesized probe molecule (**BOD-2**), its spectroscopic behavior was investigated. The UV/Vis spectrum of free **BOD-2** (CH_3CN/HEPES 1:1, pH 7.0) exhibits a single absorption band at 527 nm, which belongs to BODIPY core. As the rhodamine core is in the ring closed isomeric form, no absorption band was expected. The addition of Hg^{2+} (1 equiv.) to **BOD-2** led to the appearance of a new strong absorption band at 554 nm, one which was assigned to a ring opened rhodamine derivative.

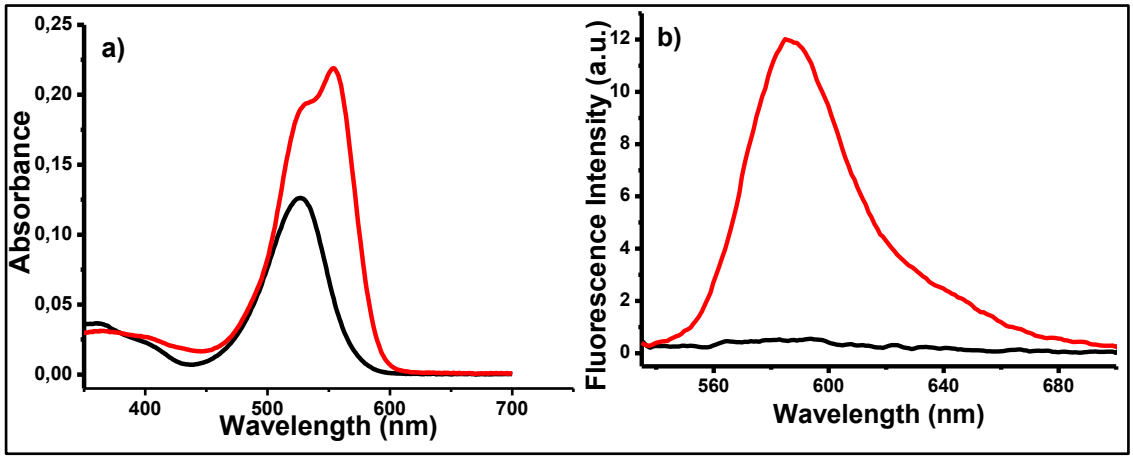

Figure 3.24. a) Absorption and b) Emission spectra of **BOD-2** (5 μM) and Hg^{2+} (1.0 equiv.) in 1:1 CH_3CN/HEPES buffer at pH = 7.0; (λ_{ex}: 525 nm, at 25 ^{o}C).

The fluorescence spectra of **BOD-2** displayed a similar behavior towards the addition of Hg^{2+} (Figure 3.25). Initially, no emission band was observed in the fluorescence spectrum of free **BOD-2** with the excitation at 525 nm. However, upon addition of Hg^{2+} ions, a new emission band with a maximum at 585 nm appeared and the intensity of this band gradually increased with the increasing concentration of the Hg^{2+}. The response of the probe towards the addition Hg^{2+} was immediate and the emission intensity became saturated when 1 equiv. of Hg^{2+} were added, creating an enhancement factor of over 50-fold.

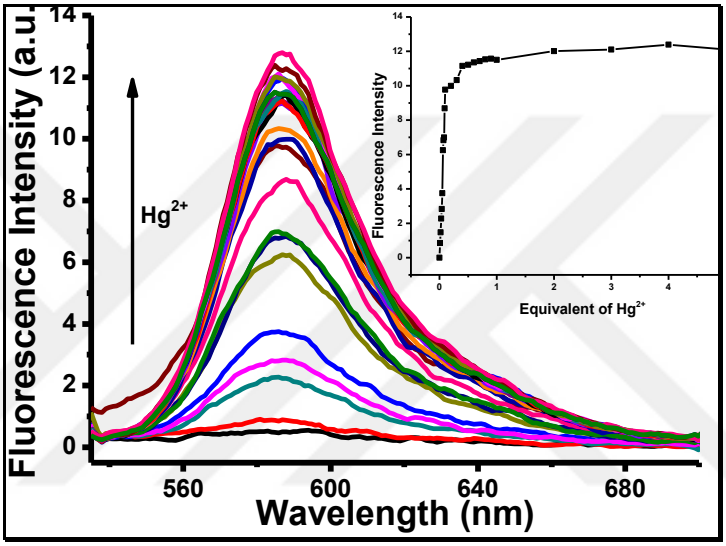

Figure 3.25. Fluorescence spectra of **BOD-2** (5 μM) in 1:1 CH_3CN/HEPES buffer at pH = 7.0 in the presence of Hg^{2+} (mole equivalents = 0.01 - 5.0). Inset: Calibration Curve.

As expected, in the presence of Hg^{2+}, **BOD-2** displayed the optical features characteristic of the rhodamine chromophore. During the process of adding the Hg^{2+}, no other accompanying emission bands were noticed in the emission spectrum that might belong to the BODIPY dye, indicating that the BODIPY was still in sleep ("off") mode.

The increase in emission intensity showed a linear relationship towards the addition of Hg^{2+} in the range of 0-0,3 μM. The minimum amount of Hg^{2+} that can be detected under these conditions was evaluated to be 8.0 nM (Figure 3.26).

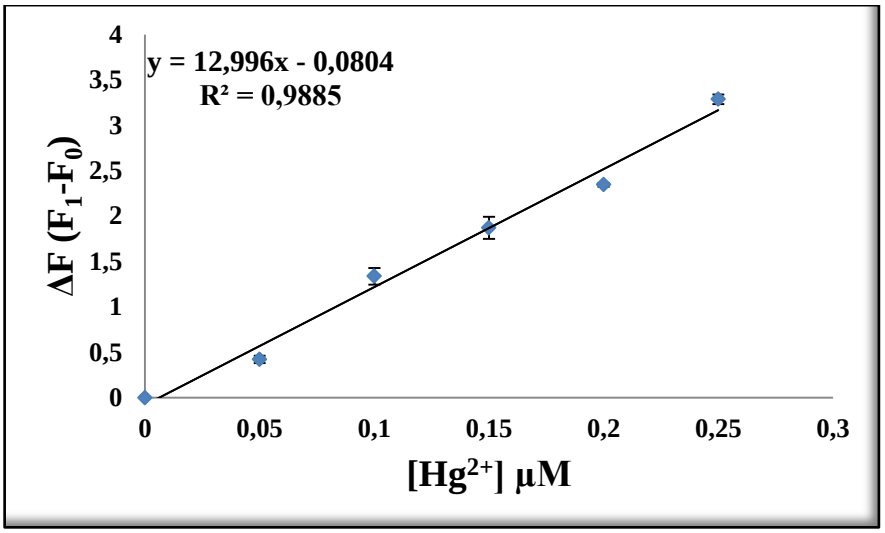

Figure 3.26. Fluorescence changes of probe 1 (5.0 µM) upon addition of Hg^{2+} (0.05 to 0.3 µM, 0.01 to 0.05 equiv.)

The selectivity profile of **BOD-2** in response to other metal ions was further investigated. For all other metal cations, such as Cu^{2+}, Ag^{+}, Zn^{2+}, Pb^{2+}, Ni^{2+}, Na^{+}, Mg^{2+}, Li^{+}, K^{+}, Pd^{2+}, Fe^{2+}, Co^{2+}, Cd^{2+}, Ca^{2+}, Ba^{2+}, Fe^{3+} and Cr^{3+}, no detectable change in the emission intensity for **BOD-2** were observed (Figure 3.27). The probe was highly selective towards Hg^{2+} and showed no spectral response to any other metals ions, except for Au^{3+} ions.

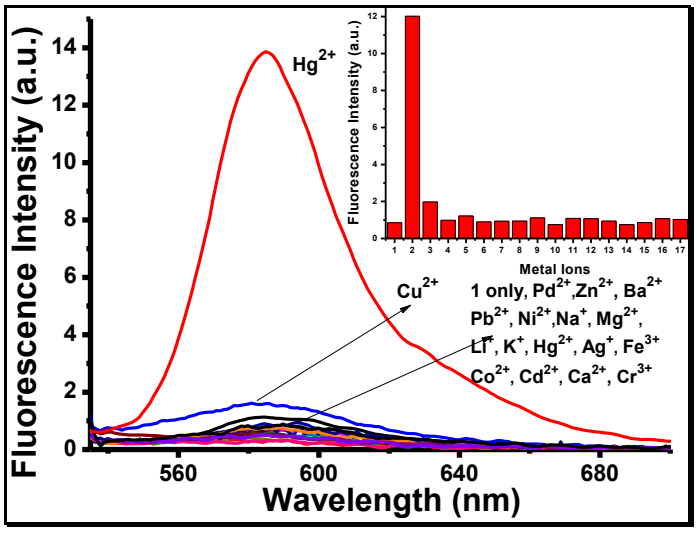

Figure 3.27. Fluorescence intensities of **BOD-2** (5 µM) in 1:1 CH_3CN/HEPES buffer at pH = 7.0 at λ_{max}: 585 nm in the presence of 10.0 equivalents of the cations of interest and Hg^{2+} (1.0 equiv.).

In addition, the interference of other metal ions was explored by performing the fluorescence experiments in the presence of mercury and other metal ions. As shown in Figure 3.28, the response of **BOD-2** towards Hg^{2+} was not affected in the presence of other competitive metal species.

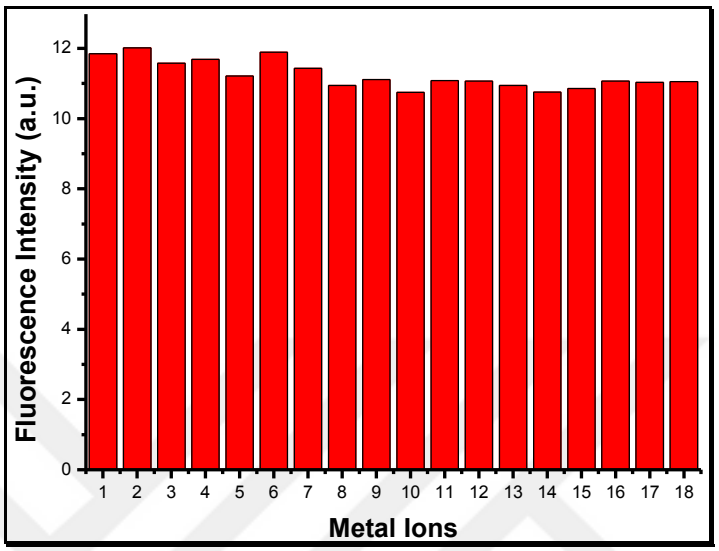

Figure 3.28. Fluorescence intensities of **BOD-2** (5 μM) in 1:1 CH_3CN/HEPES buffer at pH = 7.0 at λ_{max}: 585 nm in the presence Hg^{2+} (1.0 equiv.) and 10.0 equiv the following metal ions: 1, none; 2, Cu^{2+}; 3, Ag^{+}; 4, Zn^{2+}; 5, Pb^{2+}; 6, Ni^{2+}; 7, Na^{+}; 8, Mg^{2+}; 9, Li^{+}; 10, K^{+}, 11, Pd^{2+}; 12, Fe^{2+}; 13, Co^{2+}; 14, Cd^{2+}; 15, Ca^{2+}; 16, Ba^{2+} 17, Cr^{3+}; 18, Fe^{3+}

To check the reversibility of the Hg^{2+} sensing process, the highly emissive probe solution -pre-treated with Hg^{2+}- (**BOD-2**/Hg^{2+}) was subsequently treated with a cyanide ion source (NaCN or NH_4CN). The probe solution immediately lost its color and its emission, thus showing the sensing process is based on a reversible metal-ligand coordination process.

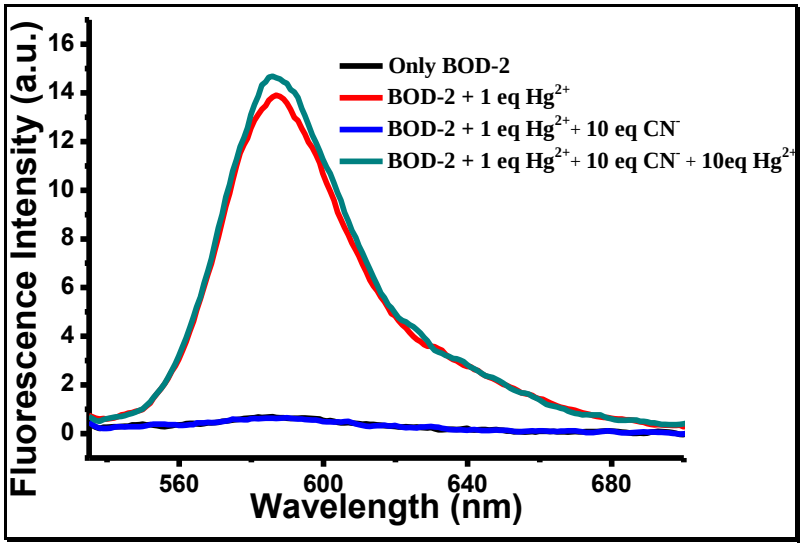

Figure 3.29. Fluorescence intensity changes of **BOD-2** (5 μM) in 1:1 CH_3CN/HEPES buffer at pH = 7.0 at λ_{max}: 585 after addition of 1 equiv. Hg^{2+} , 1 equiv. Hg^{2+} + 10 equiv. CN^- and 1 equiv. Hg^{2+} + 10 equiv. CN^- + 10 equiv. Hg^{2+} respectively.

The stoichiometry of reversible interaction of rhodamine part of **BOD-2** towards mercury ions was further investigated. The binding stoichiometry of the Hg^{2+}/**BOD-2** association was determined by Job's plot from both the UV-Vis absorption and fluorescence data (Figure 3.30). Although it was an unusual situation, both of the plots revealed a 4:1 ratio of the Hg^{2+} ions associating with each molecule of the probe.

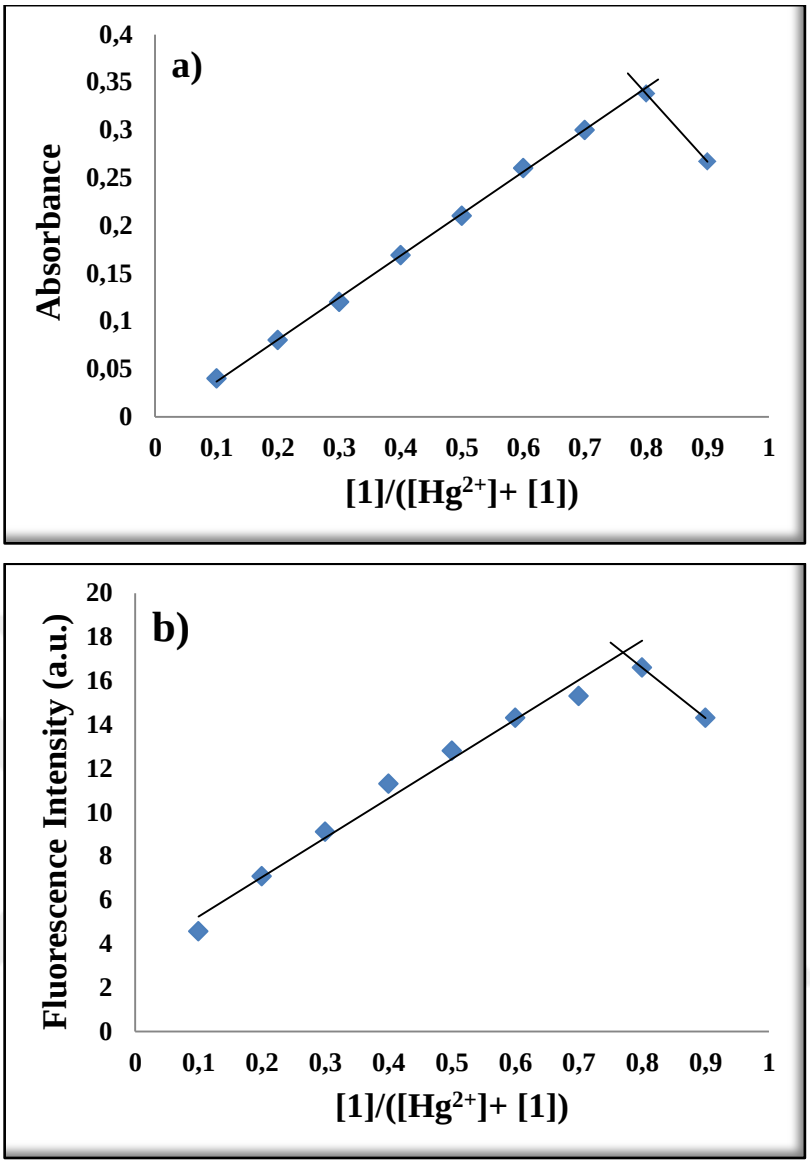

Figure 3.30. Job's plots for the **BOD-2** and Hg^{2+} in 1:1 CH_3CN/HEPES solution at pH = 7.0 from a) absorbance and b) fluorescence (λ_{max}: 585).

As discussed above, the addition of Hg^{2+} to **BOD-2** triggers a spiro-ring opening reaction and results in the formation of a highly emissive rhodamine derivative. It was noted that throughout the addition of Hg^{2+} to **BOD-2**, the BODIPY core continued to be non-emissive because the **C=N** moiety was preserved. The proposed sensing mechanism was illustrated in Figure 3.31.

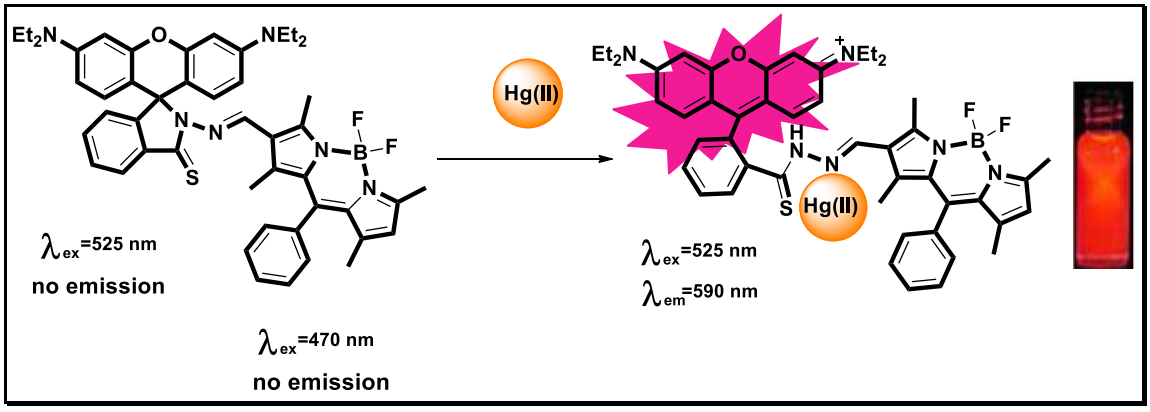

Figure 3.31. Propesed coordination of mercury to Rhodamine-BODIPY scaffold.

In the subject of this study, cell imaging was also performed (Figure 2.32). As shown in Figure 2.32 -given in previous chapter-, **BOD-2** showed similar reactivity towards mercury ions with gold ions. Mercury ions could effectively monitor in human A549 lung adenocarcinoma cell lines.

3.3.2. Mercury Ion Sensing Properties of BOD-3

As indicated before differential detection of multiple analyte species can be achieved best by recognizing each species through a different signal output (i.e., emission wavelength). Incorporating multiple binding motifs onto a single signal-transducing molecule (chromophore/fluorophore) and, as an alternative, combining different transducing molecules have both appeared as efficient routes for sensors with multiple output modes.

Despite recent advances in the field, it remains a challenge to differentiate metal species with similar chemical natures. For example, the ionic species of gold (Au^{3+}) and mercury (Hg^{2+}) share several similarities in terms of binding properties, since both have strong binding affinities toward sulphur species and unsaturated bonds.

In the field of this area a molecular probe (**BOD-3**) was developed that capable of differentiate Au^{3+} and Hg^{2+} with different emission modes. The main advantage of **BOD-3** over **BOD-2** was ability of detection with a single fluorophore group. As mentioned in previous chapter **BOD-3** synthesized from the reaction of formylated BODIPY with phenylisothiocyanate and hydrazine hydrate with a moderate yield. The title compound was characterized by using NMR spectroscopy and HRMS analysis.

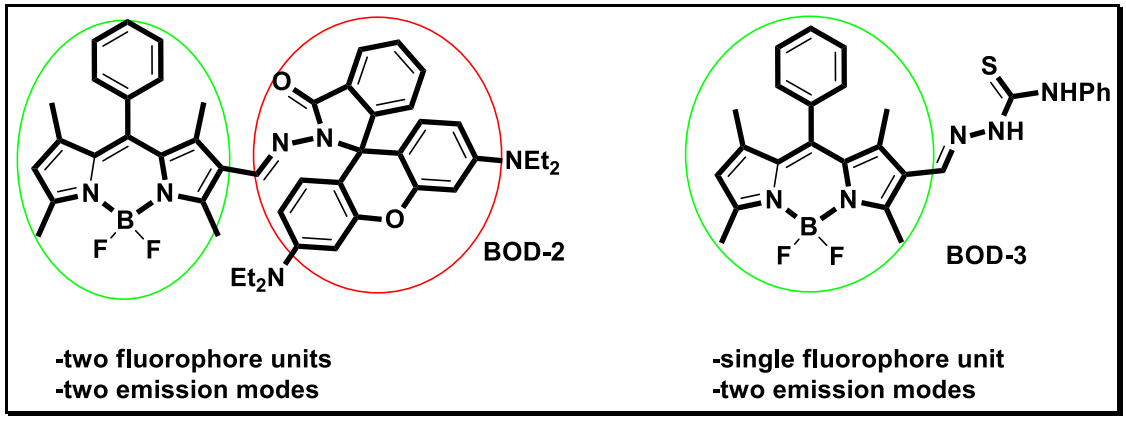

Figure 3.32. Chemical structure of **BOD-2** and **BOD-3**

During the metal screening studies for gold ion sensing, the reactivity of **BOD-3** towards Hg^{2+} ions with a different emission output was realized. To this end, the spectroscopic behaviour of **BOD-3** towards addition of mercury ions was surveyed carefully. To decide the optimum sensing conditions (% water content, pH) UV/Vis and fluorescence changes were investigated upon addition of mercury ions (Figure 3.33).

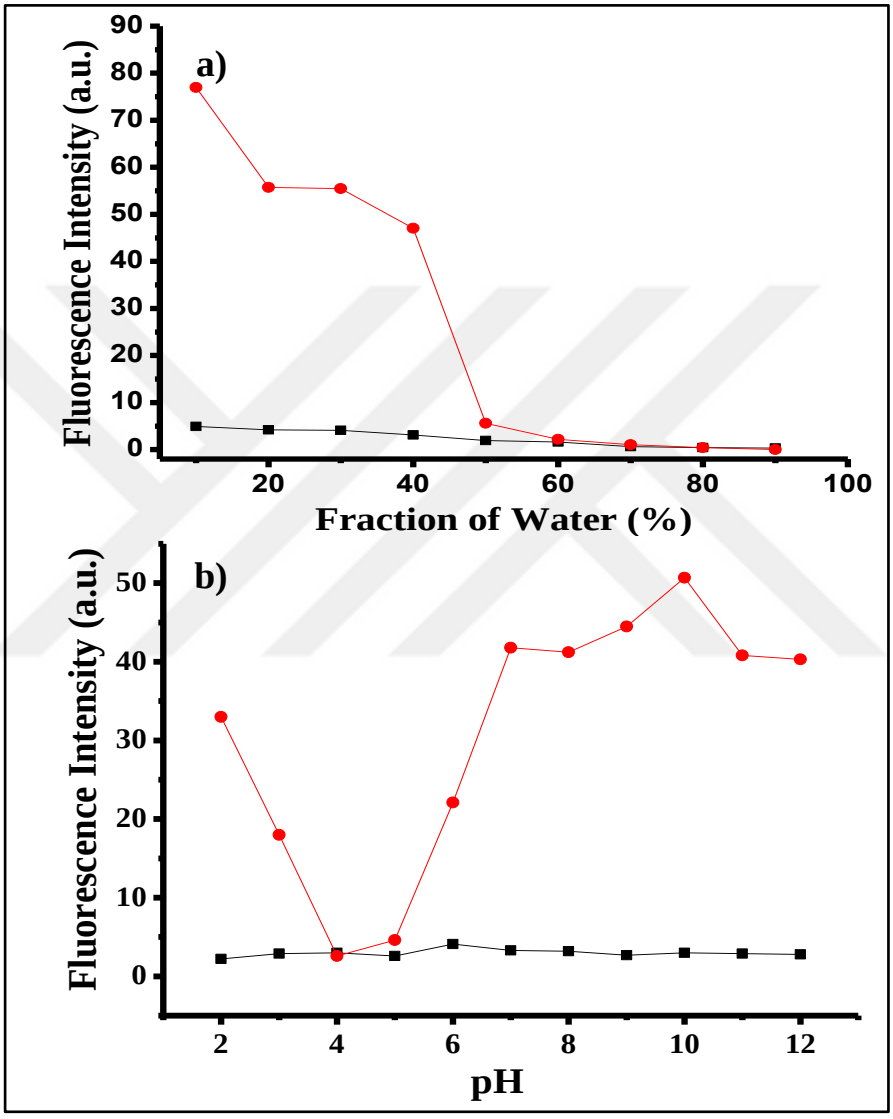

Figure 3.33. a) Effect of fraction of water (pH 7.0/EtOH) and b) Effect of pH (pH/EtOH (v/v, 1:4)) on the interaction of **BOD-3** (10 µM) (black line) with Hg^{2+} (200 µM, 20 equiv.) (red line) in 0.1M potassium phosphate buffer, (λ_{ex}: 460 nm, λ_{em}= 542 nm at 25 ^{o}C).

Given the addition of Hg^{2+}, the weakly emissive probe solution immediately (<5 sec) turned profoundly yellow, possibly due to the blockage of the free rotation around the axis, which prevents the isomerization of the **C=N** bond, and thus enhances the fluorescence emission (Figure 3.34). Meanwhile, in the fluorescence spectrum of **BOD-3**, a new emission band appeared at 542 nm and increased linearly with the increased concentration of Hg^{2+} above the range of 0.1 –100 μM (Figure 3.34.b)

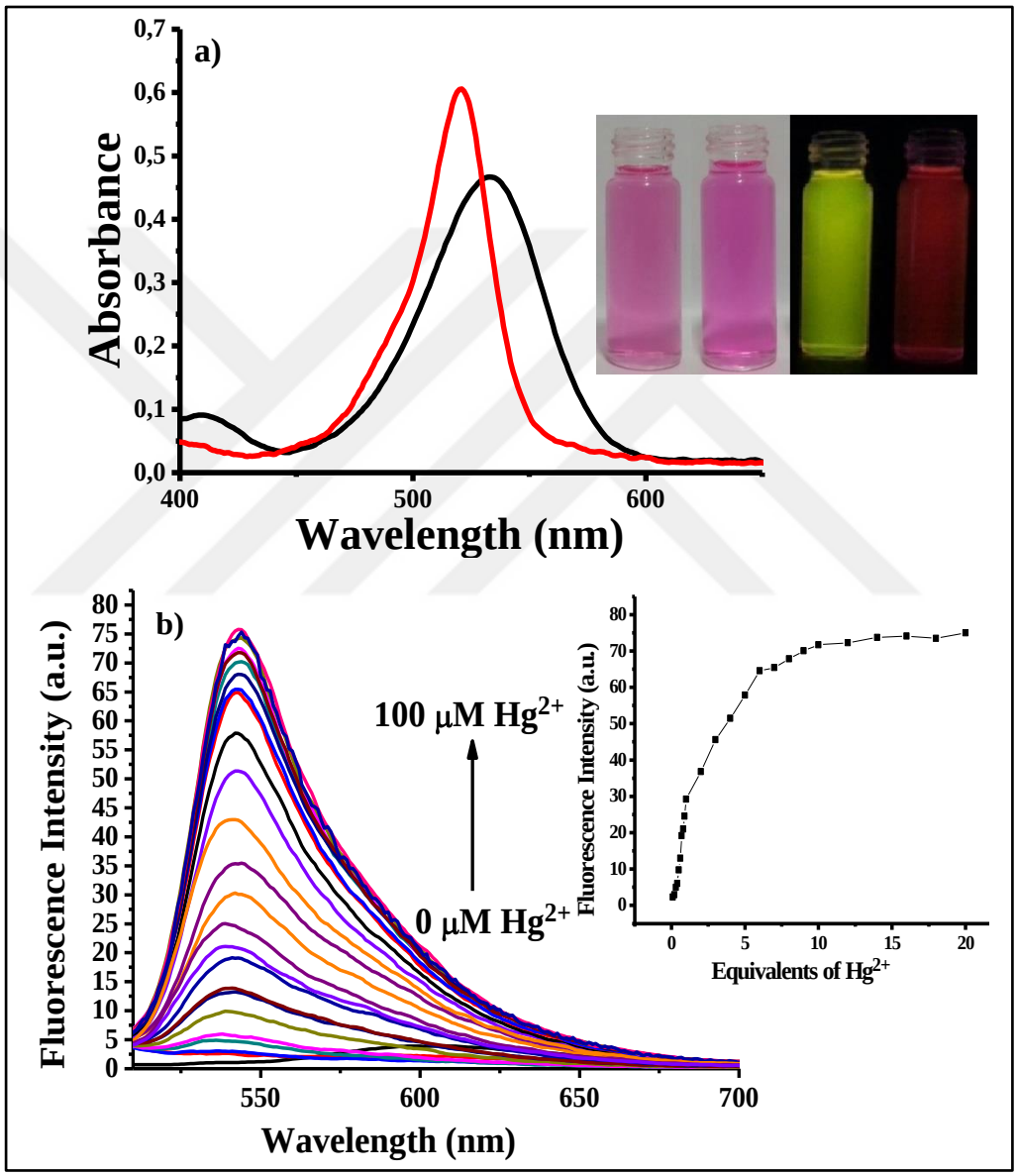

Figure 3.34. a) Absorbance spectra of **BOD-3** (10 μM) in the absence (black line) and presence (red line) of 10 equiv. (100 μM) of Hg^{2+} b) Fluorescence titration spectra of **BOD-3** (10 μM) + Hg^{2+} (0.1 to 100 μM, 0.01 to 10 equiv.) in 0.1 M phosphate buffer / EtOH (pH 7.0, v/v, 1:4) (25°C, λ_{exc}=460 nm).

The minimum detectable amount of mercury ions was evaluated with a systematic titration experiment. The detection limit of **BOD-3** was determined as 160.0 nm for Hg^{2+} ions (Figure 3.35).

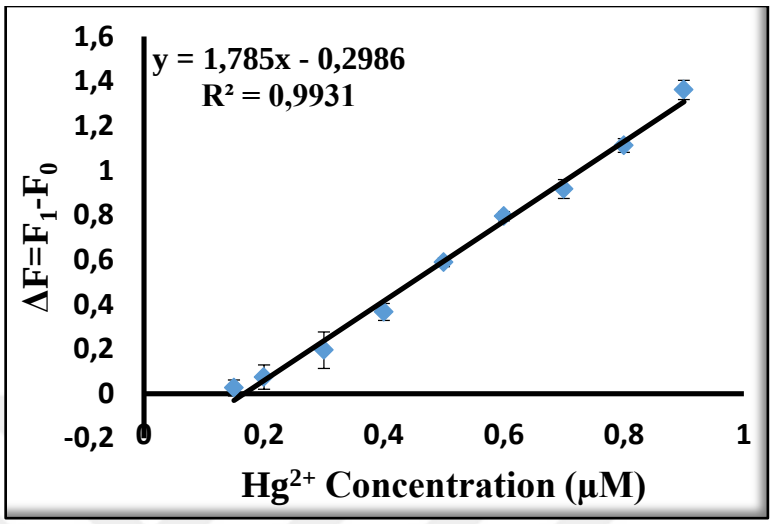

Figure 3.35. Fluorescence changes of **BOD-3** (10 µM) in 0.1 M phosphate buffer/EtOH (pH = 7.0, v/v, 1:4) upon addition of Hg^{2+} (0.01 to 0.1 equiv.) (0.1-1 µM) (λ_{ex} = 460 nm, λ_{em} = 542 nm)

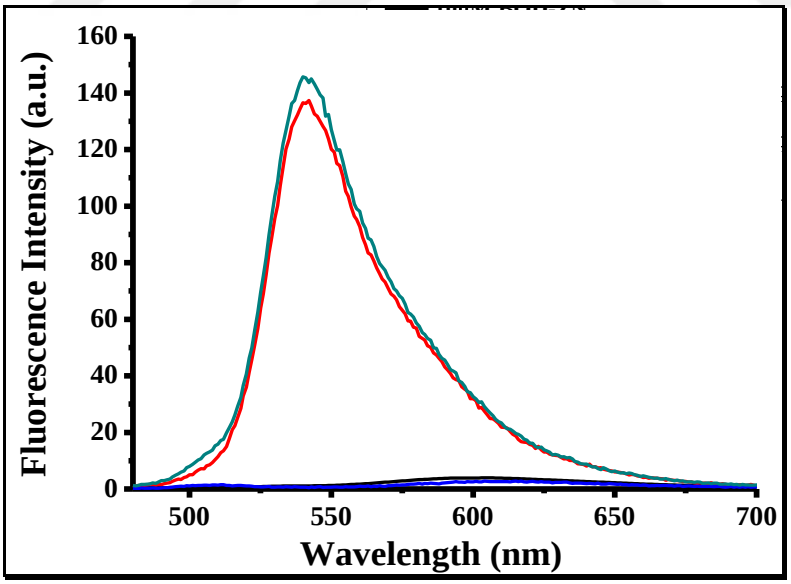

Figure 3.36. Fluorescence intensity changes of **BOD-3** (black line) (10 µM) in EtOH at pH = 7.0 at λ_{max} =542 nm after addition of 10 equiv. Hg^{2+} (red line), 10 equiv. Hg^{2+} + 10 equiv. Na_2S (blue line), 10 equiv. Hg^{2+} + 10 equiv. Na_2S + 10 equiv. Hg^{2+} (green line). (λ_{ex} = 460 nm)

In sharp contrast to the detection of Au^{3+}, detecting Hg^{2+} ions proceeded reversibly. The reversibility of the binding event between **BOD-3** and Hg^{2+} was confirmed by the addition of Na_2S to the solution pretreated with Hg^{2+}, which sharply decreased the emission intensity. The regeneration of fluorescence was again made possible by introducing Hg^{2+} ions into the solution, and the off-on switching ability of the system with Hg^{2+} proved the reversibility of the process (Figure 3.37).

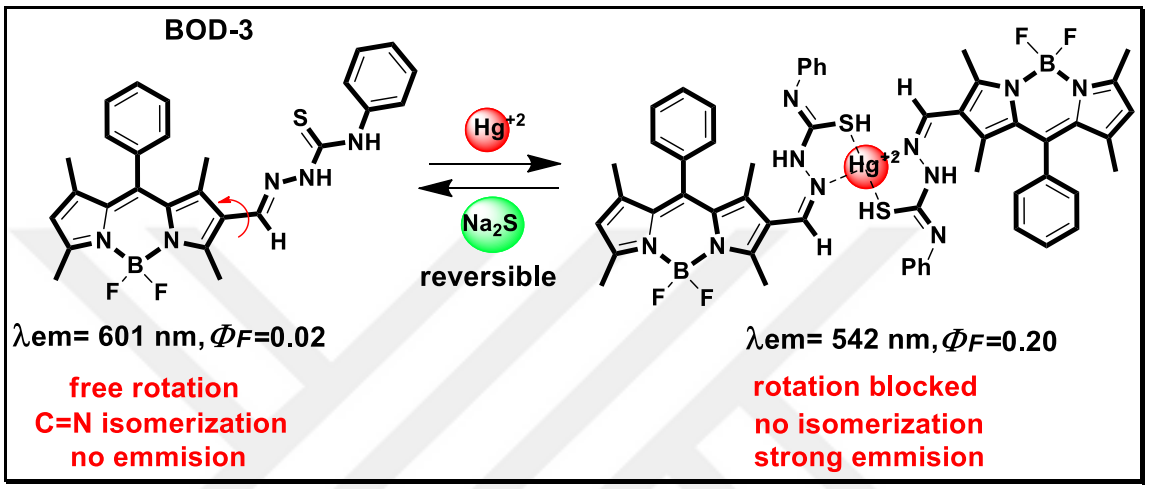

Figure 3.37. Proposed reversible binding of Hg^{2+} to **BOD-3**

At the same time, the binding process of Hg^{2+} to **BOD-3** could be clearly followed by the aid of ^{1}H-NMR spectroscopy (Figure 38). During Hg^{2+} incubation -lasting 5 min-, the pronounced differences in the ^{1}H-NMR spectrum of **BOD-3** was observed. For one, the resonance of the H_a proton signal at 8.01 ppm belonging to the hydrogen atom of the aldimine shifted to a higher frequency, while the resonance of the methyl protons (H_b and H_c) in close proximity to the recognition motif shifted to a lower frequency. Furthermore, a reorganization of the phenyl ring proton signals strongly suggests the structural modification in the phenyl thiourea motif.

With HRMS analysis, the binding of Hg^{2+} ions to **BOD-3** was also confirmed. HRMS data of the solution (Hg^{2+}/ **BOD-3**) indicated the formation of an Hg^{2+} ion complex, (m/z = 1204.368 found; 1204.364 calc.), with a binding stoichiometry of 1:2. Given all of the above, the structure of the binding complex is most likely that shown in Figure .3.37.

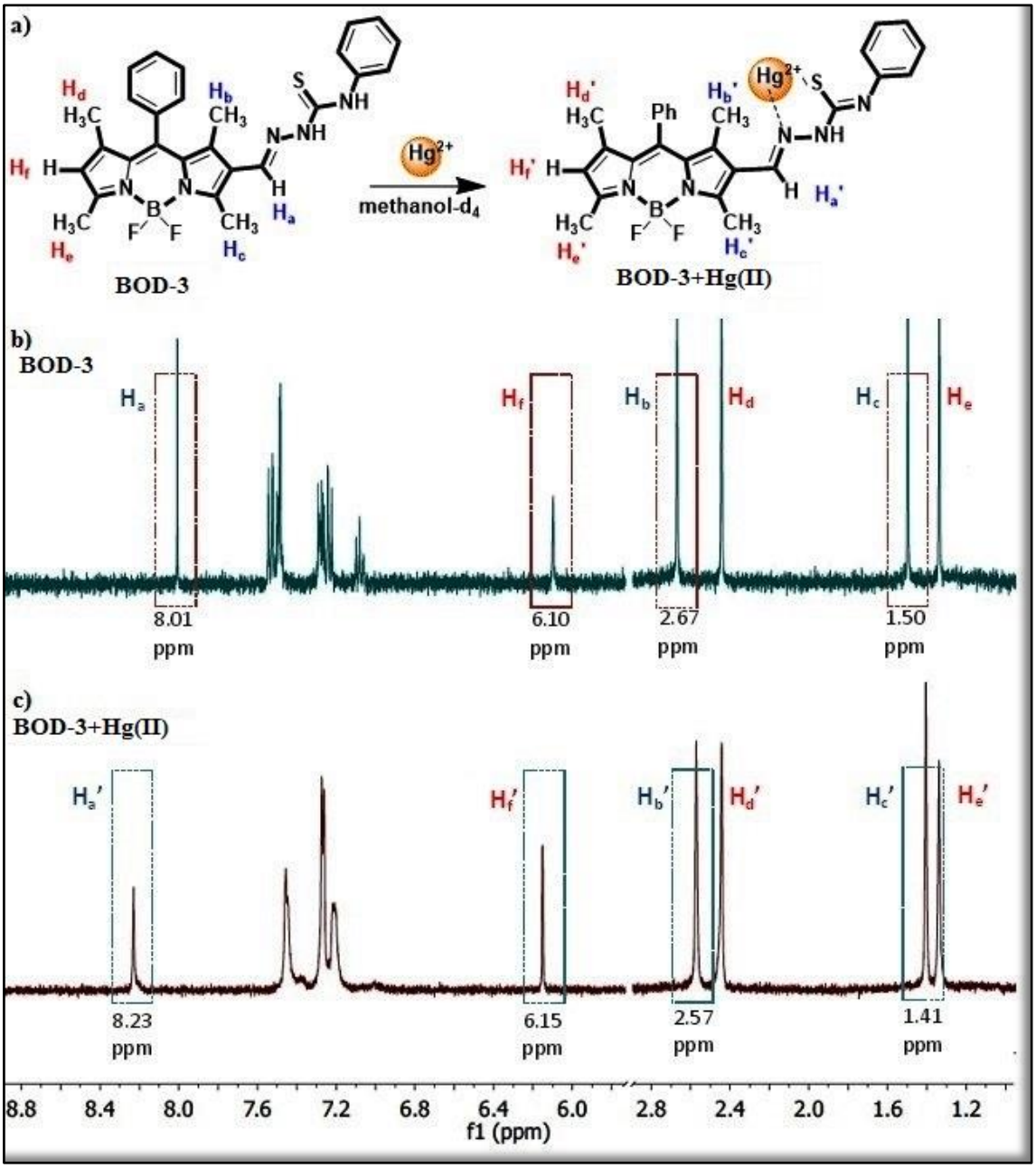

Figure 3.38. a) Proposed coordination mechanism of Hg^{2+} to **BOD-3**. b) ^{1}H-NMR of **BOD-3** in methanol-d_4. c) ^{1}H-NMR of **BOD-3** + Hg^{2+} (1 equiv.) in methanol-d_4.

Having clarified the detection of both metal species, the interference of other metal ions in the detection of Au^{3+} and Hg^{2+} was assessed. Although the spectral response of **BOD-3** induced by Au^{3+} ions showed no interference with other metal ions, the detection of Hg^{2+} was disturbed in the presence of Au^{3+} ions. More specifically, in the presence of Au^{3+} and Hg^{2+}, the fluorescence spectrum initially displayed an emission band at 542 nm for the Hg^{2+}/**BOD-3** binding complex. However, the band

disappeared within 10 min, as a new band appeared at 512 nm, which indicates that Au^{3+} ions also mediate the hydrolysis of the Hg^{2+} binding complex (Figure 3.39.b). Notably, the same sensing behaviour was also observed by adding Au^{3+} ions to a solution pretreated with Hg^{2+}.

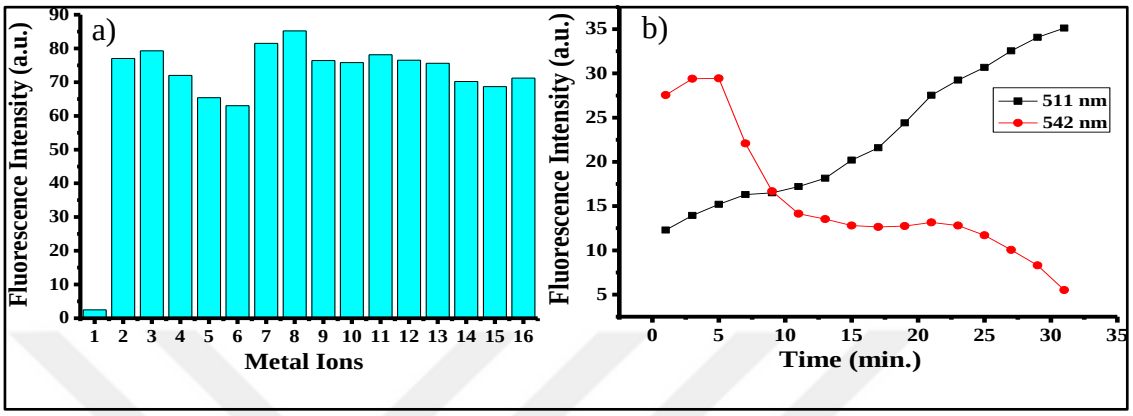

Figure 3.39 a) Fluorescence intensities of **BOD-3** (10 μM) in 0.1 M phosphate buffer/EtOH (pH = 7.0, v/v, 1:4) in the presence of 20.0 equiv. (200 μM) of the cations interest : 1, **BOD-3** only; 2, Hg^{2+}; 3, Au^{+}; 4, Ba^{2+}; 5, Ca^{2+}; 6, Cd^{3+}; 7, Cr^{2+}; 8, Cu^{2+}; 9, Fe^{2+}; 10, I^{-}; 11, Mg^{2+}; 12, Ni^{2+}; 13, Pb^{2+}; 14, Zn^{2+}; 15, Ag^{+}; 16, F^{-} . b) Selectivity profile of **BOD-3** towards Au^{3+} and Hg^{2+} ions (λ_{ex} = 460 nm, λ_{em} = 542 nm and 511nm).

The promising properties of developed chemodosimeter were also applicable in monitoring the presence of mercury ions in living cells. As shown in the Figure 2.41, **BOD-3** could successfully detect the Au^{3+} and Hg^{2+} ions in Human Lung Adenocarcinoma cells (A549). The interesting feature of cell imaging study was the emission channel of resulted dye structure. As it could be seen in Figure 2.41 the addition of both Au^{3+} and Hg^{2+} ions produced green emission due to the hydrolysis of thiosemicarbazide functionality in cell media.

The major advantage of the **BOD-3** over other synthesized probe its ability to differentiate two chemically similar metal ions with different emission modes.

3.3.3. Mercury Ion Sensing Properties of BOD-4

The alkynophilic character of mercury ions was mentioned in detail. In our design **BOD-4** included an alkyne functionality that underwent gold or mercury ion mediated irreversible cyclization reaction. Actually, the **BOD-4** probe was designed for the detection of gold ions. However, mercury ions also showed high affinty towards addition of Hg^{2+} ions with the same emission mode. This unexpected observation was reasonable, for Hg^{2+} ions similar to Au^{3+} species are known to have high affinities to alkynes.

After realizing of Hg^{2+} sensitivity of **BOD-4**, optimum sensing conditions was tried to define. The investigation was first started with screening of the effect of water and pH on the sensing event with the same solvent system (Ethanol/Phosphate buffer) of gold ions.

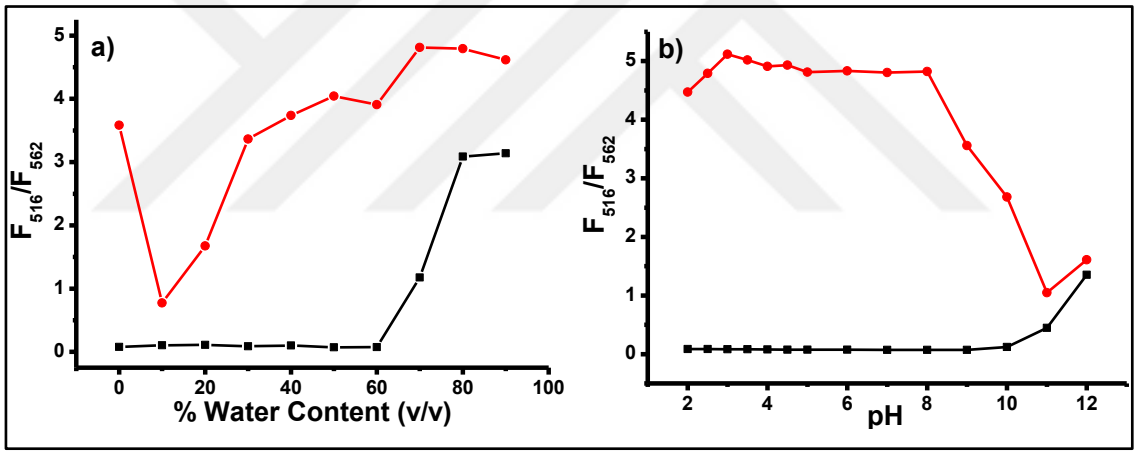

Figure 3.40. a) Effect of fraction of water (pH 7.0/EtOH) and b) Effect of pH (pH/EtOH (v/v, 6:4)) on the interaction of **BOD-4** (10 µM) (black line) with Hg^{2+} (200 µM, 20 equiv.) (red line) in 0.1M potassium phosphate buffer, (λ_{ex}: 460 nm at 25 ^{o}C).

The sensing behaviour of **BOD-4** was surveyed towards addition of Hg^{2+} ions with the aid of ultraviolet (UV) and fluorescence spectroscopy. As indicated in Figure 3.42.a, **BOD-4** has a distinct absorption band at 526 nm in UV spectrum and displays an intense emission band at 562 nm without mercury ions (Phosphate buffer: Ethanol 6:4, pH 7.0). The addition of Hg^{2+} to the sensing system caused formation of a new absorption band at 506 nm with a decrease of the band at 526 nm in absorption spectrum. The same trend was obtained in the emission spectrum of **BOD-4**. Gradual

addition of Hg^{2+} produced a ratiometric response in fluorescence spectrum. A concomitant decrease in emission band at 562 nm was clearly seen with the addition of Hg^{2+}, while a new emission band at 516 nm formed (Figure 3.41.b).

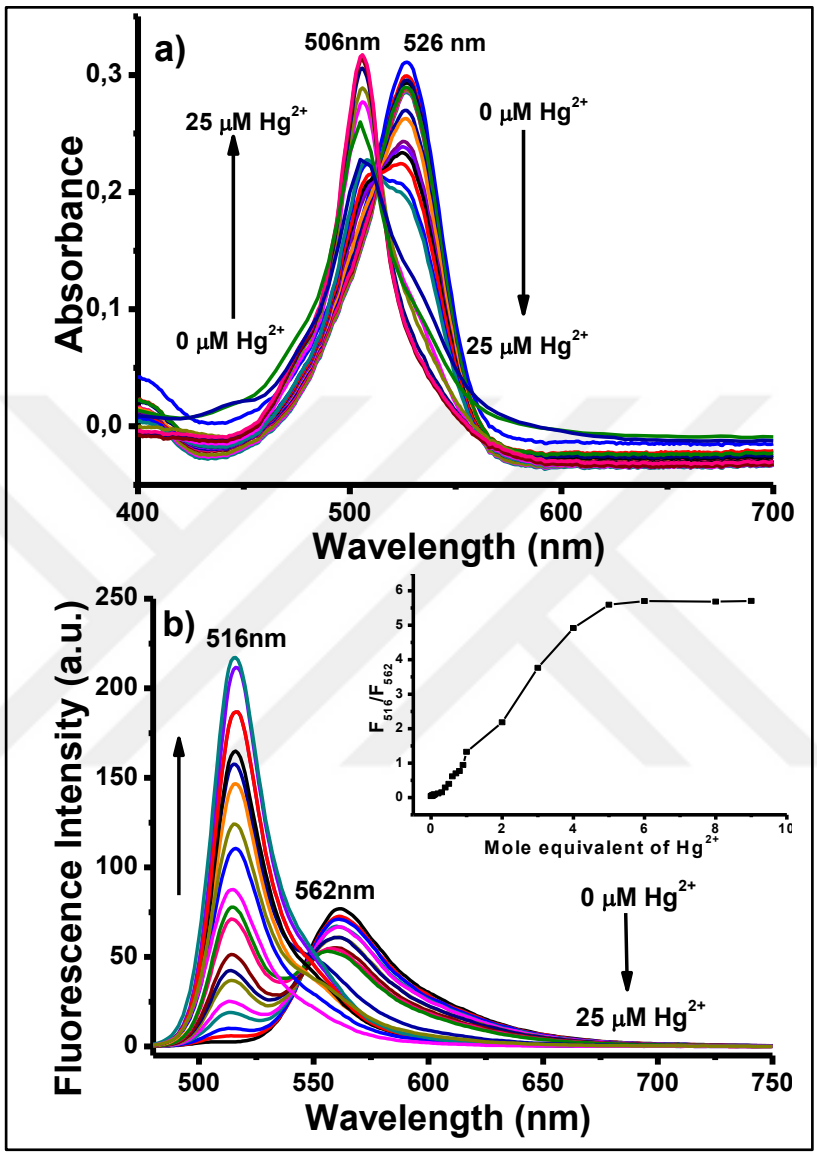

Figure 3.41. a) Absorbance and b) fluorescence spectra of BOD-4 (5 μM) in the presence of increasing amount of Hg^{2+} (0-2 μM) 0.1 M phosphate buffer/EtOH (pH 7.0, v/v, 6:4). Inset: Calibration curve. (λ_{ex}: 460 nm at 25 ^{o}C).

The saturation of sensing event was achieved with the addition of 5 equivalents of Hg^{2+} ions. The increase in emission intensity showed a linear relationship towards the addition of Hg^{2+} in the range of 0.05-0.5 μM. Notably, the detection limit for Hg^{2+} was

measured to be slightly higher than that for Au^{3+} ions (60 nM) yet still at nanomolar levels.

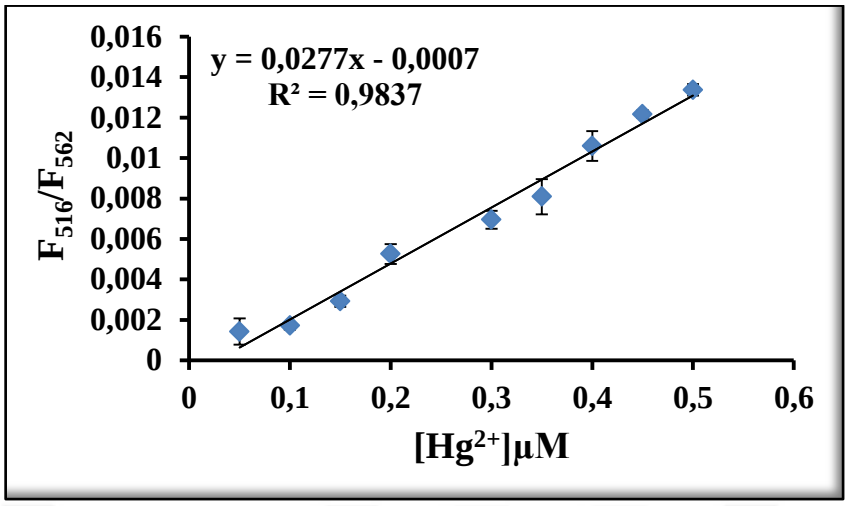

Figure 3.42. Fluorescence changes of **BOD-4** (5.0 µM) upon addition of Hg^{2+} (0.05 to 0.5 µM, 0.01 to 0.1 equiv.) in 0.1M potassium phosphate buffer, pH 7.0/EtOH (v/v, 6:4) (λ_{ex}: 460 nm, at 25 ^{o}C).

In addition, the rate of sensing event was investigated via addition of mercury ions with different concentrations. Even **BOD-4** gave a rapid response towards addition of mercury ions, the completion of reaction lasts approximitly 120 minutes (Figure 3.43).

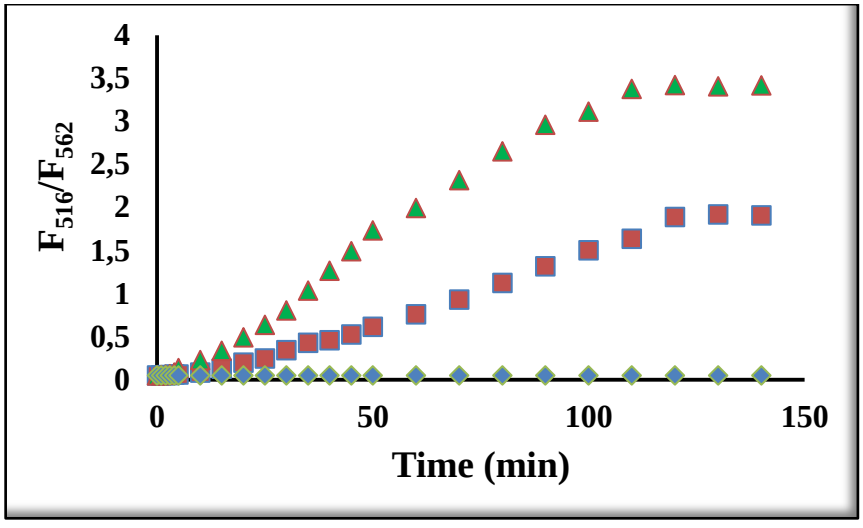

Figure 3.43. Reaction time profiles of **BOD-4** (5 µM) in the absence (♦) or presence of Hg^{2+} [5(■), 10(▲) µM]. The fluorescence intensities were continuously monitored at time intervals in 0.1 M phosphate buffer/EtOH (pH 7.0, v/v, 6:4) (λ_{exc}=460 nm at 25 ^{o}C).

Having clarified the nature of mercury ion detection, the possible interference of other metal species was next assessed. As shown in Figure 3.44, the response of **BOD-4** toward Hg^{2+} ions remained unaffected in the presence of other competitive metal species.

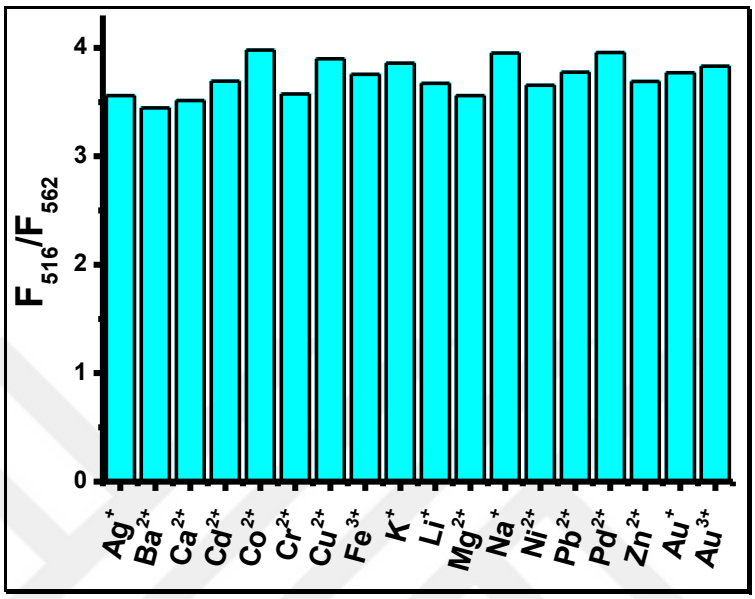

Figure 3.44. Fluorescence intensities of **BOD-4** (5 μM) in the presence of Hg^{2+} (25 μM, 2 equiv.) and 10 equiv. of other metal ions in 0.1 M phosphate buffer/EtOH (pH 7.0, v/v, 6:4) (λ_{exc}=460 nm at 25 ^{o}C).

Further experiments on improving the selectivity of the probe toward one distinct metal species -that is, either Au^{3+} or Hg^{2+}- revealed that the selectivity toward Hg^{2+} could be significantly improved by adjusting the nature of the sensing media. Remarkably, in an alternative solvent system -namely, a HEPES/acetonitrile (pH = 7.0) buffer (6:4 (v/v))- the probe displayed exceptional selectivity toward Hg^{2+} ions.

The effectiveness of methodology was investigated by screening the water ratio and pH variations. **BOD-4** displayed high sensitivity towards Hg^{2+} ions in a wide range of pH and all combinations of acetonitrile/water solutions. However, the variations of water content strongly affected the selectivity of probe because of the competitive nature of Au^{3+} and Hg^{2+} (Figure 3.45).

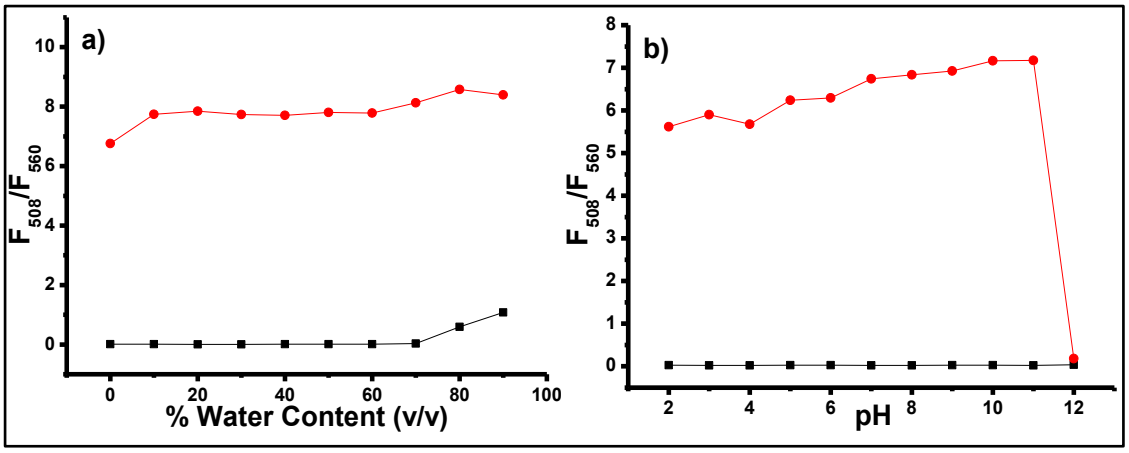

Figure 3.45. a) Effect of fraction of water (pH 7.0 HEPES/CH_3CN) and b) Effect of pH (HEPES/CH_3CN, (v/v, 6:4)) on the interaction of **BOD-4** (10 μM) (black line) with Hg^{2+} (20 μM, 2 equiv.) (red line) in 0.1M potassium phosphate buffer, (λ_{ex}: 460 nm at 25 ^{o}C).

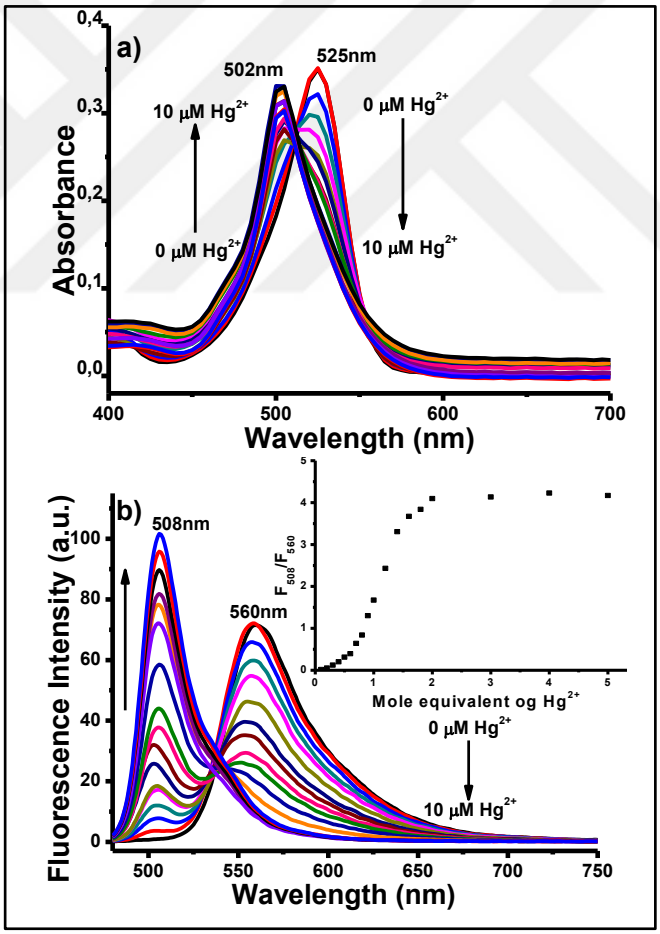

Figure 3.46. a) Absorbance and b) fluorescence spectra of **BOD-4** (5 μM) in the presence of increasing amount of Hg^{2+} (0-2 μM) in 10 mM HEPES, pH 7.0/CH_3CN (pH 7.0, v/v, 6:4). Inset: Calibration curve. (λ_{ex}: 460 nm at 25 ^{o}C).

The solvatochromic effect was observed in absorbance and fluorescence spectrum. A small blue shift was observed in both absorption emission wavelengths. **BOD-4** had a distinct absorption band at 525 nm and displayed an emission at 560 nm in its initial state. As in the case of previous conditions addition of Hg^{2+} also gave the ratiometric response with a formation of new absorption and emission bands (502 nm and 508 nm, respectively) (Figure 3.46). A systematic fluorescence titration experiment revealed a linear relationship in emission intensity towards addition of Hg^{2+} ions with in the range of 0.1-0.5 μM concentration (Figure 3.47). The minimum detectable concentration of Hg^{2+} was found as 250 nM.

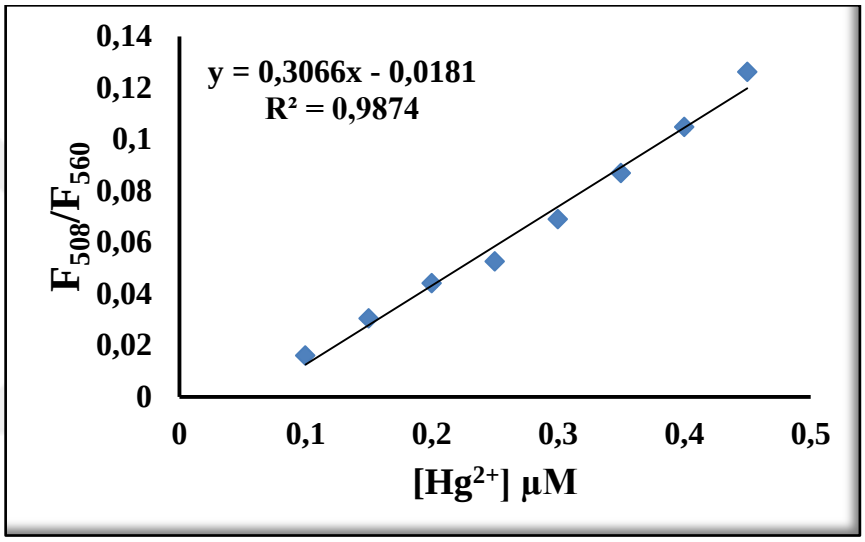

Figure 3.47. Fluorescence changes of **BOD-4** (5.0 μM) upon addition of Hg^{2+} (0,1 to 0,5 μM, 0. 02 to 0.1 equiv.) in 10mM HEPES, pH 7.0/CH_3CN (v/v, 6:4) (λ_{ex}: 460 nm, at 25 ^{o}C).

Rate of mercury mediated cyclization process was also investigated in HEPES/CH_3CN system to understand the optimal design for sensing procedure with the aid of fluorescence ratio. **BOD-4** gave a fast response (within 5 minutes) towards addition of Hg^{2+} ions in different concentrations. The saturation point was achived approximitly 45 minutes later after introduction of mercury ions (Figure 3.48).

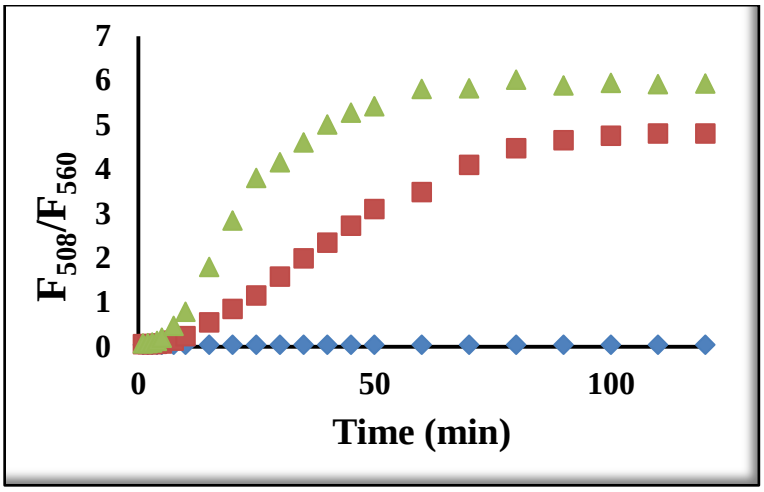

Figure 3.48. Reaction time profiles of **BOD-4** (5 μM) in the absence (♦) or presence of Hg^{2+} [5 (■), 10(▲) μM]. The fluorescence intensities were continuously monitored at time intervals in 10 mM HEPES, pH 7.0/CH_3CN (v/v, 6:4) (λ_{exc}=460 nm at 25 ^oC).

The aim of this part was to detect Hg^{2+} ions over other metal ions with a high selectivity. Because of this reason the solvent system was changed as acetonitrile/HEPES (6/4, (v/v) pH=7.0). To understand the effectivity of the system other metal ions were screened and no cross-talk was observed. The most important improvement of system was the selectivity of Hg^{2+} ions over gold ions (Figure 3.49).

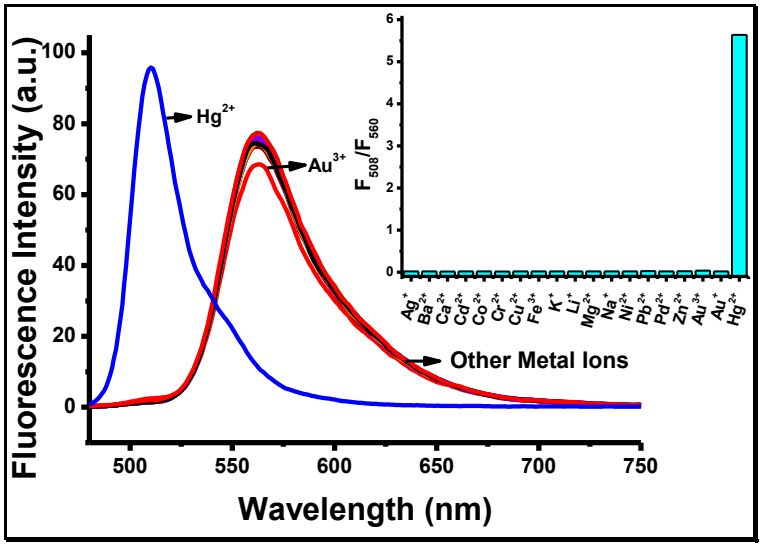

Figure 3.49. Fluorescence intensities of **BOD-4** (5 μM), **BOD-4** (5 μM) + Hg^{2+} (10 μM, 2 equiv.), **BOD-4** (5 μM) + other metal ions (50 μM, 10 equiv.) in 10 mM HEPES, pH 7.0/CH_3CN (v/v, 6:4) (λ_{ex}: 460 nm, at 25 ^oC). Inset: Bar graph notation.

The probe solution was also applicable in the mixture of other metal ions. The competitive fluorescence experiment revealed that **BOD-4** had no influence from other metal ions.

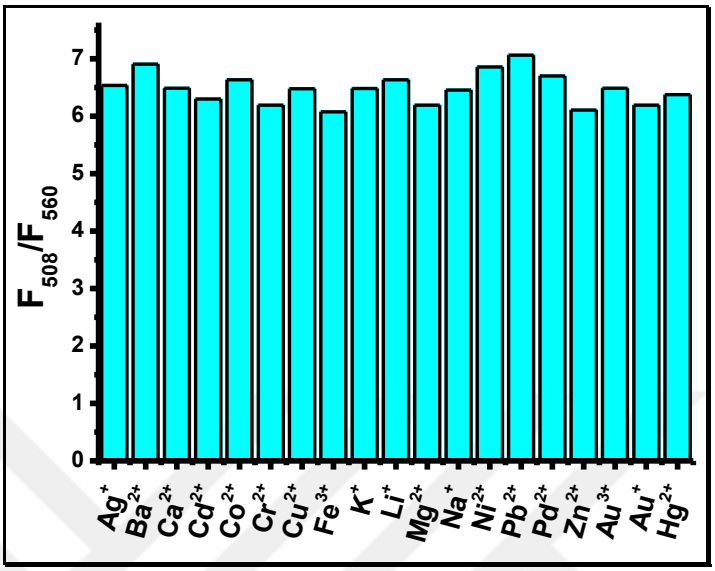

Figure 3.50. Fluorescence intensities of **BOD-4** (5 μM) in the presence of Hg^{2+} (10 μM, 2 equiv.) and 10 equiv. of other metal ions in 10 mM HEPES, pH 7.0/CH_3CN (v/v, 6:4) (λ_{exc}=460 nm at 25 ^{o}C)

In addition, the cell imaging study of **BOD-4** into the Human Lung Adenocarcinoma cells (A549) was demonstrated succesfully. The **BOD-4** displayed a red emission in its initial state and incubation of cells with mercury ions resulted in a green emission.

To sum, in this part of study, a unique BODIPY-based ratiometric fluorescent probe that shows a remarkable change in fluorescence emission toward Au^{3+} and Hg^{2+} ions with high sensitivity and selectivity over other metal ions was devised. By adjusting sensing conditions and simply switching the solvent combination, it was also possible to selectively sense Hg^{2+} ions. Apart from the rapid and specific response to both metal ions in the solution, this probe proved highly successful in imaging gold and Hg^{2+} species in living cells.

CHAPTER 4

EXPERIMENTAL STUDY

4.1. General methods

All reagents were purchased from commercial suppliers (Aldrich and Merck) and they were used without further purification unless otherwise noted. ^{1}H NMR and ^{13}C NMR were measured on a Varian VNMRJ 400 Nuclear Magnetic Resonance Spectrometer and chemical shifts were calibrated using residual solvents signals ($CDCl_3$: δ (H)= 7.26, δ (C)= 77) or TMS. Melting points were determined by using an Electrothermal Melting Point Apparatus 9200. UV absorption spectra were measured on Shimadzu UV-2550 Spectrophotometer. Fluorescence experiments were performed by using Varian Cary Eclipse Fluorescence spectrophotometer. Samples were contained in 10.0 mm path length quartz cuvettes (2.0 mL volume). All measurements were conducted at least in triplicate. The fluorescence images were acquired through an Olympus IX71 fluorescence microscope.

4.2. Determination of detection limits

The detection limit was calculated based on the fluorescence titration (Wu et al., 2011). To determine the detection limit, the emission intensity of probe molecules without metal ions was measured by 10 times and the standard deviation of blank measurements was determined. Under the present conditions, a good linear relationship between the fluorescence intensity and metal ion concentration could be obtained in a concentration range. The detection limit is then calculated with the equation: detection limit = 3σbi/m, where σbi is the standard deviation of blank measurements; m is the slope between intensity versus sample concentration (Emrullahoğlu et al., 2013).

4.3. Determination of quantum yields

Fluorescence quantum yields of synthesized probe molecules were determined by using optically matching solutions of –mostly Rhodamine 6G (Φ_F=0.95 in water)- as a standard (Brouwer, 2011). The quantum yield was calculated according to the equation;

$$\Phi_{F(X)} = \Phi_{F(S)} (A_S F_X / A_X F_S) (n_X / n_S)^2$$

Where Φ_F is the fluorescence quantum yield, A is the absorbance at the excitation wavelength, F is the area under the corrected emission curve, and n is the refractive index of the solvents used. Subscripts S and X refer to the standard and to the unknown, respectively.

4.4. Determination of association constant

The association constant of a metal ion (Au^{3+}) was determined by using fluorescence titration data with the help of following equation (Saha et al., 2010);

$$\ln[(F - F_0) / (F_{max} - F_0)] = n \ln[Au^{3+}] + n \ln(K_{asscn})$$

where n is the number of gold ions associating with each molecule of probe, K_{assoc} is the association constant, F_0 is the fluorescence of the free probe, F_{max} is the fluorescence intensity at saturation point, and F is the fluorescence of probe obtained with metai ion (Au^{3+}) addition.

4.5. Cell Imaging

A549 Human Lung Adenocarcinoma cell lines were grown in DMEM supplemented with 10% FBS (fetal bovine serum) in an atmosphere of 5 % CO_2 at 37 ^oC. The cells were plated on 12mm cover glasses in 6-well plate and allowed to grow for 24h. Before the experiments, the cells were washed with PBS buffer, and then the cells were incubated Dye molecule (5 or 10 μM) for 20 min at 37 ^oC then washed with PBS three times. After incubating with Au^{3+} or Hg^{2+} (10 or 20 μM) for 20 min at 37 ^oC, cells were rinsed with PBS three times, and DAPI for 10 min at 37 ^oC then washed with

PBS three times. Then, the fluorescence images were acquired through an Olympus IX71 fluorescence microscope.

4.6. Synthesis of Probe Molecules

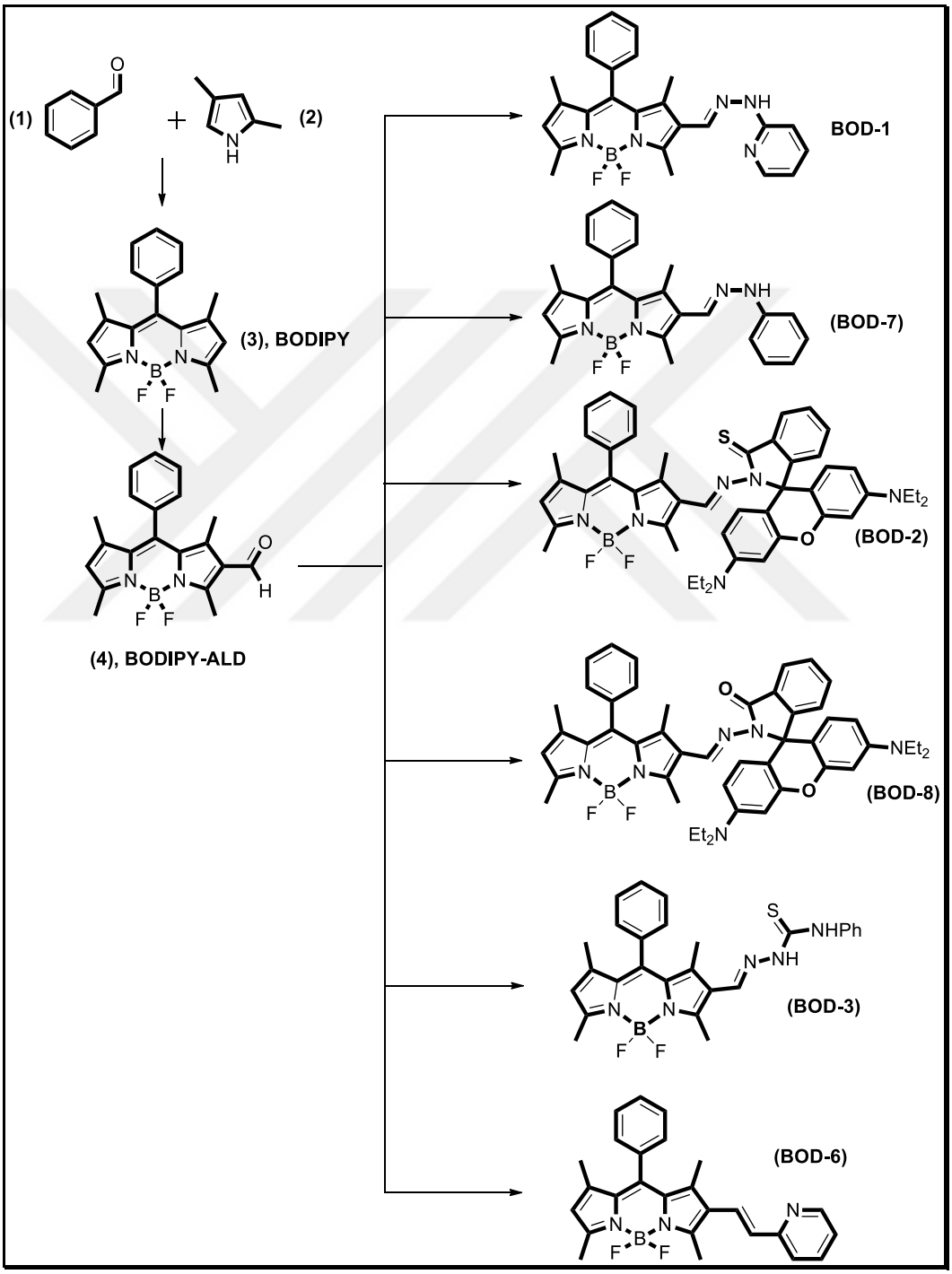

Figure 4.1. Synthetic routes of probe molecules from (4), **BODIPY-ALD**

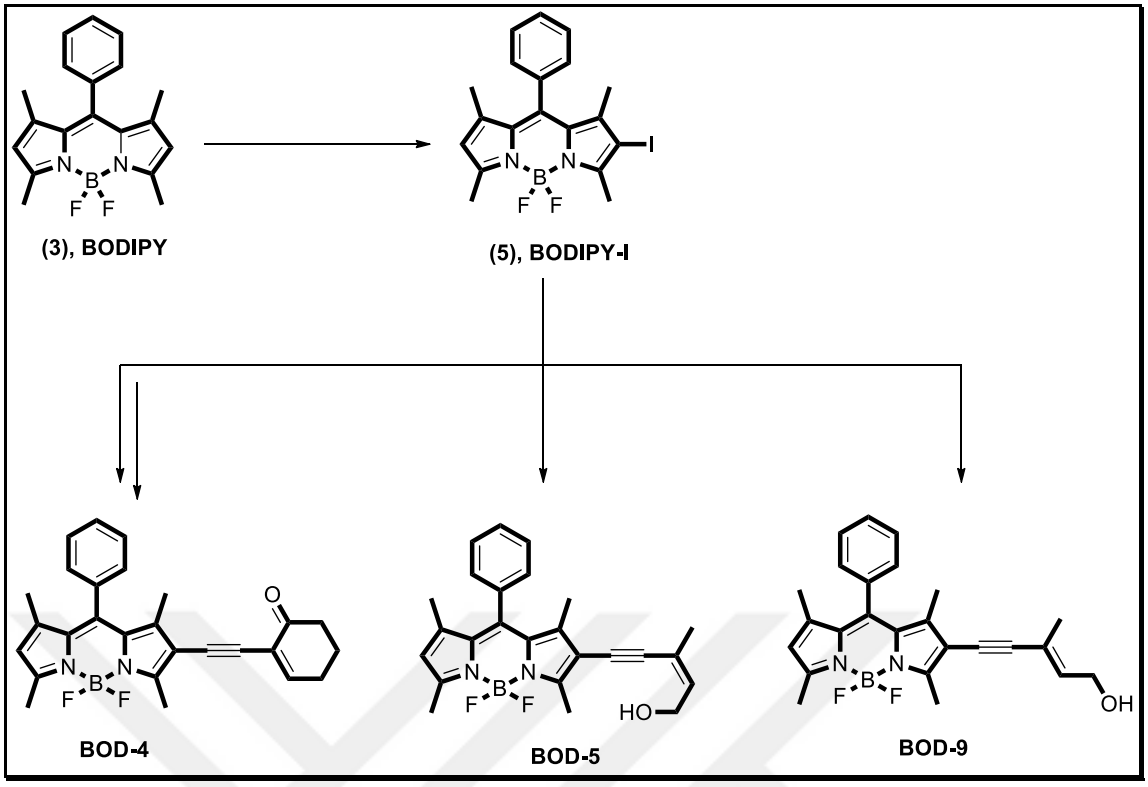

Figure 4.2. Synthetic routes of probe molecules from (5), **BODIPY-I**

4.6.1. Synthesis of (3) BODIPY

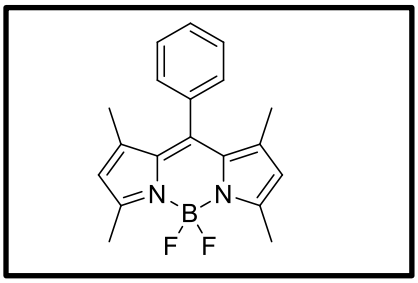

BODIPY core was synthesized by using literature procedure (Sauer et al., 2012). To a solution of 2,4-dimethylpyrrole (411 µL, 4 mmol) in 25 mL of dry THF 2 mmoles of benzaldehyde (200 µL) and 2-3 drops of trifluoroaceticacid were added successively under argon atmosphere and the solution was stirred for overnight. After overnight stirring, 455 mg of 2,3-Dichloro-5,6-dicyano-p-benzoquinone (DDQ) was dissolved into 25 mL of dry THF and added drop by drop. The resulting mixture stirred for 4 hours then, 12 mL of triethylamine added and stirred for 30 min. Finally, 13 mL of $BF_3.Et_2O$ was added and the reaction mixture was stirred overnight. At the end of reaction solvent was removed under reduced pressure and extracted with dichloromethane and dried over $MgSO_4$. Solvent was evaporated in vacuo and the resultant compound purified by column chromatography with a 40% yield (259 mg). ^{1}H NMR (400 MHz, $CDCl_3$) δ: 7.49-7.47 (m, 3H), 7.28-7.26 (m, 2H),

5.98 (s, 2H), 2.55 (s, 6H), 1.37 (s, 6H). ^{13}C NMR (100 MHz, $CDCl_3$) δ: 155.4, 143.2, 141.7, 135.0, 129.1, 128.9, 127.9, 121.29, 15.0, 14.3.

4.6.2. Synthesis of (4) BODIPY-ALD

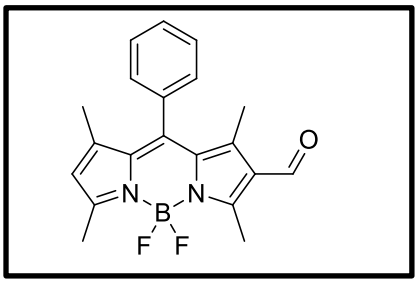

BODIPY-ALD was synthesized by using literature procedure (Isik et al., 2013). The firs step of reaction includes the formation of Vilsmeier Haack reagent via the dropwise addition of $POCl_3$ (250 μL, 1 mmol) into the dry DMF (250 μL, 3.6 mmol). The mixture was stirred for 40 min at room temperature under aargon atmosphere. Then, the solution of **(3) BODIPY** (81 mg, 0.25 mmol) in dichloroethane (DCE) was added drop by drop and the mixture stirred overnight at 60^{o}C. The reaction was quenched with the addition of 100 mL of ice cooled-$NaHCO_3$ solution and extracted with CH_2Cl_2. Combined organic phases were dried over $MgSO_4$ and they were purified with column chromatography (4:1 Hexane:Ethyl Acetate) to afford **BODIPY-ALD** as orange solid (52.1 mg, 60% yield) (Isik et al., 2013). ^{1}H NMR (400 MHz, $CDCl_3$) δ: 10.0 (s, 1H), 7.53-7.51 (m, 3H), 7.28-7.26 (m, 2H), 6.15 (s, 1H), 2.81 (s, 3H), 2.61 (s, 3H), 1.64 (s, 3H), 1.41 (s, 3H). ^{13}C NMR (100 MHz, $CDCl_3$) δ: 185.9, 161.6, 156.4, 147.3, 143.6, 142.9, 134.1, 129.5, 127.7, 126.3, 124.0, 15.1, 14.8, 13.0, 11.6.

4.6.3. Synthesis of (5) BODIPY-I

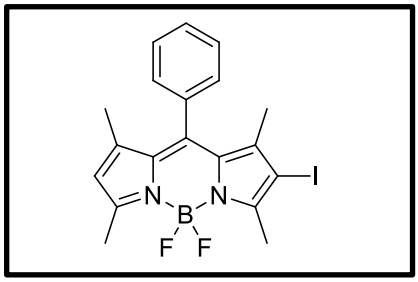

BODIPY-I was synthesized by using literature procedure (Wu et al., 2011). To a solution of (3) BODIPY (64.8 mg, 0.2 mmol) in 50 mL of dry DCM one equivalent of NIS (N-iodosuccinamide) (45 mg, 0.2 mmol) in 10 mL of DCM was added over an hour at 10-15 ^{o}C. The resulting solution was stirred further one hour and solvent was removed under reduced pressure. Title compound was passes into a short pad of silica and used in next steps without further purification.

4.6.4. Synthesis of (6) BODIPY-ACET

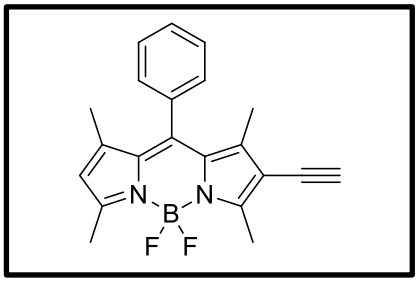

To a mixture of **BODIPY-I** (90 mg, 0.2 mmol) and trimethylsillylacetylene (56 µL, 2.0 equiv.) in THF (20 mL) $PdCl_2(PPh_3)_2$ (14 mg, 0.1 equiv.) and CuI (7.6 mg, 0.2equiv.) were added (Wu et al., 2011). The resulting mixture was degassed for 10 min and 3.9 mL of DIPA was added. The reaction mixture stirred for overnight at 50 ^oC. After completion of reaction solvent was removed under vacuum and the resulting residue extracted three times with DCM (3 x 30 mL). The organic layer was dried over MgSO4, filtered and concentrated. The resultant residue was filtered from a short pad of silica and used for deprotection without further purification. To a solution of obtained BODIPY-TMS in 25 mL of methanol 27.6 mg of K_2CO_3 (0.2 mmol) was added and the resulting mixture was stirred for 2 hours. Then the solvent removed under reduced pressure and the resultant residue was purified by column chromatography (100:2 (Hexane:Ethyl acetate)) to afford **BODIPY-ACET** as red solid (35 mg, 50 % yield).

4.6.5. Synthesis of BOD-1 and BOD-7

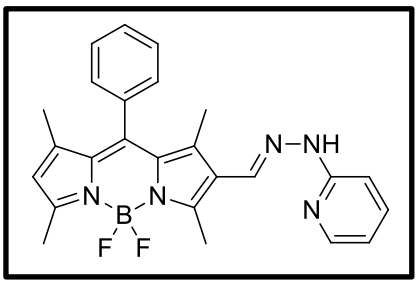

To a mixture of **(4) BODIPY-ALD** (35.2 mg, 0,1 mmol) and 2-hydrazinylpyridine (12 mg, 0,11mmol) in 4 ml ethanol and a drop of glacial acetic acid was added. The resulting solution was refluxed for two hours. After cooling room temperature, the solvent was removed under reduced pressure. The resultant residue was purified by column chromatography (2:1 (Hexane:Ethyl acetate)) to afford **BOD-1** as purple solid (34 mg, 76 % yield). Mp: 274-276 ^oC. ^1H NMR (400 MHz, $CDCl_3$) δ: 8.33 (s, 1H), 8.10 (d, J = 4.0 Hz, 1H), 7.71 (s, 1H), 7.58-7.50 (m, 3H), 7.31-7.29 (m, 2H), 7.14 (d, J = 8.0 Hz, 1H), 6.72 (t, J = 6.4 Hz, 1H), 6.03 (s, 1H), 2.82 (s, 3H), 2.59 (s, 3H), 1.68 (bs, 1H), 1.54 (s, 3H), 1.38 (s, 3H). ^{13}C NMR (100 MHz, $CDCl_3$) δ: 157.1, 156.6, 154.8, 147.5, 144.3, 142.0, 138.8, 138.2, 134.9, 133.5, 132.2, 130.7, 129.2, 129.1, 128.0, 124.3, 122.0, 115.4, 107.2, 14.7, 14.5, 14.2, 12.3.

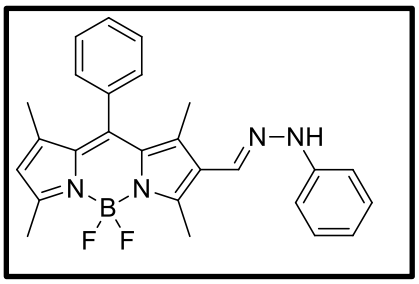

The sensor molecule, **BOD-7**, was synthesized by using above procedure as purple solid (31 mg, 70%yield). Mp: 247-249 ^{o}C. ^{1}H NMR (400 MHz, $CDCl_3$) δ: 7.64 (s, 1H), 7.50-7.48 (m, 4H), 7.26-7.20 (m, 4H), 6.95 (s, 2H), 6.81 (s, 1H), 6.01 (s, 1H), 2.81 (s, 3H), 2.58 (s, 3H), 1.52 (s, 3H), 1.35 (s, 3H). ^{13}C NMR (100 MHz, $CDCl_3$) δ: 155.9, 155.0, 143.5, 141.6, 138.2, 134.7, 131.4, 129.4, 129.3, 129.2, 129.0, 128.9, 127.9, 127.5, 125.0, 121.5, 119.2, 112.1, 14.5, 14.3, 14.1, 12.2.

4.6.6. Synthesis of BOD-8 and BOD-2

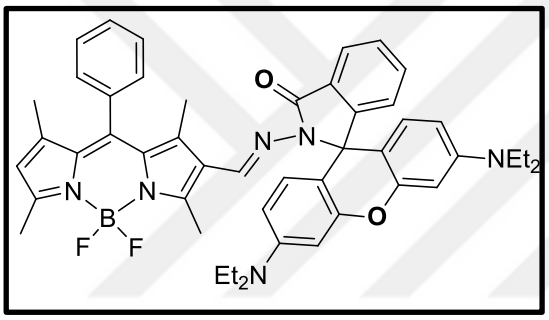

To a solution of rhodamine B hydrazide (this compound was also synthesized according to known procedure (Karakuş et al., 2013)) (150mg, 0.33 mmol) in absolute ethanol (10 ml) was added **BODIPY-ALD** (116mg, 0.33mmol). The solution was stirred overnight at reflux temperature. The reaction mixture was extracted with dichloromethane (3 x 10 mL). Then the collected organic layers were dried over anhydrous $MgSO_4$, concentrated under vacuum, and purified by column chromatography (hexane/EtOAc = 8/1) to give 156 mg of **BOD-8** (60%) as a pink solid. ^{1}H-NMR (400 MHz, $CDCl_3$) *δ*: 9.12 (s, 1H), 7.94-7.92 (m, 1H), 7.49-7.45 (m, 4H), 7.20-7.12 (m, 3H), 6.98 (t, J=7.2 Hz, 1H), 6.47-6.26 (m, 6H), 5.99 (s, 1H), 3.32 (br. s, 8H), 2.53 (s, 3H), 2.47 (s, 3H), 1.33 (s, 6H), 1.15 (br. s, 12H). ^{13}C NMR (100 MHz, $CDCl_3$) *δ*: 164.1, 156.5, 153.4, 150.8, 148.8, 143.9, 142.0, 140.9, 137.8, 134.8, 132.1, 132.0, 130.9, 130.6, 129.9, 129.2, 128.3, 127.9, 126.0, 124.0, 123.1, 121.9, 107.9, 106.3, 97.8, 66.2, 44.4, 14.7, 14.5, 14.2, 12.6, 12.0. MS (MALDI-TOF): m/z: Calcd. for $C_{48}H_{49}BF_2N_6O_2$: 791.479 $[M+H]^+$, Found: 791.471 $[M+H]^+$.

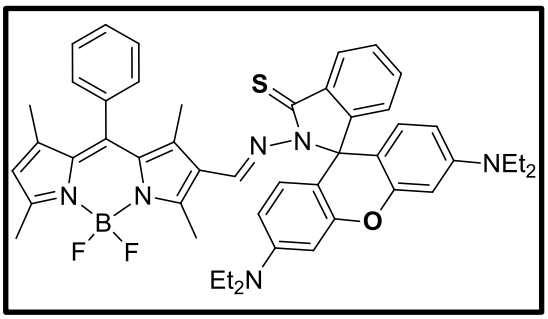

The **BOD-8** (100 mg, 0.13mmol) and Lawesson's reagent (53mg, 0.13mmol) were dissolved in dry toluene, and reaction mixture was refluxed for 2 h under N_2 atmosphere. After removal of toluene, the residue was purified by column chromatography (hexane/EtOAc = 10/1) to give 42 mg of **BOD-2** (40%) as a purple solid. ^{1}H-NMR (400 MHz, $CDCl_3$) δ: 8.63 (s, 1H), 8.07 (dd, J=6.0 Hz, 3.2 Hz, 1H), 7.48-7.47 (m, 3H), 7.39 (dd, J=6.0 Hz, 3.2 Hz, 2H), 7.27-7.26 (m, 2H), 7.10 (dd, J=6.0 Hz, 3.2 Hz, 1H), 6.76 (d, J=8.4 Hz, 2H), 6.30-6.27 (m, 4H), 6.04 (s, 1H), 3.32 (q, J=7.2 Hz, 8H), 2.81 (s, 3H), 2.58 (s, 3H), 1.59 (s, 3H), 1.38 (s, 3H), 1.15 (t, J=7.2 Hz, 12H). ^{13}C NMR (100 MHz, $CDCl_3$) δ: 170.9, 158.0, 156.6, 155.6, 152.9, 151.7, 148.1, 145.0, 142.5, 141.9, 135.0, 134.7, 132.0, 130.4, 129.2, 129.2, 127.9, 127.7, 127.1, 123.9, 122.5, 122.1, 110.6, 108.2, 97.4, 62.7, 44.3, 14.8, 14.6, 14.1, 12.9, 12.6. MS (MALDI-TOF): m/z: Calcd. for $C_{48}H_{49}BF_2N_6OS$: 807.375 $[M+H]^+$, Found: 807.451 $[M+H]^+$

4.6.7. Synthesis of BOD-3

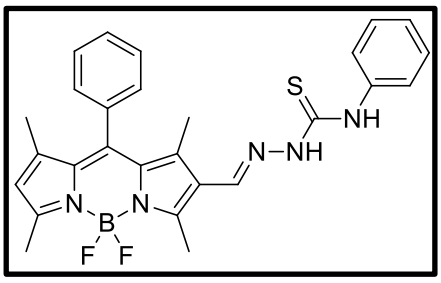

To a mixture of **BODIPY-ALD** (52.1 mg, 0.15 mmol) and hydrazine hydrate (12 µL, 0.18 mmol) in 5 ml of methanol, phenyl isothiocyanate (23 µL, 0.18 mmol) was injected. Then, a drop of glacial acetic acid was added and resulting solution was refluxed for an hour. After cooling room temperature, the solvent was removed under reduced pressure. The resultant residue was purified by column chromatography (10:1 (Hexane:Ethyl acetate)) to afford **BOD-3** as purple solid (29.4 mg, 40 % yield) (Cunha and Da Silva, 2009). Mp: 228-231 ^{o}C. ^{1}H NMR (400 MHz, $CDCl_3$) δ: 9.92 (s, 1H), 8.95 (s, 1H), 7.97 (s, 1H), 7.60 (d, J=8.0 Hz, 2H), 7.52-7.51 (m, 3H), 7.36 (t, J=8.0 Hz, 2H), 7.28-7.26 (m, 2H), 7.21 (t, J=7.2 Hz 1H), 6.09 (s, 1H), 2.75 (s, 3H), 2.59 (s, 3H), 1.50 (s, 3H), 1.40 (s, 3H). ^{13}C NMR (100 MHz, $CDCl_3$) δ: 174.7, 159.4, 153.9, 145.9, 142.5, 139.6, 138.1, 137.9, 134.5, 133.0, 130.5, 129.4, 128.7, 127.9, 125.9, 123.9, 123.1, 122.1, 14.9, 14.7, 14.1, 12.5. HRMS (EI) calc. for $C_{27}H_{26}BF_2N_5S$ $[M-H]^+$ 500.18918, found 500.18066.

4.6.8. Synthesis of BOD-4

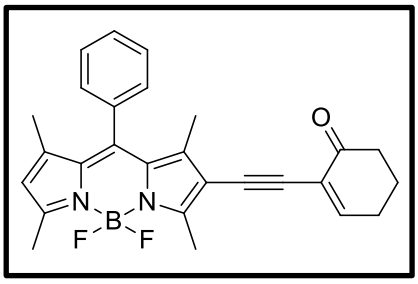

To a mixture of 2-Iodo-2-cyclohexen-1-one (22.1 mg, 0,1 mmol) in THF $PdCl_2(PPh_3)_2$ (3.51 mg, 0.05 equiv.), CuI (1.9 mg, 0.1equiv.) and **BODIPY-ACET** (69.6 mg, 2.0 equiv.) were added at 0°C. Then, diisopropylamine (42 μL, 3.0 equiv.) was added and the resulting mixture was stirred at 0°C for 1 hour. After completion of reaction THF was removed under vacuum and the resulting residue extracted three times with DCM (3 x 30 mL). The organic layer was dried over $MgSO_4$, filtered and concentrated. The resultant residue was purified by column chromatography (4:1 (Hexane:Ethyl acetate)) to afford **BOD-4** as red solid (31 mg, 70 % yield) (Yao et al., 2004). ^{1}H NMR (400 MHz, $CDCl_3$) δ: 7.49-7.48 (m, 3H), 7.27-7.22 (m, 2H), 6.02 (s, 1H), 2.66 (s, 3H), 2.56 (s, 3H), 2.52-2.45 (m, 4H), 2.04 (quint. J = 6.4 Hz, 2H), 1.47 (s, 3H), 1.18 (s, 3H). ^{13}C NMR (100 MHz, $CDCl_3$) δ: 195.1, 157.2, 156.5, 152.2, 144.4, 142.9, 141.9, 134.4, 132.1, 130.0, 129.0, 127.6, 125.3, 121.8, 114.7, 90.0, 84.7, 37.9, 26.2, 22.2, 14.5, 14.2, 13.2, 12.9. Calcd. For $C_{27}H_{25}BF_2N_2O$: 442.20280 $[M]^+$, Found: 443.20864 $[M+H]^+$.

4.6.9. Synthesis of BOD-5 and BOD-9

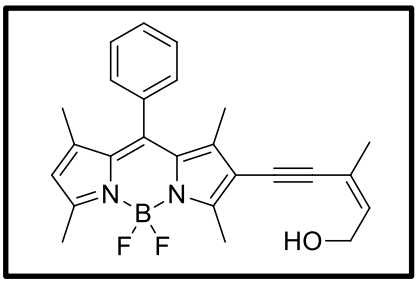

To a mixture of **BODIPY-I** (45 mg, 0.2 mmol) and **(*Z*)-3-methylpent-2-en-4-yn-1-ol** (38.8 mg, 0.4 mmol) in THF (20 mL) $PdCl_2(PPh_3)_2$ (14 mg, 0.1 equiv.) and CuI (7.6 mg, 0.2 equiv.) were added. The resulting mixture was degassed for 10 min and 3.9 mL of DIPA was added. The reaction mixture stirred for overnight at 50 °C. After completion of reaction solvent was removed under vacuum and the resulting residue extracted three times with DCM (3 x 30 mL). The organic layer was dried over $MgSO_4$, filtered and concentrated. The resultant residue was purified by column chromatography (3:1 (Hexane:Ethyl acetate)) to afford **BOD-5** as red solid (31.5 mg, 75 % yield). ^{1}H NMR (400 MHz, $CDCl_3$) δ (ppm): 7.51-7.48 (m, 3H), 7.29-7.26 (m, 2H), 6.03 (s, 1H), 5.84 (tq, J=9.2, 6.8, 1.6 Hz, 1H), 4.34 (dd, J=6.4,

1.6 Hz, 2H), 2.64 (s, 3H), 2.57 (s, 3H), 1.94 (q, J=1.2 Hz, 3H), 1.44 (s, 3H), 1.40 (s, 3H). ^{13}C NMR (100 MHz, $CDCl_3$) δ (ppm): 157.8, 156.1, 144.8, 142.4, 142.1, 134.6, 134.3 (2C), 132.5, 130.2, 129.2 (2C), 127.8, 122.2, 121.1, 114.9, 94.0, 87.2, 61.5, 23.3, 14.7, 14.5, 13.4, 13.1. MS HRMS (TOF-APCI): *m/z* Calcd. for $C_{25}H_{25}BF_2N_2O$: 417.19498 $[M-H]^+$, Found: 417.20825 $[M-H]^+$.

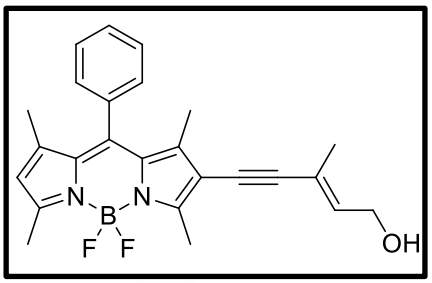

The sensor molecule, **BOD-9**, was synthesized by using above procedure as red solid (29.3 mg, 70%yield). ^{1}H NMR (400 MHz, $CDCl_3$) δ (ppm): 7.52-7.49 (m, 3H), 7.29-7.26 (m, 2H), 6.03-6.00 (m, 2H), 4.34 (dd, J=7.2, 0.8 Hz, 2H), 2.64 (s, 3H), 2.58 (s, 3H), 1.90 (t, J=0.8 Hz, 3H), 1.44 (s, 3H), 1.40 (s, 3H). ^{13}C NMR (100 MHz, $CDCl_3$) δ (ppm): 157.4, 156.4, 144.6, 142.6, 142.0, 134.6, 134.4, 132.4, 130.2, 129.2, 129.1, 127.8, 122.0, 121.1, 115.1, 98.1, 80.2, 59.2, 17.8, 14.7, 14.5, 13.4, 13.0. MS HRMS (TOF-APCI): *m/z* Calcd. for $C_{25}H_{25}BF_2N_2O$: 417.19498 $[M-H]^+$, Found: 417.20611 $[M-H]^+$.

4.6.10. Synthesis of BOD-6

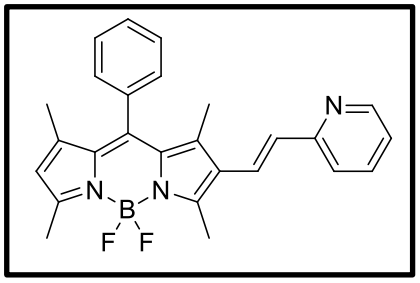

To a solution of **BODIPY-ALD** (100 mg, 0.285 mmol) in dioxane (10 mL) was added triphenyl(2-pyridylmethyl)phosphonium chloride hydrochloride (389 mg, 0.896 mmol). Then, 250 µl of triethyl amine was added drop by drop and the resultant solution was stirred at room temperature for overnight. After reaction completed, the solution was concentrated in vacuum and extracted three times with dichloromethane. The organic layer was dried over sodium sulfate and concentrated under reduced pressure. The resultant residue was purified by silica gel column chromatography (hexane / ethyl acetate (8/1)) to afford **BOD-6** as green solid (68.1mg, 56% yield). Mp: 267-269 ^{o}C. ^{1}H NMR (400 MHz, $CDCl_3$) δ: 8.56 (d, J= 4.0 Hz, 1H), 7.62 (dt, J= 8.0, 1.6 Hz 1H), 7.52-7.50 (m, 3H), 7.46 (s, 1H), 7.32-7.29 (m, 2H), 7.28 (s, 1H), 7.12-7.09 (m, 1H), 6.72 (d, J= 16.0 Hz, 1H), 6.01 (s, 1H), 2.76 (s, 3H), 2.58 (s, 3H), 1.51 (s, 3H), 1.38 (s, 3H). ^{13}C NMR (100 MHz, $CDCl_3$) δ: 156.3,

155.9, 154.9, 149.6, 143.8, 141.8, 139.3, 136.5, 135.0, 132.0, 131.0, 129.5, 129.2, 129.1, 128.1, 127.8, 123.9, 121.8, 121.8, 14.7, 14.5, 14.1, 12.9. Calcd. For $C_{26}H_{24}BF_2N_3$: 427.203 $[M]^+$, Found: 428.244 $[M+H]^+$.

4.6.11. Synthesis of (6) BODIPY-FUR

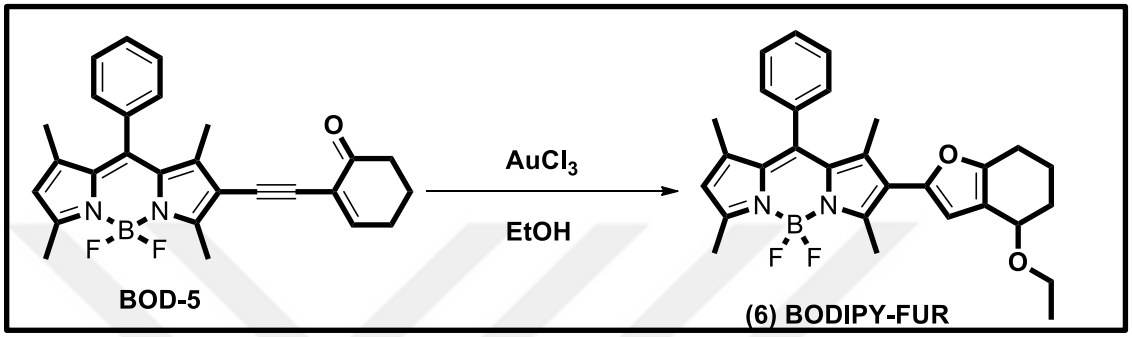

To a solution of **BOD-4** (22 mg, 0.05mmol) in phosphate/ethanol solution (10 mL, (6/4 (v/v)) 1 equivalent of $AuCl_3$ was added and the reaction mixture stirred for 1 hour. The resulting solution was extracted with DCM (3x30mL) and dried over $MgSO_4$. After evaporation of solvent, the resultant residue was purified by column chromatography. (14.5 mg, 60% yield). ^{1}H NMR (400 MHz, $CDCl_3$) δ: 7.52-7.48 (m, 3H), 7.31-7.29 (m, 2H), 6.19 (s, 1H), 6.00 (s, 1H), 4.36 (t, J = 4.0 Hz, 1H), 3.64-3.56 (m, 1H), 2.68 (s, 3H), 2.64-2.60 (m, 1H), 2.57 (s, 3H), 2.55-2.48 (m, 1H), 2.07-1.98 (m, 1H), 1.95-1.90 (m, 1H), 1.84-1.75 (m, 2H), 1.44 (s, 3H), 1.38 (s, 3H), 1.22 (t, J = 7.2, 3H). ^{13}C NMR (100 MHz, $CDCl_3$) δ: 156. 1, 154.4, 152.3, 146.2, 143.6, 141.9, 138.8, 135.1, 131.8, 130.9, 129.1, 129.0, 128.0, 123.4, 121.6, 119.5, 109.1, 70.8, 63.9, 29.7, 28.8, 23.2, 19.0, 15.7, 14.6, 14.5, 13.9, 13.0. MS HRMS (TOF-APCI): *m/z* Calcd. for $C_{29}H_{31}BF_2N_2O_2$: 488.24467 $[M]^+$, Found: 489.25052 $[M+H]^+$.

4.6.12. Synthesis of (7) BODIPY-FUR

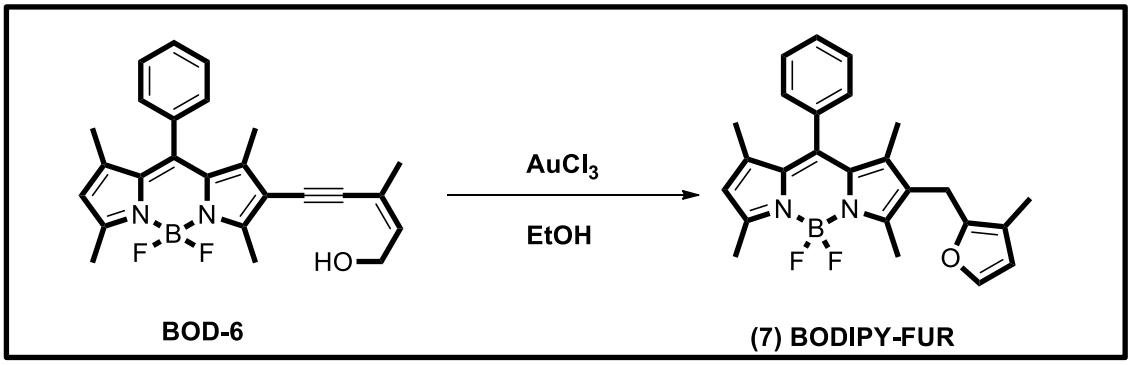

To a solution of **BOD-6** (42 mg, 0.1 mmol) in phosphate/ethanol solution (10 mL, (7/3 (v/v)) 1 equivalent of $AuCl_3$ was added and the reaction mixture stirred for 2 hour. The resulting solution was extracted with DCM (3x30mL) and dried over MgSO4. After evaporation of solvent, the resultant residue was purified by column chromatography. (2.0 mg, 5% yield). ^{1}H NMR (400 MHz, $CDCl_3$) δ (ppm): 7.48-7.46 (m, 3H), 7.29-7.26 (m, 2H), 7.16 (d, J=2.0 Hz, 1H), 6.10 (d, J=1.6 Hz, 1H), 5.95 (s, 1H), 3.57 (s, 2H), 2.56 (s, 3H), 2.54 (s, 3H), 1.94 (s, 3H), 1.34 (s, 6H). MS HRMS (TOF-APCI): *m/z* Calcd. for $C_{25}H_{25}BF_2N_2O$: 417.19498 $[M-H]^+$, Found: 417.20839 $[M-H]^+$.

CHAPTER 5

CONCLUSION

To conclude, in the subject of this thesis six new molecular probes were designed, synthesized, and characterized and their sensor abilities towards metal ions were secreened carefully (Figure 5.1). Luckily, designed probes showed high sensitivity and selectivity towards gold and mercury ions in solutions and living cells without any interference of sensing media. Another important aspect of this thesis was the discovery of a new reactive unite towards Au^{3+} ions. The **C=N** receptor unit was used for the first time which worked via gold ion mediated hydrolysis mechanism. After this invention several gold ion sensors have been developed including **C=N** receptor units (Cheng, and Qian, 2015; Feng et al., 2016; Kambama et al., 2015; Wang et al., 2016). In addition, two new probe molecules, -**BOD-4** and **BOD-5**- were constructed by exploiting their alkynophilic nature.

The main concern of thesis was to develope molecular sensors that capable to differentiate gold and mercury ions via different emission modes. To this porpose, **BOD-2** and **BOD-3** was developed. Both probes selectively detected targeted metal ions in different emission modes. In addition, gold ion selective probes –**BOD-1**, **BOD-5** and **BOD-6**- were developed and sensing properties were investigated carefully. **BOD-1**, **BOD-4** and **BOD-6** showed high selectivity towards gold ions and had no influence of other interfering metal ions bearing similar chemical nature. Furthermore, one of the improtant features of synthesized probes was their ability to detect target ions in living milleu. Except for **BOD-6** all probes displayed high sensitivity towards mercury and gold ions in living cells.

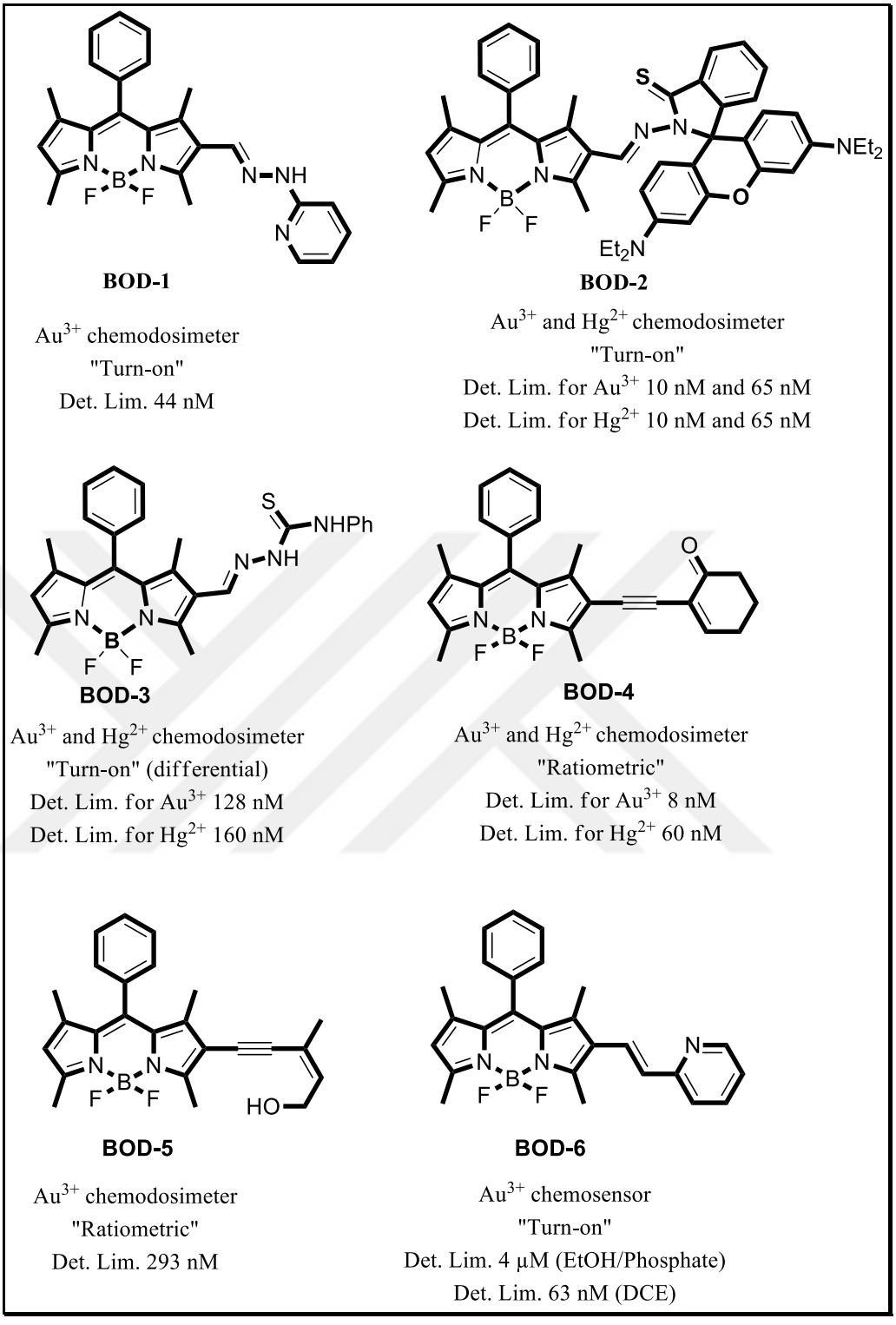

Figure 5.1. Summary of synthesized probe molecules

REFERENCES

Goppelsröder, F. On a Fluorescent Substance Extracted From Cuba Wood and on Fluorescence Analysis. J. Prakt. Chem. 1868, 104, 10–27.

Tsien, R. Y. New Calcium Indicators and Buffers with High Selectivity Against Magnesium and Protons: Design, Synthesis, and Properties of Prototype Structures. Biochemistry 1980, 19, 2396–2404.

Clevenger, W. L.; Smith, B. W.; Winefordner, J. D. Trace Determination of Mercury: A Review. Critical Reviews in Analytical Chemistry. 1997, 27, 1–26.

Powell, M. J.; Quan, E. S. K.; Boomer, D. W.; Wiederin, D. R. Inductively Coupled Plasma Mass Spectrometry with Direct Injection Nebulization for Mercury Analysis of Drinking Water. Anal. Chem. 1992, 64, 2253–2257.

Herschel, J. F. W. Phil. Trans. R. Soc. London 1845, 133, 143–145.

Baeyer, A. On A New Class of Dyes. Berichte der Deutschen chemischen Gesellschaft zu Berlin, 1871, 4, 555–558.

Perkin, W. H. On The Artificial Production of Coumarin and Formation of Its Homologues. J. Chem. Soc. 1868, 21, 53–63.

Williams, C. H. G. Researches on Chinoline and Its Homologues. Trans. R. Soc. Edinburg 1856, 21, 377.

Maity, D.; Govindaraju, T. A Differentially Selective Sensor with Fluorescence Turn-on Response to Zn^{2+} and Dual-Mode Ratiometric Response to Al^{3+} in Aqueous Media. Chem. Commun. 2012, 48, 1039–1041.

Li, Y.; Wu, J.; Jin, X.; Wang, J.; Han, S.; Wu, W.; Xu, J.; Liu, W.; Yao, X.; Tang, Y. A bimodal multianalyte simple molecule chemosensor for Mg^{2+}, Zn^{2+}, and Co^{2+}. Dalton Trans., 2014, 43, 1881–1887.

Dong, M.; Wang, Y.-W.; Peng, Y. Highly Selective Ratiometric Fluorescent Sensing For Hg^{2+} and Au^{3+}, Respectively, in Aqueous Solution. Org. Lett. 2010, 12, 5310–5313.

Onyido, I.; Norris, A. R.; Buncel, E. Metal Ion-Biomolecule Interactions. Synthesis, Spectroscopic, and Magnetic Resonance Investigations of Methylmercury(II) Complexes of The Nucleosides Guanosine and Inosine. Chem. Rev. 2004, 104, 5911–5930.

Nyarko, E.; Hara, T.; Grab, D. J.; Habib, A.; Kim, Y.; Nikolskaia, O.; Fukuma, T.; Tabata, M. In Vitro Toxicity of Palladium(II) and Gold(III) Porphyrins and Their Aqueous Metal Ion Counterparts on Trypanosoma Brucei Brucei Growth. Chem.-Biol Interact. 2004, 148, 19–25.

Zhang, J. F.; Zhou, Y.; Yoon, J.; Kim, J. S. Recent Progress in Fluorescent and Colorimetric Chemosensors for Detection of Precious Metal Ions (Silver, Gold and Platinum Ions). Chem. Soc. Rev. 2011, 40, 3416–3429.

Yan, Z.; Yuen, M. –F.; Hu, L.; Suna, P.; Lee, C. –S. Advances for The Colorimetric Detection of Hg^{2+} in Aqueous Solution. RSC Adv. 2014, 4, 48373–48388.

Chen, G.; Guo, Z.; Zeng, G.; Tang, L. Fluorescent and Colorimetric Sensors for Environmental Mercury Detection. Analyst 2015, 140, 5400–5443.

Kim, H. N.; Ren, W. X.; Kim J. S.; Yoon, J. Fluorescent and Colorimetric Sensors for Detection of Lead, Cadmium, and Mercury Ions. Chem. Soc. Rev. 2012, 41, 3210–3244.

Wu, J.; Kwon, B.; Liu, W.; Anslyn, E. V.; Wang, P.; Kim, J. S. Chromogenic/Fluorogenic Ensemble Chemosensing Systems. Chem. Rev. 2015, 115, 7893–7943.

Cheng, J.; Zhou, X.; Xiang, H. Fluorescent Metal Ion Chemosensors Via Cation Exchange Reactions of Complexes, Quantum Dots, and Metal–Organic Frameworks. Analyst 2015, 140, 7082–7115.

Mahato, P.; Saha, S.; Das, P.; Agarwallad, H.; Das, A. An Overview of The Recent Developments on Hg^{2+} Recognition. RSC Adv. 2014, 4, 36140–36174.

Singha, S.; Kim, D.; Seo, H.; Cho, S. W.; Ahn, K. H. Fluorescence Sensing Systems for Gold and Silver Species. Chem. Soc. Rev. 2015, 44, 4367–4399.

Lee, M. H.; Kim, J. S.; Sessler, J. L. Small Molecule-Based Ratiometric Fluorescence Probes for Cations, Anions, and Biomolecules. Chem. Soc. Rev. 2015, 44, 4185–4191.

Yin, J.; Hua, Y.; Yoon, J. Fluorescent Probes and Bioimaging: Alkali Metals, Alkaline Earth Metals and pH. Chem. Soc. Rev. 2015, 44, 4619–4644.

Das, S.; Dutta, M.; Das, D. Fluorescent Probes for Selective Determination of Trace Level Al^{3+}: Recent Developments and Future Prospects. Anal. Methods 2013, 5, 6262–6285.

Zhang, W.; Ma, Z.; Du, L.; Li, M. Design Strategy for Photoinduced Electron Transfer-Based Small-Molecule Fluorescent Probes of Biomacromolecules. Analyst 2014, 139, 2641–2649.

Sahoo, S. K.; Sharma, D.; Bera, R. K.; Crisponic, G.; Callan, J. F. Iron(III) Selective Molecular and Supramolecular Fluorescent Probes. Chem. Soc. Rev. 2012, 41, 7195–7227.

Culzoni, M. J.; A. De la Pena, M.; Machuca, A.; H. Goicoechea, C.; Babiano, R. Rhodamine and BODIPY Chemodosimeters and Chemosensors for The Detection of Hg^{2+}, Based on Fluorescence Enhancement Effects. Anal. Methods 2013, 5, 30–49.

Zhoua, Y.; Yoon, J. Recent Progress in Fluorescent and Colorimetric Chemosensors for Detection of Amino Acids. Chem. Soc. Rev. 2012, 41, 52–67.

Aron, A. T.; Ramos-Torres, K. M.; Cotruvo, Jr., J. A.; Chang, C. J. Recognition- and Reactivity-Based Fluorescent Probes for Studying Transition Metal Signaling in Living Systems. Acc. Chem. Res. 2015, 48, 2434−244.

Rivera-Fuentes, P.; Lippard, S. J. Metal-Based Optical Probes for Live Cell Imaging of Nitroxyl (HNO). Acc. Chem. Res. 2015, 48, 2927−2934.

Kowada, T.; Maeda, H.; Kikuchi, K. BODIPY-Based Probes for The Fluorescence Imaging of Biomolecules in Living Cells. Chem. Soc. Rev. 2015, 44, 4953–4972.

Lakshmi, V.; Rao, M. R.; Ravikanth, M. Halogenated Boron-dipyrromethenes: Synthesis, Properties and Applications. Org. Biomol. Chem. 2015, 13, 2501–2517.

Manjare, S. T.; Kim, Y.; Churchill, D. G. Selenium- and Tellurium-Containing Fluorescent Molecular Probes for the Detection of Biologically Important Analytes. Acc. Chem. Res. 2014, 47, 2985−2998.

Lu, H.; Mack, J.; Yang, Y.; Shen, Z. Structural Modification Strategies for The Rational Design of Red/NIR Region BODIPYs. Chem. Soc. Rev., 2014, 43, 4778–4823.

Ni, Y.; Wu, J. Far-red and Near Infrared BODIPY Dyes: Synthesis and Applications for Fluorescent pH Probes and Bio-imaging. Org. Biomol. Chem. 2014, 12, 3774–3791.

Kamkaew, A.; Lim, S. H.; Lee, H. B.; Kiew, L. V.; Chung, L. Y.; Burgess, K. BODIPY Dyes in Photodynamic Therapy. Chem. Soc. Rev., 2013, 42, 77–88.

Khan, T. K.; Bröring, M.; Mathura, S.; Ravikanth, M. Boron Dipyrrin-Porphyrin Conjugates. Coord. Chem. Rev. 2013, 257, 2348–2387.

Jeong, Y.; Yoon, J. Recent Progress on Fluorescent Chemosensors for Metal Ions. Inorg. Chim. Acta 2012, 381, 2–14.

Awuah, S. G.; You, Y. Boron Dipyrromethene (BODIPY)-Based Photosensitizers for Photodynamic Therapy. RSC Adv. 2012, 2, 11169–11183.

Boens, N.; Leen, V.; Dehaen, W. Fluorescent Indicators Based on Bodipy. Chem. Soc. Rev. 2012, 41, 1130–1172.

Beija, M.; Afonso, C. A. M.; Martinho, J. M. G. Synthesis and Applications of Rhodamine Derivatives As Fluorescent Probes. Chem. Soc. Rev. 2009, 38, 2410–2433.

Orndorff, W. R.; Hemmer, A. J. Fluorescein and Some of Its Derivatives. J. Am. Chem. Soc. 1927, 49, 1272–1280.

Li, X.; Gao, X.; Shi, W.; Ma, H. Design Strategies for Water-Soluble Small Molecular Chromogenic and Fluorogenic Probes. Chem. Rev. 2014, 114, 590−659.

Trenor, S. R.; Shultz, A. R.; Love, B. J.; Long, T. E. Coumarins in Polymers: From Light Harvesting to Photo-Cross-Linkable Tissue Scaffolds. Chem. Rev. 2004, 104, 3059–3077.

Sethna, S. M.; Shah, N. M. The Chemistry of Coumarins. 1944, 1–37.

Noelting, E.; Dziewoński, K. Zur Kenntniss der Rhodamine. Ber. Dtsch. Chem. Ges. 1905, 38, 3516–3527.

Liu, Z.; Wang, W.; Xu, H.; Sheng, L.; Chen, S.; Huang, D.; Suna, F. A "Naked Eye" and Ratiometric Chemosensor for Cobalt(II) Based on Coumarin Platform in Aqueous Solution. Inorg. Chem. Comm. 2015, 62, 19–23.

Hettie, K. S.; Glass, T. E. Turn-On Near-Infrared Fluorescent Sensor for Selectively Imaging Serotonin. ACS Chem. Neurosci. 2016, 7, 21−25.

Aulsebrook, M. L.; Graham, B.; Grace, M. R.; Tuck, K. L. Coumarin-Based Fluorescent Sensors for Zinc(II) and Hypochlorite. Supramolecular Chemistry, 2015, 27, 798–806.

Yan, L.; Zhou, Y.; Du, W.; Kong, Z.; Qi, Z. A New Turn on Coumarin-Based Fluorescence Probe for Ga^{3+} Detection in Aqueous Solution. Spectrochimica Acta Part A: Molecular and Biomolecular Spectroscopy 2016, 155, 116–124.

Mishra, A.; Behera, R. K.; Behera, P. K.; Mishra, B. K.; Behera, G. B. Cyanines During The 1990s: A Review. Chem. Rev. 2000, 100, 1973–2011.

Narayanan, N.; Patonay, G. A New Method for the Synthesis of Heptamethine Cyanine Dyes: Synthesis of New Near-Infrared Fluorescent Labels. J. Org. Chem. 1995, 60, 2391–2395.

Zhao, X.; Wei, R.; Chen, L.; Jin, D.; Yan, X. Glucosamine Modified Near-Infrared Cyanine As A Sensitive Colorimetric Fluorescent Chemosensor for Aspartic and Glutamic Acid and Its Applications New J.Chem. 2014, 38, 4791–4798.

Guo, Z.; Kim, G. -H.; Shin, I.; Yoon, J. A Cyanine-Based Fluorescent Sensor for Detecting Endogenous Zinc Ions in Live Cells and Organisms. Biomaterials 2012, 33, 7818–7827.

Guo, Z. Nam, S. W.; Park, S.; Yoon, J. A Highly Selective Ratiometric Near-Infrared Fluorescent Cyanine Sensor for Cysteine with Remarkable Shift and Its Application in Bioimaging. Chem. Sci. 2012, 3, 2760–2765.

Yin, J. Kwon, Y.; Kim, D.; Lee, D.; Kim, G.; Hu, Y.; Ryu, J. -H. Yoon, J. Preparation of A Cyanine-Based Fluorescent Probe for Highly Selective Detection of Glutathione and Its Use in Living Cells and Tissues of Mice. Nat. Protoc. 2015, 10, 1742–1755.

Treibs, A.; Kreuzer, F.-H. Difluorboryl-Komplexe von Di- und Tripyrrylmethenen. Justus Liebigs Ann. Chem. 1968, 718, 208–223.

Monsma, F.; Barton, A.; Kang, H.; Brassard, D.; Haugland, R.; Sibley, D. Characterization of Novel Fluorescent Ligands with High Affinity for D_1 and D_2 Dopaminergic Receptors. J. Neurochem. 1989, 52, 1641–1644.

Carter, K. P.; Young, A. M.; Palmer, A. E. Fluorescent Sensors for Measuring Metal Ions in Living Systems. Chem. Rev. 2014, 114, 4564–4601.

Fu, L.; Wang, F. F.; Gao, T.; Huang, R.; He, H.; Jiang, F. L.; Liu, Y. Highly Efficient Fluorescent BODIPY Dyes for Reaction-Based Sensing of Fluoride Ions. Sensor Actuat. B. 2015, 216, 558–562.

Sekhar, A. R.; Kaloo, M. A.; Sankar, J. Dual-mode Chemodosimetric Response of Dibromo-BODIPY with Anions. 2015, 13, 10155–10161.

Wood, T. E.; Thompson, A. Advances in The Chemistry of Dipyrrins and Their Complexes. Chem Rev. 2007, 107, 1831–1861.

Littler, B. J.; Miller, M. A.; Hung, C.-H.; Wagner, R. W.; O'Shea, D. F.; Boyle, P. D.; Lindsey, J. S. Refined Synthesis of 5-Substituted Dipyrromethanes. J. Org. Chem. 1999, 64, 1391–1396.

Li, Z.; Mintzer, E.; Bittman, R. First Synthesis of Free Cholesterol-BODIPY Conjugates. J. Org. Chem. 2006, 71, 1718–1721.

Shah, M.; Thangaraj, K.; Soong, M.-L.; Wolford, L. T.; Boyer, J. H.; Politzer, I. R.; Pavlopoulos, T. G. Pyrromethenes-BF_2 Complexes As Laser Dyes: 1. Heteroat. Chem. 1990, 1, 389–399.

Yakubovskyi, V. P.; Shandura, M. P.; Kovtun, Y. P. Boradipyrromethenecyanines. Eur. J. Org. Chem. 2009, 2009, 3237–3243

Li, L.-L.; Diau, E. W.-G. Porphyrin-Sensitized Solar Cells. Chem. Soc. Rev., 2013, 42, 291–304.

Wu, L.; Burgess, K. A New Synthesis of Symmetric Boraindacene (BODIPY) Dyes. Chem. Commun. 2008, 4933–4935.

Ulrich, G.; Ziessel, R.; Harriman, A. The Chemistry of Fluorescent Bodipy Dyes: Versatility Unsurpassed. Angew. Chem. Int. Ed. 2008, 47, 1184–1201.

Boens, N.; Verbelen, B.; Dehaen, W. Postfunctionalization of the BODIPY Core: Synthesis and Spectroscopy. Eur. J. Org. Chem. 2015, 6577–6595

Xu, W.; Ren, C.; Teoh, C. L.; Peng, J.; Gadre, S. H.; Rhee, H. –W.; Lee, C.-L. K.; Chang, Y. -T. An Artificial Tongue Fluorescent Sensor Array for Identification and Quantitation of Various Heavy Metal Ions. Anal. Chem. 2014, 86, 8763–8769.

Benstead, M.; Mehl, G. H.; Boyle, R. W. 4,4′-Difluoro-4-bora-3a,4a-diaza-s-indacenes (BODIPYs) As Components of Novel Light Active Materials. Tetrahedron 2011, 67, 3573–3601.

Arbeloa, F. L.; Bañuelos, J.; Martinez, V.; Arbeloa, T.; Arbeloa, I. L. Structural, Photophysical and Lasing Properties of Pyrromethene Dyes. Int. Rev. Phys. Chem. 2005, 24, 339–374.

Schmitt, A.; Hinkeldey, B.; Wild, M. Synthesis of the Core Compound of the BODIPY Dye Class: 4,4'- Difluoro-4-bora-(3a, 4a)-diaza-s-indacene. J. Fluoresc. 2009, 19, 755–758.

Leen, V.; Auweraer, M. V.; Boens, N.; Dehaen, W. Vicarious Nucleophilic Substitution of α-Hydrogen of BODIPY and Its Extension to Direct Ethenylation. Org. Lett. 2011, 13, 1470–1473.

Gabe, Y.; Urano, Y.; Kikuchi, K.; Kojima, H.; Nagano, T. Highly Sensitive Fluorescence Probes for Nitric Oxide Based on Boron Dipyrromethene Chromophore- Rational Design of Potentially Useful Bioimaging Fluorescence Probe. J. Am. Chem. Soc. 2004, 126, 3357–3367.

Zhao, N.; Xuan, S.; Fronczek, F. R.; Smith, K. M.; Vicente, M. G. H. Stepwise Polychlorination of 8-Chloro-BODIPY and Regioselective Functionalization of 2,3,5,6,8-Pentachloro-BODIPY. J. Org. Chem. 2015, 80, 8377–8383.

Leen, V.; Yuan, P.; Wang, L.; Boens, N.; Dehaen, W. Synthesis of Meso-Halogenated BODIPYs and Access to Meso-Substituted Analogues. Org. Lett. 2012, 14, 6150–6153.

Knoevenagel, E. Condensation von Malonsäure mit Aromatischen Aldehyden durch Ammoniak und Amine. Ber. Dtsch. Chem. Ges. 1898, 31, 2596–2619.

Haugland, R. P.; Kang, H. C. Reactive Fluorescent Dipyrrometheneboron Difluoride Dyes As Molecular Probes for Biopolymers. 1988 U.S. Patent No:4,774,339 Washington, DC: U.S. Patent and Trademark Office.

Cakmak, Y.; Akkaya, E. U. Phenylethynyl-BODIPY Oligomers: Bright Dyes and Fluorescent Building Blocks. Org. Let., 2009, 11, 85–88.

Yogo, T.; Urano, Y.; Ishitsuka, Y.; Maniwa, F.; Nagano, T. Highly Efficient and Photostable Photosensitizer Based on BODIPY Chromophore. J. Am. Chem. Soc., 2005, 127, 12162–12163.

Jiao, L.; Yu, C.; Li, J.; Wang, Z.; Wu, M.; Hao, E. β-Formyl-BODIPYs from the Vilsmeier−Haack Reaction. J. Org. Chem. 2009, 74, 7525–7528.

Zhu, S.; Bi, J.; Vegesna, G.; Zhang, J.; Luo, F.-T.; Valenzano, L.; Liu, H. Functionalization of BODIPY Dyes at 2,6-Positions Through Formyl Groups. RSC Advances, 2013, 3, 4793–4800.

Wories, H. J.; Koek, J. H.; Lodder, G.; Lugtenburg, J.; Fokkens, R.; Driessen, O.; Mohn, G. R. A Novel Water-Soluble Fluorescent Probe: Synthesis, Luminescence and Biological Properties of the Sodium Salt of the 4-sulfonato-3,3′,5,5′-tetramethyl-2,2′-pyrromethen-1,1′-BF_2 Complex. Recl. Trav. Chim. Pays-Bas 1985, 104, 288–291.

Esnal, I.; Bañuelos, J.; Arbeloa, I. L.; Costela, A.; Garcia-Moreno, I.; Garzón, M. Agarrabeitia, A. R.; Ortiz, M. J. Nitro and Amino BODIPYS: Crucial Substituents to Modulate Their Photonic Behavior. RSC Adv. 2013, 3, 1547–1556.

Rihn, S.; Retailleau, P.; Bugsaliewicz, N.; Nicola, A. D.; Ziessel, R. Versatile Synthetic Methods for the Engineering of Thiophene-Substituted Bodipy Dyes. Tetrahedron Lett. 2009, 50, 7008–7013.

Zhang, M.; Hao, E.; Zhou, J.; Yu, C.; Bai, G.; Wang, F.; Jiao, L. Synthesis of Pyrrolyldipyrrinato BF_2 Complexes by Oxidative Nucleophilic Substitution of Boron Dipyrromethene with Pyrrole. Org. Biomol. Chem. 2012, 10, 2139–2145.

Patil, N. T.; Shinde, V. S.; Thakare, M. S.; Kumar, P. H.; Pangal, P. T.; Barui, A. Y. Patra, C. R. Exploiting the Higher Alkynophilicity of Au Species: Development of a Highly Selective Fluorescent Probe For Gold Ions. Chem. Commun. 2012, 48, 11229–11231.

Karakus, E.; Ucuncu, M.; Emrullahoglu, M. Electrophilic Cyanate As a Recognition Motif for Reactive Sulfur Species: Selective Fluorescence Detection of H_2S. Anal. Chem. 2016, 88, 1039–1043.

Alcaide, B.; Almendros, P. Gold-Catalyzed Cyclization Reactions of Allenol and Alkynol Derivatives. Acc. Chem. Res., 2014, 47, 939–952.

Braun, I.; Asiri, A. M.; Hashmi, A. S. K. Gold Catalysis 2.0. ACS Catal. 2013, 3, 1902–1907.

Krause, N.; Winter, C. Gold-Catalyzed Nucleophilic Cyclization of Functionalized Allenes: A Powerful Access to Carbo- and Heterocycles. Chem. Rev. 2011, 111, 1994–2009.

Shaw III, C. F. Gold-Based Therapeutic Agents. Chem. Rev. 1999, 99, 2589–2600.

Ott, I. On the Medicinal Chemistry of Gold Complexes As Anticancer Drugs. Coord. Chem. Rev. 2009, 253, 1670–1681.

Navarro, M. Gold Complexes As Potential Anti-parasitic Agents. Coord. Chem. Rev. 2009, 253, 1619–1626.

Goodman, C. M.; McCusker, C. D.; Yilmaz, T.; Rotello, V. M. Toxicity of Gold Nanoparticles Functionalized with Cationic and Anionic Side Chains. Bioconjugate Chem. 2004, 15, 897–900.

Habib, A.; Tabata, M.; Oxidative DNA Damage Induced by HEPES (2-[4-(2-hydroxyethyl)-1-piperazinyl]ethanesulfonic Acid) Buffer in the Presence of Au(III). 2004, 98, 1696–1702.

Chen, X.; Pradhan, T.; Wang, F.; Kim, J. S.; Yoon, J. Fluorescent Chemosensors Based on Spiroring-Opening of Xanthenes and Related Derivatives. Chem. Rev. 2012, 112, 1910–1956.

Su, X.; Aprahamian, I. Hydrazone-Based Switches, Metallo-Assemblies and Sensors. Chem. Soc. Rev. 2014, 43, 1963–1981.

Yang, Y.-K; Lee, S.; Tae, J. A. Gold(III) Ion Selective Fluorescent Probe and Its Application to Bioimagings. Org. Lett. 2009, 11, 5610–5613.

Jou, M. N.; Chen, X.; Swamy, K. M. K.; Kim, H. N.; Kim, H.-J.; Lee, S.; Yoon, J. Highly Selective Fluorescent Probe For Au^{3+} Based on Cyclization of Propargylamide. Chem. Commun. 2009, 7218–7220.

Egorova, O. A.; Seo, H.; Chatterjee, A.; Ahn, K. H. Reaction-Based Fluorescent Sensing of Au(I)/Au(III) Species: Mechanistic Implications on Vinylgold Intermediates. Org. Lett. 2010, 12, 401–403.

Do, J. H.; Kim, H. N.; Yoon, J.; Kim, J. S.; Kim, H.-J. A Rationally Designed Fluorescence Turn-on Probe For the Gold(III) Ion. Org. Lett. 2010, 12, 932–934.

Cao, X.; Lin, W.; Ding, Y. Ratio-Au: A FRET-based Fluorescent Probe for Ratiometric Determination of Gold Ions and Nanoparticles. Chem. – Eur. J., 2011, 17, 9066–9069.

Seo, H.; Jun, M. E.; Egorova, O. A.; Lee, K.-H.; Kim, K.-T.; Ahn, K. H. A Reaction-Based Sensing Scheme for Gold Species: Introduction of a (2-Ethynyl)benzoate Reactive Moiety. Org. Lett., 2012, 14, 5062–5065.

Wang, J.-B.; Wu, Q.-Q.; Min, Y.-Z.; Liu, Y.-Z.; Song, Q.-H. A novel Fluorescent Probe For Au(III)/Au(I) Ions Based on an Intramolecular Hydroamination of a BODIPY Derivative and Its Application to Bioimaging. Chem. Commun. 2012, 48, 744–746.

Choi, J. Y.; Kim, G.-H.; Guo, Z.; Lee, H. Y.; Swamy, K. M. K.; Pai, J.; Shin, S.; Shin, I.; Yoon, J. Highly Selective Ratiometric Fluorescent Probe for Au^{3+} and Its Application to Bioimaging. Biosens. Bioelectron. 2013, 49, 438–441.

Wang, B.; Fu, T.; Yang, S.; Li, J.; Chen, Y. An Intramolecular Charge Transfer (ICT)-Based Dual Emission Fluorescent Probe for the Ratiometric Detection of Gold Ions. Anal. Methods 2013, 5, 3639–3641.

Emrullahoglu, M.; Karakus, E.; Ucuncu, M. A Rhodamine Based Turn-on Chemodosimeter For Monitoring Gold Ions in Synthetic Samples and Living Cells. Analyst 2013, 138, 3638–3641.

Yuan, L.; Lin, W.; Yang, Y.; Song, J. A Fast-Responsive Fluorescent Probe for Detection of Gold Ions in Water and Synthetic Products. Chem. Commun. 2011, 47, 4703–4705.

Park, J.; Choi, S.; Kim, T.-I.; Kim, Y. Highly Selective Fluorescence Turn-on Sensing of Gold Ions by a Nanoparticle Generation/C–I Bond Cleavage Sequence. Analyst 2012, 137, 4411–4414.

Park, J. E.; Choi, M. G.; Chang, S.-K. Colorimetric and Fluorescent Signaling of Au^{3+} by Desulfurization of Thiocoumarin. Inorg. Chem. 2012, 51, 2880–2884.

Wang, J.; Lin, W.; Yuan, L.; Song, J.; Gao, W. Development of A Reversible Fluorescent Gold Sensor with High Selectivity. Chem. Commun. 2011, 47, 12506–12508.

Öztaş, Z.; Pamuk, M.; Algi, F. Nonreaction-Based Fluorescent Au^{3+} Probe That Gives Fast Response in Aqueous Solution Tetrahedron 2013, 69, 2048–2051.

Yang, Y.; Yin, C.; Huo, F.; Chao, J. A Selective Fluorescent Probe for Detection of Gold(III) Ions and Its Application to Bioimaging. RSC Adv. 2013, 3, 9637–9640.

Chinapang, P.; Ruangpornvisuti, V.; Sukwattanasinitt, M.; Rashatasakhon, P. Ferrocenyl Derivative of 1,8-naphthalimide As A New Turn-on Fluorescent Sensor for Au(III) ion. Dyes Pigm. 2015, 112, 236–238.

Isik, M.; Ozdemir, T.; Turan, I. S.; Kolemen, S.; Akkaya, E. U. Chromogenic and Fluorogenic Sensing of Biological Thiols in Aqueous Solutions Using Bodipy Based Reagents. Org. Lett. 2013, 15, 216–219.

Xue, L.; Liu, Q.; Jiang, H. Ratiometric Zn^{2+} Fluorescent Sensor and New Approach for Sensing Cd^{2+} by Ratiometric Displacement. Org. Lett. 2009, 11, 3454–3457.

Komatsu, H.; Miki, T.; Citterio, D.; Kubota, T.; Shindo, Y.; Kitamura, Y.; Oka, K.; Suzuki, K. Single Molecular Multianalyte (Ca2+, Mg2+) Fluorescent Probe and Applications to Bioimaging. J. Am. Chem. Soc. 2005, 127, 10798–10799.

Yuan, M.; Zhou, W.; Liu, X.; Zhu, M.; Li, J.; Yin, X.; Zheng, H.; Zuo, Z.; Ouyang, C.; Liu, H.; Li , Y.; Zhu, D. A Multianalyte Chemosensor on a Single Molecule: Promising Structure for an Integrated Logic Gate. J. Org. Chem. 2008, 73, 5008–5014.

Yao, T.; Zhang, X.; Larock, R. C. AuCl3-Catalyzed Synthesis of Highly Substituted Furans from 2-(1-Alkynyl)-2-alken-1-ones. J. Am. Chem. Soc. 2004, 126, 11164–11165.

Deniz, E.; Isbasar, G. C.; Bozdemir, Ö. A.; Yıldırım, L. T.; Siemiarczuk, A.; Akkaya, E. U. Bidirectional Switching of Near IR Emitting Boradiazaindacene Fluorophores. Org. Lett. 2008, 10, 3401–3403.

Wagner, S.; Brödner, K.; Coombs, B. A.; Bunz, U. H. F. Pyridine-Substituted BODIPY as Fluorescent Probe for Hg^{2+}. Eur. J. Org. Chem. 2012, 11, 2237–2242.

Zhou, L.; Zhu, C.–C.; Xue, Y.–S.; He, W.–J.; Du, H.–B.; You, X.–Z.; Li, Y.–Z. Two Fluorescent 2,6-Substituted Pyridyl Boron-dipyrromethene Dyes for Selective Sensing of Cuprous Ions. Inorg. Chem. Commun. 2013, 35, 355–359.

Buynak, J. D.; Rao, A. S.; Ford, G. P.; Carver, C.; Adam, G.; Geng, B.; Bachmann, B.; Shobassy, S.; Lackey, S. 7-Alkylidenecephalosporin Esters as Inhibitors of Human Leukocyte Elastase. J. Med. Chem. 1997, 40, 3423–3433.

Tchounwou, B.; Ayensu, W. K.; Ninashvili, N.; Sutton, D. Review: Environmental Exposure to Mercury and Its Toxicopathologic Implications for Public Health. Environ. Toxicol. 2003, 18, 149–175.

De Vries, W.; Romkens, P. F.; Schutze, G. Critical Soil Concentrations of Cadmium, Lead, and Mercury in View of Health Effects on Humans and Animals. Rev. Environ. Contam. Toxicol. 2007, 191, 91–130.

Bulletin of the World Health Organization 2013, 91, 161–162

Johnson, J. Controversial EPA Mercury Study Endorsed by Science Panel. Environ. Sci. Technol. 1997, 31, 218A–219A.

Diez-Gil, C.; Martinez, R.; Ratera, I.; Hirsh, T.; Espinosa, A.; Tarraga, A.; Molina, P.; Wolfbeis, O. S.; Veciana, J. Selective Picomolar Detection of Mercury(II) Using Optical Sensors. Chem. Comm. 2011, 47, 1842–1844.

Fabbrizzi, L.; Lichelli, M.; Pallavicini, P.; Perotti, A.; Sacchi, D. An Anthracene-Based Fluorescent Sensor for Transition Metal Ions. Angew. Chem. Int. Ed. 1994, 33, 1975–1977.

Chae, M.-Y.; Czarnik, A. W. Fluorometric Chemodosimetry. Mercury(II) and Silver(I) Indication in Water via Enhanced Fluorescence Signaling. J. Am. Chem. Soc. 1992, 114, 9704-9705.

Sancenon, F.; Martinez-Manez, R.; Soto, J. Colourimetric Detection of Hg2+ by A Chromogenic Reagent Based on Methyl Orange and Open-Chain Polyazaoxaalkanes. Tetrahedron Lett. 2001, 42, 4321–4323.

Li, Y. Y.; He, S.; Lu, Y.; Zeng, X. S. Novel Hemicyanine Dye As Colorimetric and Fluorometric Dual-Modal Chemosensor for Mercury in Water. Org. Biomol. Chem. 2011, 9, 2606–2609.

Yuan, M. J.; Li, Y. L.; Li, J. B.; Li, C. H.; Liu, X. F.; Lv, J.; Xu, J. L.; Liu, H. B.; Wang, S.; Zhu, D. A Colorimetric and Fluorometric Dual-Modal Assay for Mercury Ion by a Molecule. Org. Lett. 2007, 9, 2313–2316.

Atilgan, S.; Ozdemir, T.; Akkaya, E. U. Selective Hg(II) Sensing With Improved Stokes Shift By Coupling the Internal Charge Transfer Process to Excitation Energy Transfer. Org. Lett. 2010, 12, 4792–4795.

Du, J. J.; Fan, J. L.; Peng, X. J.; Sun, P. P.; Wang, J. Y.; Li, H. L.; Sun, S. G. A New Fluorescent Chemodosimeter for Hg2+: Selectivity, Sensitivity, and Resistance to Cys and GSH. Org. Lett. 2010, 12, 476–47.

Abley, P.; Byrd, J. E.; Halpern, J. Mercury(II)- and Thallium(III)-Catalyzed Hydrolysis of Isopropenyl Acetate. J. Am. Chem. Soc. 1972, 94, 1985–1989.

Coskun, A.; Yilmaz, M. D. Akkaya, E. U. Bis(2-pyridyl)-Substituted Boratriazaindacene As an NIR-Emitting Chemosensor for Hg(II). Org. Lett. 2007, 9, 607–609.

Fan, J. L.; Peng, X. J.; Wang, S.; Liu, X. J.; Li, H. L.; Sun, S. G. A Fluorescence Turn-on Sensor for Hg^{2+} with a Simple Receptor Available in Sulphide-Rich Environments. J. Fluoresc. 2012, 22, 945–951.

Yang, Y.-K.; Yook, K-J.; Tae, J. A Rhodamine-Based Fluorescent and Colorimetric Chemodosimeter For the Rapid Detection of Hg^{2+} Ions in Aqueous Media. J. Am. Chem. Soc. 2005, 127, 16760–16761.

Wu, J.-S.; Hwang, I.-C.; Kim, K. S.; Kim, J. S. Rhodamine-Based Hg^{2+}-Selective Chemodosimeter in Aqueous Solution: Fluorescent OFF-ON. Org. Lett. 2007, 9, 907–910.

Shang, G.-Q.; Gao, X.; Chen, M.-X.; Zheng, H.; Xu, J.-G. A Novel Hg^{2+} Selective Ratiometric Fluorescent Chemodosimeter Based on an Intramolecular FRET Mechanism. J. Fluoresc. 2008, 18, 1187–1192.

Srivastava, P.; Ali, R.; Razi, S. S.; Shahid, M.; Misra, A. Thiourea Based Molecular Dyad (ANTU): Fluorogenic Hg^{2+} Selective Chemodosimeter Exhibiting Blue–Green Fluorescence in Aqueous-Ethanol Environment. Sens. Actuators, B 2013, 181, 584–595.

Yang, Y.; Zhao, Q.; Feng, W.; Li, F. Luminescent Chemodosimeters for Bioimaging. Chem. Rev. 2013, 113, 192−270.

Zhang, X.; Xu, Y.; Guo, P.; Qian, X. A Dual Channel Chemodosimeter for Hg2+ and Ag^{+} Using a 1,3-dithiane Modified BODIPY. New J. Chem. 2012, 36, 1621–1625.

Saha, S.; Agarwalla, H.; Gupta, H.; Baidya, M.; Suresh, E.; Ghosh, S. K.; Das, A. New Chemodosimetric Probe for the Specific Detection of Hg^{2+} in Physiological Condition and Its Utilisation for Cell Imaging Studies. Dalton Trans. 2013, 42, 15097–15105.

Madhu, S.; Josimuddin, S.; Ravikanth, M. 3,5-Bis(dithioacetal) meso-aryl BODIPYs: Selective Chemodosimeters for Hg(II) Ions. New J. Chem. 2014, 38, 3770–3776.

Song, F. L.; Watanabe, S.; Floreancig, P. E.; Koide, K. Oxidation-Resistant Fluorogenic Probe for Mercury Based on Alkyne Oxymercuration. J. Am. Chem. Soc. 2008, 130, 16460–16461.

Lee, H.; Kim, H. –J. Ratiometric Fluorescence Chemodosimeter for Mercuric Ions Through the Hg(II)-Mediated Propargyl Amide to Oxazole Transformation. Tetrahedron Lett. 2011, 52, 4775–4778.

Santra, M.; Ryu, D.; Chatterjee, A.; Ko, S. -K.; Shin, I.; Ahn, K. H. A Chemodosimeter Approach to Fluorescent Sensing and Imaging of Inorganic and Methylmercury Species. Chem. Commun. 2009, 2115–2117.

Santra, M.; Roy, B.; Ahn, K. H. A "Reactive" Ratiometric Fluorescent Probe for Mercury Species. Org. Lett. 2011, 13, 3422–3425.

Cho, Y. -S.; Ahn, K. H. A 'Turn-on' Fluorescent Probe That Selectively Responds to Inorganic Mercury Species. Tetrahedron Lett. 2010, 51, 3852–3854.

Lin, W.; Cao, X.; Ding, Y.; Yuan, L.; Long, L. A Highly Selective and Sensitive Fluorescent Probe for Hg^{2+} Imaging in Live Cells Based on a Rhodamine–thioamide–alkyne Scaffold. Chem. Commun. 2010,46, 3529–3531.

Sauer, R.; Turshatov, A.; Baluschev, S.; Landfester, K. One-Pot Production of Fluorescent Surface-Labeled Polymeric Nanoparticles via Miniemulsion Polymerization with Bodipy Surfmers. Macromolecules 2012, 45, 3787–3796.

Wu, W.; Guo, H.; Wu, W.; Ji, S.; Zhao, J. Organic Triplet Sensitizer Library Derived from a Single Chromophore (BODIPY) with Long-Lived Triplet Excited State for Triplet–Triplet Annihilation Based Upconversion. J. Org. Chem. 2011, 76, 7056–7064.

Cunha, S.; Da Silva, T. L. One-Pot and Catalyst-Free Synthesis of Thiosemicarbazones via Multicomponent Coupling Reactions. Tetrahedron Lett. 2009, 50, 2090–2093.

Yao, T.; Zhang, X.; Larock, R. C. $AuCl_3$-Catalyzed Synthesis of Highly Substituted Furans from 2-(1-Alkynyl)-2-alken-1-ones. J. Am. Chem. Soc., 2004, 126, 11164–11165

Brouwer, A. M. Standards for photoluminescence quantum yield measurements in solution (IUPAC Technical Report). Pure Appl. Chem., 2011, 83, 2213–2228.

Buynak, D.; Rao, A. S.; Ford, G. P.; Carver, C.; Adam, G.; Geng, B.; Bachmann, B.; Shobassy, S.; Lackey, S. 7-Alkylidenecephalosporin Esters as Inhibitors of Human Leukocyte Elastase. J. Med. Chem. 1997, 40, 3423–3433.

Hatai, J.; Pal, S.; Jose, G. P.; Sengupta, T.; Bandyopadhyay, S. A Single Molecule Multi Analyte Chemosensor Differentiates Among Zn^{2+}, Pb^{2+} and Hg^{2+}: Modulation of Selectivity by Tuning of Solvents. Rsc Adv. 2012, 2, 7033–7036.

Cheng, H.; Qian, Y. A Novel BODIPY-Schiff Base-Based Colorimetric and Fluorometric Dosimeter for Hg^{2+}, Fe^{3+} and Au^{3+}. RSC Adv. 2015, 5, 82887–82893.

Feng, Y.; Li, D.; Wang, Q.; Wang, S.; Meng, X.; Shao, Z.; Zhu, M.; Wang, X. A Carbazole-Based Mitochondria-Targeted Two-Photon Fluorescent Probe for Gold Ions and Its Application in Living Cell Imaging. . Sens. Actuators, B 2016, 225, 572–578.

Kambama, S.; Wang, B.; Wang, F.; Wang, Y.; Chen, H.; Yin, J.; Chen, X. A Highly Sensitive and Selective Fluorescein-Based Fluorescence Probe for Au^{3+} and Its Application in Living Cell Imaging. 2015, 209, 1005–1010.

Wang, E.; Pang, L.; Zhou, Y.; Zhang, J.; Yu, F.; Qiao, H.; Pang, X. A High Performance Schiff-Base Fluorescent Probe for Monitoring Au^{3+} in Zebrafish Based on BODIPY. Biosens. Bioelectron. 2016, 77, 812–817.

APPENDIX A

^{1}H-NMR AND ^{13}C-NMR SPECTRA OF COMPOUNDS

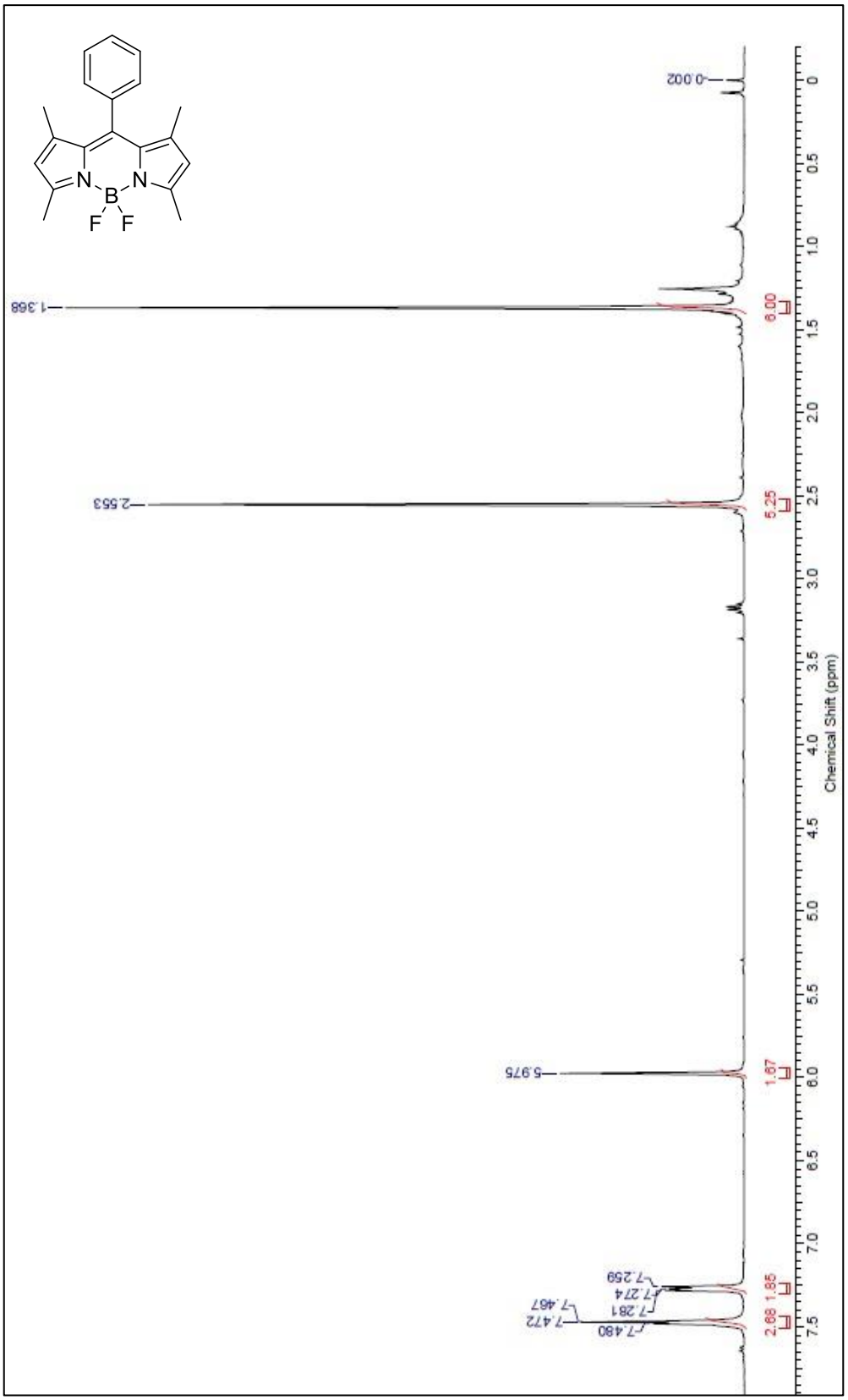

Figure A.1. ^{1}H NMR of 5,5-difluoro-1,3,7,9-tetramethyl-10-phenyl-5H-dipyrrolo[1,2-c:2',1'-f][1,3,2]diazaborinin-4-ium-5-uide

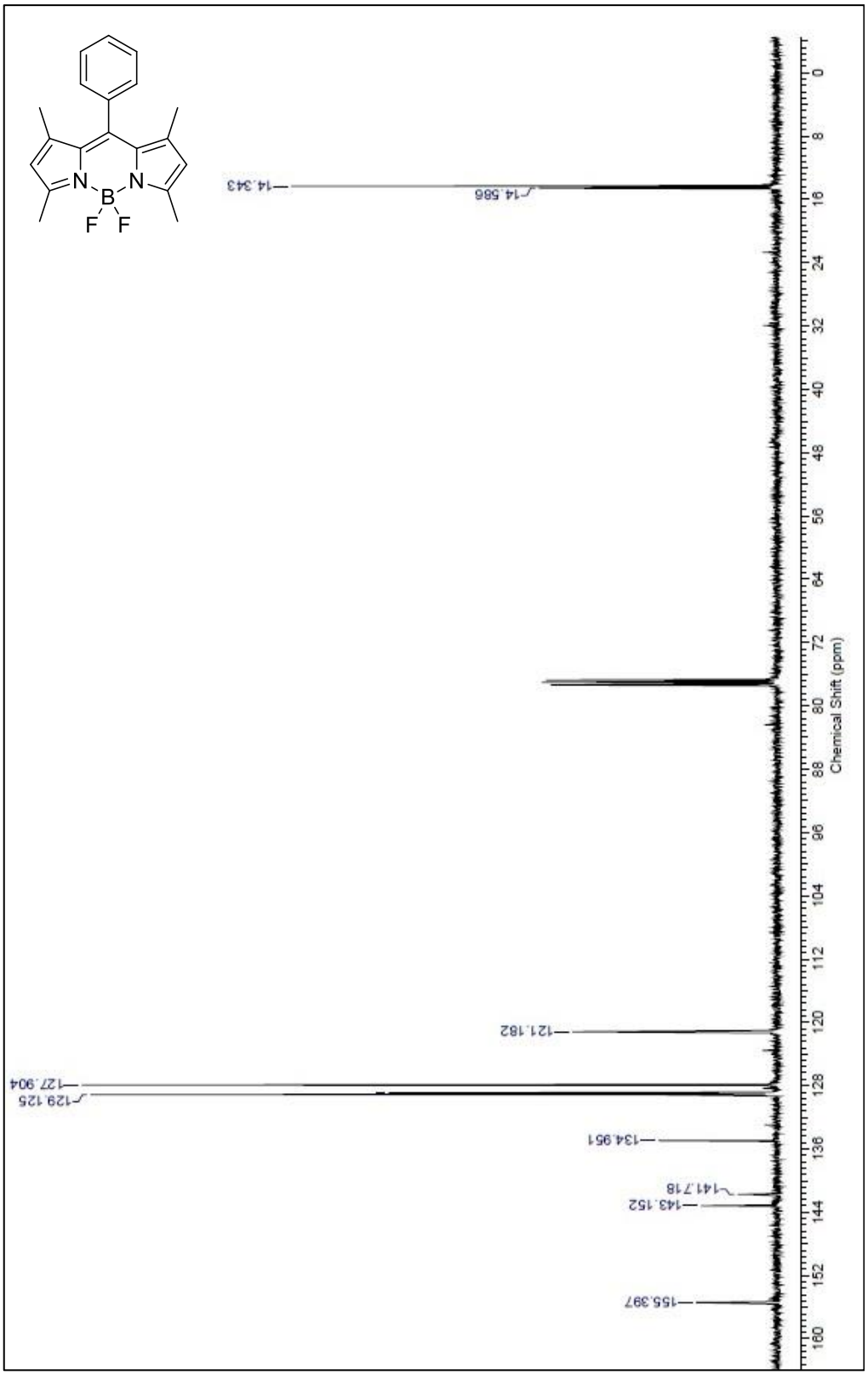

Figure A.2. ^{13}C NMR of 5,5-difluoro-1,3,7,9-tetramethyl-10-phenyl-5H-dipyrrolo[1,2-c:2',1'-f][1,3,2]diazaborinin-4-ium-5-uide

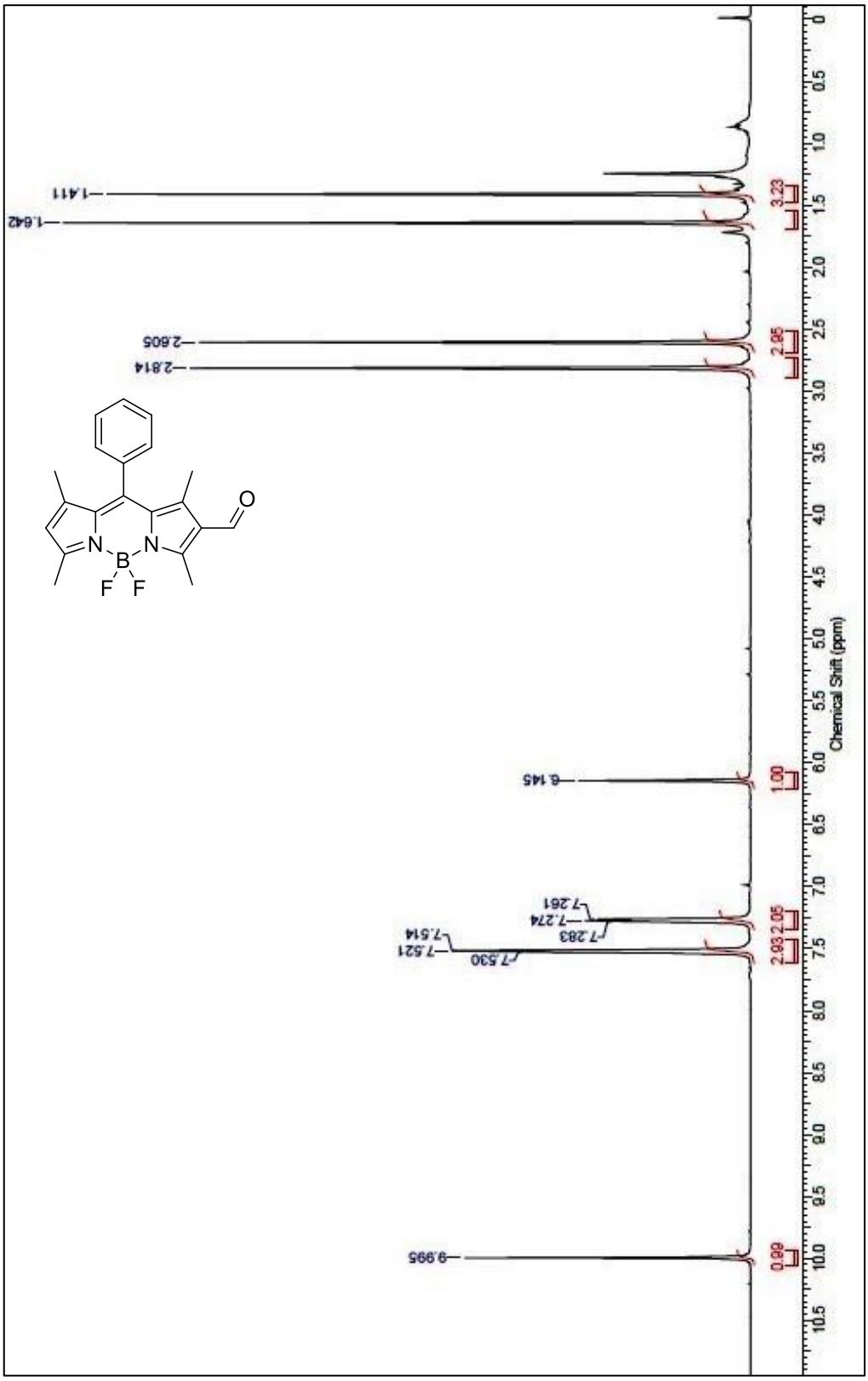

Figure A.3. ^{1}H NMR of 5,5-difluoro-8-formyl-1,3,7,9-tetramethyl-10-phenyl-5H-dipyrrolo[1,2-c:2',1'-f][1,3,2]diazaborinin-4-ium-5-uide

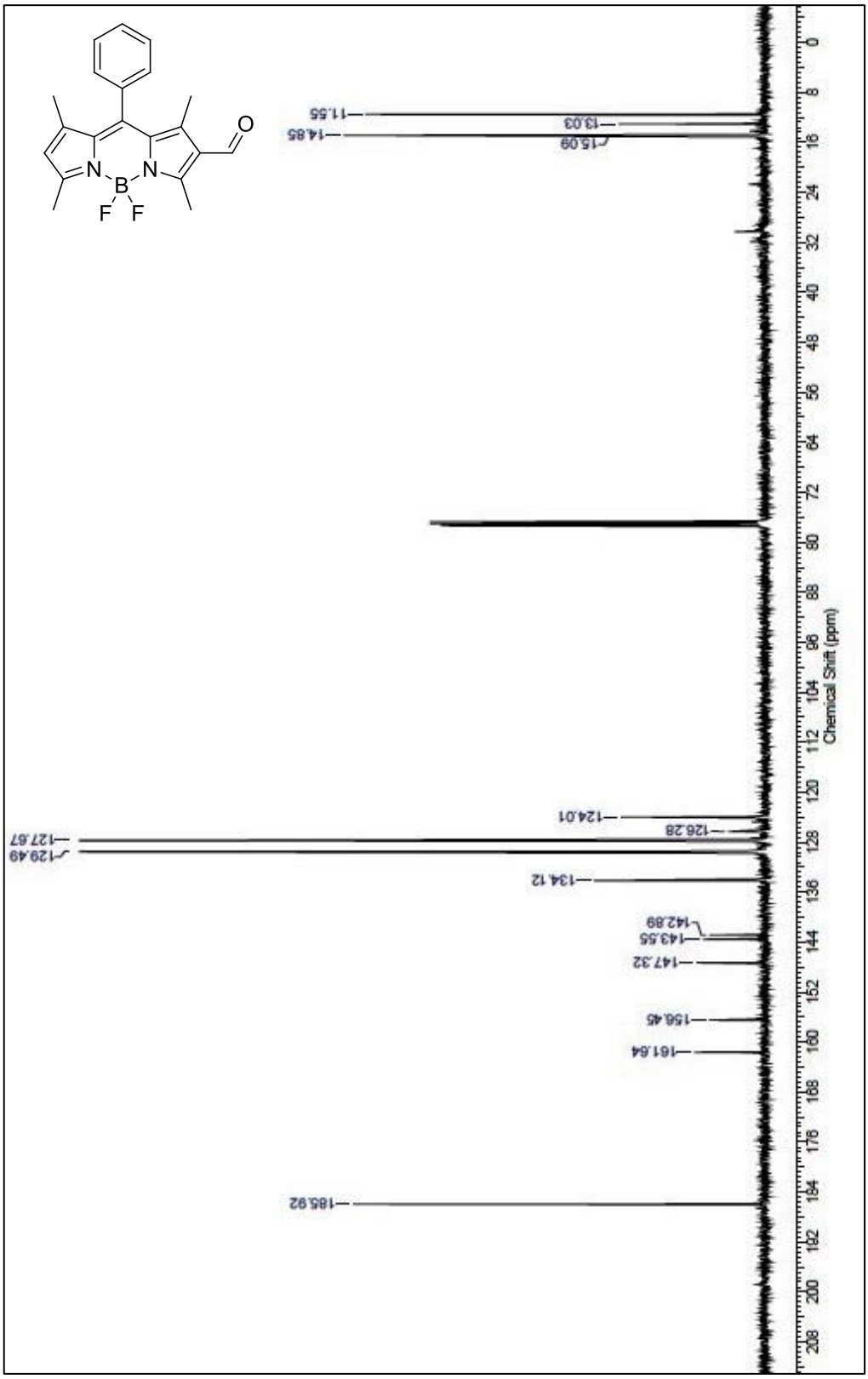

Figure A.4. ^{13}C NMR of 5,5-difluoro-8-formyl-1,3,7,9-tetramethyl-10-phenyl-5H-dipyrrolo[1,2-c:2',1'-f][1,3,2]diazaborinin-4-ium-5-uide

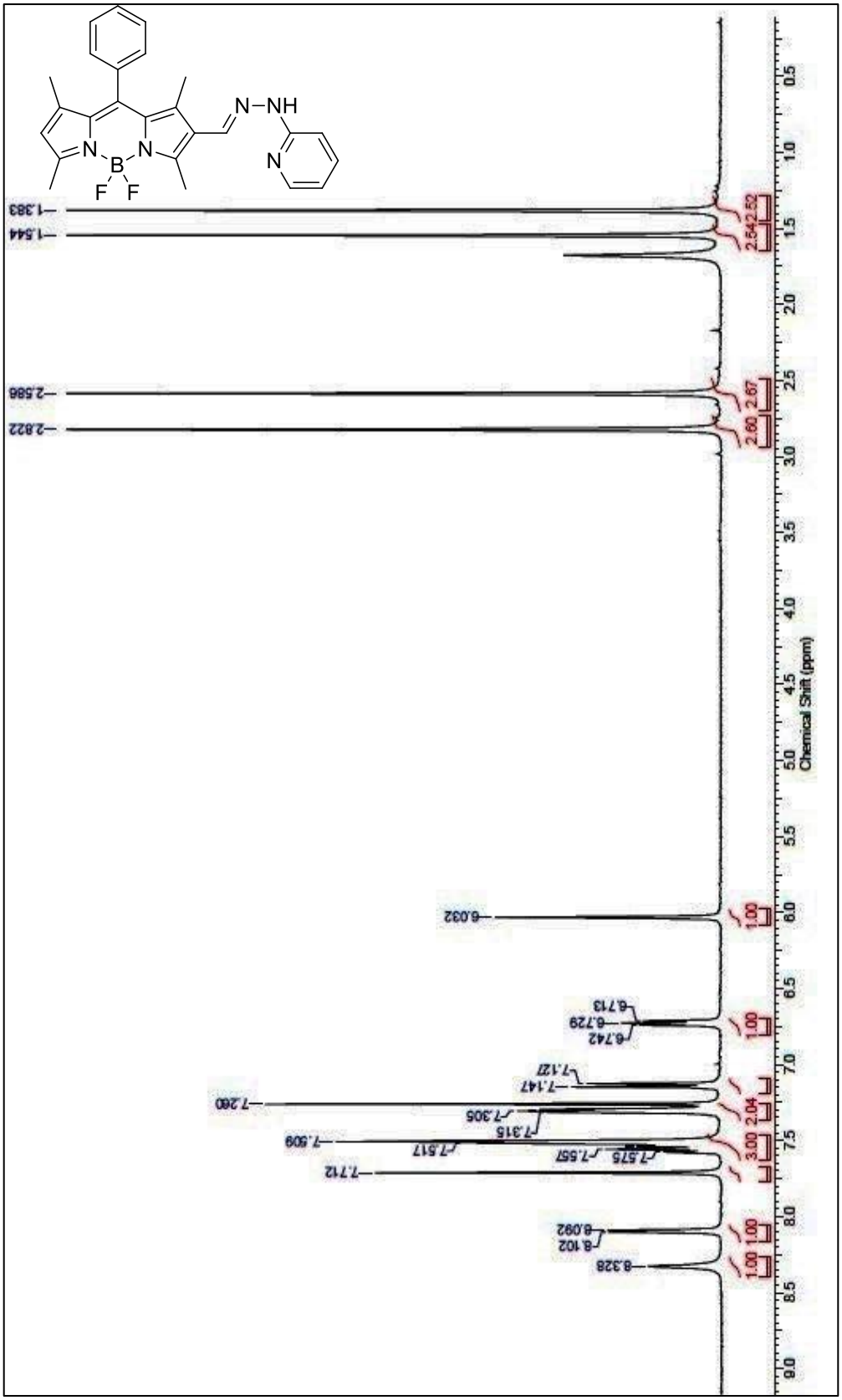

Figure A.5. ^{1}H NMR of (E)-5,5-difluoro-1,3,7,9-tetramethyl-10-phenyl-8-((2-(pyridin-2-yl)hydrazono)methyl)-5H-dipyrrolo[1,2-c:2',1'-f][1,3,2]diazaborinin-4-ium-5-uide

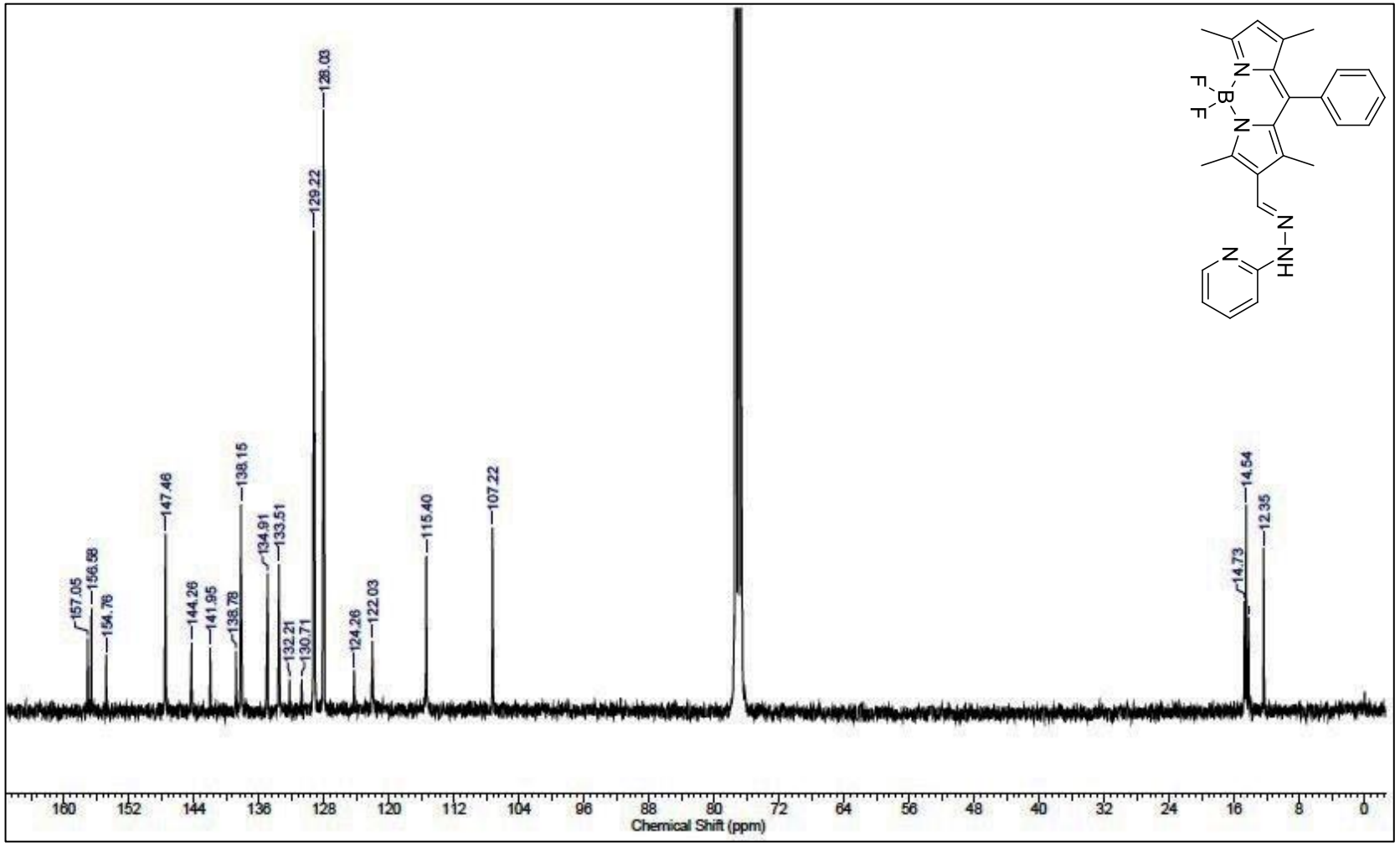

Figure A.6. ^{13}C NMR of (E)-5,5-difluoro-1,3,7,9-tetramethyl-10-phenyl-8-((2-(pyridin-2-yl)hydrazono)methyl)-5H-dipyrrolo[1,2-c:2',1'-f][1,3,2]diazaborinin-4-ium-5-uide

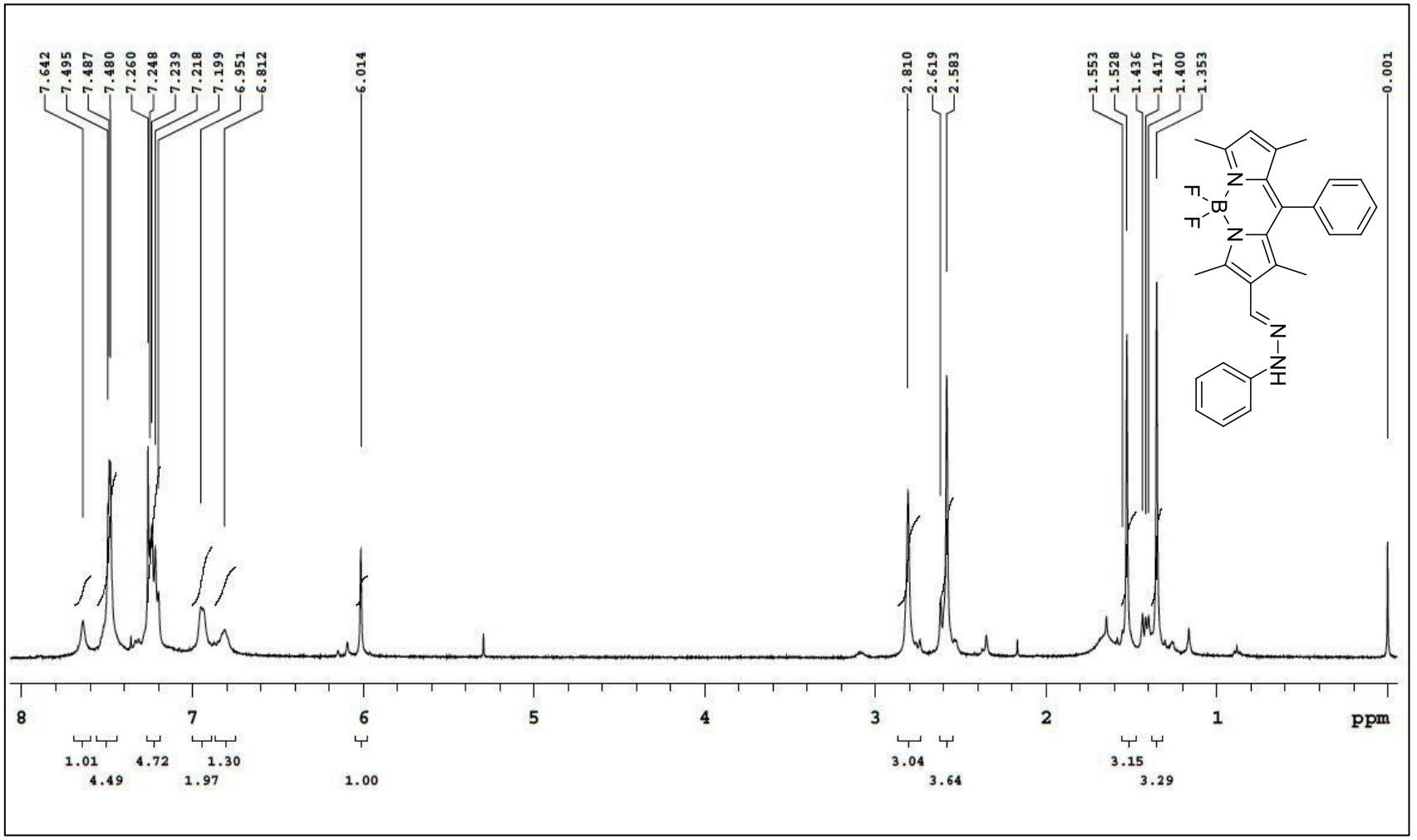

Figure A.7. ^{1}H NMR of (E)-5,5-difluoro-1,3,7,9-tetramethyl-10-phenyl-8-((2-phenylhydrazono)methyl)-5H-dipyrrolo[1,2-c:2',1'-f][1,3,2]diazaborinin-4-ium-5-uide

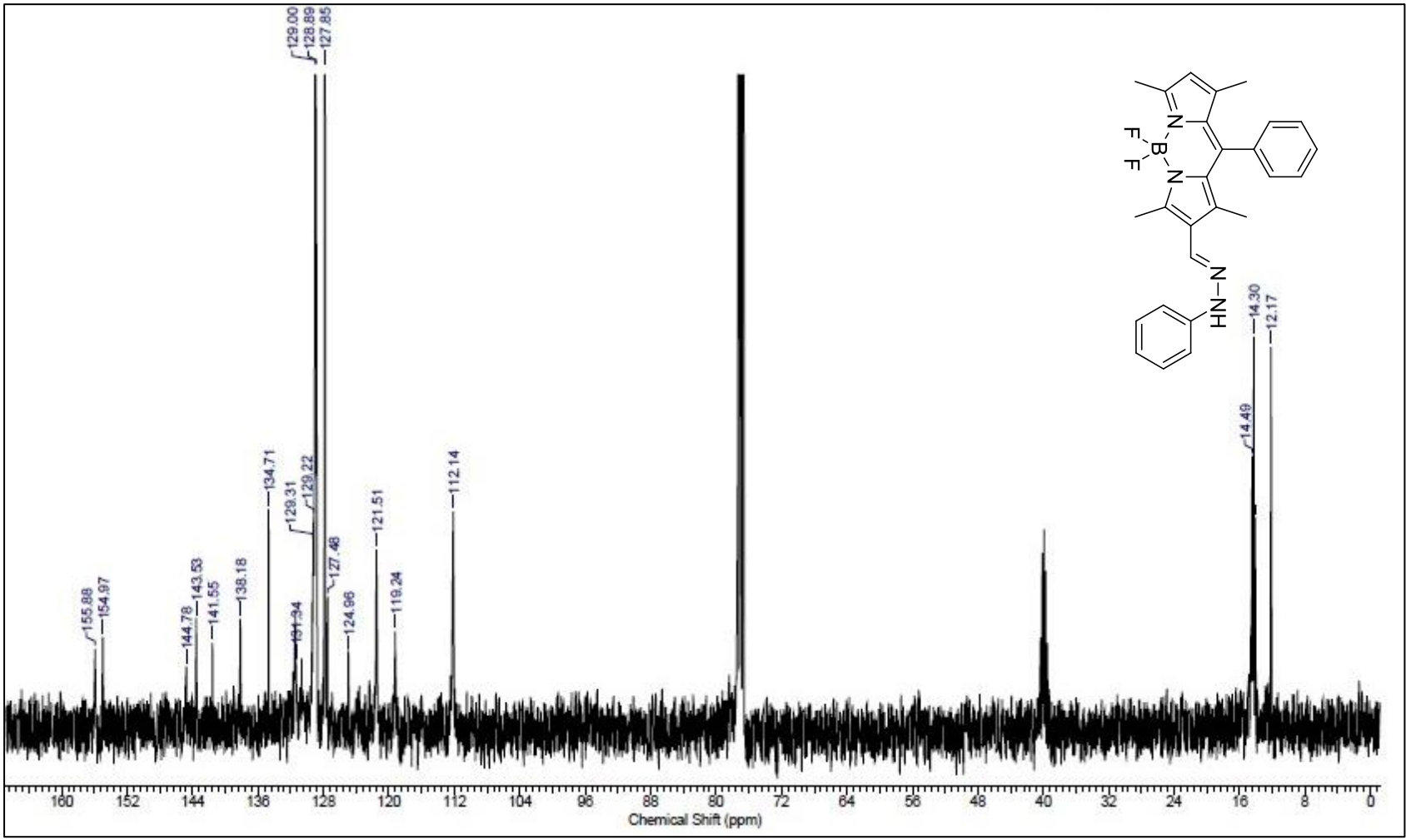

Figure A.8. ^{13}C NMR of (E)-5,5-difluoro-1,3,7,9-tetramethyl-10-phenyl-8-((2-phenylhydrazono)methyl)-5H-dipyrrolo[1,2-c:2',1'-f][1,3,2]diazaborinin-4-ium-5-uide

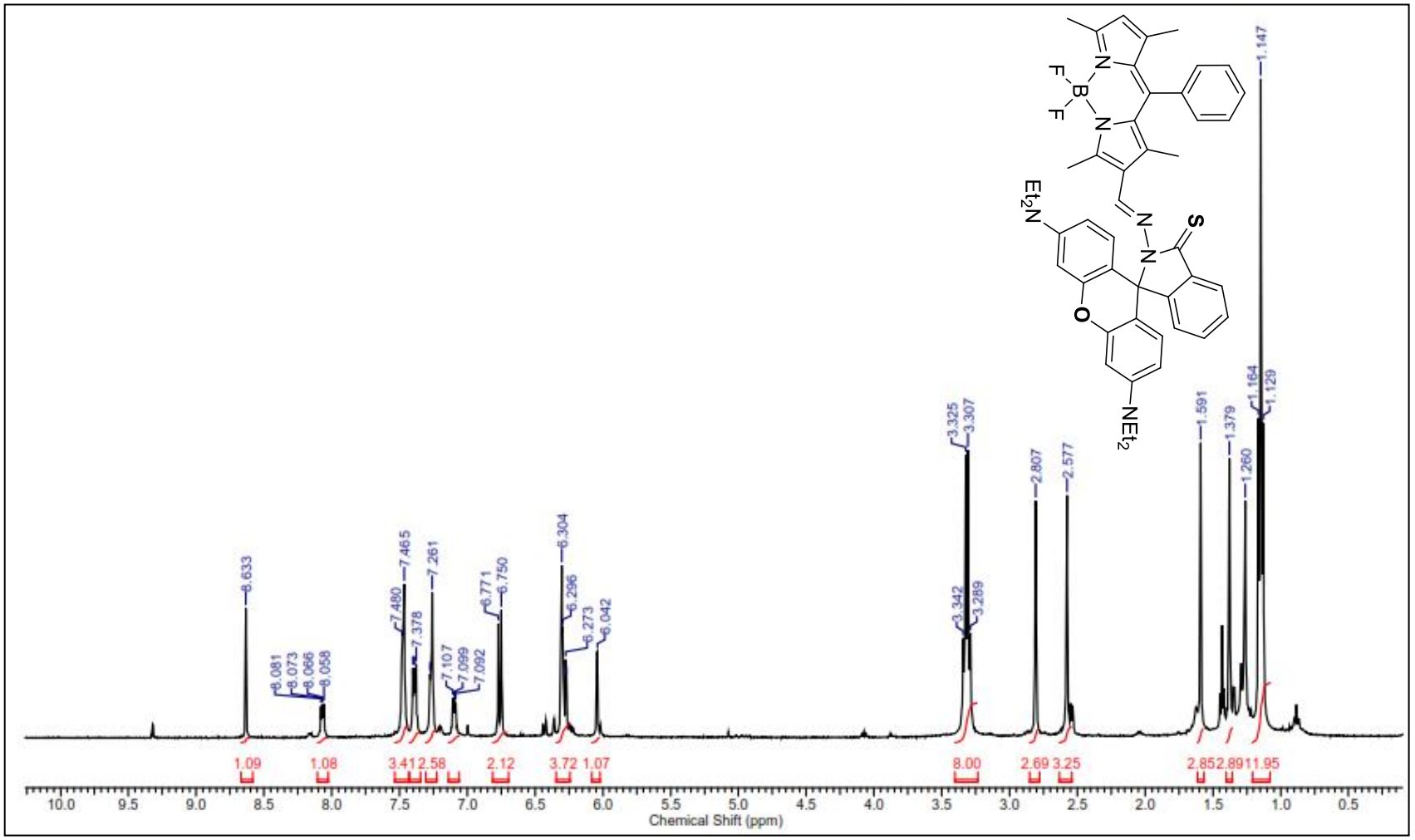

Figure A.9. ^{1}H NMR of (E)-8-(((3',6'-bis(diethylamino)-3-thioxospiro[isoindoline-1,9'-xanthen]-2-yl)imino)methyl)-5,5-difluoro-1,3,7,9-tetramethyl-10-phenyl-5H-dipyrrolo[1,2-c:2',1'-f][1,3,2]diazaborinin-4-ium-5-uide

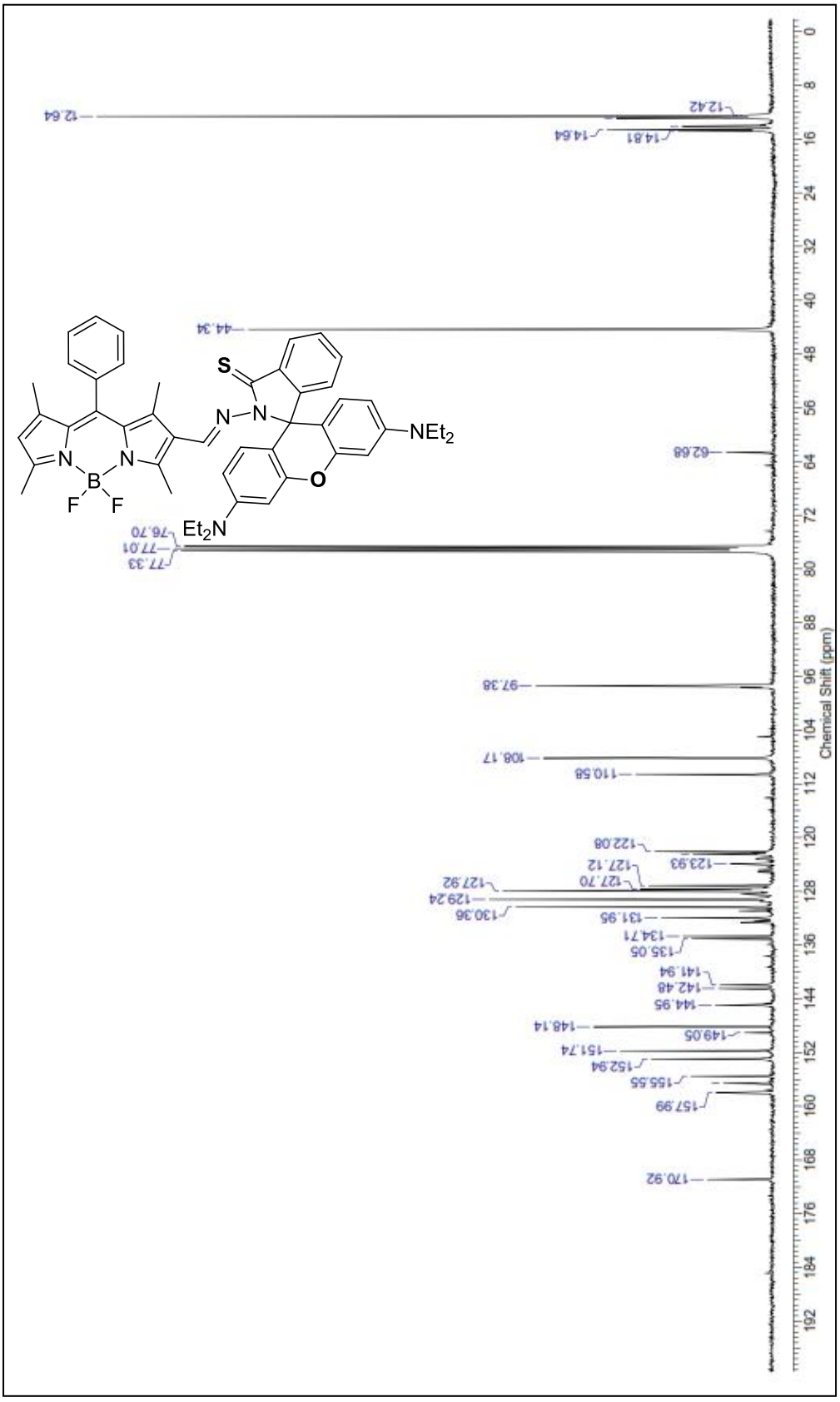

Figure A.10. ^{13}C NMR of (E)-8-(((3',6'-bis(diethylamino)-3-thioxospiro[isoindoline-1,9'-xanthen]-2-yl)imino)methyl)-5,5-difluoro-1,3,7,9-tetramethyl-10-phenyl-5H-dipyrrolo[1,2-c:2',1'-f][1,3,2]diazaborinin-4-ium-5-uide

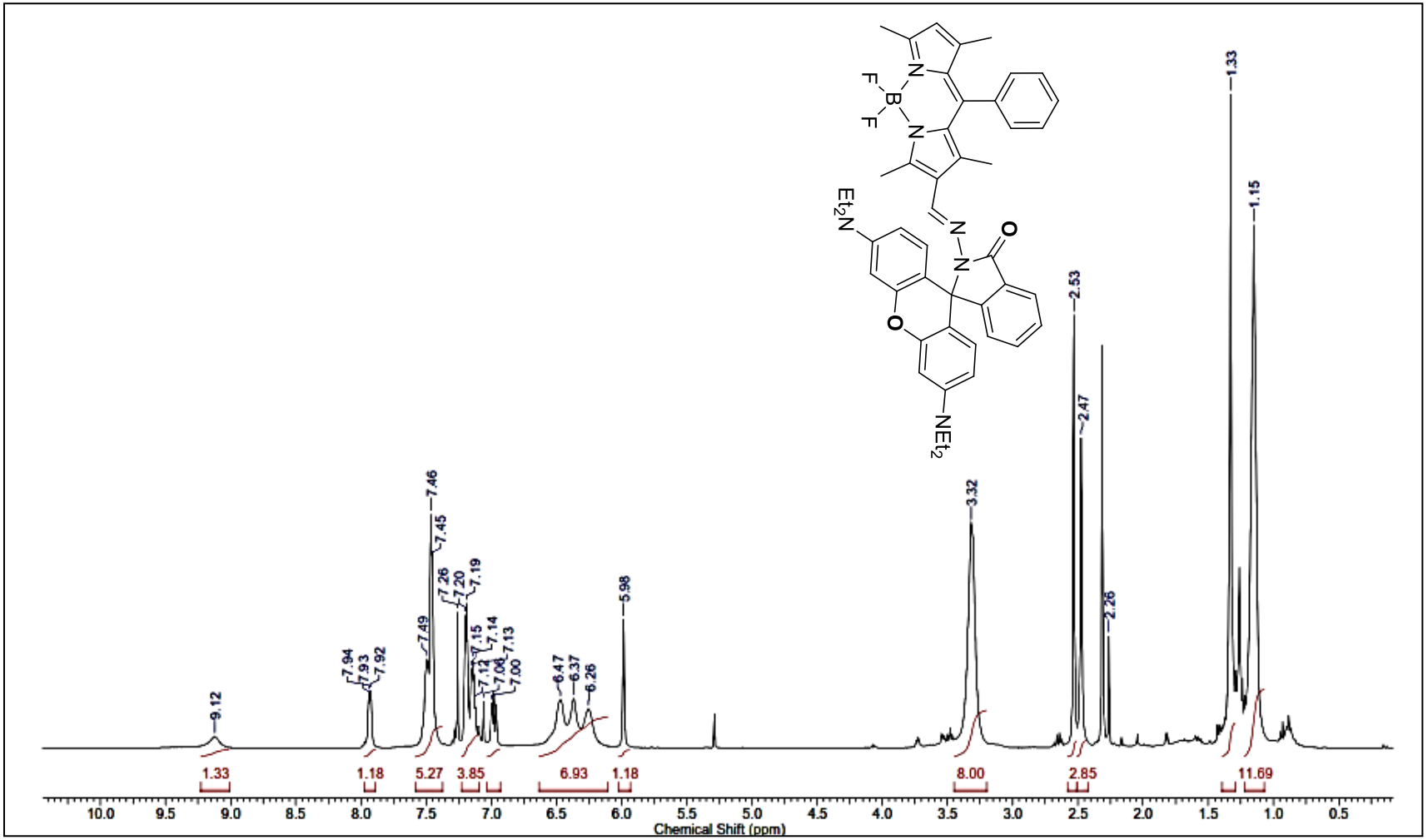

Figure A.11. ^{1}H NMR of (E)-8-(((3',6'-bis(diethylamino)-3-oxospiro[isoindoline-1,9'-xanthen]-2-yl)imino)methyl)-5,5-difluoro-1,3,7,9-tetramethyl-10-phenyl-5H-dipyrrolo[1,2-c:2',1'-f][1,3,2]diazaborinin-4-ium-5-uide

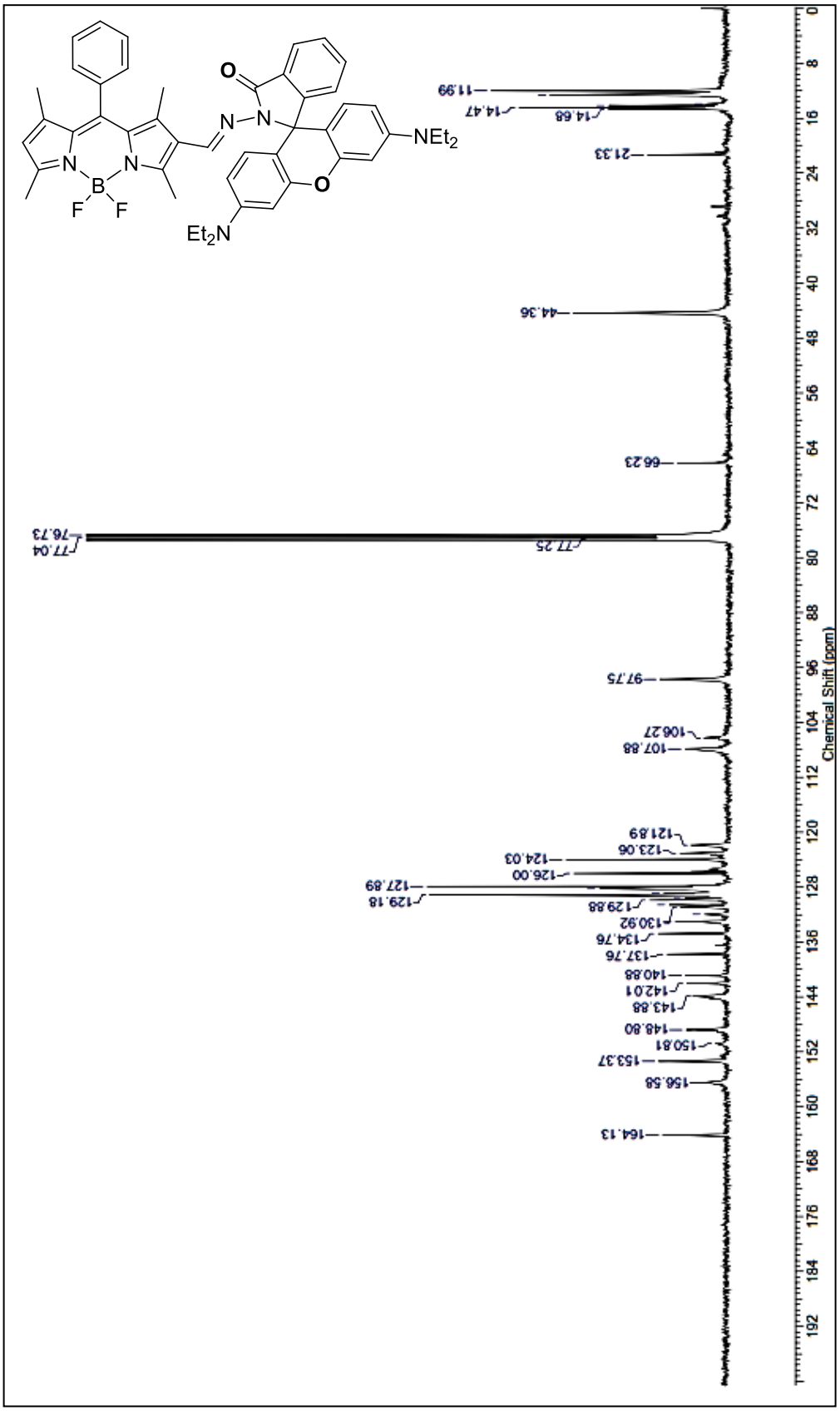

Figure A.12. ^{13}C NMR of (E)-8-(((3',6'-bis(diethylamino)-3-oxospiro[isoindoline-1,9'-xanthen]-2-yl)imino)methyl)-5,5-difluoro-1,3,7,9-tetramethyl-10-phenyl-5H-dipyrrolo[1,2-c:2',1'-f][1,3,2]diazaborinin-4-ium-5-uide

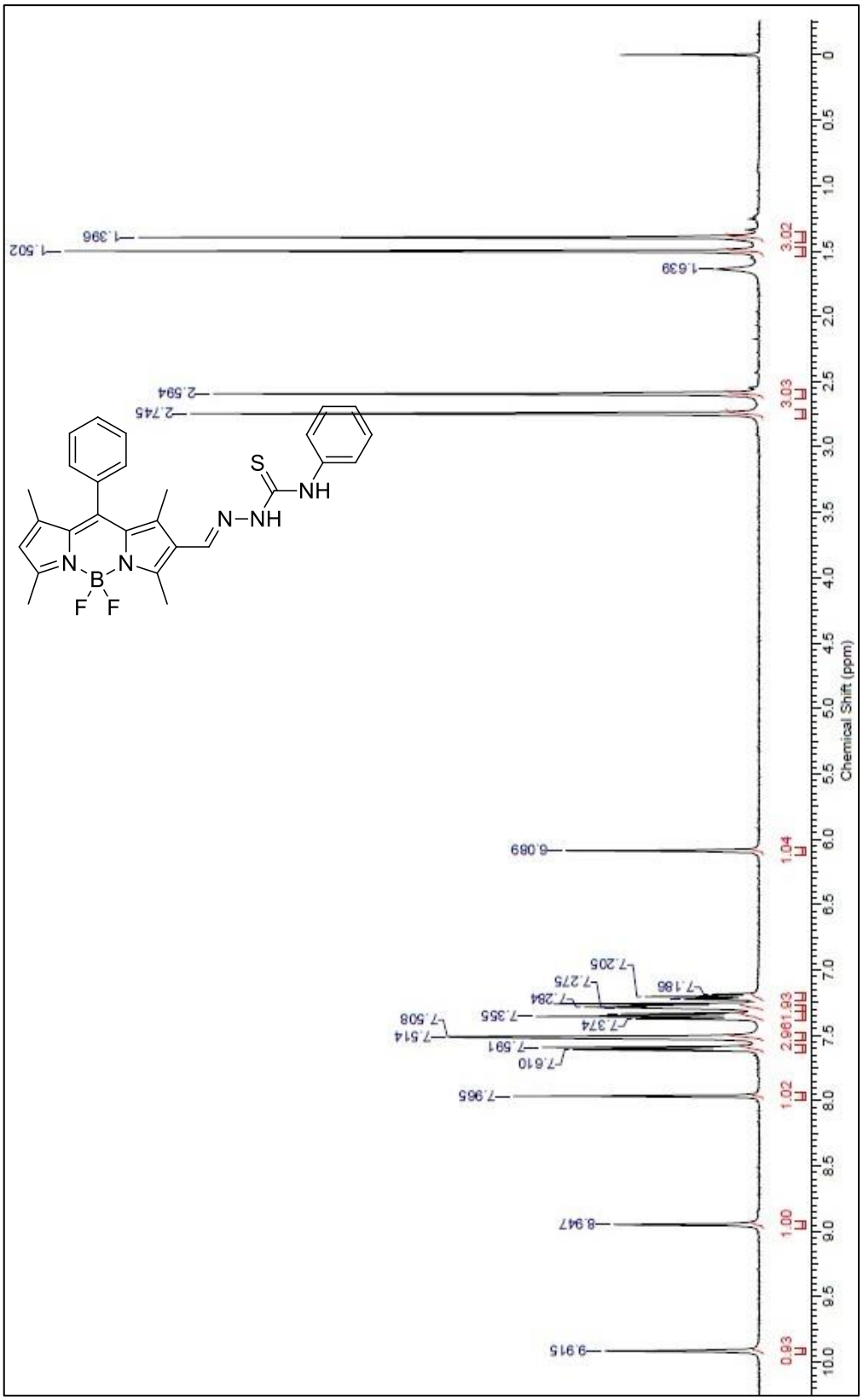

Figure A.13. ^{1}H NMR of (E)-5,5-difluoro-1,3,7,9-tetramethyl-10-phenyl-8-((2-(phenylcarbamothioyl)hydrazono) methyl)-5H-dipyrrolo[1,2-c:2',1'-f][1,3,2]diazaborinin-4-ium-5-uide

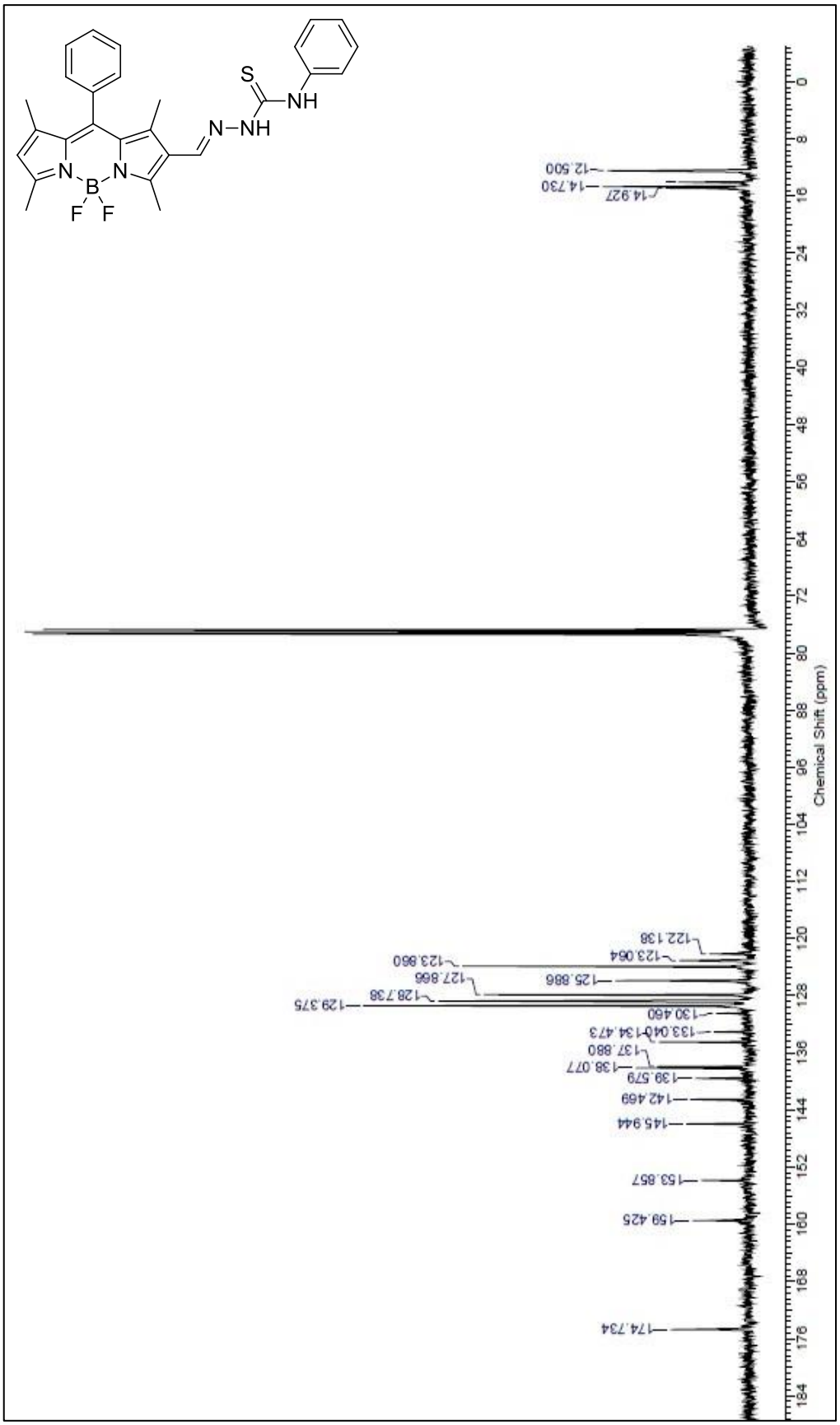

Figure A.14. ^{13}C NMR of (E)-5,5-difluoro-1,3,7,9-tetramethyl-10-phenyl-8-((2-(phenylcarbamothioyl)hydrazono) methyl)-5H-dipyrrolo[1,2-c:2',1'-f][1,3,2]diazaborinin-4-ium-5-uide

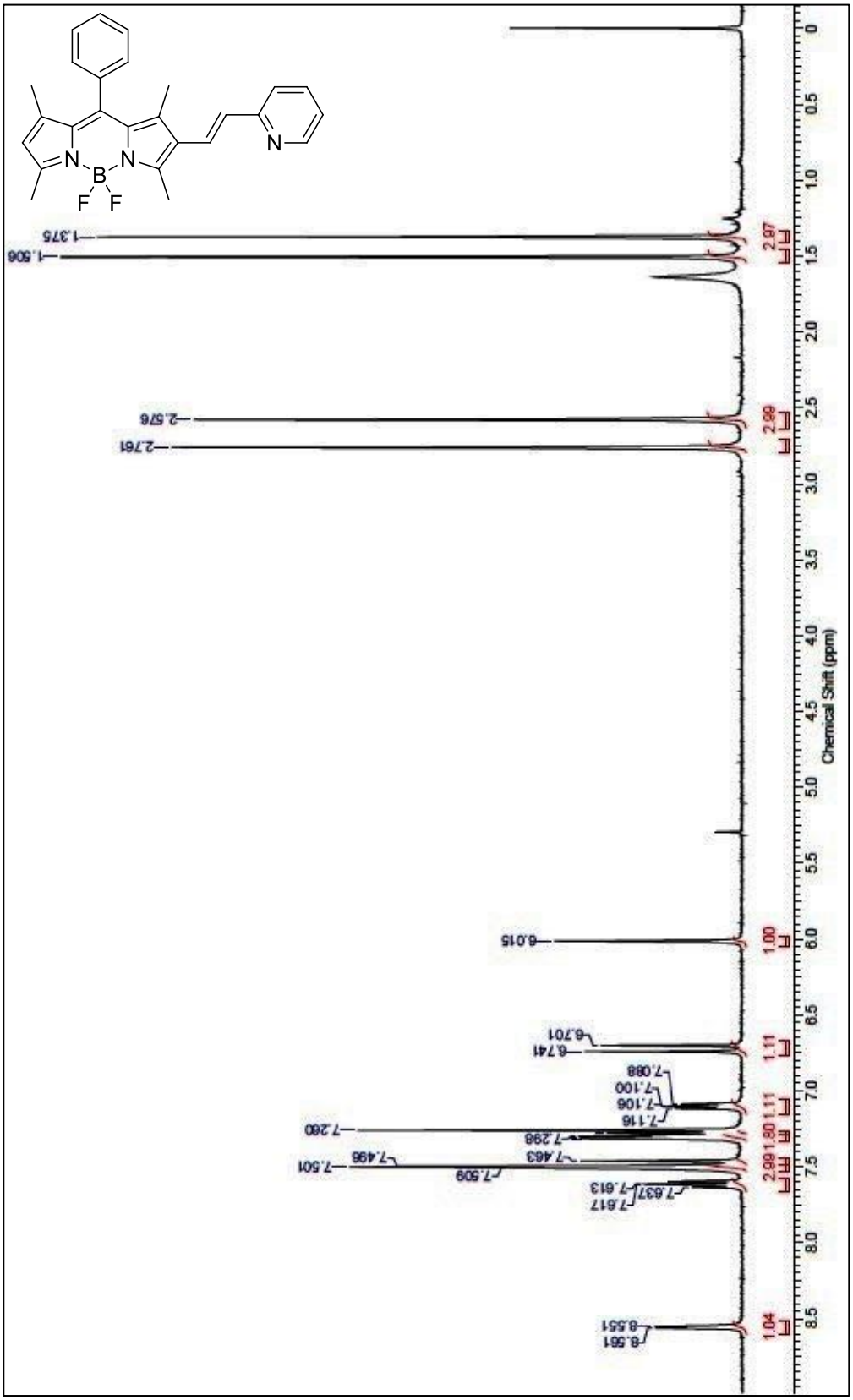

Figure A.15. ^{1}H NMR of (E)-5,5-difluoro-1,3,7,9-tetramethyl-10-phenyl-8-(2-(pyridin-2-yl)vinyl)-5H-dipyrrolo[1,2-c:2',1'-f][1,3,2]diazaborinin-4-ium-5-uide

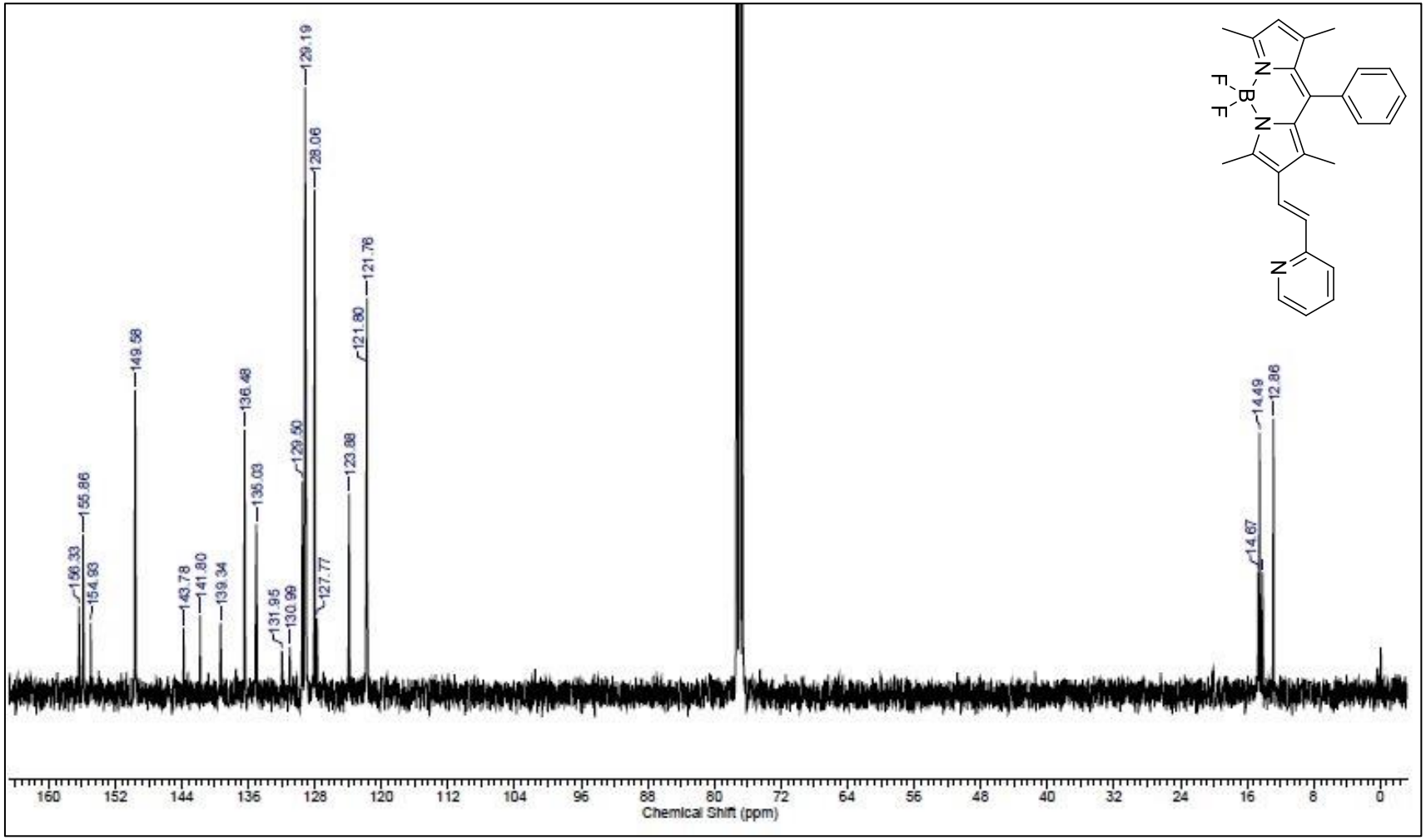

Figure A.16. ^{13}C NMR of (E)-5,5-difluoro-1,3,7,9-tetramethyl-10-phenyl-8-(2-(pyridin-2-yl)vinyl)-5H-dipyrrolo[1,2-c:2',1'-f][1,3,2]diazaborinin-4-ium-5-uide

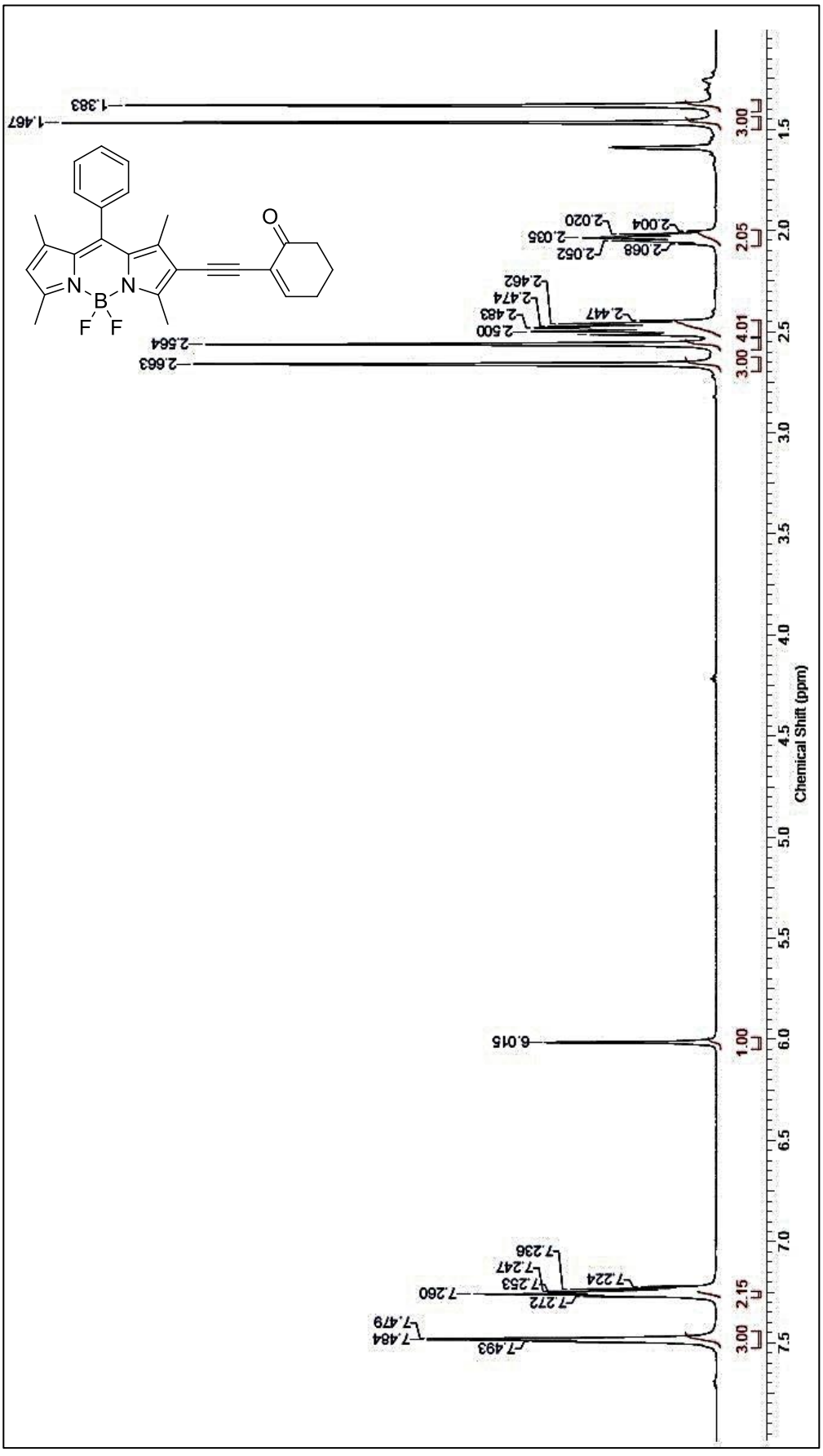

Figure A.17. ^{1}H NMR of 5,5-difluoro-1,3,7,9-tetramethyl-8-((6-oxocyclohex-1-en-1-yl)ethynyl)-10-phenyl-5H-dipyrrolo[1,2-c:2',1'-f][1,3,2]diazaborinin-4-ium-5-uide

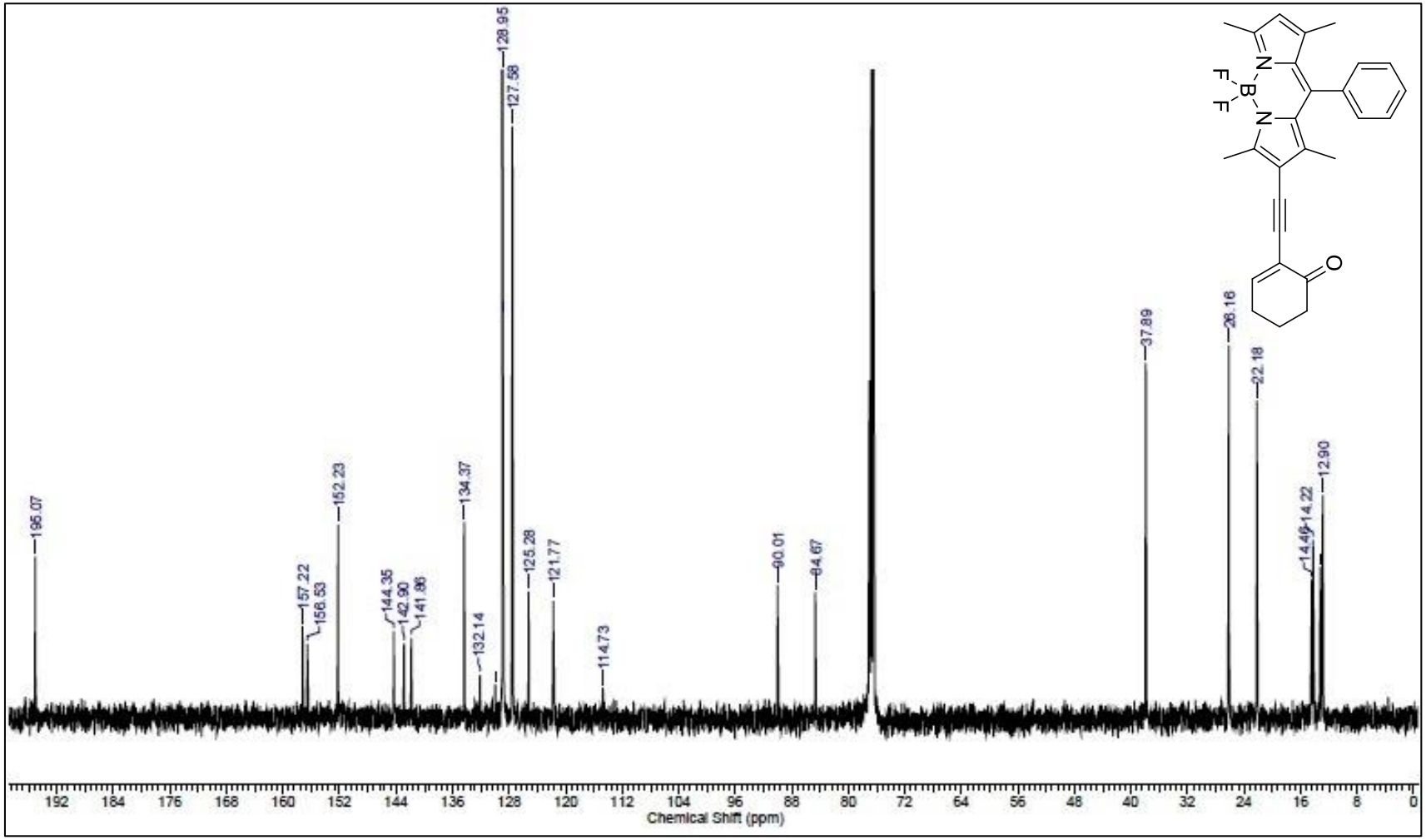

Figure A.18. ^{13}C NMR of 5,5-difluoro-1,3,7,9-tetramethyl-8-((6-oxocyclohex-1-en-1-yl)ethynyl)-10-phenyl-5H-dipyrrolo[1,2-c:2',1'-f][1,3,2]diazaborinin-4-ium-5-uide

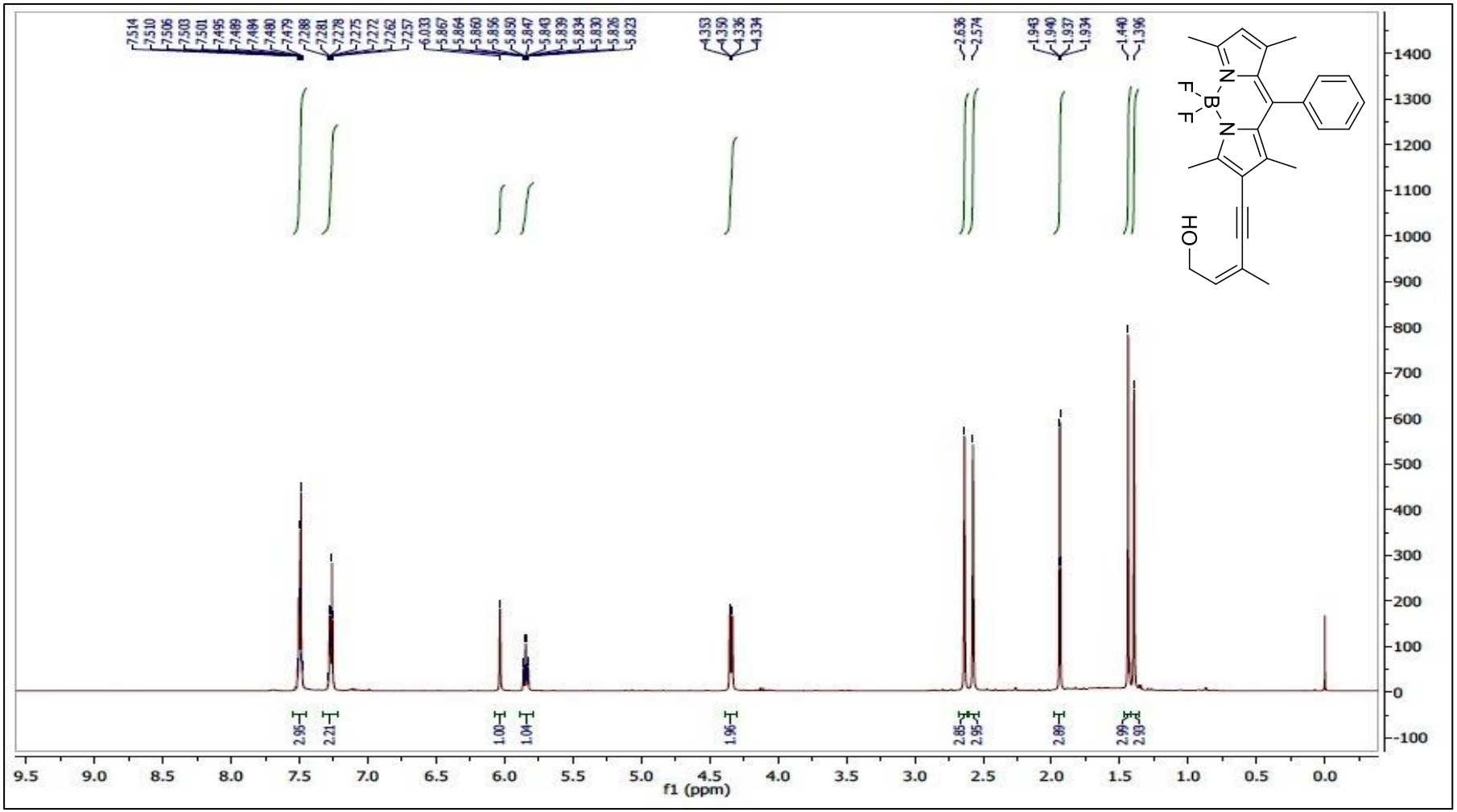

Figure A.19. ^{1}H NMR of (Z)-5,5-difluoro-8-(5-hydroxy-3-methylpent-3-en-1-yn-1-yl)-1,3,7,9-tetramethyl-10-phenyl-5H-dipyrrolo[1,2-c:2',1'-f][1,3,2]diazaborinin-4-ium-5-uide

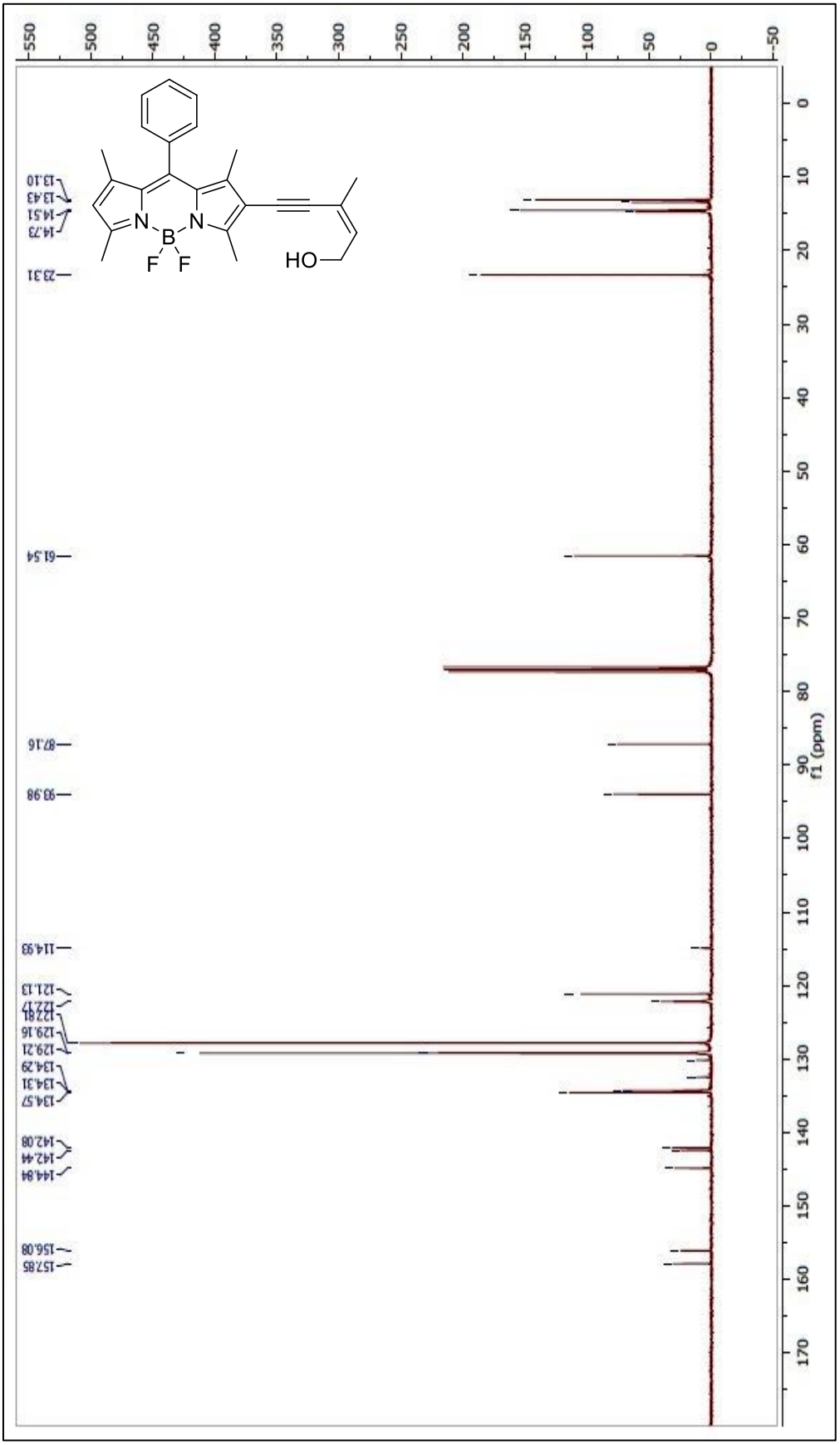

Figure A.20. ^{13}C NMR of (Z)-5,5-difluoro-8-(5-hydroxy-3-methylpent-3-en-1-yn-1-yl)-1,3,7,9-tetramethyl-10-phenyl-5H-dipyrrolo[1,2-c:2',1'-f][1,3,2]diazaborinin-4-ium-5-uide

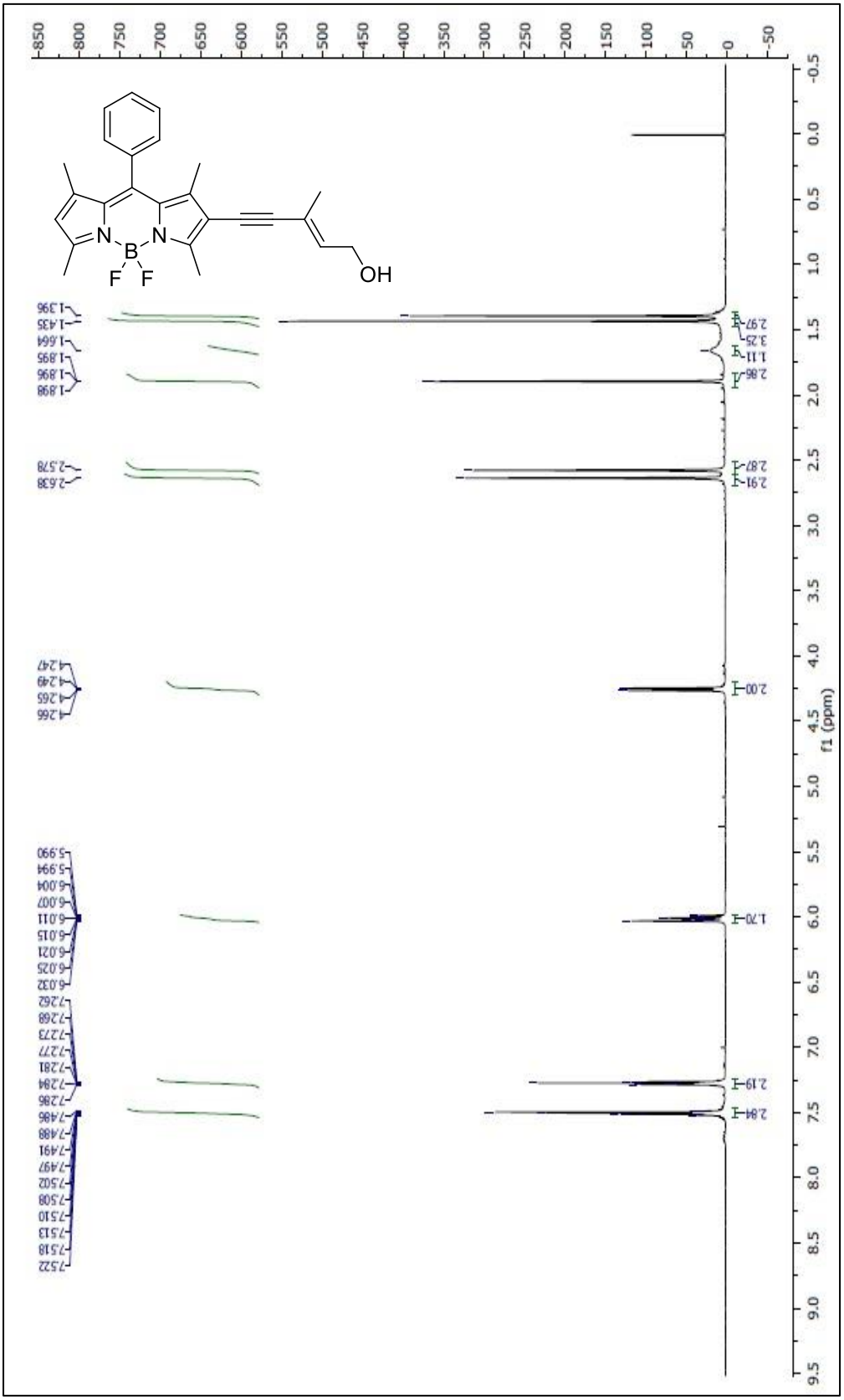

Figure A.21. ^{1}H NMR of (E)-5,5-difluoro-8-(5-hydroxy-3-methylpent-3-en-1-yn-1-yl)-1,3,7,9-tetramethyl-10-phenyl-5H-dipyrrolo[1,2-c:2',1'-f][1,3,2]diazaborinin-4-ium-5-uide

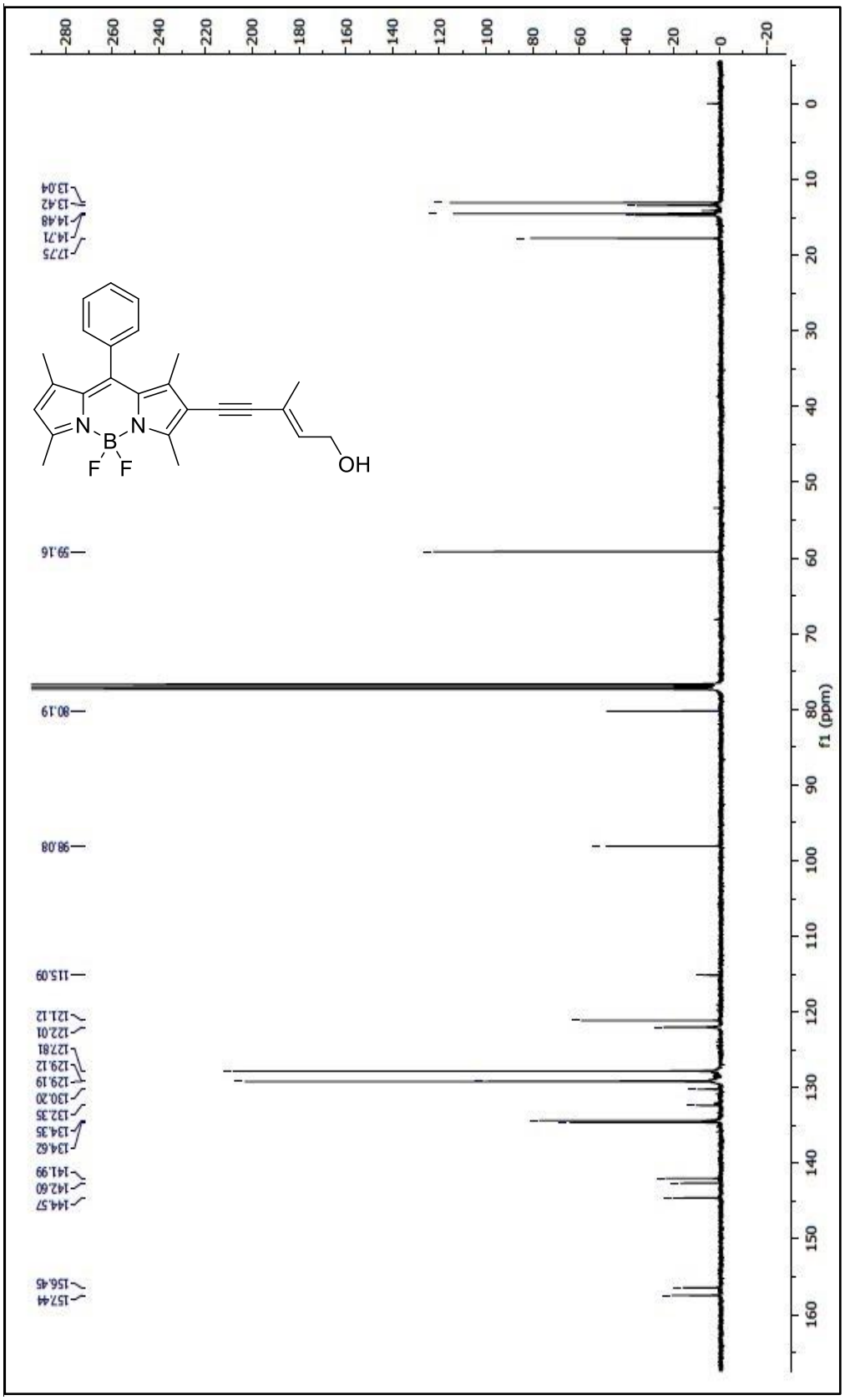

Figure A.22. ^{13}C NMR of (E)-5,5-difluoro-8-(5-hydroxy-3-methylpent-3-en-1-yn-1-yl)-1,3,7,9-tetramethyl-10-phenyl-5H-dipyrrolo[1,2-c:2',1'-f][1,3,2]diazaborinin-4-ium-5-uide

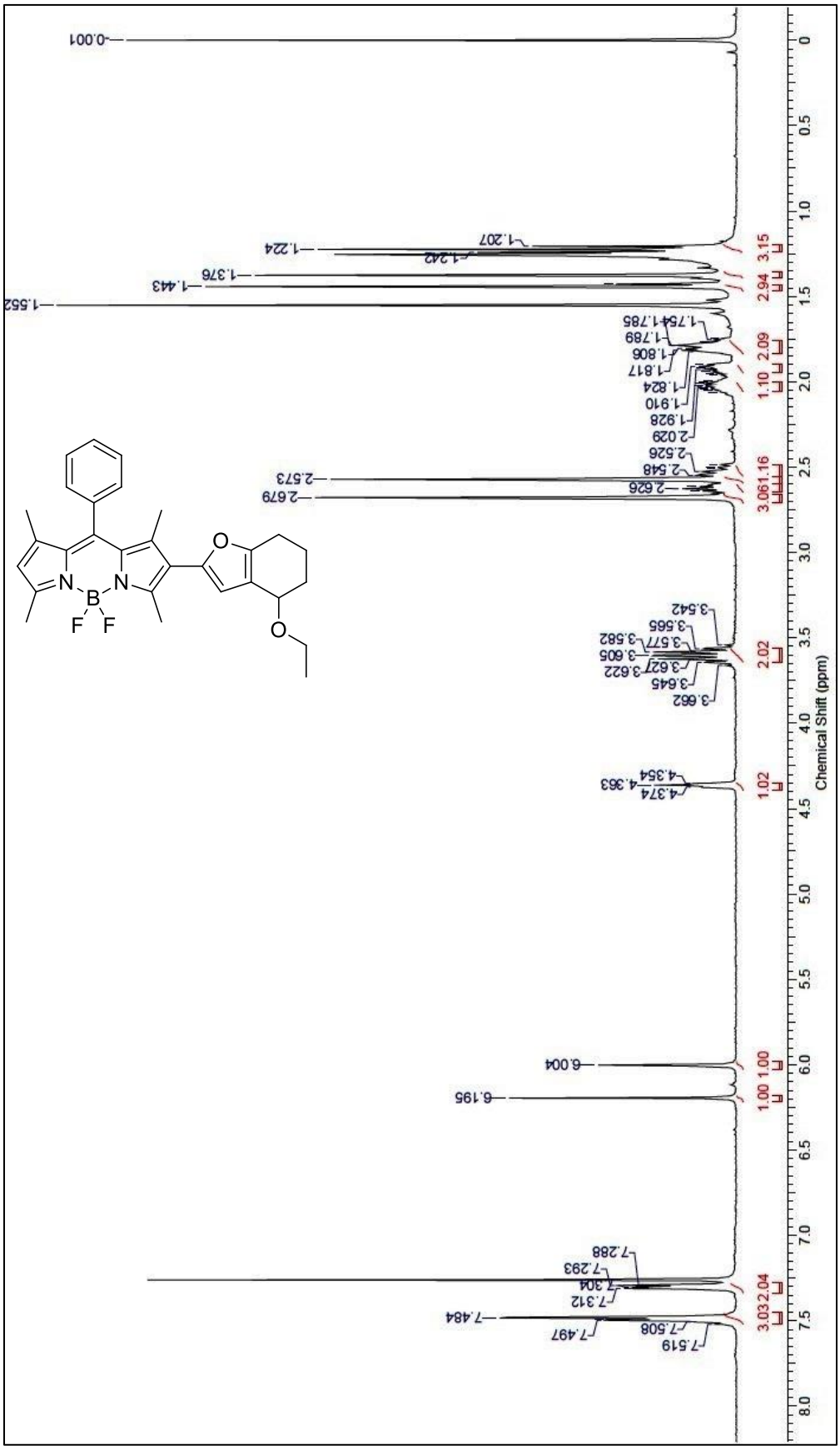

Figure A.23. ^{1}H NMR of (R)-8-(4-ethoxy-4,5,6,7-tetrahydrobenzofuran-2-yl)-5,5-difluoro-1,3,7,9-tetramethyl-10-phenyl-5H-dipyrrolo[1,2-c:2',1'-f][1,3,2]diazaborinin-4-ium-5-uide

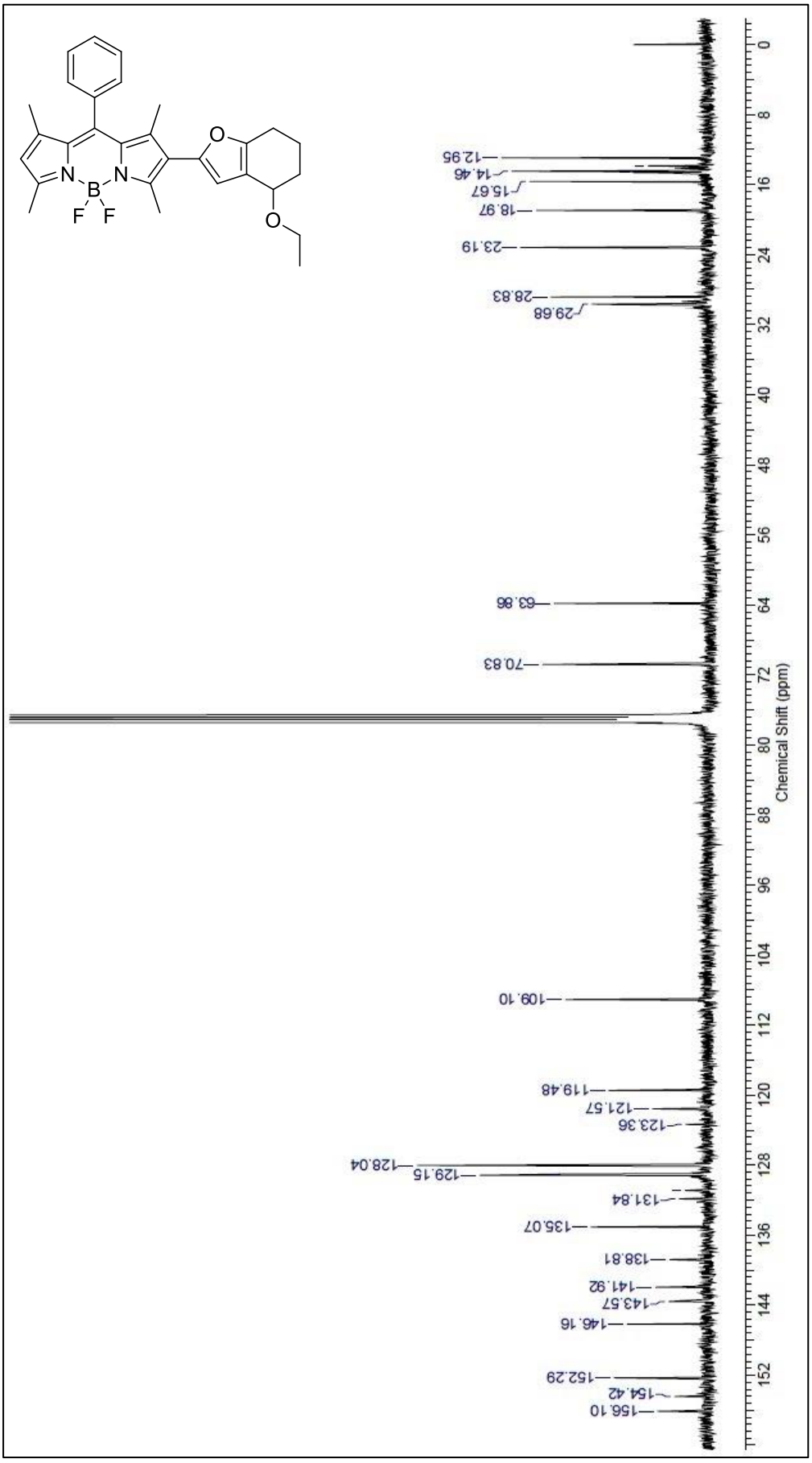

Figure A.24. ^{13}C NMR of (R)-8-(4-ethoxy-4,5,6,7-tetrahydrobenzofuran-2-yl)-5,5-difluoro-1,3,7,9-tetramethyl-10-phenyl-5H-dipyrrolo[1,2-c:2',1'-f][1,3,2]diazaborinin-4-ium-5-uide

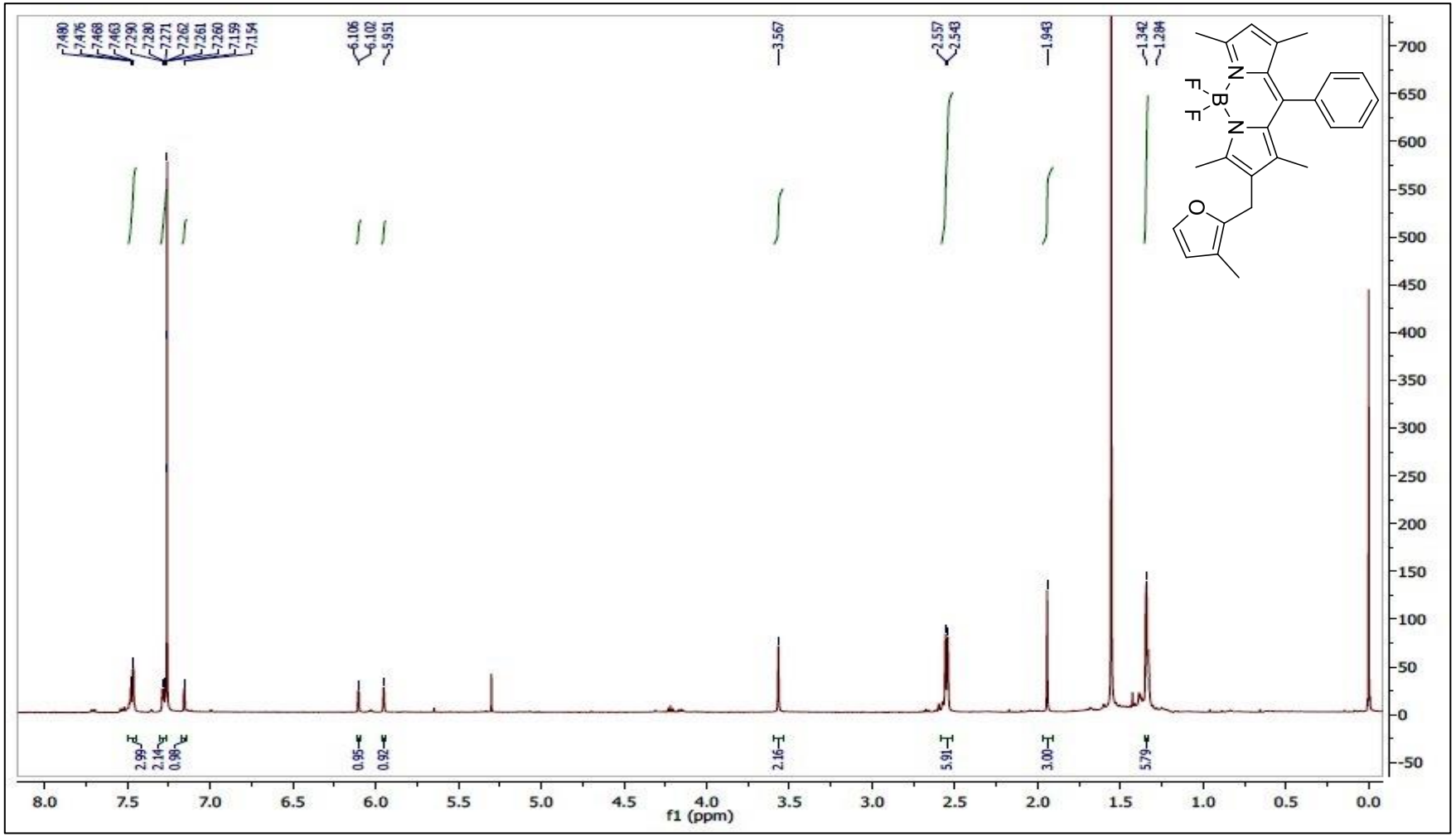

Figure A.25. ^{1}H NMR of 5,5-difluoro-1,3,7,9-tetramethyl-8-((3-methylfuran-2-yl)methyl)-10-phenyl-5H-dipyrrolo[1,2-c:2',1'-f][1,3,2]diazaborinin-4-ium-5-uide

APPENDIX B

MASS SPECTRA OF COMPOUNDS

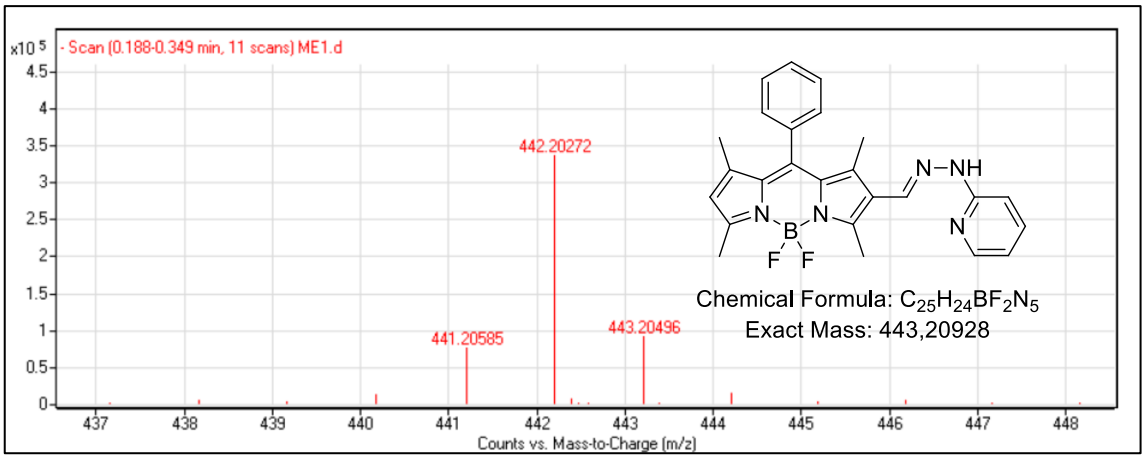

Figure B.1. (E)-5,5-difluoro-1,3,7,9-tetramethyl-10-phenyl-8-((2-(pyridin-2-yl)hydrazono)methyl)-5H-dipyrrolo[1,2-c:2',1'-f][1,3,2]diazaborinin-4-ium-5-uide

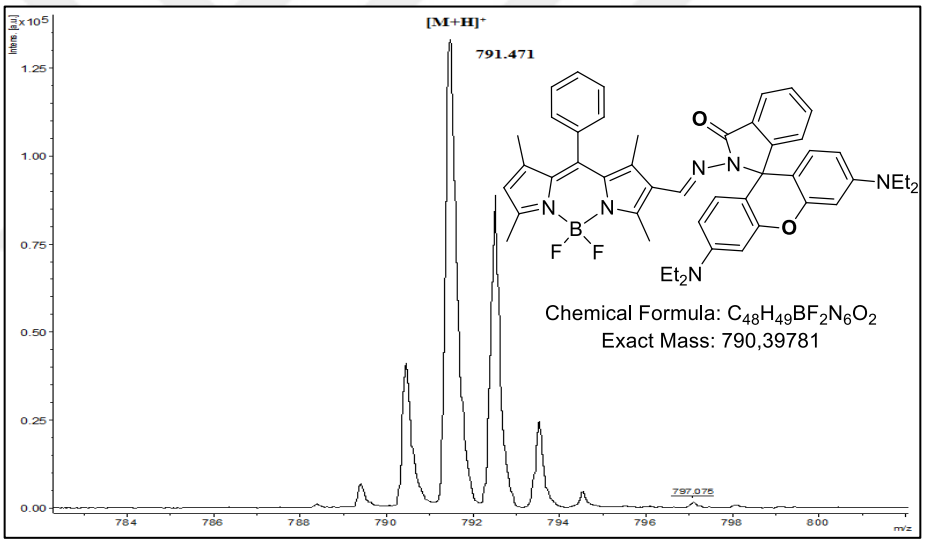

Figure B.2. MALDI-TOF Spectra of **BOD-8** ((E)-8-(((3',6'-bis(diethylamino)-3-oxospiro[isoindoline-1,9'-xanthen]-2-yl)imino)methyl)-5,5-difluoro-1,3,7,9-tetramethyl-10-phenyl-5H-dipyrrolo[1,2-c:2',1'-f][1,3,2]diazaborinin-4-ium-5-uide)

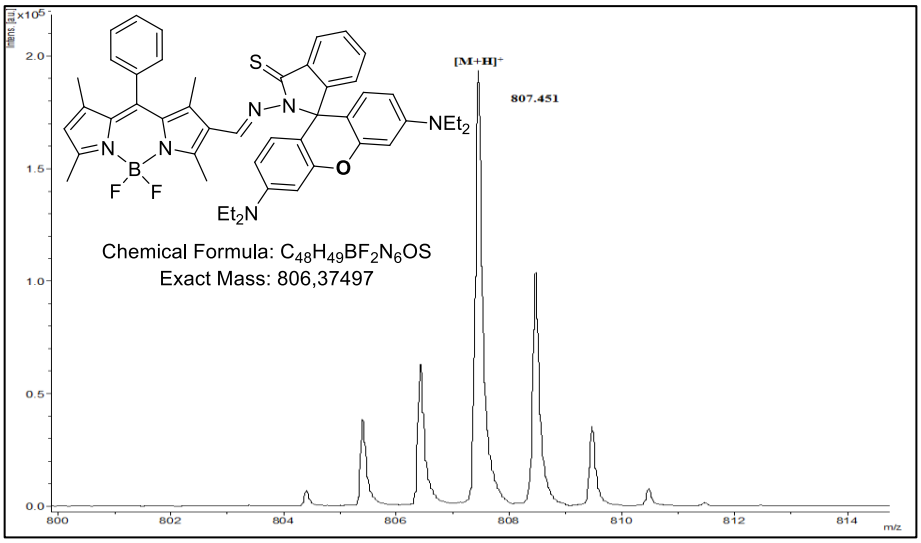

Figure B.3. MALDI-TOF Spectra of **BOD-2** ((E)-8-(((3',6'-bis(diethylamino)-3-thioxospiro[isoindoline-1,9'-xanthen]-2-yl)imino)methyl)-5,5-difluoro-1,3,7,9-tetramethyl-10-phenyl-5H-dipyrrolo[1,2-c:2',1'-f][1,3,2]diaza borinin-4-ium-5-uide)

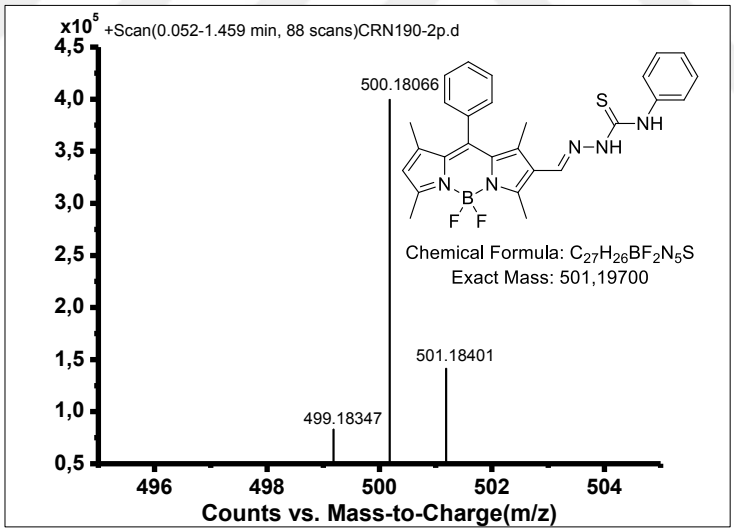

Figure B.4. Mass Spectrum of **BOD-3** ((E)-5,5-difluoro-1,3,7,9-tetramethyl-10-phenyl-8-((2-(phenylcarbamothioyl)hydrazono)methyl)-5H-dipyrrolo[1,2-c:2',1'-f] [1,3,2]diazaborinin-4-ium-5-uide)

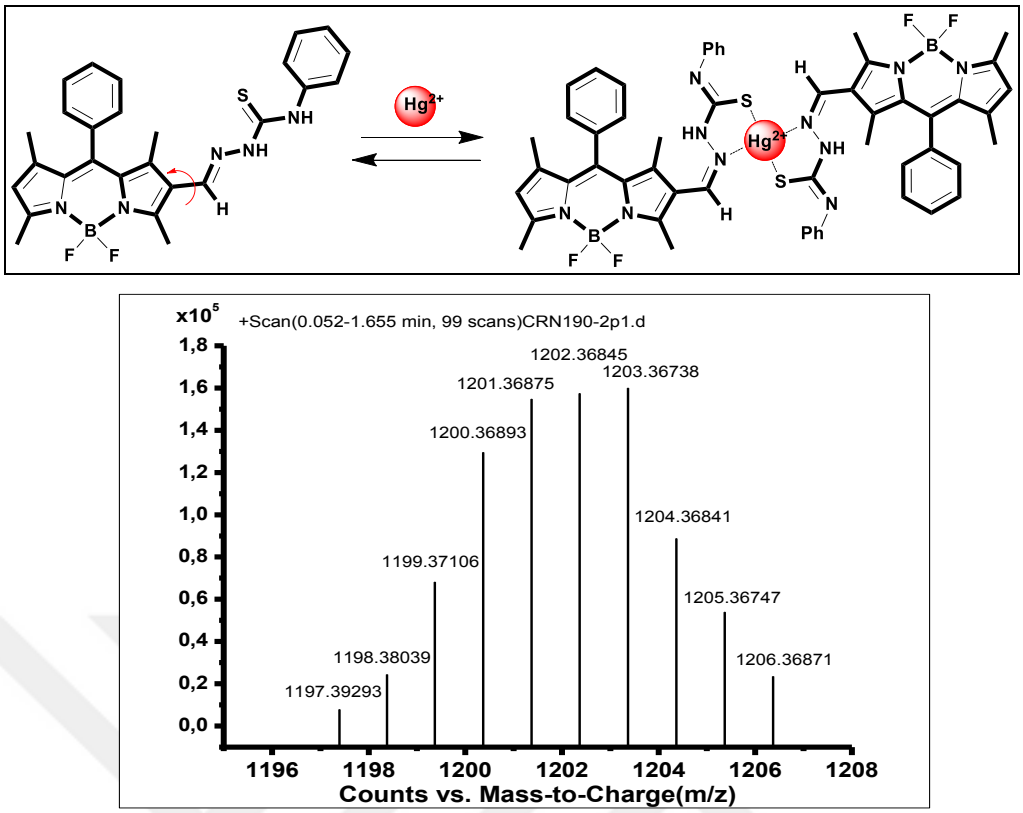

Figure B.5. Mass Spectrum of the Obtained Hg^{2+}- **BOD-3** Complex

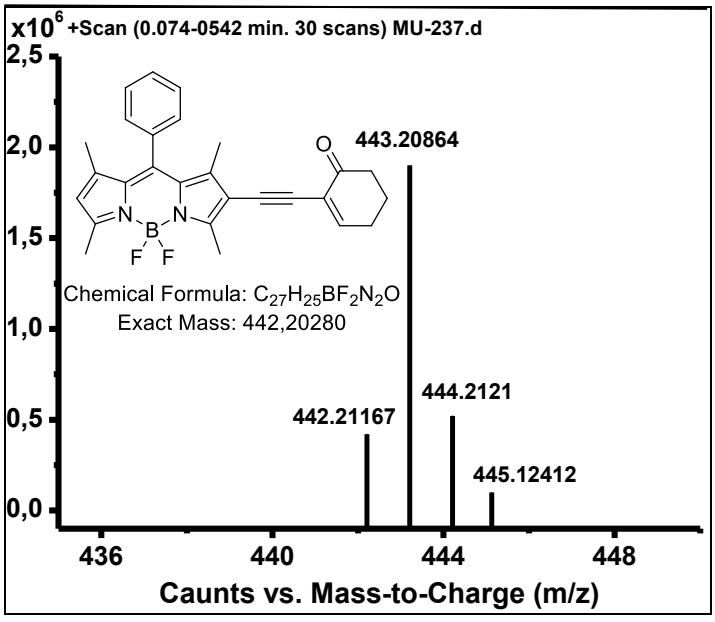

Figure B.6. Mass Spectrum of **BOD-4** (5,5-difluoro-1,3,7,9-tetramethyl-8-((6-oxocyclohex-1-en-1-yl)ethynyl)-10-phenyl-5H-dipyrrolo[1,2-c:2',1'-f][1,3,2]diazaborinin-4-ium-5-uide)

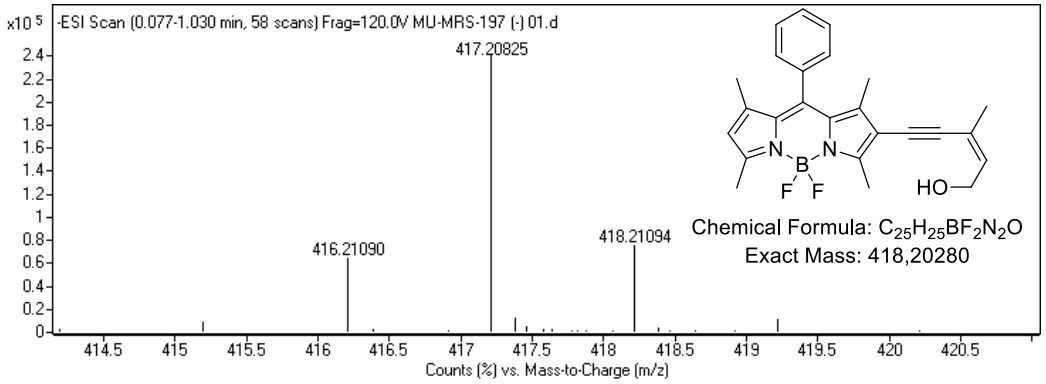

Figure B.7. Mass Spectrum of **BOD-5** ((Z)-5,5-difluoro-8-(5-hydroxy-3-methylpent-3-en-1-yn-1-yl)-1,3,7,9-tetramethyl-10-phenyl-5H-dipyrrolo[1,2-c:2',1'-f] [1,3,2]diazaborinin-4-ium-5-uide)

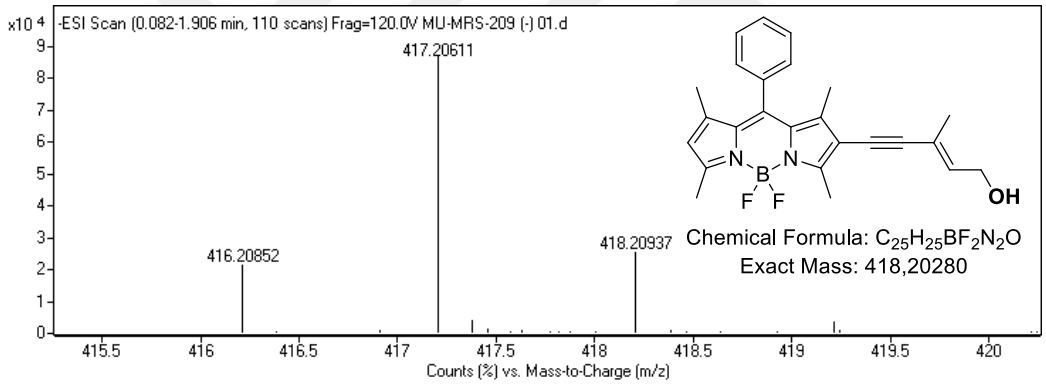

Figure B.8. Mass Spectrum of **BOD-9** ((E)-5,5-difluoro-8-(5-hydroxy-3-methylpent-3-en-1-yn-1-yl)-1,3,7,9-tetramethyl-10-phenyl-5H-dipyrrolo[1,2-c:2',1'-f] [1,3,2]diazaborinin-4-ium-5-uide)

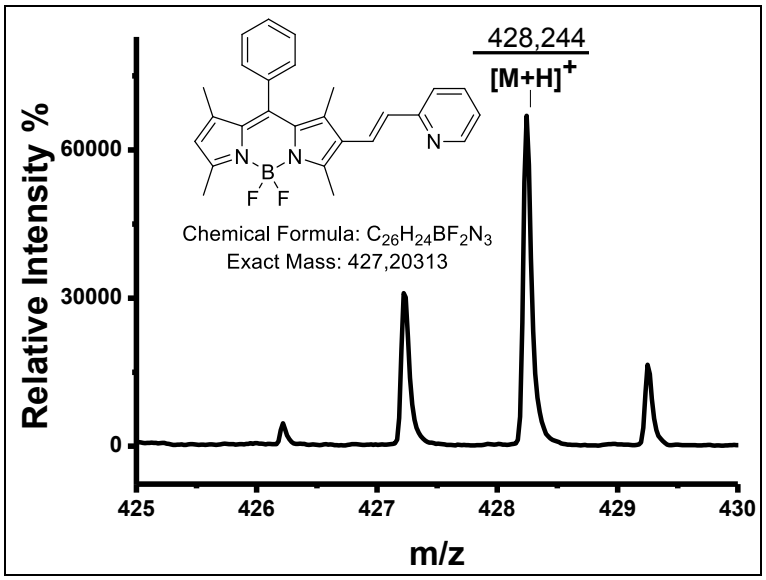

Figure B.9. Mass Spectrum of **BOD-6** ((E)-5,5-difluoro-1,3,7,9-tetramethyl-10-phenyl-8-(2-(pyridin-2-yl)vinyl)-5H-dipyrrolo[1,2-c:2',1'-f][1,3,2]diazaborinin-4-ium-5-uide)

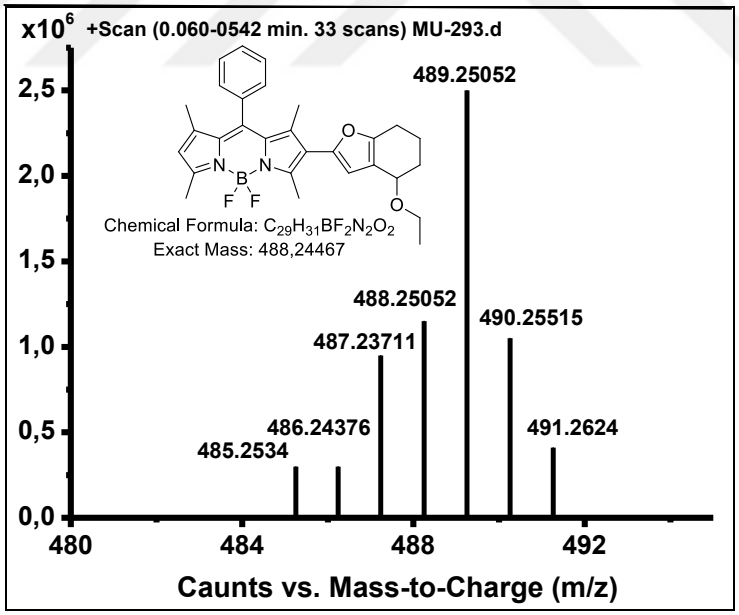

Figure B.10. Mass Spectrum of **(6)-BODIPY-FUR** (8-(4-ethoxy-4,5,6,7-tetrahydrobenzofuran-2-yl)-5,5-difluoro-1,3,7,9-tetramethyl-10-phenyl-5H-dipyrrolo[1,2-c:2',1'-f][1,3,2]diazaborinin-4-ium-5-uide)

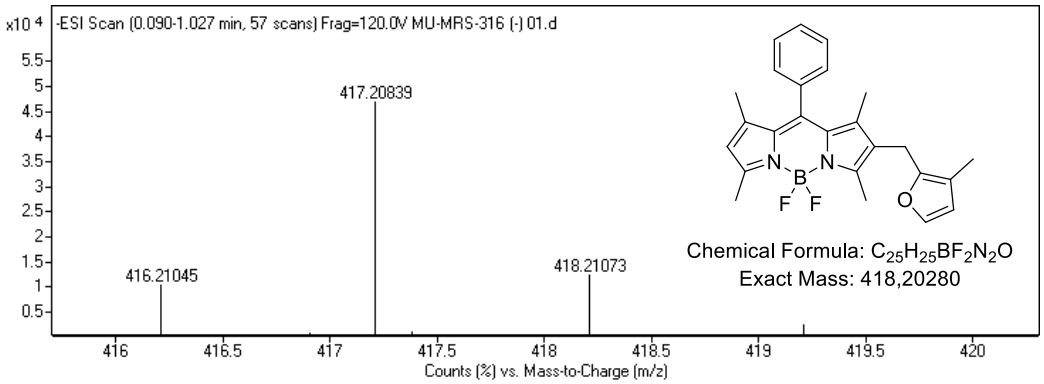

Figure B.11. Mass Spectrum of **(7)-BODIPY-FUR** 5,5-difluoro-1,3,7,9-tetramethyl-8-((3-methylfuran-2-yl)methyl)-10-phenyl-5H-dipyrrolo[1,2-c:2',1'-f][1,3,2] diazaborinin-4-ium-5-uide

VITA

PERSONAL INFORMATION

Surname, Name: ÜÇÜNCÜ Muhammed
Nationality: Turkish (T.C.)
Date and Place of Birth: 01.08.1986, Kullar/İZMİT
Marital Status: Single
Phone: (+90) 541 288 00 85
E-mail: muhammed.iyte@gmail.com

EDUCATION

Degree Institution Year of Graduation
PhD İzmir Institute of Technology 2016
MSc İzmir Institute of Technology 2011
BSc İzmir Institute of Technology 2009

WORK EXPERIENCE

2016 – Ministry of Customs and Trade, Chemist
2009 – 2016 Izmir Institute of Technology Teaching and Research Assistant
2008 – Hayat Chemical Company, Trainee

FOREIGN LANGUAGE

English (Advanced)

PUBLICATIONS

1. Üçüncü, M.; Karakuş, E.; Kuş, M.; Akpınar, G. E.; Aksın-Artok, Ö.; Krause, N.; Karaca, S.; Elmacı, N. and Artok, L. *J. Org. Chem.*, 2011, *76* (15), 5959–5971.
2. Akpınar, G. E.; Kuş, M.; Üçüncü, M.; Karakuş, E. and Artok, L. *Org. Lett.*, 2011, *13* (4), 748–751.
3. Emrullahoğlu, M.; Karakuş, E. and Üçüncü, M. *Analyst*, 2013, *138*, 3638–3641.
4. Emrullahoğlu, M.; Üçüncü, M. and Karakuş, E. *Chem. Commun.*, 2013, *49*, 7836-7838.
5. Karakuş, E.; Üçüncü M.; Eanes, R. and Emrullahoğlu, M. *New J. Chem.*, 2013, 2632-2635.
6. Karakuş, E.; Üçüncü, M. and Emrullahoğlu, M. *Chem. Commun.*, 2014, *50*, 1119-1121.
7. Üçüncü, M. and Emrullahoğlu, M. *Chem. Commun.*, 2014, *50*, 5884-5886.
8. Kurtulus I.; Yilmaz G.; Ucuncu M.; Emrullahoglu M.; Becer C. R. and Bulmus V. *Polym. Chem.*, 2014, *5*, 1593-1604.
9. Cantürk, C.; Üçüncü, M. and Emrullahoğlu, M**.** *RSC Adv.*, 2015**,** ***5***, 30522-30525.
10. Üçüncü, M.; Karakuş, E. and Emrullahoğlu, M. *Chem. Eur. J.*, 2015, *21*, 13201–13205.
11. Üçüncü, M.; Karakuş, E. and Emrullahoğlu, M. *New J. Chem.*, 2015, 39, 8337-8341.
12. Tatlıdil, D.; Üçüncü, M. and Akdoğan, Y. *Phys. Chem. Chem. Phys.*, 2015, *17*, 22678-22685.
13. Karakuş, E.; Üçüncü M. and Emrullahoğlu M. *Anal. Chem.*, 2016, *88* (1), 1039–1043.
14. Horzum, N.; Mete, D.; Karakuş E.; Üçüncü, M.; Emrullahoğlu, M. and Demir. M. M. *ChemistrySelect*, 2016, 1, 896-900.
15. Çetintaş, C.; Karakuş, E.; Üçüncü M. and Emrullahoğlu M. *Sensors Actuat B-Chem.*, 2016, 234, 109-114.
16. Üçüncü, M.; Karakuş, E. and Emrullahoğlu, M. *Chem. Commun.*, 2016, DOI: 10.1039/C6CC04100K.

AWARDS

2009 High Honor Student of Izmir Institute of Technology
2009 Highest Ranking Student of the Department
2009-2011 TUBITAK National Scholarship Program for M.Sc. Students
2013-2015 TUBITAK National Scholarship Program for Ph.D. Students
2015 (September) Best Poster-Turkey Symposium Series: Catalysis and Sensing for Health Symposium –İzmir, Turkey